Università degli Studi di Parma
Dottorato di Ricerca in Ingegneria Civile
Ciclo XXII

Investigation of Low Temperature Properties of Asphalt Mixture Containing Recycled Asphalt Materials

Dissertazione per il Conseguimento del Titolo di Dottore di Ricerca

Augusto Cannone Falchetto

Coordinatori del Dottorato
Prof. Paolo Mignosa, Prof. Gianfranco Forlani

Tutori
Prof. Antonio Montepara, Dr. Gabriele Tebaldi, Dr. Mihai O. Marasteanu

Parma, Gennaio 2011

ACKNOWLEDGEMENTS

I would like to express my deepest gratitude to my Tutors Prof. Antonio Montepara and Dr. Gabriele Tebaldi for their kind support during these years of my graduate studies. I'm deeply thankful to my advisor Dr. Mihai O. Marasteanu for his patience and guidance throughout the development of the thesis and for his advices during the three years I spent in the United States. I'm also thankful to Prof. Marco Pasetto for the time I spent at the University of Padova.

I would like to thank Mugurel I. Turos, my office mate Ki Hoon Moon, and Dr. Raul Velasquez for their help at the University of Minnesota.

I'm thankful to Dr. Elena Romeo and Valentina Rota for their kind help from Italy.

Finally I am deeply thankful to my Mother and my Father because they know that number 5 will follow number 4…and they know it very well!

ABSTRACT

The use of increased proportions of Reclaimed Asphalt Pavement (RAP) in the construction of asphalt pavements has become a top priority due to its economical and environmental benefits. Moreover other materials as Recycled Asphalt Shingles (RAS) have recently found their applicability in the same field. However in spite of a significant number of studies on the use of RAP and RAS, little was done to investigate the behavior at low temperature of pavement containing these two types of materials. In this thesis the effect of using three recycled materials RAP, Tear off Scrap Shingles (TOSS) and Manufacturer Waste Scrap Shingles (MWSS), on the asphalt mixture behavior at low temperature is investigated based on statistical analysis and modeling of an extensive set of experiments. The experimental part consisted of three-point bending creep tests performed on BBR (Bending Beam Rheometer) beams (6.25 × 12.5 × 100 mm) obtained from 17 different asphalt mixtures. Statistical analysis of the effect of RAP, TOSS and MWSS on creep stiffness, *m*-value, thermal stress and critical temperature was performed showing that TOSS and MWSS affect asphalt mixture performance only for specific amount of RAP. In the theoretical part, asphalt mixtures specimens were analyzed based on digital image analysis, micromechanical and analogical models and finite element simulations. The volumetric fractions and particle size distributions of the different asphalt mixtures were estimated from their binary images after digital processing. The volumetric fraction and the average size distribution of aggregates for the 17 asphalt mixtures investigated were found to be very similar despite of the varying amount of recycled material contained. Detailed information on the internal structure of asphalt mixture was investigated by estimating the spatial correlation functions of the beam specimens. No large fluctuation of the functions were detected meaning that the microstructure of the asphalt mixtures was not affected by the presence of RAP, TOSS and MWSS. Micromechanical and analogical models were used to backcalculate the creep stiffness of the binder for a limited number of mixtures and the prediction was compared to the creep stiffness obtained from the corresponding extracted binders. A noticeable difference was detected with the prediction having much higher values. Finally, two-dimensional finite element simulations of three point bending were used to validate the micromechanical an analogical model used.

TABLE OF CONTENTS

LIST OF TABLES

LIST OF FIGURES

Chapter 1. Introduction

Roadways are one of the most important aspects for the functionality of a country's economy nowadays as well as in the past. In the Roman Empire, roads have served to provide goods, supplies and services to human establishments (*McNichol, 2005*) as well as a faster path for army movement. Over centuries, new countries and new cities were built starting from roads allowing people to move from one region to another.

In developed countries where building new roads is not a priority, pavement maintenance and preservation have become critically important. More recently economical and environmental issues arise as some of the aspects that must also be taken into consideration when dealing with pavement design and maintenance. As the world population continues to grow, the amount and type of waste generated also continue to grow. The generation of non-decaying waste materials combined with a growing consumer population, higher disposal fees, and increased governmental and environmental regulations have resulted in significant waste disposal issues (*Watson et al., 1998*).

Over the past 20 to 30 years, a continuing search for recycling alternatives has led federal, state, and local agencies to consider a variety of potentially recyclable materials for pavements, road base, and other construction applications. The list includes Reclaimed Asphalt Pavement (RAP), reclaimed Portland cement concrete, iron blast-furnace slag, fly ash, waste tire rubber, waste glass, and roofing shingles.

Incorporating Reclaimed Asphalt Pavement (RAP) into new pavements significantly reduces the usage of new materials, conserves natural resources and solves disposal problems (*Zofka et al*., *2005*). According to Federal Highway Administration (FHWA) nearly 30 million tons of RAP are recycled into HMA pavements every year making RAP the most recycled material in the United States. To address this important issue, National Cooperative Highway Research Program has funded a number of projects such as NCHRP 9-12, Incorporation of Reclaimed Asphalt Pavements in the Superpave System, (*NCHRP, 2001*) and the still active NCHRP 9-46, Improved Mix Design, Evaluation, and Materials Management Practices for Hot Mix Asphalt with High Reclaimed Asphalt Pavement Content.

Roofing shingles is another material that is available in large quantity for recycling. According to one estimate, about 10 million tons of waste bituminous roofing materials are generated within the United States each year (*Better Roads, 1997*). According to a different reference (*Marks and Petermeier, 1997*) about 16.8 million m^3 of manufacturing and reroofing waste are generated each year within the United States and this waste is typically deposited into landfills. The Research and Development Center of Manville Service Corporation in Denver, Colorado, has estimated that asphalt roofing waste includes about 2.1 million tons of asphalt binder annually corresponding to almost 10% of all asphalt binder requirements for Hot Mix Asphalt used for asphalt pavement. At a cost of 150$/ton, this amounts to over $300 million of worth recoverable asphalt cement. As for the case of RAP, the use of recycled asphalt shingles in hot mix asphalt (HMA) has been a developing technology for more than two decades with increasing acceptance from both government agencies and construction contractors.

However the use of recycled materials into asphalt pavement can be detrimental to the overall mechanical performance of the pavement and of the asphalt mixtures especially at low service temperature, due to the presence of aged, oxidized binders that is more brittle and has worse relaxation characteristics compared to virgin binders. It is well known that asphalt binders are highly temperature-susceptible viscoelastic materials are also subject to oxidative aging during pavement service life, that leads to dramatic changes in properties that make binders more prone to cracking.

In cold regions where extreme changes in temperature occur, the typical pavement distress is thermal cracking. It manifests as a series of almost regular spaced cracks that develop when then material strength limit is overcome. Low temperature properties of asphalt binders and mixtures are evaluated according to AASHTO standards. Bending Beam Rheometer (BBR) (*AASHTO T 313-02 2006*) is used to determine creep compliance of asphalt binder, and Direct Tension (DT) Test (*AASHTO T 314-02 2002*) is used to obtain binder failure stress and strain. For asphalt mixtures, Indirect Tension Test, IDT, (*AASHTO T 322-03*) is used to obtain both creep and strength. A much simpler method was recently developed that allows obtaining mixture creep compliance using the same BBR device used for testing binders (*Marasteanu et al., 2009*).

Objective and Research Approach

The main objective of this dissertation is to investigate the effects of using Recycled Asphalt Pavement (RAP) and Recycled Asphalt Shingles (RAS), and in particular Tear-off Scrap Shingles – TOSS and Manufacturer Waste Scrap Shingles – MWSS, on asphalt mixture performance at low temperature. To accomplish this objective, the following research approach is taken:

- Investigate how the presence of RAP and RAS influence creep stiffness, *m*-value, thermal stress and critical temperature obtained from three point bending test at low temperatures performed on a set of 17 laboratory prepared asphalt mixtures.
- Based on digital image analysis and estimation of properties such as volumetric fraction, determine if the aggregates particle size distribution is affected by the use of RAP and RAS.
- Obtain detailed spatial information of the internal structure of the asphalt mixtures by means of digital imaging processing and *n*-point correlation functions and determine if the microstructure of the asphalt mixture is affected by the presence of recycled material.
- Study the effective response of the asphalt mixtures based on micromechanical and analogical models and on the back calculation of the bulk properties of the binder present in the mixtures (inverse problem).
- Validate the micromechanical and analogical models with simplified two-dimensional finite element simulations.

Organization

This thesis is divided into seven Chapters. Chapter 2 includes a general review on asphalt mixtures characterization, the use of recycled asphalt materials, the theoretical aspects of *n*-point correlation function, micromechanical models, analogical models, and a short description of the inverse problem. In Chapter 3 the materials and procedures used in the experimental phase are described. Chapter 4 presents the analysis performed on the experimental data obtained at low temperatures; visual and statistical analyses of the experimental results are also included in this Chapter. Chapter 5 contains the digital image analysis of asphalt mixtures specimens; the evaluation of the volumetric fraction of aggregate and grain size distribution is presented. This Chapter includes also the algorithm to estimate two- and three-point correlation functions of a two-phase material. Chapter 6 presents the modeling of asphalt mixtures specimens with micromechanical and analogical models and finite element simulations. Chapter

7 contains a summary of this dissertation, the conclusions, and recommendations for future research.

Chapter 2. Literature Review

First, a brief introduction to linear viscoelasticity concepts and time temperature superposition principle is presented. Some examples of research on applications of Reclaimed Asphalt Pavement (RAP) and Reclaimed Asphalt Shingle (RAS) in asphalt pavement are then described. This is followed by a summary of the theoretical aspects of the *n*-point correlation functions used for description of asphalt mixture microstructure. The chapter concludes with a review of micromechanical models for heterogeneous materials, such as asphalt mixtures, as well as analogical models for viscoleastic materials, followed by an introduction to solving inverse problem and to the correspondence principle concept.

2.1. Asphalt Mixtures

Asphalt mixtures can be classified as composite materials consisting of three phases: asphalt binder, aggregate, and air voids. A typical volumetric composition of this material is 5% of air voids, 20% of asphalt binder, and 75% of aggregate (*NCAT, 2009*). Similarly to other composite materials, the properties of asphalt mixtures are related to the properties of its components. The aggregate phase is considered linear elastic and the asphalt binder is considered viscoelastic, which results in a viscoelastic composite material with properties depending also on temperature (*Monismith and Secor, 1962*).

2.1.1. Linear Viscoelasticity

Boltzmann's superposition principle is generally used to express the constitutive relationship between stresses σ and strains ε for a linear viscoelastic non-aging material (*Christensen, 1982*; *Findley et al., 1989*) as:

$$\sigma_{ij}(t) = \int_0^t E_{ijkl}(t-\xi)\frac{\partial \varepsilon_{kl}(\xi)}{\partial \xi} d\xi \qquad [2.1]$$

$$\varepsilon_{ij}(t) = \int_0^t D_{ijkl}(t-\xi)\frac{\partial \sigma_{kl}(\xi)}{\partial \xi} d\xi \qquad [2.2]$$

Stress can be obtained from equation [2.1] knowing strain history and relaxation modulus *E(t)*. Analogously, strain can be computed using equation [2.2] knowing stress history and creep compliance function *D(t)*.

The three functions, creep compliance, relaxation modulus, and complex modulus, can fully describe the behavior of linear viscoelastic materials. The functions are not independent of each other and various interconversion methods can be used to move from one function to another (*Secor and Monismith, 1964; Mead 1994; Park and Kim, 1999; Park and Schapery, 1999; Marasteanu and Anderson, 2000*). For example, *Hopkins and Hamming* (*1957*) method has been used in many asphalt research papers to convert creep compliance to relaxation modulus; this method numerically solves the Volterra integral [2.3] assuming uniaxial state of stresses and isotropy.

$$t = \int_0^t E(t-\xi)D(t)d\xi \qquad [2.3]$$

According to different researchers, asphalt concrete can be assumed as linear viscoelastic at low temperatures (*Lytton et al., 1993; Buttlar* and *Roque, 1994; Pellinen* and *Witczak, 2002*).

2.1.2. Time-Temperature Superposition Principle (TTSP)

Time temperature superposition principle was first introduced by *Leaderman* (*1943*) who stated that temperature and time effects can be incorporated into the viscoelastic properties by a reduced time function ξ:

$$\xi(t,T) = \frac{t}{a_T(T)} \qquad [2.4]$$

where:

t	time, and
$a_T(T)$	shift factor function of temperature.

Temperature and shift factor a_T are related by the empirical expression proposed by Williams-Landel-Ferry (WLF) (*Williams et al.*, *1955*):

$$Log(a_T) = \frac{-k_1(T-T_S)}{k_2+T-T_S} \qquad [2.5]$$

where:

a_T	shift factor function of temperature,
k_1 and k_2	material constants,
T_S	reference temperature,
T	actual temperature.

Alternatively, Arrhenius law can be used to determine shift factors for asphalt concrete (*Anderson et al., 1991; Lytton et al., 1993; Marasteanu and Anderson, 1996; Di Benedetto et al., 2001; Pellinen and Witczak, 2002*). By expressing creep compliance, relaxation modulus or complex modulus in term of reduced time ξ and setting a reference temperature T_S, it is possible to construct a "master curve" that represents the variation of these parameters over different temperature regimes. When developing performance prediction models (*Wang et al., 2006; Di Benedetto et al., 2007; Masad et al., 2007*), the above considerations and the need for reliable yet simple experimental methods to determine constitutive relations for asphalt mixtures are of utmost importance.

2.2. The Use of RAP and Shingles in Asphalt Pavement

A lot of work has been done in the past to investigate the use of Reclaimed Asphalt Pavement (RAP) and Reclaimed Asphalt Shingles for asphalt pavement applications. Since an exhaustive review is beyond the scope of this thesis the next two subsections will present some of the research and work that are considered significant for the purpose of this dissertation.

2.2.1. RAP

Reclaimed asphalt pavement (RAP) has been used in the United States for more than 25 years because of the environmental benefits and costs reduction. Various percentages of RAP content are allowed by current specifications depending on the traffic level. In Minnesota, the Department of Transportation *Specification 2350/2360* (*2008*) allows up to 40% RAP based on the traffic level and binder grade. These values are based on field experience of the performance of asphalt pavements built with RAP. However, there is very little information available about the effect of RAP on the mechanical properties of the resulting asphalt mixtures.

In some previous works performed mainly in the 90's (*Little et al., 1981; Jung and Vinson, 1993; Jackson and Vinson, 1996; Zubeck and Vinson, 1996; Zubeck et al., 1996; McDaniel and Anderson, 2002*) it was shown that the structural performance of asphalt mixtures containing RAP is in general not very different compared to that of a conventional virgin asphalt mixtures. In these studies it was also showed that the properties of the mixtures containing RAP are much influenced mainly by the aged RAP binder properties and the amount of RAP in the mixture. The increase in viscosity due to aging generally translates into an increase in modulus of the asphalt, which is beneficial for the resistance to permanent deformation at high service temperatures; however, it also implies an increase in stiffness and brittleness at intermediate and low service temperatures, resulting in reduced resistance to fatigue and low temperature cracking.

Brown (*1984*) and *Meyers et al.* (*1983*) showed that blending charts based on the performance grade (PG) specification limits can be developed to determine the maximum and minimum amount of virgin or RAP asphalt binder and to select a recycling agent to produce a specific PG binder. *Kandhal and Foo* (*1997*) performed a study at National Center for Asphalt Technology to develop design procedures for asphalt mixtures containing RAP. In this study, a graphical method was developed, with a focus on arriving at the proper binder physical properties by balancing RAP amount with adjustments to the base binder grade. *Lee et al.* (*1999*) evaluated RAP effect on binder complex modulus using Rolling Thin Film Oven (RTFO) aged binder blends produced with tank binder and binder samples recovered from three types of RAP materials. It was showed that adding increased amount of RAP binder to the RTFO aged binder the complex modulus drastically increases. With a change from 0% to 100% RAP binder, the increase in complex modulus was found to exceed a factor of ten in many instances.

Kandhal et al. (*1995*) in a previous work showed that the dynamic modulus of asphalt mixtures is related to the major distress modes, such as permanent deformation, fatigue, and low temperature cracking. Dynamic modulus was also used by *Li et al*. (*2008*) to investigate the effect of different amount of RAP and different sources on the properties of asphalt mixtures. In the same study the low temperature properties of the same recycled mixtures were investigated with semicircular bend (SCB) fracture testing. Experimental results indicated that asphalt mixtures containing RAP have higher dynamic modulus values than the control mixtures containing no RAP. Experimental data also show that the RAP source is not a significant factor for the dynamic modulus at low temperatures, although it significantly affects dynamic modulus values at high temperatures. In addition to test temperature, the RAP percentage was found to significantly affect the SCB fracture resistance of mixtures.

A modeling based approach to develop a test to determine the presence and amount of RAP in post-production mixtures as a practical quality assurance tool was developed by *Buttlar and Dave* (*2005*). *Zofka et al*., (*2005*) investigated the low temperature properties of the asphalt binder present in mixtures containing RAP through an experimental work performed on

Bending Beam Rheometer (BBR) (*AASHTO T 313-02*) asphalt mixtures beams coupled with a micromechanical modeling and back calculation procedure (*Christensen et al., 2003*).

Alternative approaches to the study of Reclaimed Asphalt Pavement are also available in literature. Among those of significant relevance are the works of *Karlsson and Isacssons* (*2002* and *2003*) based on the diffusion of virgin and aged asphalt binder and on the use of FTIR-ATR (Fourier Transform Infrared Spectroscopy using Attenuated Total Reflectance).

2.2.2. Shingles

Two types of asphalt shingles are mainly available in the roofing market: organic and fiberglass. They are composed of four materials: asphalt binder, a paper backing, mineral filler and sand-sized aggregates.

ASTM D 225-07 (*2007*) standard on organic-backed shingles specifies that organic fibers should be primarily used to produce the felt. Felt is first impregnated with hot saturant asphalt, then coated on both sides with more asphalt, and finally surfaced with mineral granules. The saturant asphalt and the coating asphalt need not be identical; each has a different mechanical role within the shingle.

ASTM D 3462/3462 -10a (*2010*) presents the specification for glass felt shingles. These shingles must be comprised of one or more thicknesses of glass felt, which is defined as a thin porous sheet predominantly comprised of glass fibers containing a substantially water-insoluble binding agent. If more than one layer is used, they must be stuck to each other with a continuous layer of asphaltic material. The felt is first impregnated with saturant asphalt and then the single or laminated felt is coated on the outside with coating asphalt and granular material. This specification allows both the saturant and coating asphalts to be compounded with fibers as well as mineral stabilizer. However, since specifications in the past allowed asbestos as a backing, some glass shingles cannot be recycled and used in asphalt pavements anymore (*Newcomb et al*., *1993*).

The asphalt cement in roofing shingles is a mixture of two different asphalts, saturant and coating. Both are considerably harder than asphalt binders typically used in paving applications, with penetration values at 25°C ranging from approximately 20 dmm to about 70 dmm as opposed to typical values of 50 dmm to 300 dmm for paving asphalts; this is to prevent asphalt flow at higher temperature during the warmer season. Granular material provides the largest component (by weight) of asphalt roofing shingles. Different aggregates type are used for the production: ceramic granules, headlap granules, backsurfacer sand, and asphalt stabilizer. The most significant in terms of shingle performance are the ceramic-coated colored granules. These are small crushed rock particles coated with ceramic metal oxide, Another granular component is headlap granules. These are comprised essentially of coal slag ground to roughly the same size as the ceramic particles. They make up the largest single portion, by weight, of granular material within the shingle. Backsurfacer sand, the smallest granular contribution by weight, is washed, natural sand added in small amounts to keep the shingles from sticking together while packaged. Finally, powdered limestone is added as an asphalt stabilizer. Since shingles are manufactured to high quality standards, these granular materials are high quality aggregates typically found in paving mixtures (*Newcomb et al*., *1993*).

The use of recycled asphalt shingles in hot-mix asphalt (HMA) has been a developing technology for more than two decades showing increased interest by both construction contractors and government agencies. Several research studies on the use of recycled asphalt shingles in HMA mixtures over the past fifteen years were supported by the state of Minnesota.

Turgeon (*1991*) investigated the use of recycled tire rubber and shingle scrap in asphalt mixtures. The ground shingle scrap significantly reduced asphalt demand and increased Marshall stability, however testing on core samples showed low density, low tensile strength and high air voids than the reference control mixture. Furthermore mixtures containing shingles had lower recovered asphalt penetrations.

The influence of recycled asphalt shingles on HMA mixture properties was investigated by *Newcomb et al*. (*1993*). In that study it was found that up to 5% manufacturer waste scrap shingles (MWSS) could be used in HMA mixtures with a minimum impact on the mixture properties. However a noticeable softening of the mixture, which may result in a detrimental effect to the pavement performance, was detected for 7.5% asphalt shingle content. Softening was also seen using indirect tensile tests on mixtures containing 10% shingle showing that mixture stiffness was adversely decreased when the shingle content exceeded 5% by weight of the aggregate, which led to a general acceptance limit of 5% shingle content. In the same study the use of tear-off scrap shingles (TOSS) was also investigated; the presence of TOSS resulted in an embrittlement or stiffening of the mixture that is not desirable for low temperature cracking resistance properties. Moisture sensitivity was also investigated by *Newcomb et al*. (*1993*). The resilient modulus and tensile strength of the mixtures were tested before and after the sample were subjected to partial saturation and freezing for twenty four hours. The reduction of either tensile strength or modulus was used as an indicator of moisture induced damage. It was found that the use of MWSS did not significantly change the moisture susceptibility of the mixture, but TOSS did. Low temperature cracking was evaluated by *Newcomb et al*. (*1993*) using an indirect tensile test (IDT) (*AASHTO T 322-03*). Tensile strengths at low temperatures were shown to decrease with increasing shingle content; the mixtures made with the TOSS showed a decrease in strain capacity with increased shingle content, implying that this material will be more brittle at low temperatures.

Janisch and Turgeon (*1996*) performed a study on three test sections in Minnesota. From the testing results no significant difference was found between the laboratory data mixtures containing shingle and those without shingle. It was also found that the extracted asphalt binder in the shingle mixtures was stiffer as expected since the grade of asphalt used in shingle manufacturing is stiffer than the asphalt typically used in pavements.

Button et al. (*1996*) performed an experimental study to measure the strength, stability, creep characteristics, and water susceptibility of modified and unmodified asphalt mixtures including both manufacturing waste and consumer (tear off) waste shingles. Two different types of hot mix asphalt, dense-graded and coarse matrix-high binder (CMHB) mixtures were studied. It was found that the addition of 5% to 10% roofing waste into the dense-graded and CMHB mixtures was detrimental to the engineering properties of the mixtures investigated. However, it appeared that quantities of roofing shingles just under 5% would be satisfactory in these mixtures. Mixing and compaction temperatures of HMA was also evaluated showing that an increase of about 10 to 20°C may be required both in the laboratory and in the field to accommodate the relatively stiffer roofing-modified mixtures.

Long-term performance evaluation of hot mixed asphalt (HMA) pavements containing post-manufacturing roofing shingle material was performed by *Hanson et al*. (*1997*). The plan of study included blending aggregates from North Carolina using three different gradations with one source of shingles at three different concentration rates: 0%, 5% and 10% by weight of the aggregates. The authors found that the use of post-manufacturing roofing shingle material in HMA can produce a pavement equal to or better than a conventional HMA, especially where rutting is a principal concern.

The Georgia Department of Transportation (GDOT) has experimented with the recycling of roofing shingles in HMAC by constructing two test sections in 1994 and 1995 (*Watson et al., 1998*). From the experimental phase it was found that although viscosity of recovered asphalt from the modified test sections was slightly higher than for the virgin control sections, there does not appear to be a negative effect on performance. Due to the warm climate thermal cracking was not considered to be a problem while the increased stiffness is actually beneficial in reducing rutting susceptibility.

McGraw et al., (*2007*) investigated the use of both TOSS and MWSS combined with traditional RAP materials. Three different mixtures were prepared with the same PG 58-28: 20% RAP, 15% RAP plus 5% TOSS, and 15% RAP plus 5% MWSS. The results indicated that the two types of shingles performed differently. Both MWSS and TOSS decreased the stiffness of the mixtures. However the presence of MWSS did not affect the strength of both mixtures and extracted binders while TOSS lowered the strength of the binder significantly at the higher test temperature and increased the binder's critical temperature. The addition of RAS (Recycled Asphalt Shingles) lowered the temperature susceptibility of the binders.

Bonaquist (*2007*) proposed a method based on the Asphalt Mixture Performance Test to evaluate the effective stiffness of RAP and RAS mixtures and the amount of binder mixing taken place in those types of mixtures. Binder properties were obtained from mixture master curve data compared to recovered binder properties. The amount of binder mixing was obtained from the difference in the master curves.

Recently a study a Mn/DOT (Minnesota Department of Transportation) investigated the effect of asphalt binder grade and content, RAP source and content and different shingle sources and proportions on HMA mixture properties with the goal of giving recommendations toward a comprehensive shingle specification, including the option of using TOSS (*Johnson et al., 2010*). Currently the 2009 Minnesota Department of Transportation (Mn/DOT) specifications allow a 5% MWSS replacement for the allowable recycled asphalt pavement (RAP) in HMA pavement mixtures. Although there have been pilot projects that have used TOSS with and without RAP, there is no provision for the use of TOSS in the current specifications (*Combined 2350/2360 Mn/DOT specification, 2008*). Both laboratory and field performance were evaluated on mixtures that incorporated RAP and recycled asphalt shingles (RAS) which included both TOSS and MWSS; both asphalt binder and mixture properties were tested. Recovered asphalt binder from HMA and RAS were tested for high and low temperature properties. The mixtures appeared to be more homogenous with the finer ground TOSS, where TOSS tended to demand slightly more asphalt binder compared to MWSS. The asphalt binder contained in TOSS is typically stiffer than that contained in MWSS. The differences in binder stiffness resulted in high mixture modulus for the TOSS mixes. Decreasing the shingle content from 5% to 3% minimized the observable differences between the MWSS and TOSS shingle sources.

2.3. Microstructural Information

2.3.1. Volume Fraction Information

An extensive literature is available for the evaluation of the effective properties K_e of composite materials based on the material properties of the components K_i. Among those properties, volume fraction is the most important and simplest microstructural information. The effective properties of a two-phase material can be estimated using the simple mixture laws given by:

$$K_e = K_1\phi_1 + K_2\phi_2 \qquad \text{(arithmetic average)} \qquad [2.6]$$

$$K_e = \frac{K_1 K_2}{K_1\phi_2 + K_2\phi_1} \qquad \text{(harmonic average)} \qquad [2.7]$$

where:

K_e effective properties of the material

K_1 , K_2 properties of phase 1 and 2,

ϕ_1, ϕ_2 volume fractions of phase 1 and 2 $\left(\phi_1 = 1 - \phi_2\right)$.

Experimental results have shown that [2.6] tends to overestimate the effective property, whereas [2.7] underestimate the effective property (*Buttlar and Roque, 1996*). In the case of asphalt mixture when particles are dispersed in a matrix it is crucial to know if the particles and matrix phases are connected or not. *Hashin and Shtrikman (1963)* proposed the following bounds [2.8] and [2.9] for the bulk and shear modulus of two phase isotropic composite taking into account the connectivity information of the phases while using volume fraction only:

$$K_c^L = K_1 + \frac{\phi_2}{\dfrac{1}{K_2 - K_1} + \dfrac{3\phi_1}{3K_1 + 4G_1}} \qquad K_c^U = K_2 + \frac{\phi_1}{\dfrac{1}{K_1 - K_2} + \dfrac{3\phi_2}{3K_2 + 4G_2}} \qquad [2.8]$$

$$G_c^L = G_1 + \frac{\phi_2}{\dfrac{1}{G_2 - G_1} + \dfrac{6\phi_1(K_1 + 2G_1)}{5G_1(3K_1 + 4G_1)}} \qquad G_c^U = G_1 + \frac{\phi_1}{\dfrac{1}{G_2 - G_1} + \dfrac{6\phi_2(K_2 + 2G_2)}{5G_2(3K_2 + 4G_2)}} \qquad [2.9]$$

where:

$K_1 < K_2 \quad G_1 < G_2$,	
K_c^L, K_c^U	lower and upper bound on bulk modulus,
G_c^L, G_c^U	lower and upper bound on shear modulus,
ϕ_1, ϕ_2	volume fractions of phase 1 and 2 $\left(\phi_1 = 1 - \phi_2\right)$.

The prediction given by [2.8] and [2.9] were in good agreement with experimental results for materials with no significant clustering of particles.

Self Consistent Method proposed by *Hill* (*1965*) provides an alternative approximation for the bulk properties of two-phase composite materials. In this model a typical particle is inserted in a matrix with unknown effective mechanical properties. However when the contrast between the phases is moderate or high, as in the case of asphalt mixtures, Self Consistent Method gives poor predictions (*Torquato, 1998*). *Torquato* (*2000*) also showed that Self Consistent Methods works properly only when the material has a type of topological symmetry that is not a property of asphalt mixture. The self consistent approximations for three-dimensional two-phase composite proposed in *Hill (1965)* for the bulk and shear modulus are expressed as:

$$\phi_1\left[\frac{K_e - K_1}{4G_e/3 + K_1}\right] + \phi_2\left[\frac{K_e - K_2}{4G_e/3 + K_2}\right] = 0 \qquad [2.10]$$

$$\phi_1\left[\frac{G_e - G_1}{G_e\left(9K_e + 8G_e\right)/\left(6K_e + 12G_e\right) + G_1}\right] + \phi_2\left[\frac{G_e - G_2}{G_e\left(9K_e + 8G_e\right)/\left(6K_e + 12G_e\right) + G_2}\right] = 0 \qquad [2.11]$$

where:

K_e and G_e	effective bulk and shear modulus,
K_i, G_i and ϕ_i	bulk, shear modulus and volume fraction of the i^{th} phase.

2.3.2. *n*-point Correlation Functions

In addition to the volume fraction, information on the spatial distribution of the microcomponents is also required when modeling the effective properties of more complex microstructures. In the case of random heterogeneous materials, higher-order microstructural information is fundamental; *n*-point correlation functions, surface correlation function, lineal path function, chord-length density function, pore-size functions are some of the most used. Due to its relative simplicity compared to the others, *n*-point and especially 2- and 3-point correlation functions will be considered in this dissertation. The next paragraphs provide a brief summary of the definitions and properties of the correlation functions, while detailed definitions can be found in the works of *Beran* (*1968*), *Corson* (*1974*), *Berryman* (*1985*), *Torquato* (*2002*), and *Jiao et al. (2007*).

The *n*-point spatial correlation function measures the probability of finding *n* points all lying on the space occupied by one of the phases of the heterogeneous material (*Berryman 1985*). In the case of a two-phase heterogeneous material the 1-point correlation function is the probability that any point lies on phase 1; this correspond to the volumetric fraction of phase 1. The 2-point correlation function is the probability that two points separated by a specific distance are located both in the same phase (for example phase 1). The 3-point correlation function is the probability that all the vertices of a triangle in are all located in the same phase (phase 1). Figure 2.1 provides a schematic interpretation of the 1-, 2-, and 3-point correlation functions.

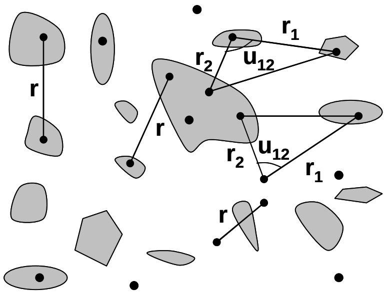

***S_1* -** probability that a randomly selected point in material belong to phase of interest, volumetric fraction of phase

***S_2* -** probability that two points separated distance *r* are located both in phase of interest

***S_3* -** probability of finding all vertices of triangle defined by r_1, r_2 and u_{12} in phase of interest

Figure 2.1. Schematic of sampling for S_1, S_2 and S_3 correlation functions calculation- *Velasquez* (*2009*)

Torquato (2002) defines the *n*-point correlation functions of a two-phase random heterogeneous material in *d*-dimensional Euclidian space R^d as:

$$S_n^{(i)}(x_1, x_2, x_3, ..., x_n) = \left\langle I^{(i)}(x_1) I^{(i)}(x_2) I^{(i)}(x_3) \cdots I^{(i)}(x_n) \right\rangle \qquad [2.12]$$

where:

$\langle\ \rangle$ ensemble averaging,

$I^{(i)}(x)$ indicator function defined as: $I^{(i)}(x) = \begin{cases} 1, & x \in V_i \\ 0, & x \in \overline{V_i} \end{cases}$ [2.13]

$V_i \in R^d$	volume occupied by the i^{th} phase,
$\overline{V_i} \in R^d$	volume occupied by the other phase.

The n-point correlation function is translationally invariant for a statistically homogeneous material (Figure 2.1).

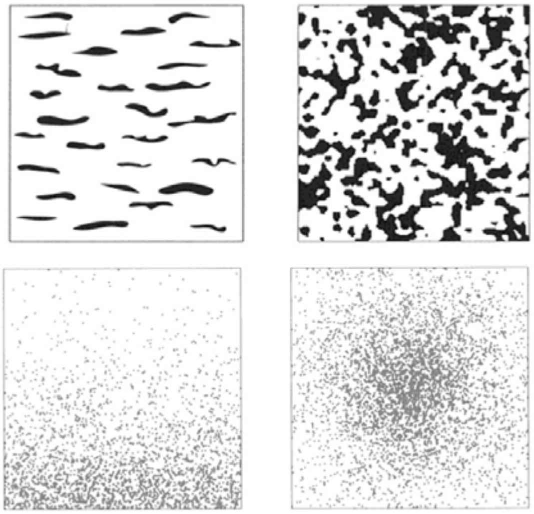

Figure 2.2. Examples of statistically homogeneous and inhomogeneous two-phase materials - *Torquato* (*2002*)

It turns out that the function depends on the differences in the coordinate values of the x_i vectors but not on their absolute position (*Torquato 2002*) meaning that the origin of the coordinate system is not important. The function can be expressed as:

$$S_n^{(i)}(x_1, x_2, x_3, ..., x_n) = S_n^{(i)}(x_{12}, x_{13}, x_{14}, ..., x_{1n}) \qquad \text{for all } n \geqslant 1 \qquad [2.14]$$

where:

$x_{ij} = x_j - x_i$	difference between the two vectors x_i and x_j,
x_1	reference vector selected.

The 1-point correlation represents the volume fraction ϕ_i of the i^{th} phase, is constant and it is the probability that a randomly selected point in the material belongs to i^{th} phase:

$$S_1^{(i)} = \left\langle I^{(i)}(x) \right\rangle = \phi_i \qquad [2.15]$$

The 2-point correlation function $S_2^{(i)}(x_1, x_2)$ is defined as (*Torquato 2002*):

$$S_2^{(i)}(x_1,x_2) = \left\langle I^{(i)}(x_1)I^{(i)}(x_2)\right\rangle \qquad [2.16]$$

In the case of a statistically homogeneous material, the 2-point correlation can be expressed as:

$$S_2^{(i)}(x_1,x_2) = S_2^{(i)}(x_{12}) = S_2^{(i)}(r) = \left\langle I^{(i)}(x_1)I^{(i)}(x_1+r)\right\rangle \qquad [2.17]$$

where:

$r = x_{12} = x_2 - x_1$.

In a more general case, when considering statistically homogeneous and isotropic materials, the 2-point correlation function does not depend on the orientation of the vector r but only on its magnitude (*Torquato, 2002*). From equation [2.13] it follows that:

$$\left(I^{(i)}(x)\right)^2 = I^{(i)}(x) \qquad [2.18]$$

and substituting [2.18] into [2.16] it can be shown that for r=0:

$$S_2^{(i)}(0) = \left\langle I^{(i)}(x_1)I^{(i)}(x_1)\right\rangle = \left\langle I^{(i)}(x_1)\right\rangle = S_1^{(i)} = \phi_i \qquad [2.19]$$

When microstructure of the material does not present long range order it can be written:

$$\lim_{r\to\infty} S_2^{(i)}(r) = \phi_i^2 \qquad [2.20]$$

Therefore, the initial value of the 2-point correlation functions is ϕ_i (r = 0) and for very large r ($r\to\infty$) it reaches the asymptotic limit of ϕ_i^2.

The 3-point correlation function for a heterogeneous material can be defined according to equation [2.12] as:

$$S_3^{(i)}(x_1,x_2,x_3) = \left\langle I^{(i)}(x_1)I^{(i)}(x_2)I^{(i)}(x_3)\right\rangle \qquad [2.21]$$

In the case of a translationally invariant isotropic material, the 3-point correlation function can be expressed as:

$$S_3^{(i)}(r_1,r_2) = S_3^{(i)}(|r_1|,|r_2|,u_{12}) \qquad [2.22]$$

where:

$r_1 = x_2 - x_1$	vector,
$r_2 = x_3 - x_1$	vector, and
u_{12}	cosine of the angle θ_{12} between vectors r_1 and r_2:

$$u_{12} = \cos\theta_{12} = \frac{r_1 \cdot r_2}{|r_1||r_2|} \qquad [2.23]$$

Thus for a statistically homogeneous and isotropic material, the 3-point correlation function depends on three variables that define a triangle: the magnitudes of two vectors r_1 and r_2, and the angle θ_{12} between these two vectors. The properties of the 3-point correlation function can be written as (*Berryman 1985*):

$$\lim_{|r_1|\to\infty} S_3^{(i)}(|r_1|,|r_2|,u_{12}) = S_2^{(i)}(|r_2|) \qquad [2.24]$$

$$\lim_{|r_1|,|r_2|\to\infty} S_3^{(i)}(|r_1|,|r_2|,u_{12}) = \phi_i^3 \qquad [2.25]$$

Assuming that there is no long-range order in the material then

$$\lim_{|r_1|\to\infty,|r_2|=fixed} S_3^{(i)}(|r_1|,|r_2|,u_{12}) = \phi_i \, S_2^{(i)}(|r_2|) \qquad [2.26]$$

The following bounds apply to the 3-point correlation function (*Berryman 1985*):

$$S_3^{(i)}(|r_1|,|r_2|,u_{12}) \le \min\left\lfloor S_2^{(i)}(|r_1|)S_2^{(i)}(|r_2|)S_2^{(i)}(|r_3|)\right\rfloor \le \max\left\lfloor S_2^{(i)}(|r_1|)S_2^{(i)}(|r_2|)S_2^{(i)}(|r_3|)\right\rfloor \le \phi_i \qquad [2.27]$$

where:

$$|r_3| = \sqrt{|r_1|^2 + |r_2|^2 - 2|r_1||r_2|u_{12}} \qquad [2.28]$$

The calculation of all the *n*-point correlation functions is required when a complete description of the microstructure of a random heterogeneous material as asphalt mixture has to be assessed. However, this computation may become particularly complex both analytically and numerically (*Torquato 2002*). Alternative microstructural descriptors are available in literature: the 2-point cluster function, for example, presents a more complex form but a lower order correlation. It is defined as the probability that two randomly selected points are located in the same cluster of the i^{th} phase (*Torquato 2002*). Lineal path function, which is the probability that an entire line segment is located in the i^{th} phase, provides a further option when describing the microstructure of a material from a statistical point of view.

2.4 Composite Materials Models for Asphalt Mixture Characterization

2.4.1. Micromechanical Models

At the macroscopic level composite materials are made of two or more phases. Generally one phase acts as a continuous matrix, while the others act as inclusion or reinforcement. The advantage of mixing two or more materials is given by the possibility of designing a new material with specific properties not achievable by a single phase. However, in order to predict the performance of the new composite both the properties of the constituents and high order microstructural information are needed. Several types of models, which provide solution for the estimation of the microstructural correlation functions for composite materials, are available in literature (*Torquato, 2002*). The effective response $\boldsymbol{K_{eff}}$ of a composite material can be written as:

$$\mathbf{K_{eff}} = f(\mathbf{K_i}, \phi_i, \mathbf{\Omega}) \quad [2.29]$$

where $\boldsymbol{K_i}$ and ϕ_i are the intrinsic properties of the i^{th} phase and its corresponding volumetric fraction, and $\mathbf{\Omega}$ is a parameter that gives the higher-order microstructural information.

Asphalt mixtures can be classified as particulate composites that contain aggregate particles of various sizes and shapes randomly distributed in matrix of asphalt binder. In several research studies, asphalt mixtures are considered as two-phase materials (binder or mastic and aggregate) (*Papagiannakis et al., 2002*; *Masad and Somadevan, 2002*; *Yue et al., 2003; Abbas et al., 2004*). Asphalt mixture was also evaluated as a three-phase material (large aggregate, small aggregate and mastic) with a two step method by *Buttlar and Roque* (*1996*)*, Wang et al.* (*2004*) and *Li and Metcalf* (*2005*).

For example the effective properties of asphalt mixture at low temperature were evaluated by *Buttlar and Roque* (*1996*) using classical micromechanical models. Due to the low order microstructural information (volume fractions) used in the models, the response was significantly underpredicted.

The Generalized Self-Consistent Scheme (GSCS) model was implemented by *Buttlar et al.* (*1999*) to model asphalt mastic. The predictions of the GSCS model was compared to the test results of specimens with different concentrations of particles and investigating three filler reinforcement regimes: volume filling, physiochemical effects, and particle interaction. The authors concluded that the physiochemical interaction between the particles and the binder is mainly responsible for the reinforcement effect of the particles on the mastics. The GSCS is a three phase model and represents a special case of the composite spheres model proposed by *Hashin* (*Hashin and Shtrikman, 1963*). This model consists of an infinite matrix of homogeneous material where a spherical inclusion is embedded in and does not take into account interaction between particles. Based on finite element simulations and mastic micromechanical modeling *Masad and Somadevan* (*2002*) found that the average strain in the asphalt mastic is three to five times higher than the strain in the mixture The authors also found that the mastic can be three to ten times stiffer than the binder.

Hashin-Shtrikman (H-S) bounds [2.8] and [2.9] were used by *Kim and Little* (*2004*) to investigate the stiffening effect of two fillers. Based on experimental results and micromechanical analysis it was found that H-S model provides good prediction only for low volume fraction of the filler.

Buttlar and Dave (*2005*) developed blending charts for Recycled Asphalt Pavements (RAP) based on micromechanical modeling. Simple mixture laws ([2.6] and [2.7]), first order models and second order models ([2.8] and [2.9]) were used to obtain the effective properties of a two-phase material and to construct the charts.

2.4.2. Higher Order Micromechanical Models

Zofka et al. (*2006*) compared different micromechanical models with finite element simulations and experimental results of asphalt concrete tested in 3-point bending at low temperatures. The finite element simulation was closely matched by the *Milton* (*1981*) bounds model. Milton's simplified bounds are described in the following equations [2.30]:

$$K_e^U = \langle K \rangle - \frac{3\phi_1\phi_2\left(K_1 - K_2\right)^2}{3\langle \overline{K} \rangle + 4\langle G \rangle_\zeta} \qquad K_e^L = \left[\left\langle \frac{1}{K} \right\rangle - \frac{4\phi_1\phi_2\left(\frac{1}{K_1} - \frac{1}{K_2}\right)^2}{4\left\langle \frac{1}{\overline{K}} \right\rangle + 3\left\langle \frac{1}{G} \right\rangle_\zeta} \right]^{-1} \qquad [2.30]$$

where:

$$\left\langle \frac{1}{K} \right\rangle = \frac{\phi_1}{K_1} + \frac{\phi_2}{K_2}$$

$$\langle K \rangle = \phi_1 K_1 + \phi_2 K_2$$

$$\left\langle \frac{1}{\overline{K}} \right\rangle = \frac{\phi_1}{K_2} + \frac{\phi_2}{K_1}$$

$$\langle \overline{K} \rangle = \phi_1 K_2 + \phi_2 K_1$$

$$\left\langle \frac{1}{G} \right\rangle_\zeta = \frac{\zeta_1}{G_1} + \frac{\zeta_2}{G_2}$$

$$\langle G \rangle_\zeta = \zeta_1 G_1 + \zeta_2 G_2$$

$$\zeta_1 = 1 - \zeta_2$$

$$P_2(u) = \frac{1}{2}(3u^2 - 1) \text{ (Legendre polynomial)}$$

Milton's number ζ_1 (geometry parameter) can be calculated with:

$$\zeta_1 = \lim_{\Delta \to 0} \lim_{\beta \to \infty} \frac{9}{2\phi_1\phi_2} \int_{\Delta}^{\beta} dr \int_{\Delta}^{\beta} ds \int_{-1}^{1} \frac{S_3^{(1)}(r,s,u)}{rs} P_2(u) du \qquad [2.31]$$

where $S_3^{(1)}(r,s,u)$ is the 3-point correlation function of the material. *Berryman* (*1985*), *Torquato* (*1991*), and *Zofka* (*2007*) proposed approximate expressions for ζ_1 as a function of the volume fractions. *Velasquez* (*2009*), *Velasquez et al.* (*2010*) also investigated this model to predict the experimental data obtained form 3-point bending test on asphalt mixtures at low temperature showing that Milton bounds are wide and poor predictors of the experimental results (Figure 2.3).

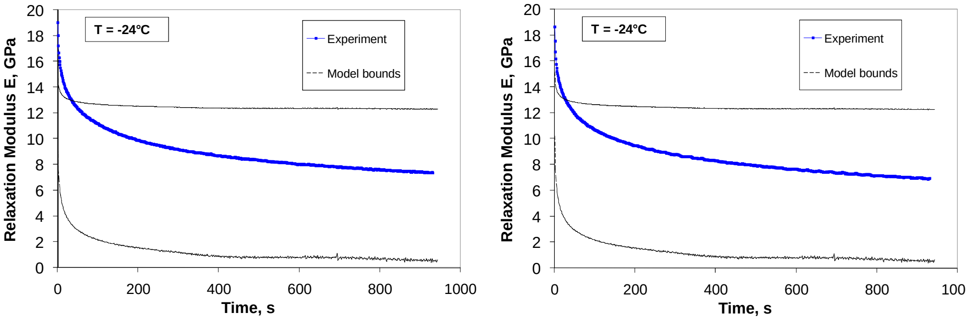

Figure 2.3. Milton bounds for granite and limestone mixtures – *Velasquez et al.* (*2010*)

Torquato (*1998*) proposed a three dimensional isotropic two-phase model ([2.32] and [2.33]). It presents the geometry parameters ζ_2 and η_2 similar to [2.31], but including, the 2-point correlation function as part of the integral. To ensure convergence of the integral, the 2-point correlation function is included in the integrand of [2.36] and [2.37]. The effective bulk and shear modulus can be expressed as:

$$\frac{K_e}{K_1} = \frac{1 + \frac{4G_1}{3K_1}\kappa\phi_2 - \frac{10G_1}{3(K_1 + 2G_1)}\kappa\mu\phi_1\zeta_2}{1 - \kappa\phi_2 - \frac{10G_1}{3(K_1 + 2G_1)}\kappa\mu\phi_1\zeta_2} \qquad [2.32]$$

$$\frac{G_e}{G_1}=\frac{1+\frac{9K_1+8G_1}{6(K_1+2G_1)}\mu\phi_2-\frac{2\kappa\mu G_1}{3(K_1+2G_1)}\phi_1\zeta_2-\frac{\mu^2}{6}\left\{\left[\frac{3K_1+G_1}{K_1+2G_1}\right]^2\phi_1\eta_2+5G_1\left[\frac{2K_1+3G_1}{(K_1+2G_1)^2}\right]\phi_1\zeta_2\right\}}{1-\mu\phi_2-\frac{2\kappa\mu G_1}{3(K_1+2G_1)}\phi_1\zeta_2-\frac{\mu^2}{6}\left\{\left[\frac{3K_1+G_1}{K_1+2G_1}\right]^2\phi_1\eta_2+5G_1\left[\frac{2K_1+3G_1}{(K_1+2G_1)^2}\right]\phi_1\zeta_2\right\}} \quad [2.33]$$

where:

$$\kappa\equiv\kappa_{21}=\frac{K_2-K_1}{K_2+\frac{4G_1}{3}} \quad [2.34]$$

$$\mu\equiv\mu_{21}=\frac{G_2-G_1}{G_2+G_1\left[\frac{9K_1+8G_1}{6(K_1+2G_1)}\right]} \quad [2.35]$$

with phase one and two corresponding to the matrix and dispersions, respectively. The three point parameters ζ_2 and η_2 are defined by the following integrals:

$$\zeta_2=\frac{9}{2\phi_1\phi_2}\int_0^\infty\frac{dr}{r}\int_0^\infty\frac{ds}{s}\int_{-1}^{1}\left[S_3^{(2)}(r,s,u)-\frac{S_2^{(2)}(r)S_2^{(2)}(s)}{\phi_2}\right]P_2(u)du \quad [2.36]$$

$$\eta_2=\frac{5\zeta_2}{21}+\frac{150}{7\phi_1\phi_2}\int_0^\infty\frac{dr}{r}\int_0^\infty\frac{ds}{s}\int_{-1}^{1}\left[S_3^{(2)}(r,s,u)-\frac{S_2^{(2)}(r)S_2^{(2)}(s)}{\phi_2}\right]P_4(u)du \quad [2.37]$$

where, P_2 and P_4 are the Legendre polynomials of order 2 and 4, respectively. The expressions for the Torquato model [2.32] and [2.33] were obtained by truncating an exact series expansion for the effective elastic stiffness tensor of two phase materials. For this model there is no assumption regarding the geometry of the microstructure but it requires statistical homogeneity (*Torquato, 1998*). Torquato model was applied by *Velasquez* (*2009*) and *Velasquez et al.* (*2010*) to the prediction of the asphalt mixture properties obtained form 3-point bending test. Torquato model resulted to be a poor predictor since the estimated relaxation did not match the experimental data. The high contrast between the stiffness of the phases and the inability to simulate contacts between particles are the main reasons why this model fails.

2.4.3 Semi-empirical Model

A semi-empirical model, based on Hirsch model (*Hirsch, 1962*) was proposed by *Christensen et al.* (*2003*) to estimate the extensional and shear dynamic modulus. The effective response is obtained assembling the elements of the mixture in parallel and in series (Figure 2.4).

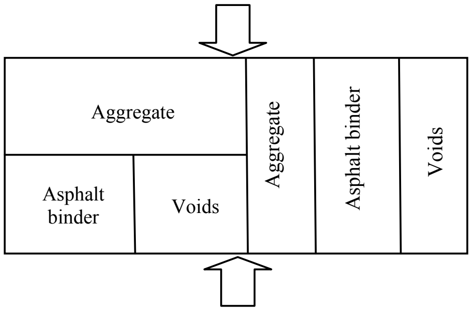

Figure 2.4. Semi-empirical model proposed by *Christensen et al.* (*2003)*

The empirical factor *Pc* determines the amount of parallel or series elements in the mixtures. The general equation for this semi-empirical model is:

$$E_{mix} = Pc\left[E_{agg}V_{agg} + E_{binder}V_{binder}\right] + (1-Pc)\left[\frac{V_{agg}}{E_{agg}} + \frac{(1-V_{agg})^2}{E_{binder}V_{binder}}\right]^{-1} \quad [2.38]$$

where:

E_{mix}	effective modulus of the mixture,
E_{agg}, V_{agg}	modulus and volume fraction of the aggregate,
E_{binder}, V_{binder}	modulus and volume fraction of binder, and
Pc	contact volume is an empirical factor defined as:

$$Pc = \frac{\left(P_0 + \frac{VFA \cdot E_{binder}}{VMA}\right)^{P_1}}{P_2 + \left(\frac{VFA \cdot E_{binder}}{VMA}\right)^{P_1}} \quad [2.39]$$

where:

VFA	voids filled with asphalt binder (%),
VMA	voids between mineral aggregate (%),and
P_0, P_1, P_2	fitting parameters.

Zofka et al. (*2005*) evaluated the use of Hirsch model (*Hirsch, 1962*) proposed by Christensen (*Christensen et al., 2003*) to predict the BBR mixture stiffness from the properties of the binder. The asphalt binders from the mixtures prepared in this study were extracted and tested in the BBR to obtain the stiffness and the m-values. The experimentally determined binder stiffness values were input in equations [2.38] and [2.39] to predict the mixture stiffness based on the volumetric properties measured from the gyratory specimens. Since the predicted values were always higher than the measured stiffness values, equation [2.38] was modified. The aggregate modulus, E_{agg}, which is equal to 4,200,000 psi, was replaced with a value of 2,750,000 psi based on these results and on numerical manipulation. In order to improve the prediction of the laboratory mixture results, a further modification of the Hirsch model was proposed by *Zofka* (*2007*) introducing a new expression for the parameter *Pc* [2.40]:

$$P_c = 0.1 \ln\left(\frac{E_{binder}}{a}\right) + 0.609 \qquad [2.40]$$

where:

E_{binder}	relaxation modulus of the binder in GPa, and
a	constant equal to 1 GPa.

The original Hirsch model consistently overpredicted the measured E_{mix} values while with the new expression for *Pc* the model predicted measured E_{mix} relatively well. Hirsch model was used by *Velasquez* (*2009*) and *Velasquez et al.* (*2010*) to estimate the asphalt mixture modulus obtained from BBR testing. It was found that Hirsch model predicts fairly well the relaxation modulus of the majority of the mixtures investigated. *Cannone Falchetto* (*2010*) and *Cannone Falchetto et al*., (*2011*) applied the Hirsch model to predicts the asphalt mixtures creep stiffness starting from the experimental data obtained from binder testing on three point bending at low temperature with the Bending Beam Rheometer. Expression [2.38] was coupled both with expression [2.39] and [2.40] showing that the two predicted mixtures creep stiffness give a lower and upper bound for the experimental curves obtained testing small asphalt mixtures beams.

2.5. Analogical Models

Different analogical models are available in literature. They may be very simple or much more complex and work on discrete or on continuous spectrum. The following paragraphs provide a short description of the most interesting models applied to asphalt mixture.

2.5.1. Discrete Spectrum Models

Dashpot and springs constitute the simplest analogical linear viscoelastic models (*Ferry, 1980*; *Findley, 1989*). When spring and dashpot are assembled is series and in parallel Maxwell and Kelvin-Voigt model can be constructed respectively (Figure 2.5).

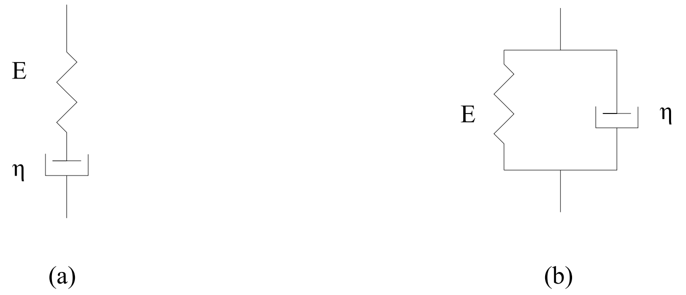

Figure 2.5. Maxwell model (a) and Kelvin-Voigt model (b)

Expressions [2.41], [2.42] provide the creep compliance *D(t)* and the relaxation function *R(t)* for the Maxwell model.

$$D(t)=\frac{1}{E}+\frac{t}{\eta} \qquad [2.41]$$

$$R(t)=Ee^{-\frac{t}{\tau}} \qquad [2.42]$$

where:

τ relaxation time $\tau=\eta/E$.

The complex modulus for the Maxwell model is:

$$E^*(i\omega)=E\frac{i\omega\tau}{1+i\omega\tau}=\frac{E\omega^2\eta^2+iE^2\omega\eta}{E^2+\omega^2\eta^2} \qquad [2.42]$$

where:

i complex number (i^2=-1)

Expressions [2.43], [2.44] provide the creep function *D(t)* and the relaxation function *R(t)* for the Kelvin-Voigt model.

$$D(t)=\frac{1}{E}\left(1-e^{-\frac{t}{\tau}}\right) \qquad [2.43]$$

$$R(t)=E+\eta\delta(t) \qquad [2.44]$$

where:

τ relaxation time $\tau=\eta/E$,

δ Dirac function.

The complex modulus for the Kelvin-Voigt model is:

$$E^*(i\omega) = E + i\omega\eta \qquad [2.45]$$

These two models are not able to describe the complex properties of asphalt material but can be used as basic components of more sophisticated models. A satisfactory description of the behavior of asphalt binder and concrete (*Neifar and Di Benedetto, 2001*) can be obtained combining two previous model into a Generalized Maxwell Model (*n* Maxwell elements in parallel plus one spring) or into a Generalized Kelvin-Voigt Model (*n* Kelvin-Voigt elements in series plus one spring and one linear dashpot) (Figure 2.6 and Figure 2.7).

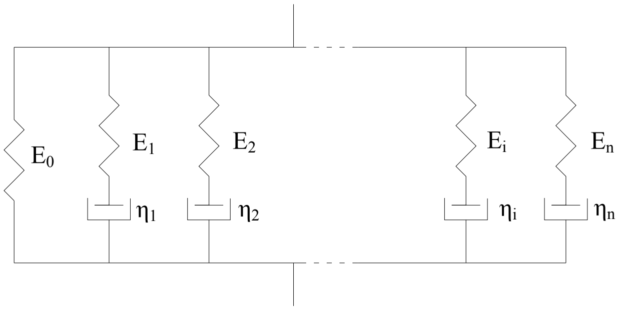

Figure 2.6. Generalized Maxwell model

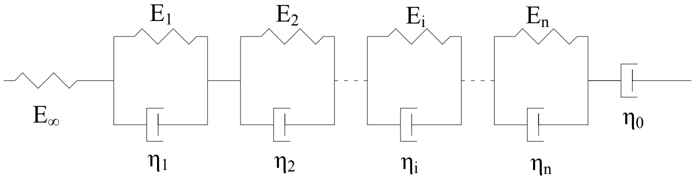

Figure 2.7. Generalized Kelvin-Voigt model

In the case of discrete number of element and thus for a discrete spectrum the relaxation modulus for the Generalized Maxwell model can be expressed as (*Ferry, 1980*):

$$R(t) = E_\infty + \sum_{i=1}^{n} E_i e^{-\frac{t}{\tau_i}} \qquad [2.46]$$

where:

τ_i relaxation time of the i^{th} Maxwell element,

E_i spectral strength of the i^{th} Maxwell element.

The complex modulus presents the following expression:

$$E^*(i\omega) = E_\infty + \sum_{i=1}^{n} E_i \frac{i\omega\tau_i}{1+i\omega\tau_i} \qquad [2.47]$$

Increasing the number of element without limit in the Maxwell model it is possible to obtain a continuous spectrum representation of the relaxation and complex modulus functions [2.48] and [2.49] respectively:

$$R(t) = E_\infty + \int_{\ln(\tau)=-\infty}^{\ln(\tau)=+\infty} H(\tau) e^{-\frac{t}{\tau}} d\ln\tau \qquad [2.48]$$

$$E^*(i\omega) = \int_{\ln(\tau)=-\infty}^{\ln(\tau)=+\infty} H(\tau) \frac{i\omega\tau}{1+i\omega\tau} d\ln\tau \qquad [2.49]$$

where:

$H(\tau)\ d\ln(\tau)$ is the modulus associated with the relaxation time.

For a discrete spectrum the relaxation modulus for the Generalized Kelvin-Voigt model can be expressed as:

$$D(t) = \sum_{i=1}^{n} \frac{1}{E_i}\left(1 - e^{-\frac{t}{\tau_i}}\right) + \frac{1}{E_\infty} + \frac{1}{\eta_0} \qquad [2.50]$$

$$E^*(i\omega) = \left(\sum_{i}^{n} \frac{1}{E_i + i\eta_i\omega} + \frac{1}{E_\infty} + \frac{1}{i\eta_0\omega}\right) \qquad [2.51]$$

2.5.2. Continuous Spectrum Models

The discrete numbers of elements included into the Generalized Maxwell or Kelvin-Voigt models are not always enough to have a satisfactory representation of a complex linear viscoelastic material, even though the number of elements can be increased. More advanced analogical models with continuous spectrum were proposed by other authors and they can be represented by an infinite number of Kelvin-Voigt or Maxwell elements.

2.5.2.1. Parabolic Element

A parabolic element is an analogical model that can be schematized as in Figure 2.8.

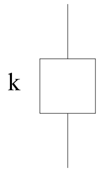

Figure 2.8. Parabolic element

Creep function *D(t)* and complex modulus E^* can be expressed as:

$$D(t) = \delta\left(\frac{t}{\tau}\right)^k \qquad [2.52]$$

$$E^*(i\omega\tau) = \frac{(i\omega\tau)^k}{\delta\Gamma(k+1)} \qquad [2.53]$$

where:

i	complex number (i^2=-1)
E^*	complex modulus,
k	exponent,
δ	dimensionless constant,
ω	2π*frequency,
τ	characteristic time varying with temperature accounting for the Time Temperature Superposition Principle (TTSP): $\tau = a_T(T)\tau_0(T_S)$
a_T	shift factor at temperature T (can be determined from equation [2.5] WLF),
τ_0	characteristic time determined at reference temperature T_S
Γ	gamma function that can be expressed as: $\Gamma(n) = \int_0^\infty t^{n-1}e^{-t}dt$ $\Gamma(n+1) = n\Gamma(n)$ n>0 or Re(n)>0 t integration variable, n argument of the gamma function.

2.5.2.2. Huet Model

The Huet analogical model (*Huet, 1963*) is composed of two parabolic elements $J_1(t)=at^h$ and $J_2(t)=bt^k$ plus a spring (stiffness E_∞) combined in series. (Figure 2.9)

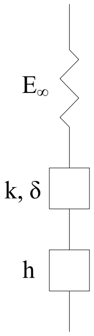

Figure 2.9. Huet model – (*Huet, 1963*)

The Huet model was proposed for binders and mixtures and presents a continuous spectrum that means it can be schematized by infinity of Kelvin-Voigt elements in series or Maxwell elements in parallel. The analytical expression of the Huet model for the creep compliance is:

$$D(t) = \frac{1}{E_\infty}\left(1 + \delta \frac{(t/\tau)^k}{\Gamma(k+1)} + \frac{(t/\tau)^h}{\Gamma(h+1)}\right) \qquad [2.54]$$

where:

$D(t)$	creep compliance
E_∞	glassy modulus,
h, k	exponents such that $0<k<h<1$,
δ	dimensionless constant,
t	time,
Γ	gamma function,
τ	characteristic time varying with temperature accounting for the Time Temperature Superposition Principle (TTSP): $\tau = a_T(T)\tau_0(T_S)$
a_T	shift factor at temperature T (can be determined from equation [2.5] WLF),
τ_0	characteristic time determined at reference temperature T_S.

An expression of the complex modulus for this model is also available [2.55], while there is no analytical formula for the relaxation function:

$$E^*(i\omega\tau) = \frac{E_\infty}{1+\delta(i\omega\tau)^{-k}+(i\omega\tau)^{-h}} \qquad [2.55]$$

where:

i complex number (i^2=-1)

E_∞ limit of the complex modulus for $\omega\tau\rightarrow\infty$ (Glassy modulus),

ω 2π*frequency

A modified expression of the Huet model which includes a third term function of τ and representing a dashpot in series was proposed by Maillard (*Maillard, 2005*). The modified model was applied to asphalt binder and a sensitivity study in the time domain was performed. Huet Model was also used by *Cannone Falchetto* (*2010*) and *Cannone Falchetto et al*., (*2011*) to investigate the creep stiffness of eight binders and sixteen corresponding mixtures obtained from three-point bending configuration at low temperatures. The models fitted the data very well both for binder and for mixtures.

2.5.2.3. Huet-Sayegh Model

Since the Huet model does not perform well for mixes response at very low frequencies and/or high temperature, due to the inability to take into account the limiting value of the mixtures modulus related to the aggregate skeleton, *Sayegh* (*1965*) proposed a new expression [2.56] for the complex modulus introducing a spring in parallel into the Huet model (Figure 2.10).

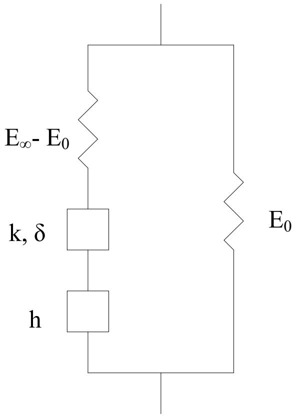

Figure 2.10. Huet-Sayegh model – (*Sayegh, 1965*)

$$E^*(i\omega\tau) = E_0 + \frac{E_\infty - E_0}{1 + \delta(i\omega\tau)^{-k} + (i\omega\tau)^{-h}} \qquad [2.56]$$

where:

i	complex number (i^2=-1)
E_∞	limit of the complex modulus for $\omega\tau \rightarrow \infty$ (Glassy modulus),
E_0	limit of the complex modulus for $\omega\tau \rightarrow 0$,
h, k	exponents such that $0<k<h<1$,
δ	dimensionless constant,
τ	characteristic time varying with temperature accounting for the Time Temperature Superposition Principle (TTSP), and
ω	2π*frequency.

Six constants are required from this model (δ, k, h, E_∞, E_0, and τ_0), one more than the Huet model. This model was applied by several authors (*De La Roche, 1996; Neifar, 1997; Olard – Di Benedetto, 2003; Bodin et al., 2004; Wistuba et al., 2006; Chabot et al., 2010*) with good results in the small strain domain for any range of frequencies and temperatures. It should be mentioned that this model presents some limitation when predicting binder modulus at very low frequencies where a parabolic element behavior is showed while a linear dashpot would be more appropriate. The model was also used by *Neifar and Di Benedetto.* (*2001*) to calibrate a thermo-visco-plastic law named DBN law. This law allows describing with the same formalism different types of mixture behaviors according to the considered loading domain (*Olard and Di Benedetto, 2005*). A three dimensional extension of the DBN was also proposed by the same authors (*Di Benedetto et al., 2007*). It must be finally mentioned that there is no analytical expression for creep compliance in the time domain for this model.

2.5.2.4. 2S2P1D Model and ENTPE Transformation

An improved Huet-Sayegh model that takes into account the drawback for binder characterization was proposed by Di Benedetto and Olard et al. (*Olard et al., 2003; Olard, 2003; Di Benedetto et al. 2004*). This model is obtained by the Huet-Sayegh model and adding a linear dashpot in series with the two parabolic elements and the spring of rigidity E_∞-E_0 so that at low frequency it is equivalent to a linear dashpot in parallel with a spring of rigidity E_0.

The scheme of the model is shown in Figure 2.11 and the analytical expression of the complex modulus is given by [2.57].

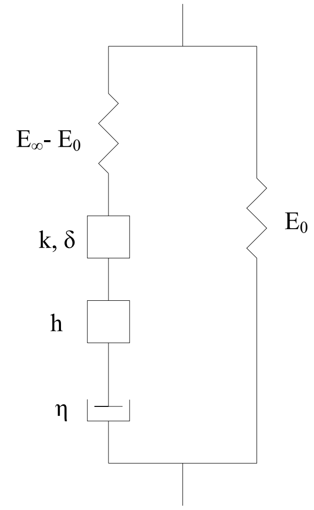

Figure 2.11. 2S2P1D model – (*Olard et al., 2003*)

$$E^{*}(i\omega\tau) = E_0 + \frac{E_\infty - E_0}{1 + \delta(i\omega\tau)^{-k} + (i\omega\tau)^{-h} + (i\omega\beta\tau)^{-1}} \qquad [2.57]$$

where:

i	complex number (i^2=-1)
E_∞	limit of the complex modulus for $\omega\tau \to \infty$ (Glassy modulus),
E_0	limit of the complex modulus for $\omega\tau \to 0$,
h, k	exponents such that $0<k<h<1$,
δ	dimensionless constant,
β	dimensionless parameter introduced to take into account the newtonian viscosity of the linear dashpot
τ	characteristic time varying with temperature accounting for the Time Temperature Superposition Principle (TTSP), and
ω	2π*frequency.

The seven constants (δ, β, k, h, E_∞, E_0, and τ_0) required were determined with a minimization process from the experimental data at a reference temperature T_S=10ºC for a series of binders and corresponding mixtures. Each mixture showed the same parameters δ, k, h and β of the associated binder while only the static and glassy modulus (E_0 and E_∞) and τ_0 seemed to be peculiar of the specific binder and mixtures. The values of E_0 and E_∞ for the mixtures were in the range of 250 to 1050MPa and 41500 to 45400MPa respectively. From the simple regression of the characteristic time of the mixture, τ_{0mix}, on the characteristic time of the corresponding binder, $\tau_{0binder}$, at the reference temperature in log scale the authors found the following relationship:

$$\tau_{0mix} = 10^{\alpha}\,\tau_{0binder} \qquad [2.58]$$

and applying the time temperature superposition principle:

$$\tau_{mix}(T) = 10^{\alpha}\,\tau_{binder}(T) \qquad [2.59]$$

where:

τ_{0mix}	characteristic time of mixture determined at reference temperature T_S,
$\tau_{0binder}$	characteristic time of binder determined at reference temperature T_S,
τ_{mix}	characteristic time of mixture at temperature T,
τ_{binder}	characteristic time of binder at temperature T,
α	regression coefficient depending on mixture and aging.

The value of α was determined in the range 2.66 to 2.82 according to the different mixtures and binders investigated for a characteristic time evaluated at T_S=10ºC (*Olard et al., 2003; Olard, 2003; Di Benedetto et al. 2004*).

Based on this findings a relationship between the binder and the mix complex moduli (considering both the phase angle and the norm of the complex) was proposed [2.60] (*Olard et al., 2003; Olard, 2003; Di Benedetto et al. 2004*):

$$E^*_{mix}(\omega,T) = E_{0mix} + \left[E^*_{binder}(10^{\alpha}\omega,T) - E_{0binder}\right]\frac{E_{\infty mix} - E_{0mix}}{E_{\infty binder} - E_{0binder}} \qquad [2.60]$$

where:

E^*_{mix}	complex modulus of the mixture,
E^*_{binder}	complex modulus of the binder,
$E_{\infty mix}$	glassy modulus of the mixture,
E_{0mix}	static modulus of the mixture,
$E_{\infty binder}$	glassy modulus of the binder,
$\mathrm{E_{0binder}}$	static modulus of the binder,
T	temperature,

ω 2π*frequency,

α regression coefficient depending on mixture and aging.

The expression [2.60] is independent of the rheological model used to construct it and can be interpreted as a combination of three transformations (Figure 2.12):

- a negative translation of value E_{0_binder} along the real axis,
- a homothetic expansion starting from the origin with a ratio of $(E_{\infty\_mix} - E_{0\_mix})/(E_{\infty\_binder} - E_{0\_binder})$,
- a positive translation of value E_{0_mix} along the real axis.

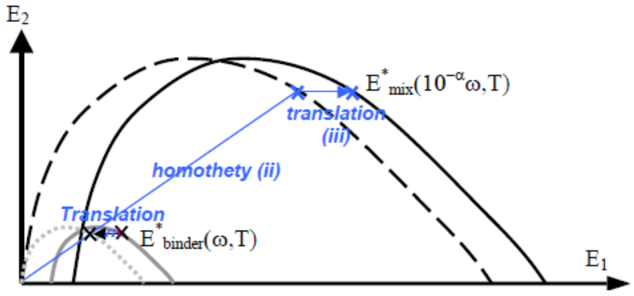

Figure 2.12. Binder to Mixture model scheme – (*Di Benedetto et al., 2004*)

Expression [2.60] was also validated by *Di Benedetto et al.* (*2004*) for different mixtures and binders other than those used to derive the transformation. Delaporte et al. (*Delaporte et al., 2007*) used the same approach to investigate the linear viscoelastic properties of asphalt binder and mastics with and without aging.

Note that equation [2.60] can be simply rearranged to obtain E^*_{binder} from E^*_{mix}:

$$E^*_{binder}(\omega,T) = E_{0binder} + \left[E^*_{mix}(10^{-\alpha}\,\omega,T) - E_{0mix}\right]\frac{E_{\infty binder} - E_{0binder}}{E_{\infty mix} - E_{0mix}} \qquad [2.61]$$

Expressions [2.60] and [2.61] are called ENTPE (École Nationale des Travaux Publics de l’État) transformations.

Cannone Falchetto (*2010*) and *Cannone Falchetto et al.*, (*2011*) obtained a formula analogous to [2.60] to predict the creep stiffness of asphalt mixtures from the creep stiffness of the corresponding asphalt binder (Forward Problem) determined experimentally on the Bending Beam Rheometer (BBR) at low temperatures:

$$S_{mix}(t) = S_{binder}(t10^{-\alpha})\frac{E_{\infty\_mix}}{E_{\infty\_binder}} \qquad [2.62]$$

where:

$S_{mix}(t)$	creep stiffness of mixture,
$S_{binder}(t)$	creep stiffness of binder,
E_{∞_mix}	glassy modulus of mixture,
E_{∞_binder}	glassy modulus of binder,
t	time,
α	regression parameter which may depend on mix design, expressed as:

$$\tau_{mix} = 10^{\alpha}\tau_{binder} \qquad [2.63]$$

where:

τ_{binder}	characteristic time of binder,
τ_{mix}	characteristic time of mixture,

Expression [2.62] provided very good predictions for all the eight binder and sixteen mixtures investigated.

2.6. Inverse Problem

The prediction of a material property based on the measured (or observed) material response constitutes the objective of an inverse problem in mechanics. This process is called a parameter identification procedure. Two procedures for parameter identification for viscoelastic materials were proposed by *Ohkami and Swoboda* (*1999*). Both methods contain boundary control concept introduced by *Ichikawa and Ohkami* (*1992*).

Amin et al (*2002*) developed a similar approach by combining FEM simulations with inverse scheme. The viscoelastic behavior was modeled by the authors using a 3-parameter solid model (Maxwell model parallel with a spring). With a similar approach, FEM simulations combined with measured data was used by *Bocciarelli et al.* (*2005)* to construct objective function; this function was then minimized using trust-region approach.

Kim and Kreider (*2006*) used numerical inversion for 2D problem for linear viscoelastic homogenous material with 3-7 parameters. Several potential problems with this scheme were detected. The solution might not be unique and might depend on the initial guess for optimization method and moreover there is no unique optimization approach that is suitable for all problem and material types.

Zofka et al. (*2005*) obtained mixture stiffness (inverse of creep compliance) by performing Bending Beam Rheometer (BBR) tests on beams of asphalt mixture. The author used a modified Hirsch (*Hirsch, 1962*) model proposed by Christensen (*Christensen et al., 2003*) to "back-calculate" the asphalt binder stiffness and m-value. Since brute force was time consuming the original equation [2.38] was combined with an alternative procedure to the numerical minimization based on the observation that a simple function could be fitted to the mix stiffness versus binder stiffness data. *Velasquez et al.* (*2010*) using additional experimental data developed two expressions for the *Pc* parameter [2.39] and [2.40].

Cannone Falchetto (*2010*) and *Cannone Falchetto et al*., (*2011*) investigated the possibility to obtain the creep stiffness of asphalt binder from the creep stiffness of the corresponding asphalt mixtures (Inverse Problem) determined experimentally on the Bending Beam Rheometer (BBR) at low temperatures. Hirsch model and Huet model coupled with ENTPE transformation were used. However Hirsch model results to be a poor predictor, while using the inverse of expression [2.62] the experimental curves were matched very well by the predicted asphalt binder creep stiffness.

Zofka (*2007*) used an inverse scheme based on the Zevin's method of iterative functions (*Zevin, 1979; Arutyunyan and Zevin, 1988*). The asphalt mixture is treated as a 2-phase composite material consisting of elastic aggregate particles of arbitrary shape and viscoelastic asphalt mastic.

2.7. Correspondence Principle

One of the most widely used approach for solving mechanics problems in linear viscoelasticity is represented by the correspondence principle (*Alfrey*, *1944*; *Tsien*, *1950* and *Lee 1955*). The solution of a viscoelastic problem is generally complicated by the presence of both time and space variables in the governing differential equations. However, when temperature and boundary conditions remain constant, correspondence principle allows the reformulation of the viscoelastic problem in Laplace domain (*s*-domain) as associated elastic problem. Analytical or numerical solution such as finite element or boundary element method can then be applied to solve the fictitious elastic problem in Laplace space. The inverse Laplace transform can be finally used to invert the *s*-domain results back to the time domain using either analytical or numerical methods. One of the limitations of the correspondence principle is represented by the Laplace inversion process that in some cases may be source of large errors (*Schapery*, *1965*; *Graham*, *1968*; *Jordaan and Khalifa 1977*, *Lee and Kim 1995., Paulino and Jin 2001*, *Ahn et al. 2003, Huang et al. 2006*).

Different approximate inversion methods were proposed and applied to viscoelastic problems involving asphalt binders and asphalt mixtures by several authors (*Kim et al.*, *1995*; *Schapery*, *1965*; *Daniel et al.*, *1998*; *Lundstrom and* Isacsson, *2004*). However, the accuracy of these methods is strongly affected by the complexity of the original viscoelastic problem and thus, they might not be satisfactory when solving inverse problems.

Chapter 3. Materials and Testing

3.1. Test Methods for low temperature characterization of asphalt binders and mixtures

The following paragraphs provide a short description of the current test methods used to characterize the behavior of asphalt binders and mixtures at low temperature.

3.1.1. Asphalt Binder Testing

During the Strategic Highway Research Program (SHRP) two test methods were developed for the evaluation of the properties of asphalt binders at low temperatures: the Bending Beam Rheometer (BBR) and the Direct Tension (DT) test (*Anderson et al*., 1994).

3.1.1.1. Bending Beam Rheometer (BBR)

The BBR is used to perform low-temperature creep tests on thin beams of asphalt binders conditioned at the desired temperature for one hour (*AASHTO T 313-02 2006*). The asphalt beam (101.6x12.5x6.25mm) is tested in a three-point bending configuration (Figure 3.1).

Figure 3.1. BBR equipment for asphalt binder testing

A constant load is applied instantaneously and maintained for all the duration of the test (240s) while the deflection at the mid span of the beam is continuously recorded. Correspondence principle and elastic solution for a simply supported beam are used to obtain the creep compliance. The creep stiffness, *S(t)*, equal to the inverse of the creep compliance, *D(t)*, is calculated as:

$$S(t) = \frac{\sigma}{\varepsilon(t)} = \frac{P \cdot l^3}{4 \cdot b \cdot h^3 \cdot \delta(t)} \qquad [3.1]$$

where

S(t)	flexural creep stiffness, function of time,
σ	maximum bending stress in the beam, MPa,
ε(t)	bending strain (mm/mm), unction of time,
P	constant load = 980±50mN ,
l	length of specimen (101.6mm),
b	width of specimen (12.5mm),
h	height of specimen (6.25mm),
δ(t)	deflection at the midspan of the beam at time t, and
t	time.

The *m*-value which is the slope of log stiffness versus log time curve is computed according to:

$$m(t) = \left| \frac{d \log S(t)}{d \log(t)} \right| \qquad [3.2]$$

Both stiffness and the *m*-value are used to determine the critical temperature.

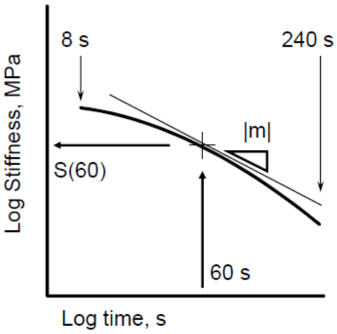

Figure 3.2. BBR stiffness and m-value

The *m*-value can be computed by fitting a polynomial curve of second order to the log of the stiffness (log(*S*(*t*)) versus log(*t*) curve:

$$\log S(t) = a \cdot (\log(t))^2 + b \cdot \log(t) + c \qquad [3.3]$$

and

$$m(t) = \left| 2a \cdot \log(t) + b \right| \qquad [3.4]$$

The critical temperature T_{CR}, (the temperature at which cracking occurs) can be determined as the lowest temperature at which the following conditions are satisfied (*AASHTO T313-02, 2006*):

$$S(t_{60}) \leq 300MPa \tag{3.5}$$

$$m(t_{60}) \geq 0.300 \tag{3.6}$$

where

t_{60} time equal to 60 seconds.

The binder PG (Performance Grade) low temperature is then determined subtracting 10ºC from the temperature determined from the *S*(*t*) and *m*-value limits. This temperature correction, based on Time-Temperature Superposition (TTS) principle for linear viscoelastic materials (*Anderson and Kennedy*, *1993*) is needed since low temperature pavement performance is correlated to creep stiffness obtained after two hours of loading.

3.1.1.2. Direct Tension (DT) Test

The Direct Tension (DT) is used to perform uniaxial tension tests at a constant strain rate of 1% per minute on dog-bone shaped specimens of asphalt binders until failure (*AASHTO T 314-02 2002*). The average stress and strain at failure are obtained from six replicates and for the same temperature for which creep stiffness and m-value are measured on BBR. DT strength and thermal stress calculation can be used to calculate the critical cracking temperature for the specific binder (*Bouldin et al., 2000*).

3.1.2. Asphalt Mixture Testing

3.1.2.1. Indirect Tensile Test (IDT)

Indirect Tensile test (IDT) (*AASHTO T 322-03*) is currently used to obtain creep compliance and strength of asphalt mixtures at low temperatures (*Roque and Buttlar, 1992; Buttlar and Roque, 1994; Zhang et al., 1997; Christensen, 1998; Roque et al., 2002*). During creep testing the cylindrical specimen is vertically loaded with a constant load resulting in an almost uniform tensile stress along the diameter of the sample. Four Linear Variable Differential Transducers (LDVT's) are used to measure the vertical and horizontal displacement on both sides of the specimen for 1000±2.5s and from this the creep curve is obtained. Creep compliance *D(t)* is calculated according to elastic-viscoelastic correspondence principle, elastic solutions for horizontal and vertical stresses and plane stress Hooke's law. Strength test of asphalt mixtures can also be performed on IDT configuration when appropriate loading mode is applied to the specimen.

3.1.2.2. Bending Beam Rheometer (BBR) test for Asphalt Mixtures

Three-point bending test is currently the standard procedure used to determine creep compliance of asphalt binders at low temperatures (*AASHTO T 313-02 2006*). The device used to perform this test is the Bending Beam Rheometer (BBR) developed during the Strategic Highway Research Program (SHRP) (*Bahia et al. 1992*). In recent years, *Zofka et al.* (*2005, 2006*) and *Zofka* (*2007*) investigated the use of BBR to determine the creep compliance of asphalt concrete. Good agreement was found between the BBR and IDT testing procedures. *Velasquez* (*2009*) investigated the representative volume element (RVE) when using BBR to test asphalt mixtures beams, and determined that a representative creep stiffness of asphalt concrete can be obtained from testing a minimum of three replicates of the thin mixture beams. A procedure similar to the one used for binders was proposed by *Marasteanu et al.*, (*2009*) to test thin asphalt mixtures beams with BBR equipment. A description of the beam preparation is detailed in the NCHRP 133 Final report (*Marasteanu et al., 2009*) and it include several cutting steps from the gyratory compacted cylinder through IDT specimens and finally to actual BBR beams. An example of a BBR asphalt mixture beam is shown in Figure 3.3, while Figure 3.4 illustrates a scheme on how the beams are obtained from a cylindrical specimen.

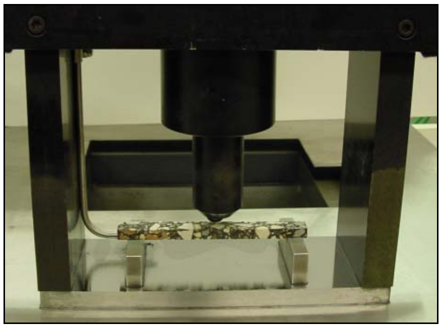

Figure 3.3. Bending Beam Rheometer with thin asphalt mixture beam (*Marasteanu et al., 2009*)

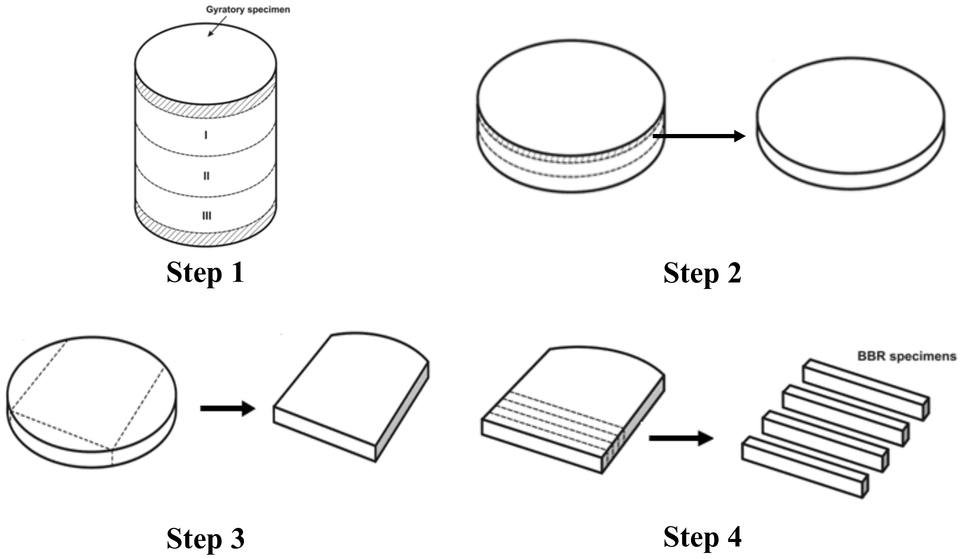

Step 1 Step 2

Step 3 Step 4

Figure 3.4. Asphalt mixture beam preparation – *(Marasteanu et al., 2009)*

Testing was performed according to *AASHTO T 313-02* standard, using higher loads due to the higher stiffness of the mixtures and for a longer time (1000s). It was found that good creep stiffness results can be obtained using test loads of 1961 mN and 4413 mN at high (PG low temperature + 22˚C) and intermediate low temperature levels (PG low temperature + 10˚C), respectively. For the lowest temperature level (PG low temperature - 2˚C), the creep stiffness can be predicted from the data obtained at the higher two temperatures and from time-temperature superposition (*Marasteanu et al., 2009*).

3.2. Materials and Experimental Work

The asphalt mixtures used in this study were provided by Minnesota Department of Transportation (Mn/DOT) and are part of Mn/DOT research project 2010-08 performed by Mn/DOT and Minnesota Pollution Control Agency (MPCA) to determine the effects of using varying proportions of recycled asphalt shingles (RAS), reclaimed asphalt pavement (RAP), and two different virgin binders on pavement performance (*Johnson et al., 2010*). Thirty four gyratory compacted specimens, two for each of the 17 mixtures investigated, were delivered to the Asphalt Pavement Laboratory of the Department of Civil Engineering at University of

Minnesota. No information was available about gradation of aggregates and recycled materials used. The design of the HMA laboratory mixtures consisted of:

- Virgin binder and aggregates (No recycled materials);
- Virgin binder and aggregate plus Recycled Asphalt Pavement (RAP);
- Virgin binder and aggregate plus Manufacturer Waste Scrap Shingles (MWSS) and RAP;
- Virgin binder and aggregate plus Tear-off Scrap Shingles (TOSS);
- Virgin binder and aggregate plus Tear-off Scrap Shingles (TOSS) and RAP.

The virgin aggregate materials used in the mixtures consisted of a pit-run-sand, a quarried ¾ in. (19 mm) dolostone, quarried dolostone manufactured sand; it is worth to note that dolostone presents similar characteristics to limestone with a very similar stiffness modulus (*Martinez et al., 2006*). It is also known that a limestone with the carbonate component mainly made up of magnesium calcium carbonate (dolomite) is termed dolostone (*Bell, 2000*). The recycled material included in the mixtures consisted of ¾ in. (19 mm) RAP and RAS (either MWSS or TOSS). Figure 3.5 presents two pictures of Manufacturer Waste Scrap Shingles (MWSS) and Tear-off Scrap Shingles (TOSS).

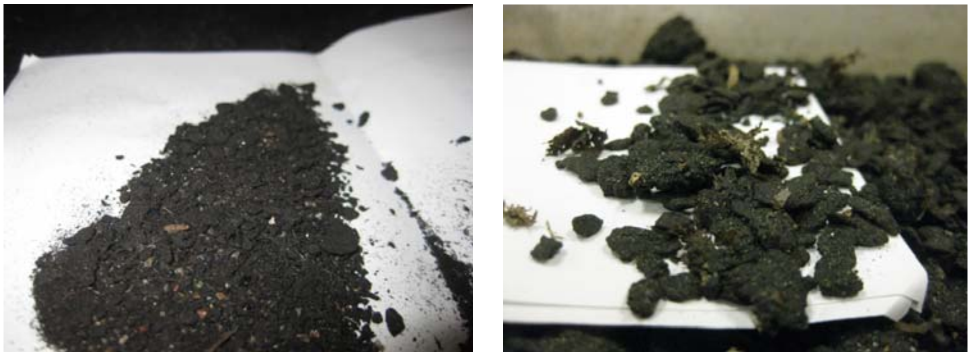

Figure 3.5. TOSS (right) and MWSS (left) – (*Johnson et al., 2010*)

A PG 58-28, non-polymer modified, asphalt binder with specific gravity of 1.036, was used in all but two of the RAS/RAP mixtures were a PG 52-34, non-polymer modified, asphalt binder was selected in order to investigate the binder and mixture properties resulting from using a softer binder. Table 3.1 presents the mixture design for the 17 mixtures investigated:

Table 3.1. Mixture design for the 17 mixtures investigated

Mix		Recycled Material			Binder PG		VMA	VFA	Air Voids
ID	Description	RAP (%)	TOSS (%)	MWSS (%)	58-28	52-34	%	%	%
1	PG 58-28 Control	0	0	0	x		15.9	76.6	3.7
2	15% RAP	15	0	0	x		15.2	72.9	4.1
3	25% RAP	25	0	0	x		15.3	73.0	4.1
4	30% RAP	30	0	0	x		15.0	45.4	3.7
5	15% RAP 5% MWSS	15	0	5	x		15.6	75.0	3.9
6	15% RAP 5% TOSS	15	5	0	x		15.9	77.2	3.6
7	25% RAP 5% TOSS	25	5	0	x		15.4	73.9	4.0
8	25% RAP 5% MWSS	25	0	5	x		14.8	72.5	4.1
9	25% RAP 5% TOSS	25	5	0		x	15.8	71.8	4.5
10	25% RAP 5% MWSS	25	0	5		x	15.0	73.5	4.0
11	25% RAP 3% TOSS	25	3	0	x		15.5	75.3	3.8
12	25% RAP 3% MWSS	25	0	3	x		15.3	73.7	4.0
13	15% RAP 3% TOSS	15	3	0	x		16.1	79.4	4.0
14	15% RAP 3% MWSS	15	0	3	x		16.1	73.8	4.2
15	10% RAP 5% TOSS	10	5	0	x		16.6	75.0	4.2
16	15% RAP 5% TOSS*	15*	5	0	x		16.7	77.2	3.8
17	5% TOSS	0	5	0	x		16.6	76.3	4.0

*Different RAP Source – millings containing 4.0% asphalt binder

The cylindrical specimens were cut into small beams, six for each of two gyratory compacted specimens available for each mixture. A total of 204 beams were obtained (see Appendix A for geometric properties of the beams). The asphalt mixture beams were tested in the BBR according to the procedure proposed by *Marasteanu et al.,* (*2009*). Two Test temperatures and corresponding loads were selected: a high low temperature level (PG low temperature + 22˚C) , corresponding at -6°C with a loads of 1961 mN and an intermediate low temperature level (PG low temperature + 10˚C), corresponding at -18°C with a loads of 4413 mN respectively. The mixture prepared with PG 52-34 binder were also tested at these two temperatures.

BBR tests were also performed on the binder extracted from the mixtures according to *AASHTO T 313-02* (*2006*). Extraction and tests were performed at Mn/DOT laboratory and were not under the control of the author of this thesis. Moreover, the extracted binders were not obtained from the gyratory cylinders from which the asphalt mixture BBR beams were cut, but from different cylinder replicates of the same mixtures. For this reason different numbers of replicates were tested according to the amount of material the Mn/DOT technicians were able to extract. Furthermore, extracted binder was not available for all the mixtures, but only for mixtures # 2, 3, 5, 6, 7 and 8. Since BBR results for the original or the extracted binders from the control mixture (virgin materials) were not available, no further details are presented in this section about the extracted binder test and no analysis of this data will be performed in Chapter 4. The data will only be used for comparison in Chapter 6 (Modeling).

Chapter 4. Experimental Data Analysis

In this chapter, the experimental data obtained from BBR creep testing on the seventeen asphalt mixtures investigated are analyzed. First, the values of the creep stiffness and the *m*-value at 60 seconds are considered and analysis of variance (ANOVA) (*Cook and Weisberg*, *1999*; *Oehlert*, *2000*; *Moore et al.*, *2008*) is used to determine which factors, RAP, TOSS, MWSS, binder type and temperature affect the response (stiffness and *m*-value). Then the procedure to compute thermal stress and critical temperature are outlined and a second set of ANOVA is run to evaluate if RAP, TOSS, MWSS, binder type and cooling rate affect thermal stress, at the low temperature PG (performance grade), and the critical temperature as well. Two pieces of software were used to perform the statistical analysis; Mac ANOVA (*MacANOVA v.5.05 release 1, 2006*), a free open source program, and SPSS (*SPSS v.17.1, 2008*), a commercial available software.

4.1. Creep Stiffness and *m*-value

The creep stiffness *S*(t) and the *m*-value for the different mixture were calculated according to [3.1] to [3.4] and to *Marasteanu et al.*, (*2009*), for the entire duration of the BBR asphalt mixture creep test (1000s). For the purpose of statistical analysis, a reference time of 60s (as in the case binder procedure reported in *AASHTO T313-02, 2006*) was selected. The average values for each mixture of the creep stiffness *S*(*t*) and the *m*-value, at *t*=60s, for the two testing temperatures (-6 ºC and -18ºC) and the corresponding coefficients of variation are showed in Table 4.1 and plotted in Figure 4.1 and Figure 4.2. A detailed table of the values of creep stiffness *S*(*t*) and the *m*-value at *t*=60s for all the replicates can be found in Appendix B.

Table 4.1. ***S*(t) and the *m*-value, at t=60s, and corresponding CV's**

Mixture ID	T °C	S(60) Mean (GPa)	CV S(60) %	m(60) Mean -	CV m(60) %
1	-6.0	4.627	18.4	0.287	6.2
2		6.567	22.1	0.173	7.1
3		8.626	4.4	0.159	8.2
4		7.524	8.1	0.168	4.7
5		7.653	8.5	0.174	7.5
6		9.612	7.4	0.154	9.7
7		9.542	5.2	0.130	7.7
8		9.596	14.1	0.136	11.2
9		6.850	21.3	0.180	10.1
10		7.599	19.5	0.193	8.1
11		10.307	8.9	0.125	23.9
12		9.972	23.0	0.135	19.3
13		7.416	8.0	0.153	6.5
14		6.568	12.9	0.172	4.2
15		6.491	11.8	0.164	4.6
16		8.335	20.7	0.164	5.8
17		6.377	17.2	0.177	5.6
1	-18.0	12.886	10.2	0.153	5.4
2		15.198	9.3	0.123	7.9
3		16.885	21.3	0.119	7.1
4		13.249	9.2	0.117	9.7
5		16.617	11.6	0.129	5.4
6		14.943	20.8	0.120	7.5
7		15.824	18.7	0.111	12.3
8		14.051	2.6	0.105	6.0
9		15.023	8.1	0.130	26.3
10		14.483	12.7	0.145	12.9
11		17.229	9.0	0.108	5.8
12		14.586	13.6	0.123	13.3
13		12.513	8.5	0.117	16.3
14		13.596	6.5	0.122	12.8
15		14.187	17.0	0.130	3.0
16		18.039	22.3	0.129	8.4
17		14.312	19.6	0.123	14.4

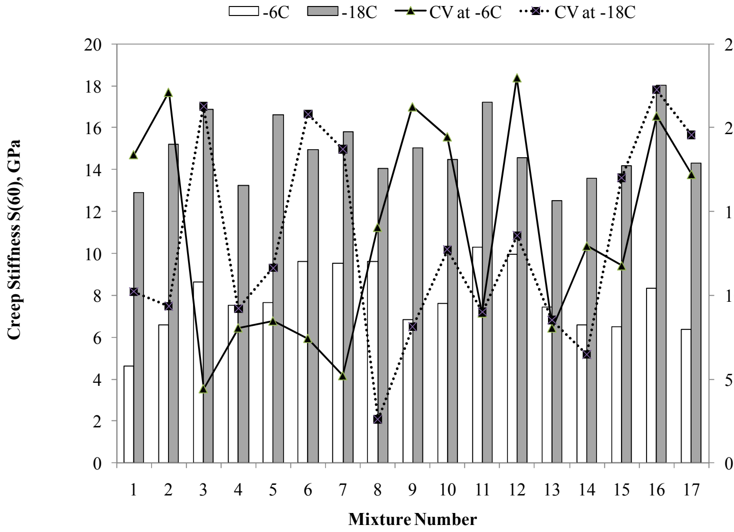

Figure 4.1. Creep stiffness *S*(*t*) at 60s and CV's

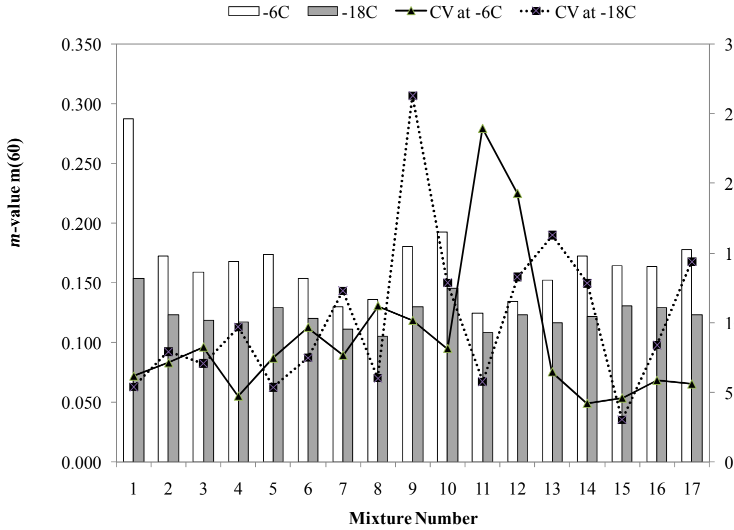

Figure 4.2. *m*-value at 60s and CV's

4.1.1. Statistical Analysis

In the following paragraphs the creep stiffness *S*(*t*) and the *m*-value for different groups of mixtures with common characteristics as RAP, TOSS and MWSS content or binder are analyzed from a statistical point of view using ANOVA procedure. Creep stiffness S(*t*) and *m*-value are set in turn as response and, according to the different mixture groups selected for the analysis, RAP, TOSS, MWSS, binder and temperature were set as factors. As a general procedure a full ANOVA analysis based on a linear model is first run taking into account all the possible interactions between the factors considered. The assumption of normality and constant variance are verified through the use of Box-Cox plot, Residuals plot and Normal Probability plot. If required a transformation of the response is performed and the analysis is repeated using the transformed data. Then if some interaction terms are not statistically significant, they are pulled into the error term and a reduced linear model is used. From this, a final estimate of *t*-statistic and *p*-value for each term is obtained assuming a significance level of 0.05.

4.1.1.1. Effect of RAP Amount on Creep Stiffness and m-value

For this analysis the first four mixtures were selected since they don't include any recycled material other than RAP (Reclaimed Asphalt Pavement). Mixture 1 was set as control mixture because of the absence of any recycled material in its mix design, while mixtures 2 (15% RAP), 3 (25% RAP) and 4 (30% RAP) are the test mixtures. The selected response for the ANOVA are the creep stiffness *S*(*t*) and the *m*-value at *t*=60s. Amount of RAP (0%, 15%, 25% and 30%) and temperature (-6°C and -18°C) are the factors selected for the analysis. Tables 4.2 and 4.3 summarize the experimental design and the average values of the selected responses with the corresponding coefficients of variation.

Table 4.2. Experimental design for mixtures 1, 2, 3 and 4

Mixture ID	**RAP %**	TOSS %	MWSS %	Binder PG	Description Statistics
1	**0**	0	0	58-28	Control
2	**15**	0	0	58-28	Test
3	**25**	0	0	58-28	Test
4	**30**	0	0	58-28	Test

Table 4.3. *S*(t) and *m*-value at t=60s, for mixtures 1, 2, 3 and 4 and CV's

Mixture ID	Temp °C	Creep Stiffness(60) Original (GPa)	Creep Stiffness(60) CV(%)	m-value(60) m-value	m-value(60) CV(%)
1	-6	4.627	18.4	0.287	6.2
	-18	12.886	10.2	0.153	5.4
2	-6	6.567	22.1	0.173	7.1
	-18	15.198	9.3	0.123	7.9
3	-6	8.626	4.4	0.159	8.2
	-18	16.885	21.3	0.119	7.1
4	-6	7.524	8.1	0.168	4.7
	-18	13.249	9.2	0.117	9.7

Figure 4.3 shows the histograms of the creep stiffness and *m*-value for mixtures 1, 2, 3 and 4, with the corresponding CV's for the two testing temperatures.

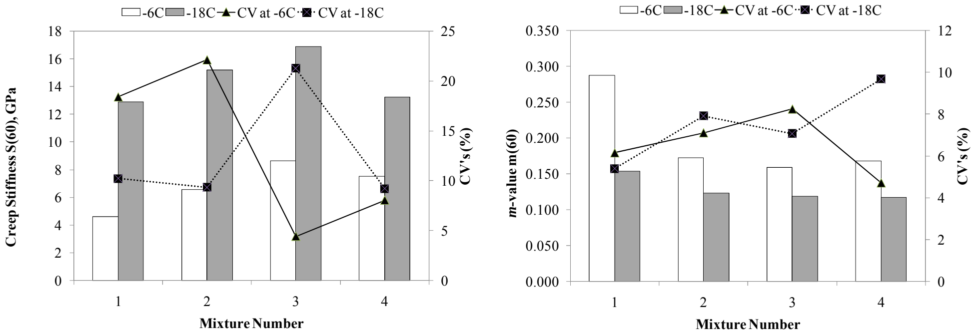

Figure 4.3. Creep stiffness and *m*-value at 60s and CV's for mixtures 1, 2, 3 and 4

Normality and constant variance were checked and log transformation of the stiffness was suggested to satisfy the assumptions for ANOVA while no transformation was required for the *m*-value. Full ANOVA including all the interactions between factors (RAP and temperature) was performed. The results are shown in Tables 4.4 to 4.7 where:

SS	Sums of Squares
df	degrees of freedom
MS	Mean Squares
F	F-statistics
p-value	values to compare to the assumed significance level (0.05).

Table 4.4. ANOVA for creep stiffness *S*(*t*) at 60s – mixtures 1, 2, 3 and 4

Source	SS	df	MS	F	**p-value**
Intercept	749.050	1	749.050	175294.0	**0.000**
RAP	0.229	3	0.076	17.8	**0.000**
Temperature	1.310	1	1.310	306.5	**0.000**
RAP• Temperature	0.074	3	0.025	5.8	**0.002**
Error	0.167	39	0.004		
Total	750.830	47			

Table 4.5. ANOVA for *m*-value at 60s– mixtures 1, 2, 3 and 4

Source	SS	df	MS	F	**p-value**
Intercept	1.243	1	1.243	5100.0	**0.000**
RAP	0.053	3	0.018	72.6	**0.000**
Temperature	0.057	1	0.057	233.9	**0.000**
RAP• Temperature	0.017	3	0.006	22.9	**0.000**
Error	0.010	39	0.000		
Total	1.380	47			

Table 4.6. Coefficient estimates for creep stiffness *S*(*t*) at 60s – mixtures 1, 2, 3 and 4

Coefficients	Estimate	Std. error	t	**p-value**
Intercept	4.108	0.027	153.94	0.000
RAP 15%	0.070	0.038	1.85	0.072
RAP 25%	0.111	0.038	2.94	**0.006**
RAP 30%	0.011	0.038	0.29	0.774
Temperature	-0.449	0.038	-11.90	**0.000**

Table 4.7. Coefficient estimates for *m*-value at 60s – mixtures 1, 2, 3 and 4

Coefficients	Estimate	Std. error	t	**p-value**
Intercept	0.154	0.006	24.08	**0.000**
RAP 15%	-0.030	0.009	-3.34	**0.002**
RAP 25%	-0.035	0.009	-3.86	**0.000**
RAP 30%	-0.036	0.009	-3.99	**0.000**
Temperature	0.134	0.009	14.83	**0.000**

RAP temperature and their interaction are significant at a 0.05 significance level for the creep stiffness at 60s. Overall adding RAP increases the creep stiffness, but when looking at the single level only the inclusion of 25% of RAP produces a statistically significant creep stiffness increment compared to the other levels. As expected, lower creep stiffness is obtained at the higher testing temperature (-6^{o}C) compared to the lower temperature level (-18^{o}C) (see negative coefficient -0.449 in Table 4.6 for Temperature). In case of *m*-value at 60s, all RAP levels are statistically significant. Also temperature and its interaction with RAP are significant. Adding RAP results in lower *m*-values, meaning reduced relaxation properties of the mixtures.

4.1.1.2. Effect of TOSS and MWSS Amounts on Creep Stiffness and m-value

In this section two mixtures groups were identified. In each of them a constant amount of RAP is presents: 15% and 25% for mixtures 2, 5, 6, 13 and 14 and mixtures 3, 7, 8, 11 and 12 respectively. Tear-off Scrap Shingles (TOSS) and Manufacturer Waste Scrap Shingles (MWSS) are included in those mixture groups with three different percentages: 0%, 3% and 5%. Tables 4.8 and 4.9 exhibit the experimental design for the two mixture groups evaluated.

Table 4.8. Experimental design for mixtures 2, 5, 6, 13 and 14

Mixture ID	RAP %	**TOSS %**	**MWSS %**	Binder PG	Description Statistics
2	15	**0**	**0**	58-28	Control
5	15	**0**	**5**	58-28	Test
6	15	**5**	**0**	58-28	Test
13	15	**3**	**0**	58-28	Test
14	15	**0**	**3**	58-28	Test

Table 4.9. Experimental design for mixtures 3, 7, 8, 11 and 12

Mixture ID	RAP %	**TOSS %**	**MWSS %**	Binder PG	Description statistics
3	25	**0**	**0**	58-28	Control
7	25	**5**	**0**	58-28	Test
8	25	**0**	**5**	58-28	Test
11	25	**3**	**0**	58-28	Test
12	25	**0**	**3**	58-28	Test

Two separated ANOVA's were performed for the two different mixtures groups so that the influence of RAP on the effect of the other factors could be disregarded. TOSS (0%, 3% and 5%), MWSS (0%, 3% and 5%) and temperature (-6°C and -18°C) were set as factors for the analysis of variance, while creep stiffness $S(t)$ and *m*-value at 60s are still the responses. The average values of the selected responses and the corresponding CV's are shown in Tables 4.10 and 4.11.

Table 4.10. *S*(t) and *m*-value at t=60s, for mixtures 2, 5, 6, 13 and 14 and CV's

Mixture ID	T °C	Creep Stiffness(60) Original (GPa)	Creep Stiffness(60) CV(%)	m-value(60) m-value	m-value(60) CV(%)
2	-6	6.567	22.1	0.173	7.1
	-18	15.198	9.3	0.123	7.9
5	-6	7.653	8.5	0.174	7.5
	-18	16.617	11.6	0.129	5.4
6	-6	9.612	7.4	0.154	9.7
	-18	14.943	20.8	0.120	7.5
13	-6	7.416	8.0	0.153	6.5
	-18	12.513	8.5	0.117	16.3
14	-6	6.568	12.9	0.172	4.2
	-18	13.596	6.5	0.122	12.8

Table 4.11. *S*(t) and *m*-value at t=60s, for mixtures 3, 7, 8, 11 and 12 and CV's

Mixture ID	T °C	Creep Stiffness(60) Original (GPa)	Creep Stiffness(60) CV(%)	m-value(60) m-value	m-value(60) CV(%)
3	-6	8.626	4.4	0.159	8.2
	-18	16.885	21.3	0.119	7.1
7	-6	9.542	5.2	0.130	7.7
	-18	15.824	18.7	0.111	12.3
8	-6	9.596	14.1	0.136	11.2
	-18	14.051	2.6	0.105	6.0
11	-6	10.307	8.9	0.125	23.9
	-18	17.229	9.0	0.108	5.8
12	-6	9.972	23.0	0.135	19.3
	-18	14.586	13.6	0.123	13.3

Figures 4.4 and 4.5 show the histograms of the creep stiffness and *m*-value for mixtures 2, 5, 6, 13 and 14 and or mixtures 3, 7, 8, 11 and 12 with the corresponding CV's for the two temperature levels.

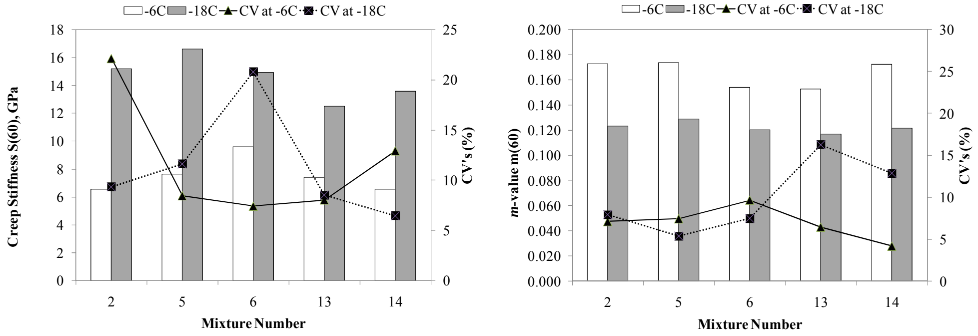

Figure 4.4. Creep stiffness and *m*-value at 60s and CV's for mixtures 2, 5, 6, 13 and 14

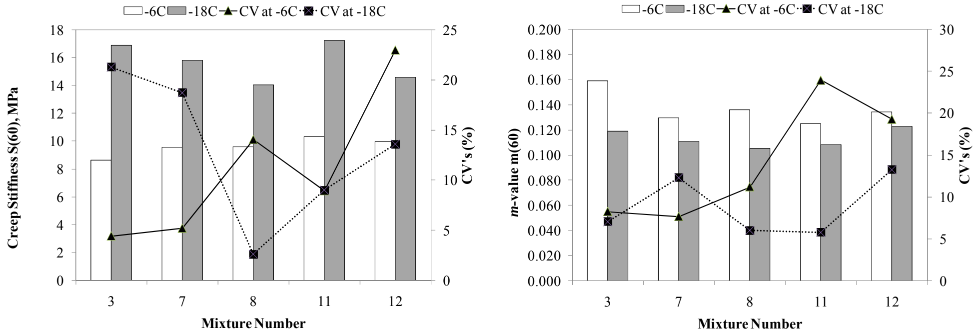

Figure 4.5. Creep stiffness and *m*-value at 60s and CV's for mixtures 3, 7, 8, 11 and 12

After checking normality and constant variance assumptions a log transformation of the creep stiffness was assumed also for this analysis, while the *m*-value could be evaluated in natural scale. The full ANOVA linear model applied to mixtures 2, 5, 6, 13 and 14 showed that, in the case of creep stiffness, the interaction term between MWSS and temperature is not significant at 0.05 level. Thus, a reduced model without this term was assumed. On the other hand, the statistical analysis results for *m*-value showed that all the terms but temperature are not statistically significant (Tables 4.12 and 4.13) and thus no significant change of the relaxation properties can be expected adding TOSS and MWSS for a 15% RAP content. However, from the coefficients tables (Tables 4.14 and 4.15), it is evident that in the case of creep stiffness, only TOSS at 3% content has a significant p-value with a negative contribution to the stiffness, while the other significant factor, MWSS, affect positively the creep stiffness only when present at 5%.

Table 4.12. ANOVA for creep stiffness *S*(*t*) at 60s – mixtures 2, 5, 6, 13 and 14

Source	SS	df	MS	F	**p-value**
Intercept	952.753	1	952.753	291792.0	**0.000**
Temperature	1.194	1	1.194	365.8	**0.000**
TOSS	0.057	2	0.028	8.7	**0.001**
MWSS	0.037	2	0.018	5.7	**0.006**
Temperature •TOSS	0.064	2	0.032	9.9	**0.000**
Error	0.167	51	0.003		
Total	954.272	59			

Table 4.13. ANOVA for *m*-value at 60s – mixtures 2, 5, 6, 13 and 14

Source	SS	df	MS	F	**p-value**
Intercept	1.214	1	1.214	4768.4	**0.000**
Temperature	0.028	1	0.028	109.6	**0.000**
TOSS	0.001	2	0.001	2.8	0.068
MWSS	0.000	2	0.000	0.2	0.805
Temperature •TOSS	0.001	2	0.001	1.4	0.264
Temperature •MWSS	0.000	2	0.000	0.2	0.789
Error	0.012	49	0.000		
Total	1.256	59			

Table 4.14. Coefficient estimates for creep stiffness *S*(*t*) at 60s – mixtures 2, 5, 6, 13 and 14

Coefficients	Estimate	Std. error	t	**p-value**
Intercept	4.167	0.019	215.42	**0.000**
TOSS 3%	-0.071	0.030	-2.35	**0.023**
TOSS 5%	0.001	0.030	0.03	0.973
MWSS 3%	-0.025	0.024	-1.03	0.309
MWSS 5%	0.052	0.024	2.20	**0.033**
Temperature	-0.339	0.019	-17.51	**0.000**

Table 4.15. Coefficient estimates for *m*-value at 60s – mixtures 2, 5, 6, 13 and 14

Coefficients	Estimate	Std. error	t	**p-value**
Intercept	0.123	0.007	18.92	**0.000**
TOSS 3%	-0.007	0.009	-0.71	0.479
TOSS 5%	-0.003	0.009	-0.31	0.759
MWSS 3%	-0.002	0.009	-0.18	0.859
MWSS 5%	0.006	0.009	0.60	0.549
Temperature	0.054	0.010	5.57	**0.000**

The full analysis of variance linear model for mixtures 3, 7, 8, 11 and 12 showed that only temperature is statistically significant when creep stiffness is the response investigated. This is also confirmed when the coefficients for the singles factor levels are estimated. In the case of *m*-value only temperature and TOSS main term with both 3% and 5% content affect the response when 25% RAP is present in the mixture, thus a decrease in the relaxation properties can be expected. It must be mentioned that model assumptions still required a log transformation of the creep stiffness.

Tables 4.16, 4.17, 4.18 and 4.19 present the results of ANOVA and coefficients estimation.

Table 4.16. ANOVA for creep stiffness *S*(*t*) at 60s – mixtures 3, 7, 8, 11 and 12

Source	SS	df	MS	F	**p-value**
Intercept	902.421	1	902.421	184946.0	**0.000**
Temperature	0.693	1	0.693	142.1	**0.000**
TOSS	0.022	2	0.011	2.2	0.121
MW	0.000	2	0.000	0.0	0.995
Temperature •TOSS	0.012	2	0.006	1.2	0.303
Temperature •MWSS	0.011	2	0.006	1.1	0.330
Error	0.215	44	0.005		
Total	903.374	54			

Table 4.17. ANOVA for *m*-value at 60s – mixtures 3, 7, 8, 11 and 12

Source	SS	df	MS	F	**p-value**
Intercept	0.879	1	0.879	2652.7	**0.000**
Temperature	0.009	1	0.009	27.3	**0.000**
TOSS	0.003	2	0.002	5.0	**0.011**
MWSS	0.001	2	0.001	1.9	0.166
Error	0.016	48	0.000		
Total	0.908	54			

Table 4.18. Coefficient estimates for creep stiffness *S*(*t*) at 60s – mixtures 3, 7, 8, 11 and 12

Coefficients	Estimate	Std. error	t	**p-value**
Intercept	4.219	0.029	147.94	**0.000**
TOSS 3%	0.010	0.042	0.23	0.822
TOSS 5%	-0.026	0.040	-0.64	0.524
MWSS 3%	-0.030	0.042	-0.71	0.483
MWSS 5%	-0.042	0.042	-1.00	0.321
Temperature	-0.283	0.040	-7.03	**0.000**

Table 4.19. Coefficient estimates for *m*-value at 60s – mixtures 3, 7, 8, 11 and 12

Coefficients	Estimate	Std. error	t	**p-value**
Intercept	0.126	0.006	21.67	**0.000**
TOSS 3%	-0.021	0.008	-2.64	**0.011**
TOSS 5%	-0.021	0.008	-2.77	**0.008**
MWSS 3%	-0.002	0.008	-0.26	0.796
MWSS 5%	-0.014	0.008	-1.82	0.076
Temperature	0.026	0.005	5.22	**0.000**

4.1.1.3. Effect of Binder Type on Creep Stiffness and m-value

Two mixtures groups (mixtures 7 and 9 and mixtures 8 and 10) were identified based on the different type of binder used to prepare them (PG 58-28 and PG 52-34). The mixtures contained 25% of RAP. Tables 4.20 and 4.21 show the experimental design.

Table 4.20. Experimental design for mixtures 7 and 9

Mixture ID	RAP **%**	**TOSS %**	**MWSS %**	Binder PG	Description statistics
7	25	**5**	**0**	58-28	Control
9	25	**5**	**0**	52-34	Test

Table 4.21. Experimental design for mixtures 8 and 10

Mixture ID	RAP **%**	**TOSS %**	**MWSS %**	Binder PG	Description statistics
8	25	**0**	**5**	58-28	Control
10	25	**0**	**5**	52-34	Test

The two ANOVA mixtures group were selected in such a way that the other factors, TOSS and MWSS, couldn't mask the effect of binder. Temperature (-6°C and -18°C) was also considered in the statistical analysis. Tables 4.22 and 4.23 present the average values of the creep stiffness $S(t)$ and m-value at 60s used as response in the statistical analysis while Figure 4.6 shows the bar charts of the same parameters for the mixtures evaluated with the corresponding CV's for the two temperature levels.

Table 4.22. *S*(t) and *m*-value at t=60s, for mixtures 7 and 9 and CV’s

Mixture	T	Creep Stiffness(60)		m-value(60)	
ID	°C	Original (MPa)	CV(%)	m-value	CV(%)
7	-6	9542	5.2	0.130	7.7
	-18	15824	18.7	0.111	12.3
9	-6	6850	21.3	0.180	10.1
	-18	15023	8.1	0.130	26.3

Table 4.23. *S*(t) and *m*-value at t=60s, for mixtures 8 and 10 and CV’s

Mixture	T	Creep Stiffness(60)		m-value(60)	
ID	°C	Original (MPa)	CV(%)	m-value	CV(%)
8	-6	9596	14.1	0.136	11.2
	-18	14051	2.6	0.105	6.0
10	-6	7599	19.5	0.193	8.1
	-18	14483	12.7	0.145	12.9

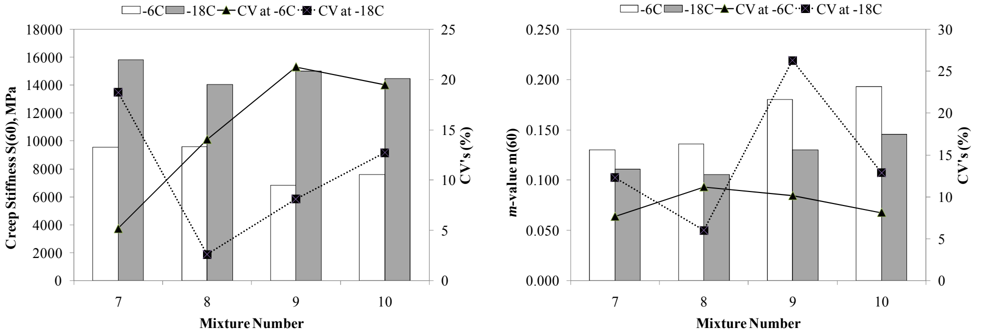

Figure 4.6. Creep stiffness and *m*-value at 60s and CV’s for mixtures 7, 8, 9 and 10

After a transformation of the creep stiffness to a log scale, in order to satisfy the conditions of normality and constant variance, a full linear model ANOVA was run for both mixtures 7 and 9 and mixtures 8 and 10. In both cases, all interaction terms were not statistically significant, and only the main effects were further considered. In the following tables the analysis results and the coefficient estimates are presented for the mixtures investigated.

Table 4.24. ANOVA for creep stiffness *S*(*t*) at 60s – mixtures 7 and 9

Source	SS	df	MS	F	**p-value**
Intercept	372.344	1	372.344	55056.0	**0.000**
Temperature	0.434	1	0.434	64.1	**0.000**
Binder	0.045	1	0.045	6.7	**0.018**
Error	0.135	20	0.007		
Total	372.958	23			

Table 4.25. ANOVA for *m*-value at 60s – mixtures 7 and 9

Source	SS	df	MS	F	**p-value**
Intercept	0.428	1	0.428	801.3	**0.000**
Temperature	0.009	1	0.009	17.0	**0.001**
Binder	0.008	1	0.008	14.5	**0.001**
Error	0.011	20	0.001		
Total	0.456	23			

Table 4.26. Coefficient estimates for creep stiffness *S*(*t*) at 60s – mixtures 7 and 9

Coefficients	Estimate	Std. error	t	**p-value**
Intercept	4.214	0.029	143.78	**0.000**
Temperature	-0.275	0.034	-8.01	**0.000**
Binder	-0.089	0.034	-2.59	**0.018**

Table 4.27. Coefficient estimates for *m*-value at 60s – mixtures 7 and 9

Coefficients	Estimate	Std. error	t	**p-value**
Intercept	0.098	0.008	11.94	**0.000**
Temperature	0.040	0.010	4.13	**0.001**
Binder	0.037	0.010	3.81	**0.001**

Table 4.28. ANOVA for creep stiffness *S*(*t*) at 60s – mixtures 8 and 10

Source	SS	df	MS	F	**p-value**
Intercept	375.216	1	375.216	64205.0	**0.000**
Temperature	0.341	1	0.341	58.3	**0.000**
Binder	0.025	1	0.025	4.2	0.054
Error	0.117	20	0.006		
Total	375.699	23			

Table 4.29. ANOVA for *m*-value at 60s – mixtures 8 and 10

Source	SS	df	MS	F	**p-value**
Intercept	0.494	1	0.494	1175.5	**0.000**
Temperature	0.007	1	0.007	16.8	**0.001**
Binder	0.011	1	0.011	26.8	**0.000**
Error	0.008	20	0.000		
Total	0.520	23			

Table 4.30. Coefficient estimates for creep stiffness *S*(*t*) at 60s – mixtures 8 and 10

Coefficients	Estimate	Std. error	t	**p-value**
Intercept	4.202	0.029	145.42	**0.000**
Temperature	-2.44	0.032	-7.64	**0.000**
Binder	-0.065	0.032	-2.04	0.054

Table 4.31. Coefficient estimates for *m*-value at 60s – mixtures 8 and 10

Coefficients	Estimate	Std. error	t	**p-value**
Intercept	0.107	0.008	13.82	**0.000**
Temperature	0.035	0.009	4.10	**0.001**
Binder	0.044	0.009	5.18	**0.000**

Binder PG 52-34 has lower creep stiffness for mixture containing TOSS, while no effect of binder is detectable when MWSS are included in the mix design. However, PG 52-34 binder has higher *m*-values compared to PG 58-28 binder providing an indication of better relaxation properties.

4.2. Thermal Stress and Critical Temperature

One of the most significant pavement distresses in the Northern states of US and in Canada is represented by thermal cracking. Thermal stress (σ_{TS}) starts to increase in the restrained asphalt pavement layers when temperature drops to values well below 0°C. When stress exceeds material strength, cracking occurs in the pavement; the critical value of the temperature at which this phenomenon takes place is called critical temperature, T_{CR}. A brief description of the thermal stress calculation method is hereafter presented. A detailed procedure can be found in Appendix B and in *Basu* (*2002*) and *Moon* (*2010*).

4.2.1. Thermal Stress Computation Method

Assuming a simplified case of a restrained uniaxial viscoelastic beam, thermal strain can be computed as [5.1]:

$$\varepsilon = \alpha \cdot \Delta T \tag*{[5.1]}$$

where:

ε	thermal strain,
α	coefficient of thermal expansion or contraction,
Δt	temperature variation.

Considering the constitutive equation [2.1] and expression [2.4] in Chapter 2, substituting [5.1] into [2.1] and expressing everything in term of reduced time, a general expression for the computation of the thermal stress is obtained [5.2]:

$$\sigma(\xi) = \int_{-\infty}^{\xi} \frac{d\varepsilon(\xi')}{d\xi'} \cdot E(\xi - \xi')d\xi' = \int_{-\infty}^{t} \frac{d(\alpha \Delta T)}{dt'} \cdot E(\xi(t) - \xi'(t))dt' \tag*{[5.2]}$$

where:

$E(\xi - \xi')$	relaxation modulus,
$\varepsilon(\xi')$	strain,
ξ'	integration variable.

In this dissertation the procedure used to calculate the thermal stress involves several steps. First creep stiffness $S(t)$ and, its inverse, creep compliance $D(t)$ are obtained from the BBR experimental deflection data (equation [3.1] and [5.3]):

$$D(t) = \frac{1}{S(t)} \tag*{[5.3]}$$

where:

$D(t)$	creep compliance,
$S(t)$	creep stiffness,
t	time.

Relaxation modulus $E(t)$ is obtained from creep compliance $D(t)$ using *Hopkins and Hamming* (*1957*) method and CAM model (*Marasteanu and Anderson, 1996*) is used to generate relaxation modulus master curves:

$$E(t) = E_g \cdot \left[1 + \left(\frac{t}{t_c} \right)^{v} \right]^{-w/v} \tag*{[5.4]}$$

where:

$E(t)$	relaxation modulus,
E_g	glassy modulus (generally 3GPa for binder and 30GPa for mixtures),
v, w	model parameters,
t_c	cross over time,
t	time.

According to the different test temperatures used during the experimental phase the curve shift factor can be also expressed as:

$$a_T = 10^{C_1 + C_2 \cdot T} \qquad [5.5]$$

where:

C_1 C_2	fitting parameters,
T	reference temperature, °C,

In this thesis only two testing temperatures were used: -6°C, and the reference temperature -18°C. For this reason only one shift factor was required when generating the relaxation modulus master curves.

Thermal stress can then be calculated solving the one dimensional hereditary integral [5.2] with numerical Gaussian quadrature with 24 Gauss (*Basu. A, 2002*).

It must be mentioned that, when BBR binder creep data is used to obtain mixture thermal stress, the values obtained from equation [5.1] have to be multiplied by the empirical Pavement Constant (PC=18) proposed by *Bouldin et al*. (*2000*). If BBR mixture experimental data are available then thermal stresses are calculated directly from equation [5.2].

4.2.2. Critical Temperature Evaluation Method

Thermal stress can be used to determine the critical temperature at which pavement experiences cracking. Two methods are generally available (*Shenoy*, *2002*).

The first requires the use of two experimental devices, Bending Beam Rheometer (BBR) (*AASHTO T313-02, 2006*) and the Direct Tension Tester (*AASHTO T314-02, 2002*) and it is known as dual instrument method (DIM). In the case of asphalt binder critical cracking temperature T_{CR} is obtained at the intersection of thermal stress curve with the strength curve as shown in Figure 4.7. This approach can be also applied to mixtures, however in this dissertation no strength tests were performed on the asphalt mixtures investigated. For this reason the alternative procedure proposed by *Shenoy*, (*2002*) was considered for the evaluation of the critical temperature.

In this method, called single asymptote procedure (SAP) a line is fitted to the lowest temperature part of the thermal stress curve and the intersection with the temperature axis is assumed as critical temperature T_{CR} (Figure 4.8).

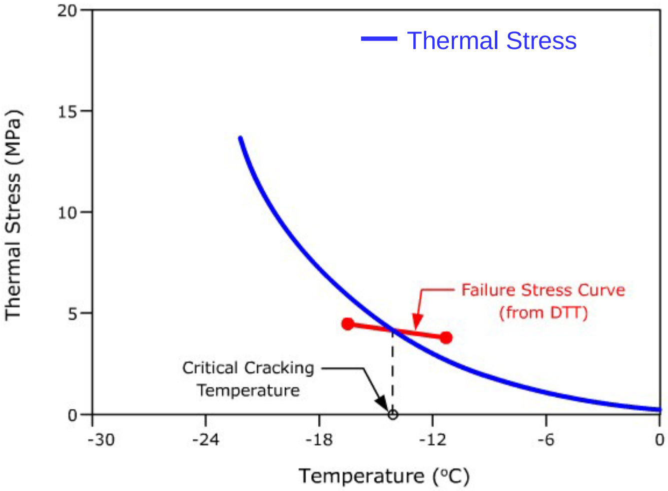

Figure 4.7. Critical temperature T_{CR} – dual instrument method – (*NAPA, 2005*)

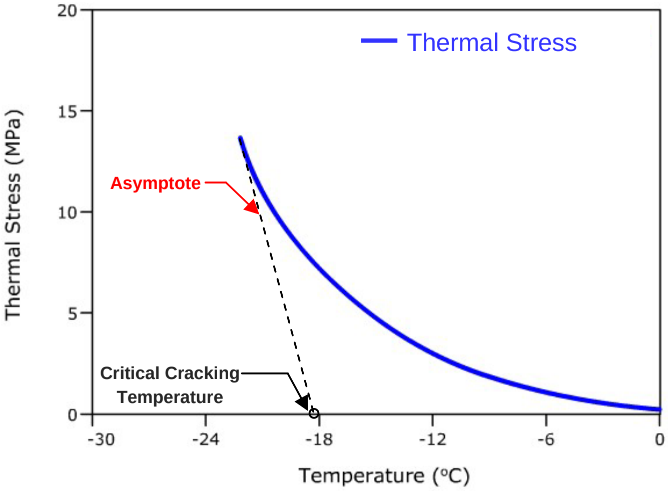

Figure 4.8. Critical temperature T_{CR} – single asymptote method – (*Shenoy, 2002*)

4.2.3. Thermal Stress and Critical Temperature Results Summaries

In this thesis thermal stress was calculated for the case in which the temperature drops from 22°C to -40°C in 0.5°C steps at two different rates: 1°C/h and 10°C/h, respectively. The single asymptote line was fitted to the two final points of the thermal stress curves:

Point 1: (x_{i-1},y_{i-1}) = (-39.5°C, $\sigma_{TS}(-39.5^{o}C)$) and

Point 2: (x_i,y_i) = (-40.0°C, $\sigma_{TS}\,(-40.0^{o}C)$) [5.6]

Table 4.32 presents the average values of thermal stress at the low PG grade corresponding at the testing temperature of -18°C for both cooling rates and the corresponding critical temperatures, T_{CR}. Thermal stress average value was analyzed at the testing temperature of -18°C, corresponding to PG low temperature +10°C, since this was the lowest testing temperature used.

Table 4.32. Critical temperature T_{CR} and thermal stress for all mixtures

Mixture ID	σ_{TS} -1ºC/h (MPa)	σ_{TS} -10ºC/h (MPa)	T_{CR} SAP -1ºC/h ºC	T_{CR} SAP -10ºC/h ºC
1	1.0	1.9	-26.1	-22.7
2	2.1	3.6	-21.7	-18.2
3	2.8	4.5	-20.8	-17.3
4	2.1	3.6	-20.8	-17.5
5	2.3	3.9	-22.2	-18.6
6	3.1	5.0	-17.5	-14.7
7	3.8	5.8	-18.4	-15.4
8	3.8	5.6	-18.2	-15.1
9	1.9	1.7	-22.4	-19.3
10	1.8	3.4	-21.4	-18.0
11	3.6	5.6	-17.5	-14.2
12	3.1	5.0	-17.1	-14.8
13	2.6	4.1	-19.7	-16.8
14	2.0	3.5	-20.8	-17.6
15	1.7	3.0	-22.0	-18.9
16	2.5	4.0	-22.4	-19.0
17	2.3	3.9	-21.3	-17.7

Thermal stress curves including critical temperature (SAP) plots for all the mixtures can be found in Appendix B.

Figures 4.9 and 4.10 present the bar charts of the thermal stress and critical temperatures for all the seventeen mixtures evaluated and for the corresponding temperature cooling rates.

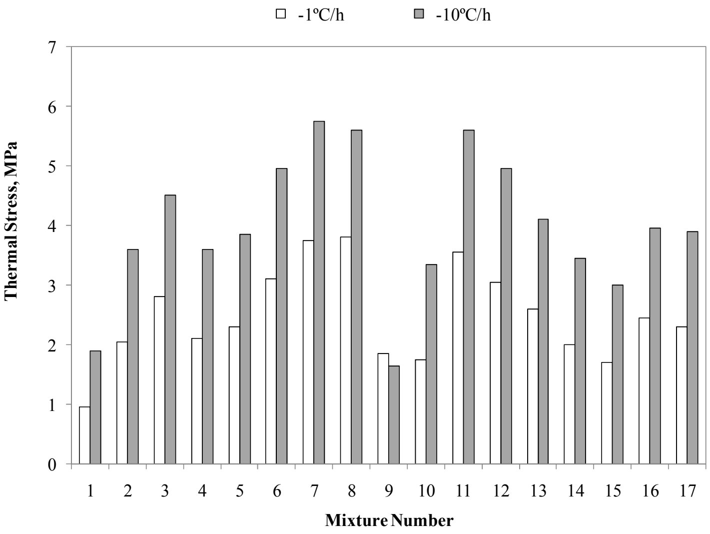

Figure 4.9. Thermal stress

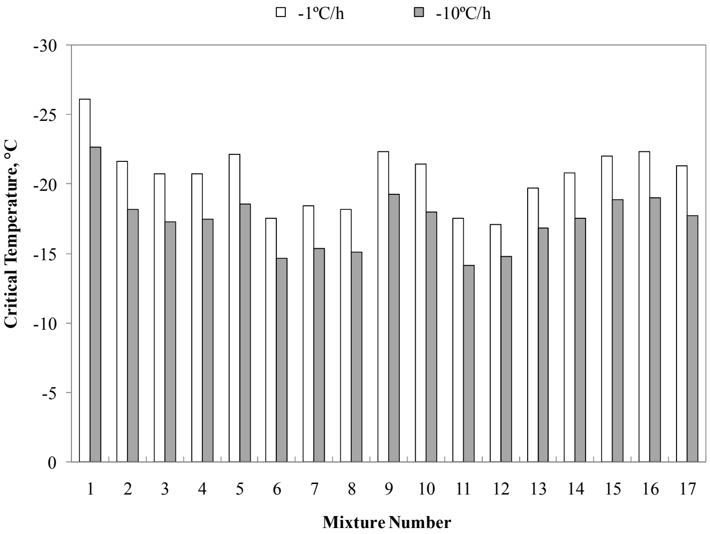

Figure 4.10. Critical temperature

4.2.4. Statistical Analysis

Analogously to what was done for the creep stiffness *S*(*t*) and the *m*-value, different groups of mixtures with common characteristics are analyzed using ANOVA procedure. Thermal stress and critical temperature at PG low temperature +10°C (-18°C) are set as response while RAP, TOSS, MWSS, binder and temperature cooling rate are used as factors. ANOVA analysis based on a linear model is first run and normality and constant variance assumption are evaluated using Box-Cox plot, Residuals plot and Normal Probability plot. If required, a transformation of the response is applied and the analysis is repeated using the transformed data. When interaction terms are not statistically significant, they are pulled into the error term and a reduced linear model is used. From this, a final estimate of *t*-statistic and p-value for each term is obtained assuming a significance level of 0.05.

4.2.4.1. Effect of RAP Amount on Thermal Stress and Critical Temperature

The first four mixtures were selected as in section 4.1.1.1 since they don't include any recycled material other than RAP. Control was assigned to mixture 1 due to the absence of any recycled material in its mix design, while mixtures 2 (15% RAP), 3 (25% RAP) and 4 (30% RAP) are set as test mixtures. Thermal stress and critical temperature (T_{CR}) at PG low temperature +10°C (-18°C) are the selected response for the ANOVA. Amount of RAP (0%, 15%, 25% and 30%) and temperature drop rate (-1°C/h and -10°C/h) are the factors selected for the analysis. Tables 4.2 and 4.33 summarize the experimental design and the average values of the selected responses respectively.

Table 4.33. Thermal stress and critical temperature, T_{CR}, for mixtures 1, 2, 3 and 4

Mixture ID	σ_{TS} -1ºC/h (MPa)	σ_{TS} -10ºC/h (MPa)	T_{CR} SAP -1ºC/h ºC	T_{CR} SAP -10ºC/h ºC
1	1.0	1.9	-26.1	-22.7
2	2.1	3.6	-21.7	-18.2
3	2.8	4.5	-20.8	-17.3
4	2.1	3.6	-20.8	-17.5

Thermal stress and critical temperature (T_{CR}) for mixtures 1, 2, 3 and 4 are shown in Figure 4.11 for the two different cooling rate (-1°C/h and -10°C/h) used during testing.

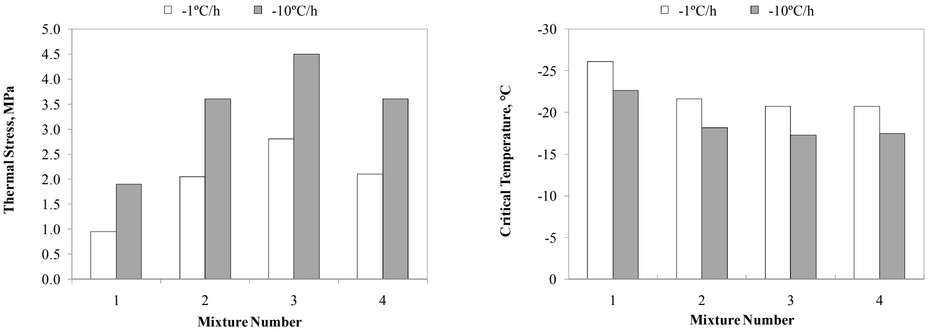

Figure 4.11. Thermal stress and critical temperature, T_{CR}, for mixtures 1, 2, 3 and 4

Normality and constant variance were checked and no transformation was necessary. Full ANOVA including all the interactions between factors (RAP and cooling Rate) was performed showing that the interaction is not significant both for thermal stress and critical temperature analysis. Tables 4.34 to 4.37 present the results of ANOVA and coefficients evaluation.

Table 4.34. ANOVA for thermal stress - mixtures 1, 2, 3 and 4

Source	SS	df	MS	F	**p-value**
Intercept	115.563	1	115.563	983.5	**0.000**
RAP	10.263	3	3.421	29.1	**0.000**
Rate	8.123	1	8.123	69.1	**0.000**
Error	1.293	11	0.118		
Total	135.240	16			

Table 4.35. ANOVA for critical temperature, T_{CR} - mixtures 1, 2, 3 and 4

Source	SS	df	MS	F	**p-value**
Intercept	6789.760	1	6789.760	7284.8	**0.000**
RAP	77.885	3	25.962	27.9	**0.000**
Rate	46.923	1	46.923	50.3	**0.000**
Error	10.253	11	0.932		
Total	6924.820	16			

Table 4.36. Coefficient estimates for thermal stress – mixtures 1, 2, 3 and 4

Coefficients	Estimate	Std. error	t	**p-value**
Intercept	0.712	0.192	3.72	**0.003**
RAP 15%	1.425	0.242	5.88	**0.000**
RAP 25%	2.225	0.242	9.18	**0.000**
RAP 30%	1.400	0.242	5.78	**0.000**
Rate	1.425	0.171	8.31	**0.000**

Table 4.37. Coefficient estimates for critical temperature, T_{CR} - mixtures 1, 2, 3 and 4

Coefficients	Estimate	Std. error	t	**p-value**
Intercept	-26.088	0.540	-48.34	**0.000**
RAP 15%	5.275	0.683	7.73	**0.000**
RAP 25%	5.350	0.683	7.84	**0.000**
RAP 30%	4.475	0.683	6.56	**0.000**
Rate	3.425	0.483	7.10	**0.000**

Both RAP and cooling rate are highly significant for both thermal stress and critical temperature. All the levels of RAP are highly significant too; increasing RAP content cause an increase of thermal stress and of the critical temperature showing a reduced relaxation capability of the mixture. As obvious an increase in cooling rate implies an increase of thermal stress and of the critical temperature as well.

4.2.1.2. Effect of TOSS and MWSS Amounts on Thermal Stress and Critical Temperature

The same mixtures groups used in 4.1.1.2 were analyzed in this section. The experimental design for the two mixture groups evaluated are shown in Tables 4.8 and 4.9

For the two different mixture groups two separated ANOVA's were run; in this way the other factors effect was not influenced by the RAP levels. Cooling rate (-1°C/h and -10°C/h), TOSS (0%, 3% and 5%) and MWSS (0%, 3% and 5%) were set as factors while thermal stress and critical temperature (T_{CR}) at low PG low temperature +10°C (-18°C) are the investigated responses. Tables 4.38 and 4.39 show the average values of the selected responses.

Table 4.38. Thermal stress and critical temperature, T_{CR}, for mixtures 2, 5, 6, 13 and 14

Mixture ID	σ_{TS} -1ºC/h (MPa)	σ_{TS} -10ºC/h (MPa)	T_{CR} SAP -1ºC/h ºC	T_{CR} SAP -10ºC/h ºC
2	2.1	3.6	-21.7	-18.2
5	2.3	3.9	-22.2	-18.6
6	3.1	5.0	-17.5	-14.7
13	2.6	4.1	-19.7	-16.8
14	2.0	3.5	-20.8	-17.6

Table 4.39. Thermal stress and critical temperature, T_{CR}, for mixtures 3, 7, 8, 11 and 12

Mixture ID	σ_{TS} -1ºC/h (MPa)	σ_{TS} -10ºC/h (MPa)	T_{CR} SAP -1ºC/h ºC	T_{CR} SAP -10ºC/h ºC
3	2.8	4.5	-20.8	-17.3
7	3.8	5.8	-18.4	-15.4
8	3.8	5.6	-18.2	-15.1
11	3.6	5.6	-17.5	-14.2
12	3.1	5.0	-17.1	-14.8

Figures 4.12 and 4.13 show the histograms of the thermal stress and critical temperature for mixtures 2, 5, 6, 13 and 14 and or mixtures 3, 7, 8, 11 and 12 for the two cooling rate assumed (-1°C/h and -10°C/h).

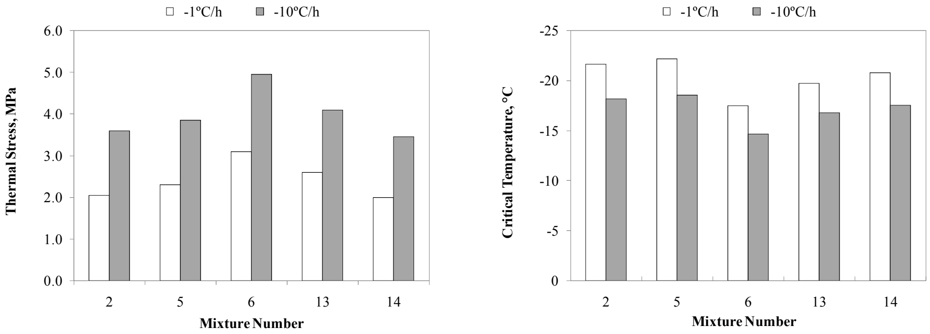

Figure 4.12. Thermal stress and critical temperature, T_{CR}, for mixtures 2, 5, 6, 13 and 14

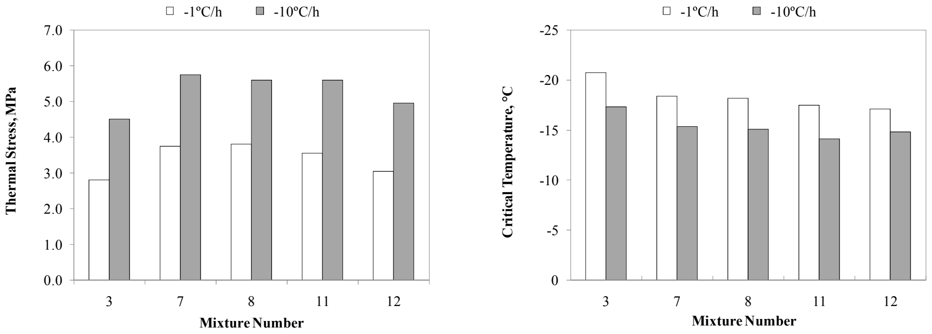

Figure 4.13. Thermal stress and critical temperature, T_{CR}, for mixtures 3, 7, 8, 11 and 12

Assumptions of normality and constant variance were verified. In the case of mixtures 2, 5, 6, 13 and 14 no transformation was required for thermal stress response while the Box-Cox showed that critical temperature was just outside the 95% confidence interval and thus a simple log transformation was used to normalize the data. That was not true in the case of mixtures 3, 7, 8, 11 and 12 were no transformation was needed both for thermal stress and critical temperature. However to have a fair comparison critical temperature was log transformed since also after transformation the experimental data of T_{CR} were inside the 95% confidence interval suggested by the Box-Cox plot.

After a first analysis of variance it was found that all the possible interactions terms between factors were statistically not significant at a 0.05 level. A reduced linear model including only the main effect was then assumed both for thermal stress and critical temperature for both mixtures 2, 5, 6, 13 and 14 and mixtures 3, 7, 8, 11 and 12.

Tables 4.40 to 4.43 show the ANOVA results and the coefficients estimates for thermal stress and critical temperature in the case of mixtures 2, 5, 6, 13 and 14, when the reduced model is applied.

Table 4.40. ANOVA for thermal stress – mixtures 2, 5, 6, 13 and 14

Source	SS	df	MS	F	**p-value**
Intercept	77.224	1	77.224	331.6	**0.000**
TOSS	3.362	2	1.681	7.2	**0.007**
MWSS	0.552	2	0.276	1.2	0.335
Rate	12.013	1	12.013	51.6	**0.000**
Error	3.260	14	0.233		
Total	211.830	20			

Table 4.41. ANOVA for critical temperature, T_{CR} - mixtures 2, 5, 6, 13 and 14

Source	SS	df	MS	F	**p-value**
Intercept	60.570	1	60.570	8773.9	**0.000**
TOSS	0.097	2	0.048	7.0	**0.008**
MWSS	0.003	2	0.002	0.2	0.805
Rate	0.145	1	0.145	21.0	**0.000**
Error	0.097	14	0.007		
Total	172.577	20			

Table 4.42. Coefficient estimates for thermal stress – mixtures 2, 5, 6, 13 and 14

Coefficients	Estimate	Std. error	t	**p-value**
Intercept	2.050	0.264	7.76	**0.000**
TOSS 3%	1.200	0.341	3.52	**0.003**
TOSS 5%	0.175	0.341	0.51	0.616
MWSS 3%	0.250	0.341	0.73	0.476
MWSS 5%	-0.275	0.341	-0.81	0.434
Rate	1.550	0.216	7.18	**0.000**

Table 4.43. Coefficient estimates for critical temperature, T_{CR} - mixtures 2, 5, 6, 13 and 14

Coefficients	Estimate	Std. error	t	**p-value**
Intercept	3.069	0.046	67.44	**0.000**
TOSS 3%	-0.219	0.059	-3.73	**0.002**
TOSS 5%	-0.095	0.059	-1.61	0.130
MWSS 3%	0.025	0.059	0.42	0.678
MWSS 5%	0.038	0.059	0.66	0.523
Rate	-0.170	0.037	-4.59	**0.000**

In the case of thermal stress only, TOSS and cooling rate are statistically significant (Table 4.40). An increase in TOSS causes an increase in thermal stress, but only for a 3% content as is shown in table 4.42. Critical temperature is also affected by temperature cooling rate and TOSS content, but only up to 3%, beyond which no significant variation in the response is expected. MWSS is not statistically significant for both levels.

The ANOVA results and the coefficients estimates for thermal stress and critical temperature in the case mixtures 3, 7, 8, 11 and 12 are presented in Tables 4.44 to 4.47.

Table 4.44. ANOVA for thermal stress – mixtures 3, 7, 8, 11 and 12

Source	SS	df	MS	F	**p-value**
Intercept	165.313	1	165.313	381.5	**0.000**
TOSS	2.795	2	1.398	3.2	0.070
MWSS	2.287	2	1.143	2.6	0.107
Rate	17.861	1	17.861	41.2	**0.000**
Error	6.067	14	0.433		
Total	403.550	20			

Table 4.45. ANOVA for critical temperature, T_{CR} - mixtures 3, 7, 8, 11 and 12

Source	SS	df	MS	F	**p-value**
Intercept	53.785	1	53.785	8977.8	**0.000**
TOSS	0.072	2	0.036	6.0	**0.013**
MWSS	0.070	2	0.035	5.8	**0.015**
Rate	0.164	1	0.164	27.4	**0.000**
Error	0.084	14	0.006		
Total	158.996	20			

Table 4.46. Coefficient estimates for thermal stress – mixtures 3, 7, 8, 11 and 12

Coefficients	Estimate	Std. error	t	**p-value**
Intercept	2.705	0.361	7.50	**0.000**
TOSS 3%	1.100	0.465	2.36	**0.033**
TOSS 5%	0.925	0.465	1.99	0.067
MWSS 3%	1.050	0.465	2.26	**0.041**
MWSS 5%	0.350	0.465	0.75	0.465
Rate	1.890	0.294	6.42	**0.000**

Table 4.47. Coefficient estimates for critical temperature, T_{CR} – mixtures 3, 7, 8, 11 and 12

Coefficients	Estimate	Std. error	t	**p-value**
Intercept	3.032	0.042	71.53	**0.000**
TOSS 3%	-0.120	0.055	-2.20	**0.045**
TOSS 5%	-0.187	0.055	-3.41	**0.004**
MWSS 3%	-0.144	0.055	-2.62	**0.020**
MWSS 5%	-0.175	0.055	-3.19	**0.007**
Rate	-0.181	0.035	-5.24	**0.000**

From the general ANOVA table (Table 4.44) neither TOSS nor MWSS appear to be statistically significant for thermal stress. However also for mixtures 3, 7, 8, 11 and 12 as for the previous group of mixtures (2, 5, 6, 13 and 14) those results mask the fact that both TOSS and MWSS are significant up to 3% content inducing an increase in thermal stress. Cooling rate is statistically significant as well.

TOSS and MWSS are both affecting the critical temperature. This is shown by the ANOVA table and the coefficients estimate. As for thermal stress, a temperature cooling rate increment is positively correlated with the critical temperature.

4.2.1.3. Effect of Binder Type on Thermal Stress and Critical Temperature

The same mixtures analyzed in 4.1.1.3 are used hereafter (mixtures 7 and 9 and mixtures 8 and 10). Binders PG 58-28 and PG 52-34 were used to prepare them; the same amount of RAP, 25%, is present in each mixture. The mixtures experimental design is shown in Tables 4.20 and 4.21. Thermal stress and critical temperature are used in this analysis as response while PG and cooling rate are set as factors. The average values of the response are summarized in Tables 4.48 and 4.49 while Figure 4.14 shows the histograms of responses for the mixtures evaluated.

Table 4.48. Thermal stress and critical temperature, T_{CR}, for mixtures 7 and 9

Mixture ID	σ_{TS} -1ºC/h (MPa)	σ_{TS} -10ºC/h (MPa)	T_{CR} SAP -1ºC/h ºC	T_{CR} SAP -10ºC/h ºC
7	3.8	5.8	-18.4	-15.4
9	1.9	1.7	-22.4	-19.3

Table 4.49. Thermal stress and critical temperature, T_{CR}, for mixtures 8 and 10

Mixture ID	σ_{TS} -1ºC/h (MPa)	σ_{TS} -10ºC/h (MPa)	T_{CR} SAP -1ºC/h ºC	T_{CR} SAP -10ºC/h ºC
8	3.8	5.6	-18.2	-15.1
10	1.8	3.4	-21.4	-18.0

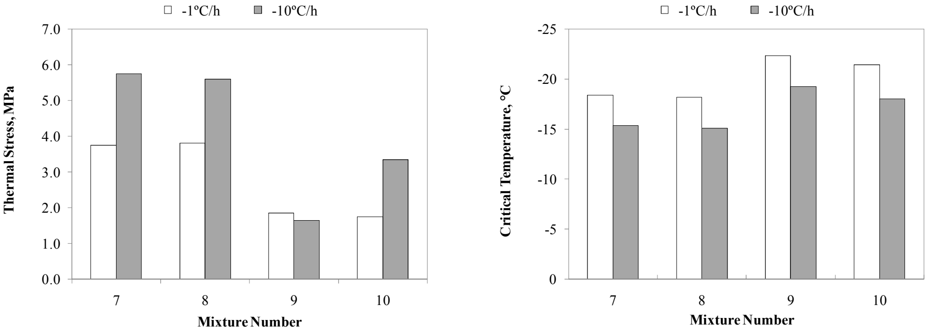

Figure 4.14. Thermal stress and critical temperature, T_{CR}, for mixtures 7, 8, 9 and 10

No transformation of the thermal stress and critical temperature was required to satisfy normality and constant variance for both mixtures 7 and 9 and mixtures 8 and 10. The full ANOVA model showed that for all the responses no interaction term between PG and cooling rate was statistically significant. Tables 4.50 to 4.57 present the analysis results and the coefficient estimates for the mixtures investigated.

Table 4.50. ANOVA for thermal stress – mixtures 7 and 9

Source	SS	df	MS	F	**p-value**
Intercept	106.580	1	106.580	124.5	**0.000**
Binder	9.680	1	9.680	11.3	**0.020**
Rate	5.780	1	5.780	6.8	**0.048**
Error	4.280	5	0.856		
Total	126.320	8			

Table 4.51. ANOVA for critical temperature, T_{CR} – mixtures 7 and 9

Source	SS	df	MS	F	**p-value**
Intercept	2838.811	1	2838.811	18769.0	**0.000**
Binder	30.811	1	30.811	203.7	**0.000**
Rate	18.911	1	18.911	125.0	**0.000**
Error	0.756	5	0.151		
Total	2889.290	8			

Table 4.52. Coefficient estimates for thermal stress – mixtures 7 and 9

Coefficients	Estimate	Std. error	t	**p-value**
Intercept	3.900	0.567	6.88	**0.001**
Binder	-2.200	0.654	-3.36	**0.020**
Rate	1.700	0.654	2.60	**0.048**

Table 4.53. Coefficient estimates for critical temperature, T_{CR} – mixtures 7 and 9

Coefficients	Estimate	Std. error	t	**p-value**
Intercept	-18.413	0.238	-77.31	**0.000**
Binder	-3.925	0.275	-14.27	**0.000**
Rate	3.075	0.275	11.18	**0.000**

Table 4.54. ANOVA for thermal stress – mixtures 8 and 10

Source	SS	df	MS	F	**p-value**
Intercept	105.125	1	105.125	3091.9	**0.000**
Binder	9.245	1	9.245	271.9	**0.000**
Rate	5.780	1	5.780	170.0	**0.000**
Error	0.170	5	0.034		
Total	120.320	8			

Table 4.55. ANOVA for critical temperature, T_{CR} – mixtures 8 and 10

Source	SS	df	MS	F	**p-value**
Intercept	2639.011	1	2639.011	359.1	**0.000**
Binder	18.911	1	18.911	2.6	0.170
Rate	20.801	1	20.801	2.8	0.153
Error	36.746	5	7.349		
Total	2715.470	8			

Table 4.56. Coefficient estimates for thermal stress – mixtures 8 and 10

Coefficients	Estimate	Std. error	t	**p-value**
Intercept	3.850	0.113	34.10	**0.000**
Binder	-2.150	0.130	-16.49	**0.000**
Rate	1.700	0.130	13.04	**0.000**

Table 4.57. Coefficient estimates for critical temperature, T_{CR} – mixtures 8 and 10

Coefficients	Estimate	Std. error	t	**p-value**
Intercept	-18.238	1.660	-10.99	**0.000**
Binder	-3.075	1.917	-1.60	0.170
Rate	3.225	1.917	1.68	0.153

In the case of mixtures 7 and 9, both binder type (PG) and cooling rate are significant at 0.05 level both for thermal stress and critical temperature. Moreover, the Performance Grade (PG) is negatively correlated with the responses, meaning that using a softer binder (PG 52-34) decreases the critical temperature and the stress at the reference low PG grade for the control binder (58-28) that in this case is equal to -18°C.

The same conclusions are not valid in the case of mixtures 8 and 10. In fact, while a softer binder reduces thermal stress, as well as a slower rate, it seems that critical temperature is unaffected by rate and PG. It must be notice that for the same amount of RAP (25%) mixtures 7 and 9 contain 5% of TOSS while mixtures 8 and10 contains 5% of MWSS. This may be the reason why no significant effect in critical temperature is detected when changing binder grade in the last two mixtures.

Chapter 5. Image Analysis

This chapter is divided into three parts. In the first part a short introduction to the digital image processing is proposed and the results for the estimation of the volume fraction of the aggregate phase for the seventeen mixtures evaluated in this thesis are presented. In the second part a simple grain size distribution estimation procedure is outlined and visual comparisons between some of the investigated mixtures with common characteristics as RAP, MWSS and TOSS are shown. Finally two- and three-point correlation functions are obtained for all the mixtures based on a numerical procedure.

5.1. Digital Image Processing

The internal structure of heterogeneous materials as asphalt mixtures can be described and quantified by processing digital images of the materials. A digital image can be considered as a two-dimensional discrete function $f(x,y)$, where f is the intensity of the image at that point (x,y) and x and y are spatial its coordinates. Pixels are the elements that from a digital image; each pixel has a specific location and intensity value (*Gonzales et al. 2004*).

An image can be represented by pixel matrix; in the case of binary images the intensity can take the values of 0 for black pixels and 1 for white pixels. The matrix representation of and $M \times N$ binary image is shown in Figure 5.1.

$$f(x,y)=\begin{bmatrix} f(0,0) & f(0,1) & . & f(0,N-1) \\ f(1,0) & f(1,1) & . & f(1,N-1) \\ . & . & . & . \\ f(M-1,0) & f(M-1,1) & . & f(M-1,N-1) \end{bmatrix}$$

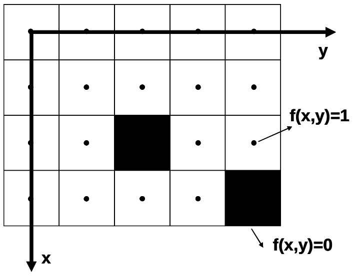

Figure 5.1. Matrix representation and schematic of a M × N binary image (*Velasquez et al., 2010*)

Digital image processing (DIP) involves different manipulation tools; they usually are mathematical functions as filters or geometric transformation that are applied to the matrix that is behind the image representation.

Eriksen and Wegan (*1993*) were among the first to make use of image analysis to characterize the microstructure of asphalt mixtures. In their work they use images of asphalt binders and asphalt mixtures to investigate the microstructure. *Yue et al*. (*1995*) estimated gradation, shape, and orientation of aggregates in asphalt mixtures using digital image processing.

Digital image analysis and X-ray tomography was used by *Masad et al.* (*1999*) to characterize the internal structure of asphalt mixtures prepared in the laboratory with the Superpave Gyratory Compactor at different compaction levels. After measuring aggregate orientation, gradation, and air void distribution, they concluded that aggregates tend to have a preferred orientation up to a certain level of compaction, after which aggregates tend to be randomly distributed.

Traditional and digital image processing methods for characterization of the internal structure of asphalt mixtures were compared by *Masad and Button* (*2004*). The distribution of the aggregates, air voids, and voids in the mineral aggregate (VMA) were quantified with conventional volumetric methods that rely on bulk measurements of the material and digital imaging methods. Camera and an X-ray computed tomography system were used to capture two- and three- dimensional images respectively. It was found that image analysis can be use to study differences among compaction methods in the laboratory, to improve the laboratory method in connection with what is done in the field, and to evaluate the prediction of the asphalt mixtures permeability.

Aggregate orientations and their effects on engineering properties of asphalt mixtures were also well investigated in other works and characterized using imaging techniques (*Masad et al., 1998*; *Chen et al., 2001, 2002, 2005*). More automated techniques were proposed by *Kose et al*., (*2000*), *Yue et al.*, (*2003*), *Offrell and Magnusson*, (*2004*) where the manual/subjective component of the analysis (usually the selection of the gray scale or black and white threshold) is correlated with experimental results.

Zelelew et al., (*2008*) and *Zelelw* (*2008*) used X-ray CT images to characterize and reconstruct the microstructure of asphalt mixture. An improved volumetric threshold algorithm based on global minima percent error and volumetric properties of asphalt mixture was implemented for the purpose.

More Recently *Velasquez* (*2009*) and *Velasquez et al*., (*2010*) used Digital Image Processing to obtain volumetric, microstructure and RVE (Representative Volume Element) information on asphalt mixtures to use it as input in micromechanical models.

5.1.1. Digital Processing Procedure

A CanoScan D2400u scanner was used to acquire the color (RGB) images of the BBR small thin beams on the four major surfaces. However the resolution used was limited to 300dpi due hardware and software compatibility issues and also to reduce the amount of disk space required to store all the images. This resolution allows for detection of aggregates larger than 85 μm. Since sieve #200 corresponds to 75 μm and sieve #100 corresponds to 150 μm it is more realistic to expect to be able to detect aggregates larger then sieve #100.

The following procedure was implemented using MATLAB Image Processing Toolbox (*2008*) to convert RGB images of asphalt concrete to binary images, black (0) represents voids + asphalt binder + aggregates smaller than 150 μm and where white (1) represents aggregates larger than 150 μm.

1) Function *rgb2gray* is used to convert the original RGB image (Figure 5.2a) to gray scale (Figure 5.2b).
2) Function *histeq* is applied to perform histogram equalization and enhance contrast between the two phases (asphalt mastic and aggregates). The gray scale pixel values are transformed in such a way that the histogram of the transformed image is uniform (Figure 5.2c).
3) In order to reduce the noise present in the image, especially in large aggregates, maximum spatial filter function, *ordfilt2*, was used (Figure 5.2d). This function is a non-linear spatial filter based on the ranking of the pixels contained in the specific region of the image. The pixel located in the center of that specific region is replaced with the value found from the ranking analysis (*Gonzales et al.*, *2004*).
4) Finally function *im2bw* is applied to convert the gray scale image to a binary image assuming an average threshold of 0.35 (Figure 5.2e). Threshold value selection is a well known problem in digital image analysis of asphalt concrete mainly due to the difficulty arises from the fact that aggregates in the mix have different colors

depending on their origin. Dark colored aggregates can potentially be confused for asphalt binder in the analysis. However the threshold in this case was selected based the on the known value of VMA (Voids in the Mineral Aggregate) and VFA (Voids Filled with Asphalt) and on the image resolution. Since it was known that aggregates smaller than 150μm couldn't be detected and that they would became part of the mastic (black phase) a threshold value of 0.35 was found appropriate also taking into account that all the mixtures have very similar VFA and VMA values.

Figure 5.2 presents the output example of the digital image analysis procedure used in this thesis for one side of a asphalt mixture BBR beam.

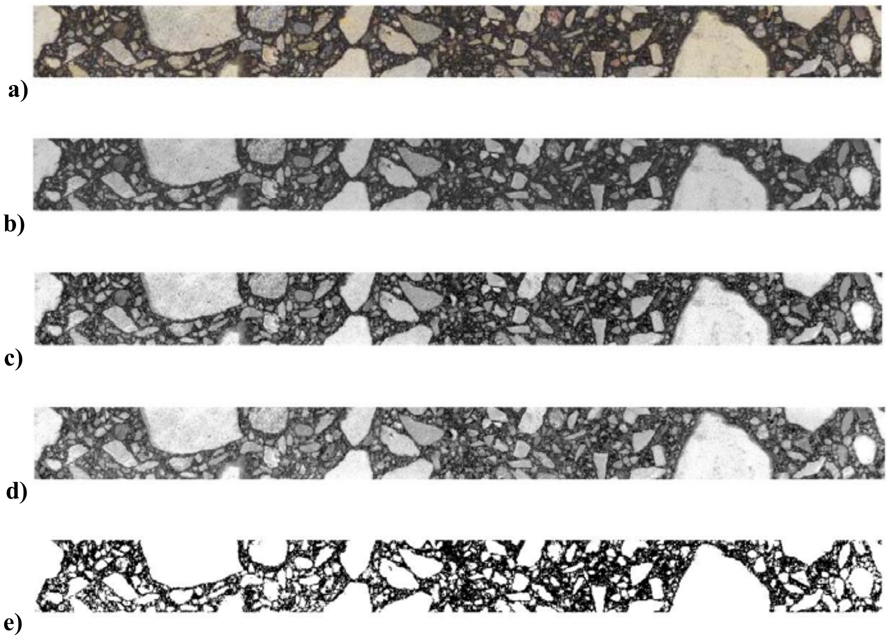

Figure 5.2. Digital processing of asphalt mixture BBR beam images

5.1.2. Volume Fraction

Volume fractions can be obtained from area fractions when a sufficient large number of two-dimensional sections of the material are used (*Underwood*, *1970)*. However, as a mentioned before, due to the images resolution (300dpi), aggregates smaller than 150 μm (i.e. passing sieve #100) can not be detected and thus the volumetric fractions of the aggregates obtained from the two-dimensional binary images are an underestimation of the real value. In the binary image, represented by a matrix of ones and zeros, the aggregate phase is represented by an intensity value of one. The total volumetric fraction of the aggregate can be estimated as the ratio between the sum of all the elements of the binary matrix and its size (i.e. M x N). For each replicate - BBR asphalt mixture beam - the volumetric fraction was obtained as the average between the two larger sides of the specimen (~115 × 11.8 mm). Then the volumetric fraction for each mixture was calculated averaging the volumetric fraction of the twelve replicates (six for each slice of mixture obtained from the gyratory compacted specimen as described in Chapter 3). Table 5.1 and Figure 5.3 present the value of the volumetric fraction for the seventeen mixtures investigated and the corresponding coefficient of variation.

Table 5.1. Estimated aggregates volumetric fraction and CV's

Mixture ID	Volumetric Fraction %	CV %
1	75.8	1.43
2	74.9	2.12
3	76.4	1.78
4	75.4	1.30
5	75.5	2.21
6	76.8	1.60
7	75.8	0.99
8	75.2	1.03
9	76.7	1.85
10	75.3	2.86
11	75.8	1.83
12	77.0	1.15
13	77.4	1.99
14	77.6	1.25
15	77.5	1.67
16	76.9	1.76
17	75.7	2.62

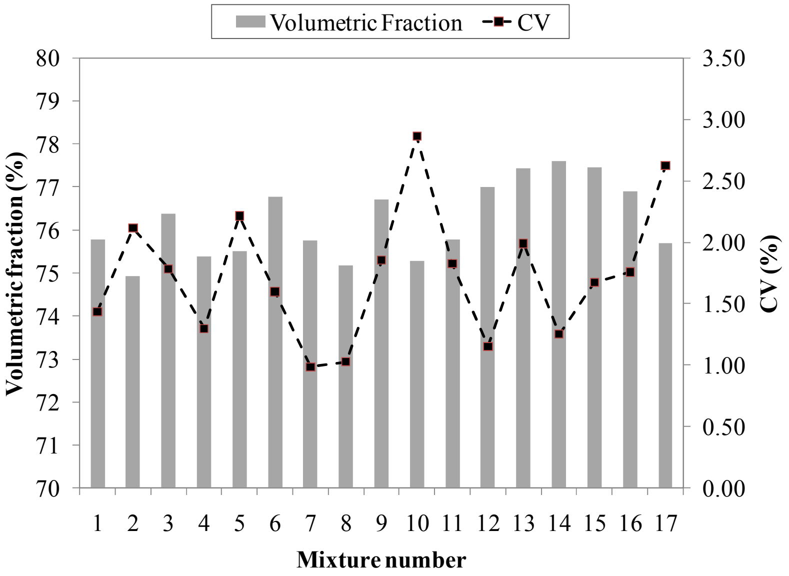

Figure 5.3. Estimated mixtures volumetric fraction and CV's

Since from Table 5.1 the values of the volumetric fractions didn't seem to be very different from mixture to mixture, an ANOVA analysis was run to verify it and a pairwise comparison of the mixtures based on the volumetric fraction was also performed. It was found that there is no statistically significant difference between the different mixtures evaluated meaning that probably all the mixtures were designed with a very similar amount of aggregates even though different recycled material are added.

5.2. Grain Size Distribution

It is known that true particle size distribution of mixtures containing irregular particles, such as asphalt concrete, can not be obtained from 2D image. *Schafer and Teyssen* (*1987*) demonstrated that aggregate size distributions extracted from two-dimensional sections are generally biased towards the finer side due to the random cut of the aggregates. However, two-dimensional approximations of the grain size distribution can be useful to compare gradations from different type of mixtures and provide a indicative idea on how the asphalt mixtures differ.

Some difficulties may arise when estimating the grain size distribution contained in an asphalt mixture specimen from two-dimensional images:

- Not detecting smaller particles due to the resolution of the images,
- Recognizing two or more particles in contact as one large particle,
- Assuming that the irregular geometry of the particles is described by ellipses or circles.

In this thesis the procedure proposed by *Velasquez* (*2009*) was adopted and the grain size distribution of BBR asphalt mixture beams specimens was estimated using *ImageJ v.1.43* (*2010*), a public domain *Java* (*Java 1.6.0_10, 2010*) image processing program. The following procedure, implemented into a macro, is used for the calculation of the gradation curves (*Velasquez, 2009*):

- The original RGB (color) image is converted to gray scale (Figure 5.4a).
- A smooth filter that replaces each pixel with the average of its 3 x 3 neighborhood is applied to the gray scale image (Figure 5.4b).
- Histogram equalization of the original image is applied to enhance contrast (Figure 5.4c)
- The conversion of gray scale image to a binary image is performed using a threshold cut off and pixels from the edges of black objects are removed by an erosion procedure (Figure 5.4d).
- After deselecting the particles edges in the binary image and the area of each particle is calculated. Then, by assuming that particles are circles, the size of each particle is estimated by calculating its diameter.

Obviously, the assumption of having spherical particles, introduces a large degree of approximation in the calculations. However, for the purpose of this thesis, it was considered appropriate since no further investigation on the orientation of the aggregates is performed. A more advanced and precise technique was proposed by the *University of Wisconsin* in an AASHTO draft standard (*2010*).

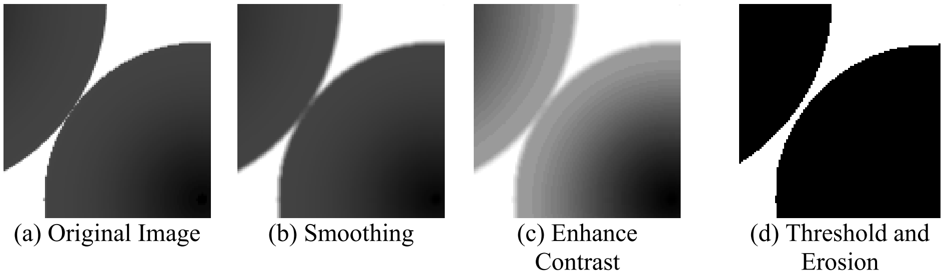
(a) Original Image (b) Smoothing (c) Enhance Contrast (d) Threshold and Erosion

Figure 5.4. Digital image procedure for grain size distribution – (*Velasquez, 2009*)

Velasquez (*2009*) investigated the error obtained from using the previous procedure when several particles are or are not in contact from a computer-generated material with known particle size distribution. It was found that the gradation curves for the computer-generated material with and without contacting particle are similar with a slight difference of 5% for the percent passing of particles with 0.6 mm size (Figure 5.5).

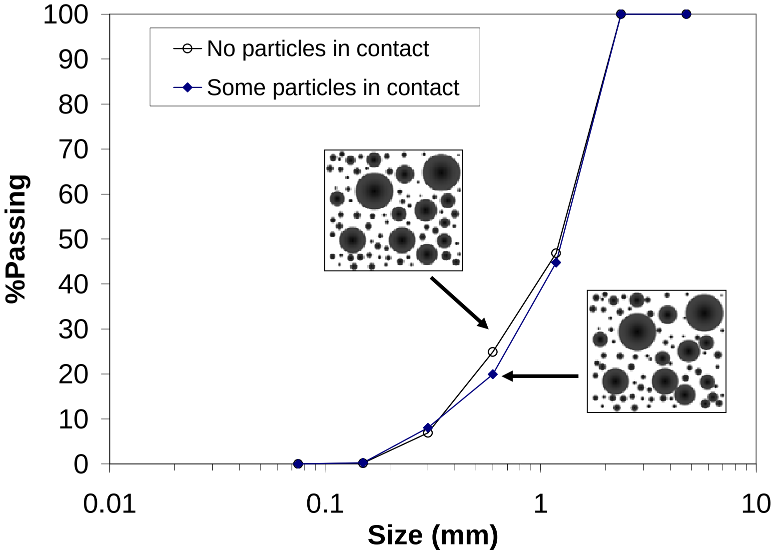

Figure 5.5. Grain size distribution for computer-generated material – (*Velasquez, 2009*)

The gradation of the material containing some particles in contact was slightly coarser than the gradation of the same material with no particles in contact. This result suggested that the proposed procedure for estimation of grain size distribution was unable to remove all possible contact between particles, however a good estimation of the gradation of the mixtures investigated was obtained by using this procedure.

The grain size distribution for each asphalt mixtures BBR beam specimen used in this thesis was obtained as the average of the grain size distribution calculated on both major sides of the beams (~115 × 11.8 mm). The average gradation curves calculated from twelve replicates (six BBR asphalt mixtures beams from each of the two asphalt mixture slices cut from two gyratory compacted specimen respectively for each mixture type) and the corresponding coefficients of variation are presented in Figures 5.6 - 5.14. Appendix C presents the gradation curves for all the specimens from each gyratory cylinder asphalt mixture slice.

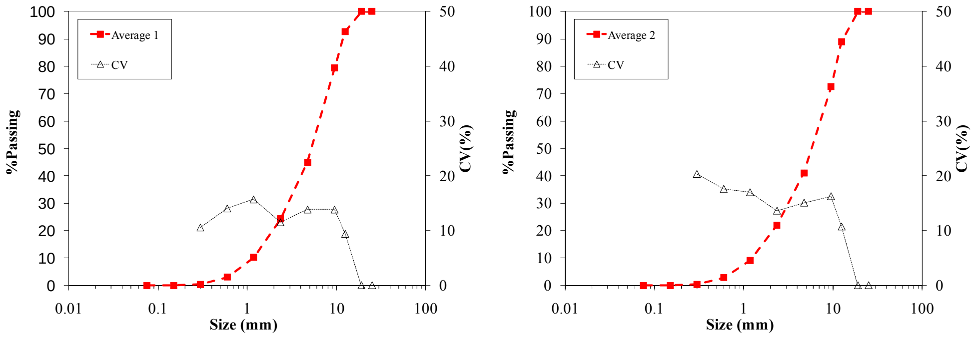

Figure 5.6. Grain size distribution for mixtures 1 and 2 and CV

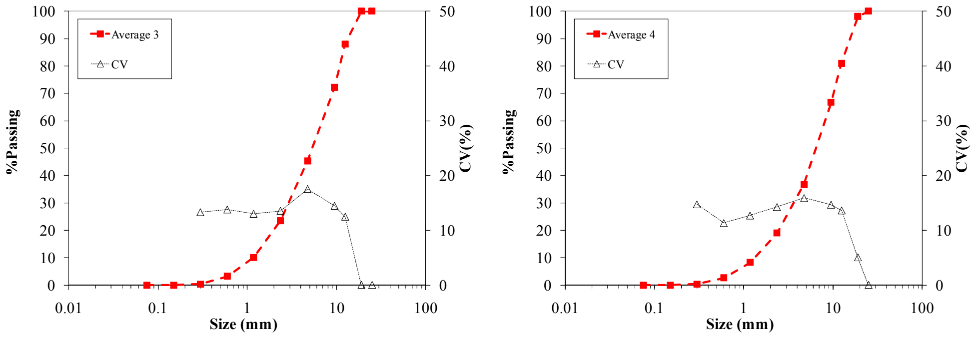

Figure 5.7. Grain size distribution for mixtures 3 and 4 and CV

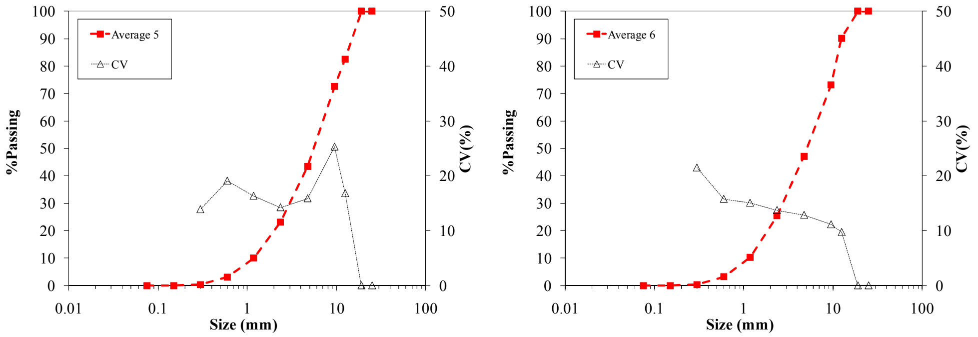

Figure 5.8. Grain size distribution for mixtures 5 and 6 and CV

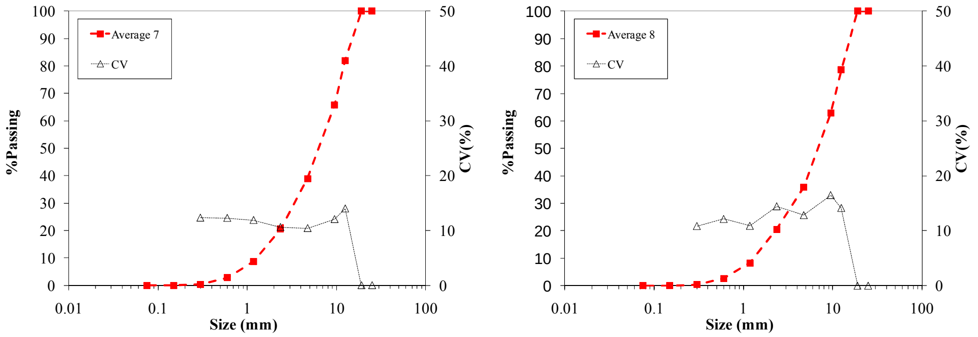

Figure 5.9. Grain size distribution for mixtures 7 and 8 and CV

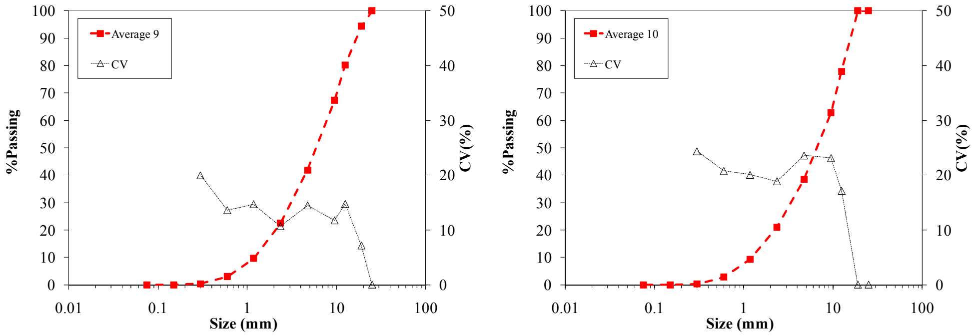

Figure 5.10. Grain size distribution for mixtures 9 and 10 and CV

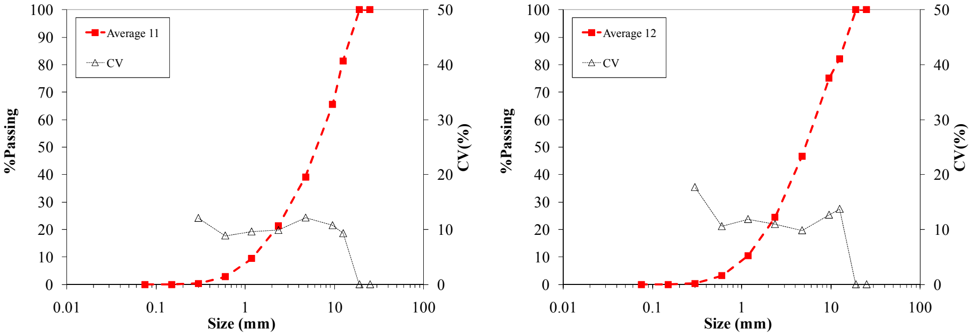

Figure 5.11. Grain size distribution for mixtures 11 and 12 and CV

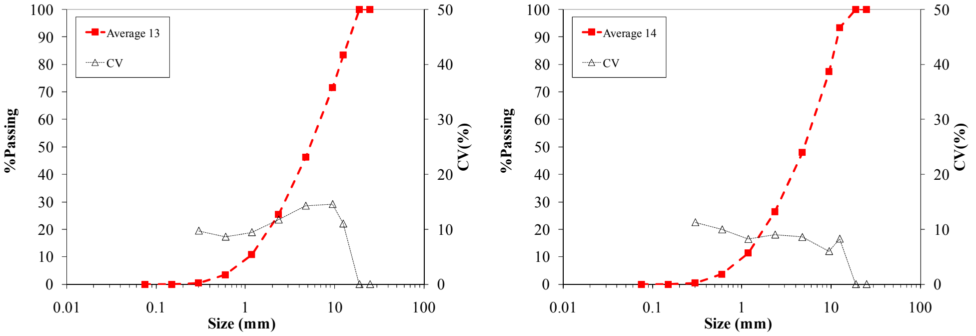

Figure 5.12. Grain size distribution for mixtures 13 and 14 and CV

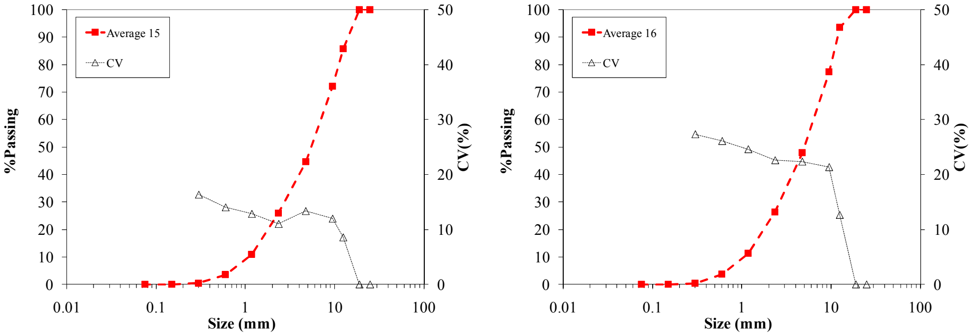

Figure 5.13. Grain size distribution for mixtures 15 and 16 and CV

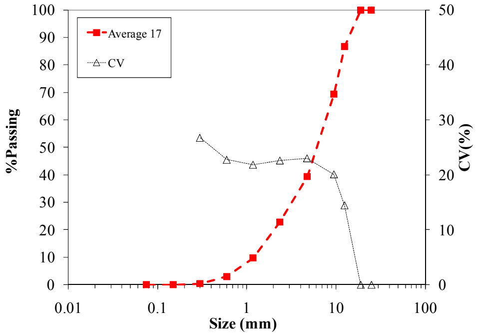

Figure 5.14. Grain size distribution for mixture 17 and CV

A visual comparison the same mixtures groups for which statistical analysis was performed in Chapter 4 are hereafter presented.

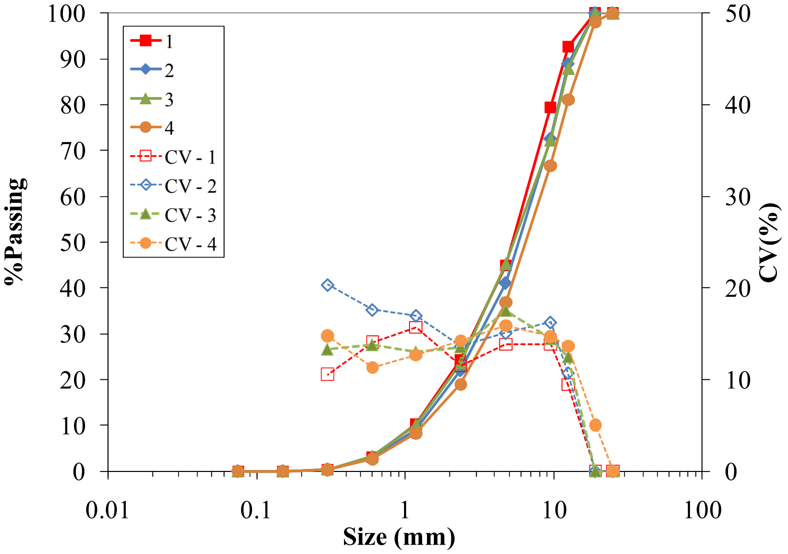

Figure 5.15. Grain size distribution for mixtures 1, 2, 3, and 4 and CV's

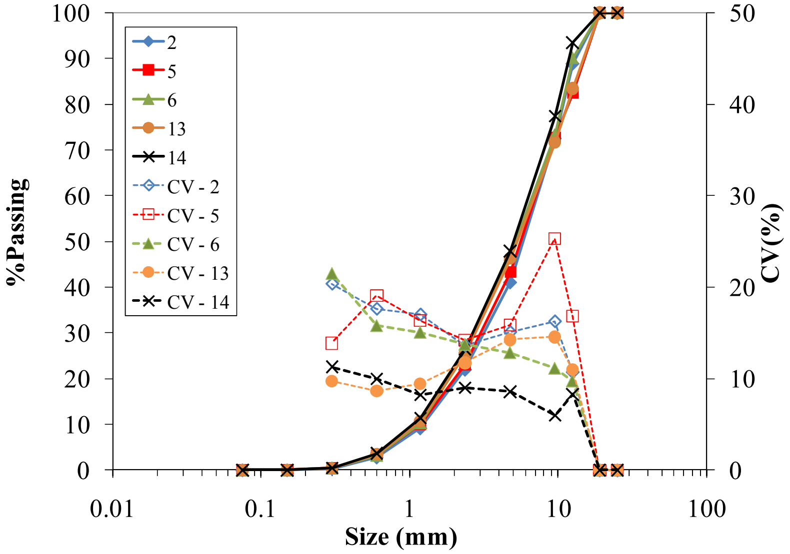

Figure 5.16. Grain size distribution for mixtures 2, 5, 6, 13 and 14 and CV's

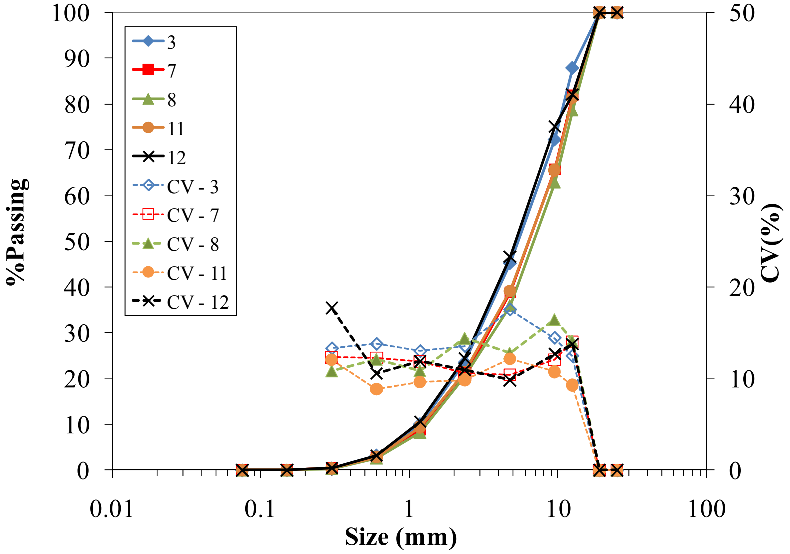

Figure 5.17. Grain size distribution for mixtures 3, 7, 8, 11 and 12 and CV's

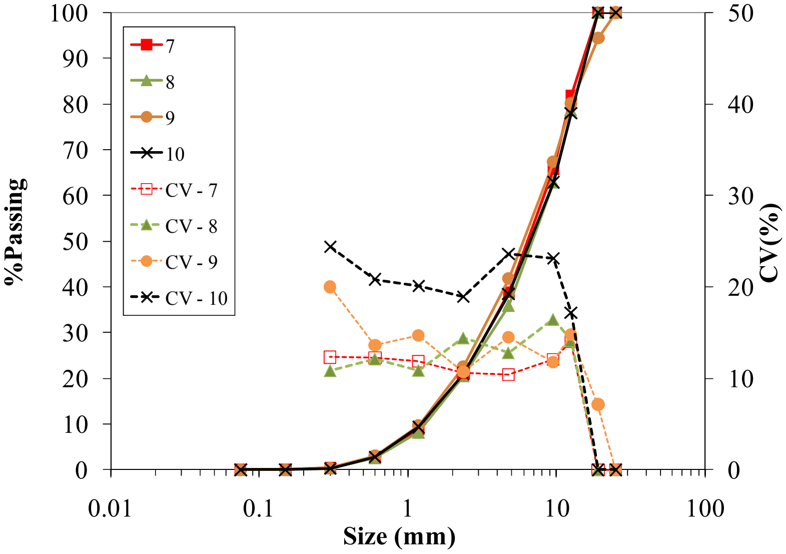

Figure 5.18. Grain size distribution for mixtures 7, 8, 9 and 10 and CV's

From a visual comparison, the gradation curves for the four asphalt mixture groups presented in Figures 5.15, 5.16, 5.17 and 5.18 are very similar. This may suggest that the gradation curves for all mixtures, whether they are made only using virgin material or they contain RAP, TOSS or MWSS recycled material, are very similar.

5.3. *n*-point Correlation Functions

Statistical tools are available to characterize the microstructures of complex materials such as asphalt mixture. *Jiao et al.* (*2007*) found that the effective mechanical and transport properties of heterogeneous materials are function of the microconstituents spatial distribution and not only of their volume fraction. Important information for the calculation of improved upper and lower bounds of the mechanical properties of materials can be obtained from higher-order microstructural functions such as the *n*-point correlation functions (*Torquato 2000*).

In a two-phase heterogeneous material, with the same volume fraction, the spatial distribution of its particles can dramatically affect the mechanical properties, as well as the failure characteristics (*Torquato 2000*). For this reason spatial correlation functions can be used as a tool to identify fluctuations on the microstructure of a heterogeneous material. An example of a

2-point correlation function for two materials with the same volume fraction but with variability on spatial distribution of particles is presented in Figure 5.19.

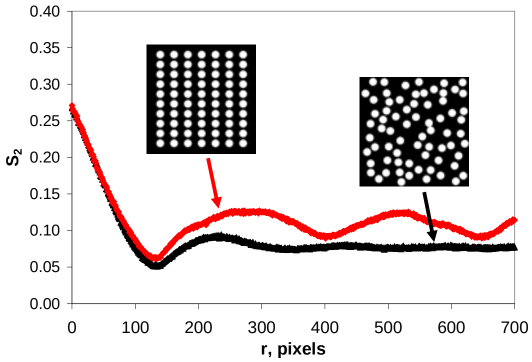

Figure 5.19. 2-pint correlation function for two materials with the same volume fraction and different particles spatial distribution – (*Velasquez, 2009*)

Very similar algorithms to those proposed by *Velasquez* (*2009*) and *Velasquez et al.*, (*2010*) are adopted in this dissertation to estimate the 2- and 3-point correlation functions of asphalt mixtures. These procedures, described in the next sections of this Chapter, make use of Monte Carlo simulations to approximate the correlation functions of the material. The binary images of the BBR asphalt mixtures specimens obtained in section 5.1 are used for the estimation of the spatial correlation functions. However since computation of the 3-point correlation function was prohibitive for a laptop computational power it was decide to simply the algorithm in order to have at least a one dimensional response of this function.

5.3.1. 2-point Correlation Function

The 2- point correlation function can be computed using a discretized expression of equation [2.17] and binary images of the microstructure of the investigated material. The following discretized version of equation [2.17] was proposed by *Berryman* (*1985*) to estimate S_2:

$$\hat{S}_2(x,y) = \frac{1}{(M-x)(N-y)} \sum_{i=1}^{M-x} \sum_{j=1}^{N-y} I(i,j) I(i+x, j+y) \qquad [5.1]$$

where:

M	height of the digital image, and
N	width of the digital image.

The isotropic 2-point correlation function $S_2(k)$ is calculated as the average of the values of $S_2(x, y)$ at a fixed radius k, where $S_2(x, y)$ is the two-dimensional estimate provided by equation [5.1]. However, since the values of $S_2(x, y)$ are generally not known at the specific points of interest, *Berryman* (*1985*) introduced the following function:

$$\bar{S}_2(k,\theta) \equiv \hat{S}_2(k\cos\theta, k\sin\theta) \qquad [5.2]$$

When $k \cdot cos\theta$ and $k \cdot sin\theta$ are not integers, bilinear interpolation can be applied to the right-hand side of equation [5.2]. Knowing the values of [5.2], the average 2-point correlation function can be evaluated as:

$$S_2(k) = \frac{1}{2k+1}\sum_{l=0}^{2k}\bar{S}_2\left(k, \frac{\pi l}{4k}\right) \qquad [5.3]$$

where:

k	less than or equal to half of the minimum dimension of the image.

However for high resolution images containing a large number of pixels, a brute force method is computationally very expensive and therefore prohibited to use in an extensive experimental program especially if the computational power available is that of a standard laptop. For this reason an alternative approach is represented by Monte Carlo simulations; this can be used to estimate the 2-point correlation function of heterogeneous materials at a lower computational cost in comparison to brute force methods.

For the 2-point correlation, the algorithm drops vectors of specific length inclined at a random angle in the digital image N number of times and calculates the number of times the end points of the vector are in the phase of interest (Figure 5.20). The procedure is repeated for vectors of lengths varying from zero to half the size of the image. The function *rand(),* available in *MATLAB* (*2008*)*,* was used to randomly generate the location and inclination of each vector.

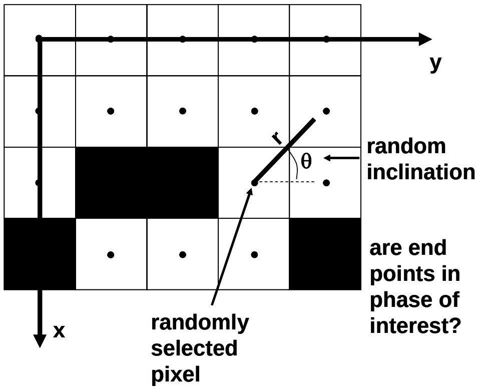

Figure 5.20. Schematic for 2-point correlation function algorithm – (*Velasquez et al., 2010*)

Velasquez (*2009*) and *Velasquez et al*., (*2010*) using a two-phase randomly generated material with ϕ_1 = 0.5 determined its 2-point correlation function (Figure 5.21) showing, as expected, that the correlation function has the material volumetric fraction ϕ_1 as initial value and instantaneously decays to ϕ_1^2, which is the probability of randomly finding two points in phase 1.

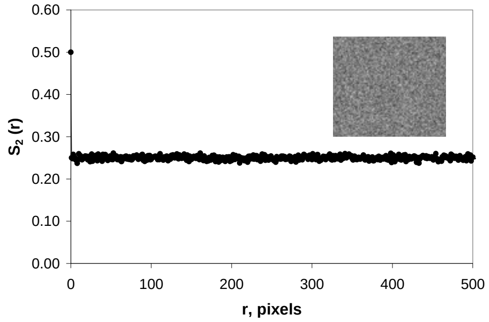

Figure 5.21. 2-point correlation function for phase 1 of a randomly generated material – (*Velasquez et al., 2010*)

The simplified method was also validated by the same authors comparing the results to the analytical exact solution for the Penetrable Sphere Model (*Weissberg 1963; Torquato and Stell 1983; Berryman 1985*) and it was found that the results from using the implemented algorithm are in good agreement with the theoretical solution. The number of drops *N* for the estimation of the correlation function was determined from the Penetrable Sphere model as well using a material with ϕ_{matrix} = 0.26 (white phase) as a balance between computational time and results fluctuation. $N > 10{,}000$ provided the best compromise. A comparison of the brute force method and the simplified algorithm for a material containing overlapping particles with $\phi_{particles} = 0.26$ also indicated that the method based on Monte Carlo simulations provides a good approximation of the spatial correlation function with less computational time (*Velasquez, 2009*; and *Velasquez et al*., *2010*).

5.3.1.1. 2-point Correlation Function for Asphalt Mixture

The binary images of the different specimens were used to compute the 2-point correlation functions of the aggregate phase. The 2-point correlation functions for each specimen of the seventeen mixtures analyzed in this study are presented in Appendix C. As in the case of volume fraction and gradation the single values of the 2-point correlation function for each specimen is calculated as average of the two larger sides of the specimen (~115 × 11.8 mm). An example of the 2- point correlation function for the six specimen obtained from slice 2 of mixture 7 is presented in Figure 5.22.

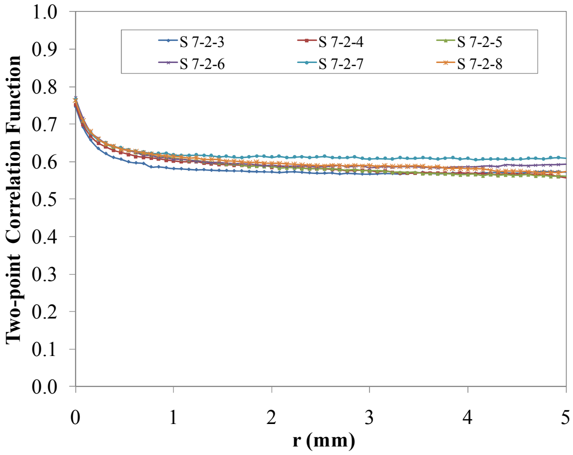

Figure 5.22. 2-point correlation function for aggregate phase, mixture 7 slice 2

Table 5.2 presents a comparison between the 1-point correlation function (the volume fraction of aggregate, ϕ_I), the calculated 2-point correlation function and the theoretical 2-point correlation function (ϕ_I^2) at r=5mm for all the asphalt mixtures. The average and coefficient of variation of the 2-point correlation function of the aggregate phase for all the different asphalt mixtures are presented in Figures 5.23-5.31.

Table 5.2. 2-point correlation function values comparison

Mixture ID	Volume fraction -	S_2 at r=5mm -	S_2 Theoretical at r=5mm -	Difference at r=5mm %
1	0.758	0.555	0.574	3.44
2	0.749	0.540	0.561	3.78
3	0.764	0.569	0.583	2.44
4	0.754	0.549	0.568	3.43
5	0.755	0.557	0.570	2.25
6	0.768	0.568	0.589	3.67
7	0.758	0.561	0.574	2.27
8	0.752	0.560	0.565	0.94
9	0.767	0.581	0.589	1.27
10	0.753	0.562	0.567	0.78
11	0.758	0.560	0.574	2.43
12	0.770	0.583	0.593	1.60
13	0.774	0.597	0.600	0.41
14	0.776	0.595	0.602	1.23
15	0.775	0.593	0.600	1.16
16	0.769	0.591	0.591	0.04
17	0.757	0.559	0.573	2.38

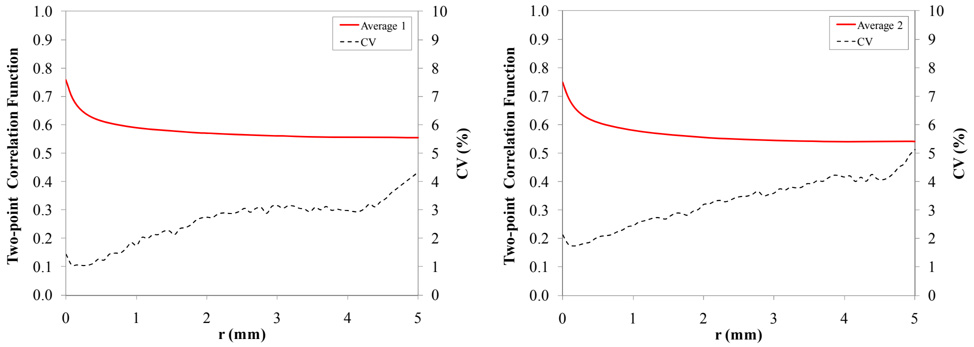

Figure 5.23. 2-point correlation function for mixtures 1 and 2 and CV

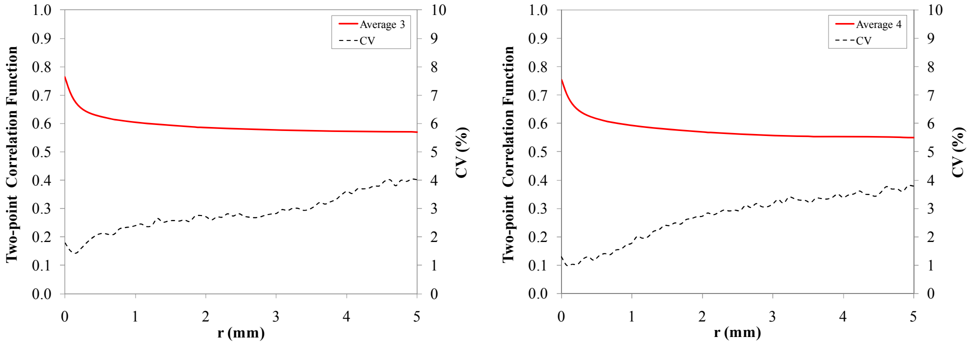

Figure 5.24. 2-point correlation function for mixtures 3 and 4 and CV

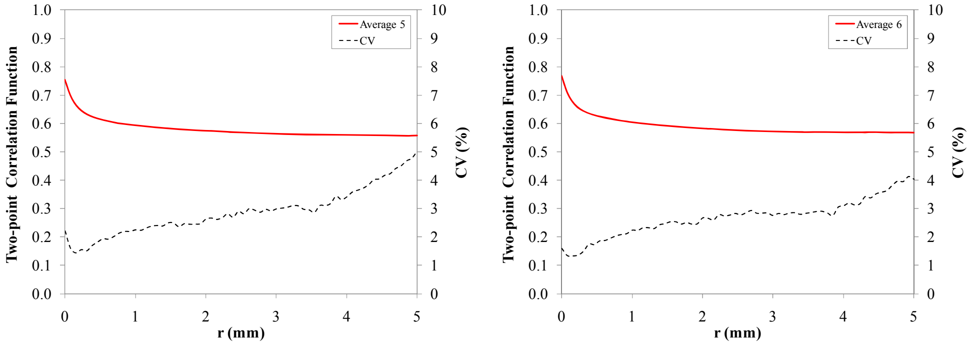

Figure 5.25. 2-point correlation function for mixtures 5 and 6 and CV

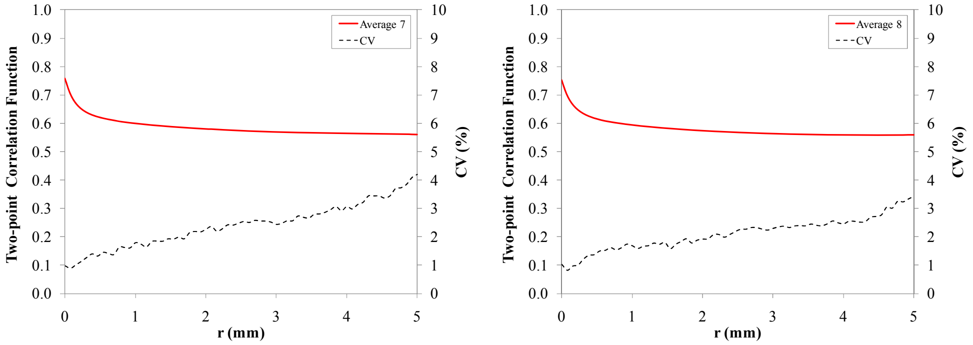

Figure 5.26. 2-point correlation function for mixtures 7 and 8 and CV

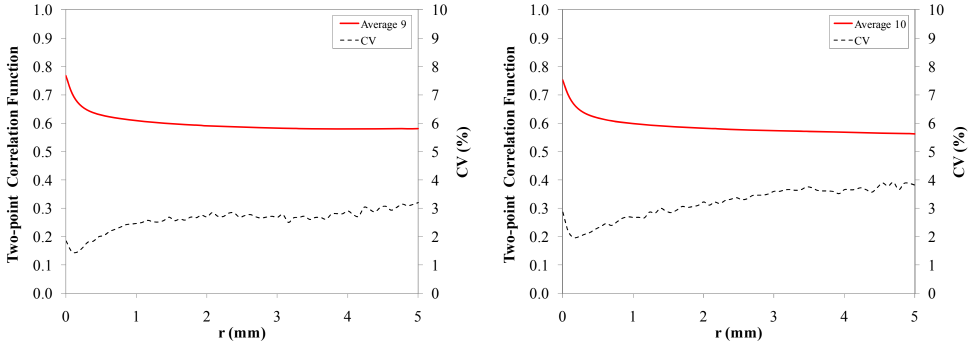

Figure 5.27. 2-point correlation function for mixtures 9 and 10 and CV

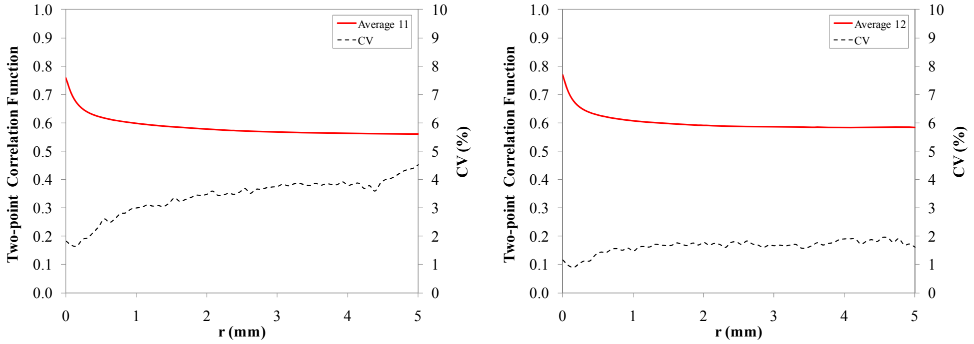

Figure 5.28. 2-point correlation function for mixtures 11 and 12 and CV

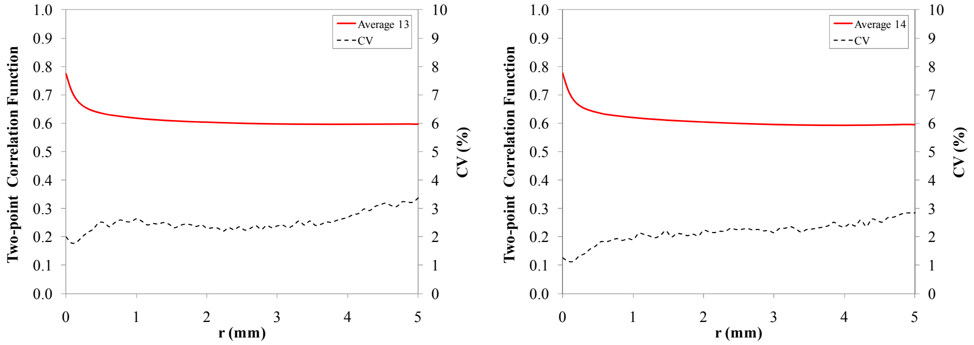

Figure 5.29. 2-point correlation function for mixtures 13 and 14 and CV

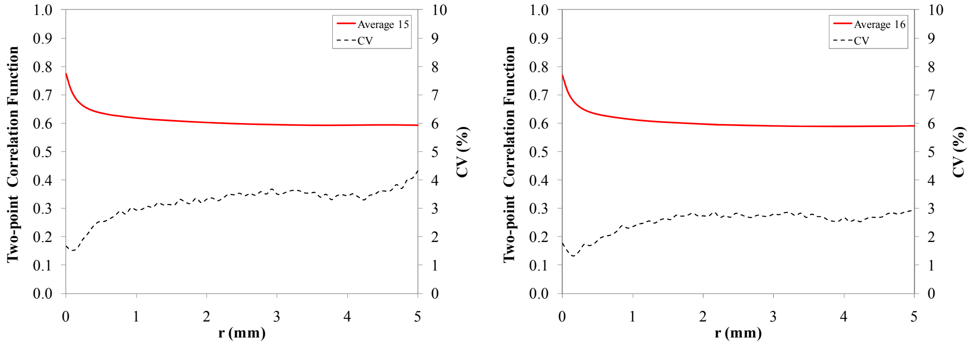

Figure 5.30. 2-point correlation function for mixtures 15 and 16 and CV

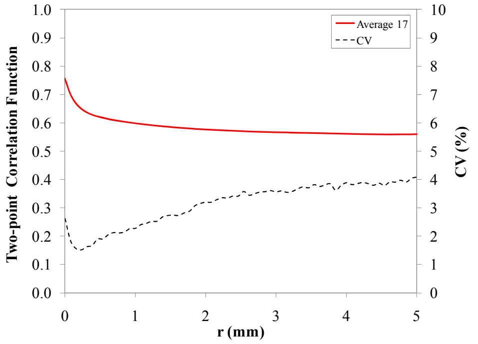

Figure 5.31. 2-point correlation function for mixture 17 and CV

The 2-point correlation functions calculated for asphalt mixtures materials (Figures 5.23 - 5.31) behave similarly for all the seventeen asphalt mixtures investigated. The value of the correlation function does not fluctuate as the distance (*r*) increases. The 2-point correlation function starts at approximately $\phi_{aggregate}$ and smoothly drops to $\phi_{aggregate}^{2}$ as also shown by the difference between the computed and theoretical value (Table 5.2). For each mixture, no large coefficients of variation are observed between the correlation function measured from the twelve BBR beam sspecimens. The maximum coefficient of variation calculated is 5.13%.

5.3.2. 3-point Correlation Function

Several approaches are available to compute the 3-point correlation function. The use of brute force applied to the discretized version of equation [2.21] is however prohibitive in terms of computational time. *Berryman* (*1985*) proposed a simplified algorithm based on Monte Carlo simulations and on a set of lattice commensurate triangles to approximate the 3-point correlation function. He showed that, by using the symmetries of the 3-point correlation function, computational time can be reduced. For an isotropic and statistically homogeneous material, the 3-point correlation function does not depend on the location or orientation of the triangle but only on the size and shape of it. A procedure was proposed by *Berryman* (*1985*) to define the set of triangles used for the estimation of the spatial correlation function. Three integer *l*, *m*, and *n* are used to characterize each triangle (Figure 5.32). In order to avoid calculating the probability of the same triangle more than once (redundancy) the following conditions are imposed:

- The length of the longest side of the triangle *l* is not larger than half of the size of the image,
- A local coordinate system (x', y') with origin at the vertex formed by the intersection of the longest and shortest side of the triangle is a defined,
- The longest side *l* of the triangle is place along the x' axes. Then, with respect to this local coordinate system, the second and third vertex of the triangle are located at (*l*, *0*) and (*m*, *n*), respectively.
- To avoid calculating the correlation function for the same triangle more than once then:

$$m \leq l/2 \qquad [5.4]$$

$$m^2 + n^2 \leq 2ml \qquad [5.5]$$

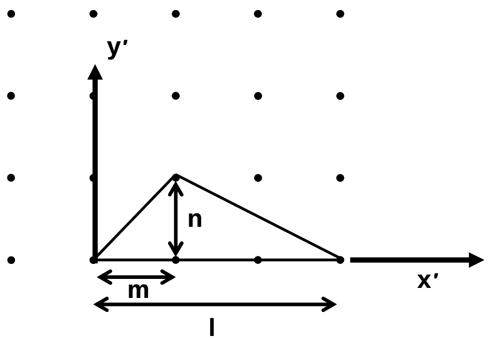

Figure 5.32. Schematic of triangles used for calculation of 3-point correlation function – (*Velasquez et al., 2010*)

Each triangle defined by the integers (*l*, *m*, *n*) was randomly dropped *N* number of times in the digital image and the number of times (N_{hits}) the three vertices of the triangle were in the phase of interest was counted (Figure 5.23). The value of the 3-point correlation function for that specific triangle is:

$$S_3(l,m,n) = N_{hits} / N \qquad [5.6]$$

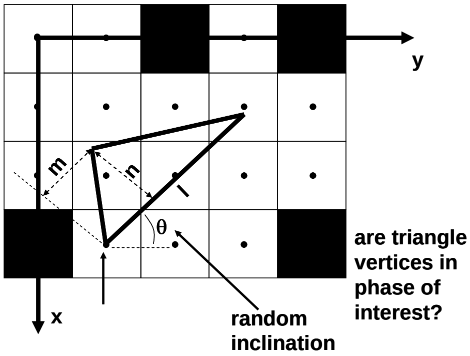

Figure 5.33. Schematic of Monte Carlo simulations for 3-point correlation function – (*Velasquez et al., 2010*)

The 3-point correlation function was applied by *Velasquez* (*2009*) and *Velasquez et al*., (*2010*) to study the effect of different sizes of beams of asphalt mixture specimen and the microstructure of the material. The 3-point correlation function for a randomly generated material and the penetrable sphere material was calculated using a set of triangles with the same shape but different sizes. The shape of the triangle was defined by $L = 3$ pixels and $M = N = 1$ pixel and the size of the triangle was determined by a factor *p*, that varied from 1 to half the size of the image. The set of triangles used to calculate S_3 was determined by the following triplets:

$$(l,m,n) = p \times (L,M,N) \qquad [5.7]$$

It was found that S_3 can capture differences in the microstructure of two completely different materials, similar to what 2-point correlation function (S_2) does. For the random material, the spatial correlation function starts at the volumetric fraction of the matrix phase (i.e. white pixels) and then instantaneously drops to $\phi_{matrix}{}^3$. The authors also showed that, as expected, the 3-point correlation function of the random material reflects no patterns in the internal structure of the material and that the 3-point correlation function for the penetrable spheres model behaves similarly to previous research (*Berryman, 1985*) when N = 100,000 triangle drops are used during the simulations.

5.3.2.1. 3-point Correlation Function for Asphalt Mixture

The same binary images of the asphalt mixtures BBR beams used for the calculation of the 2-point correlation function of the different specimens were used also for the computation of the 3-point correlation function. First a simplified algorithm based on the conditions stated above, and very similar to what was proposed by *Velasquez* (*2009*) and *Velasquez et al*., (*2010*) was coded in *MATLAB* using the random number generator function for the Monte Carlo simulations. This algorithm should generate a three-dimensional output. However it was found that this is prohibitive for a computational power available in a standard laptop and thus this approach was dropped. It was decided to select only a single triangle with fixed proportion and varying dimension from one point to half of the size the smaller side of the specimen larger face (~115 × 11.8 mm). The set of triangles defined by L = 2, M = 1, N = 1, and p = 0 - 32, was selected. This helped to drastically reduce the computation time form more that 5 days for a single simulation to few minutes. It must be underlined that this single triangle procedure does not provide the entire 3-point correlation function; however, for the purpose of this dissertation it was considered a good compromise between computation power and an appropriate response. An example of the 3- point correlation function for the six specimen obtained from slice 2 of mixture 7 is presented in Figure 5.34.

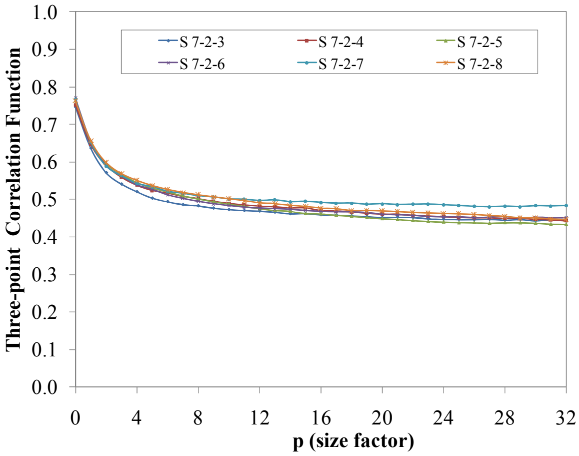

Figure 5.34. 3-point correlation function for aggregate phase, mixture 2 slice 2

Table 5.3 presents a comparison between the 1-point correlation function (the volume fraction aggregate, ϕ_I), the calculated 3-point correlation function and the theoretical 3-point correlation function (ϕ_I^3) for all the asphalt mixtures at p=32. The average and coefficient of variation of the 3-point correlation function of the aggregate phase for all the different asphalt mixtures are presented in Figures 5.35-5.43. Appendix C contains the plots for the 3-point correlation functions for each specimen of the seventeen mixtures analyzed in this dissertation.

Table 5.3. 3-point correlation function values comparison

Mixture ID	Volume fraction -	S_3 at p=32 -	S_3 Theoretical at p=32 -	Difference at p=32 %
1	0.758	0.424	0.435	2.55
2	0.749	0.410	0.421	2.57
3	0.764	0.442	0.446	0.86
4	0.754	0.421	0.428	1.68
5	0.755	0.430	0.431	0.22
6	0.768	0.441	0.452	2.58
7	0.758	0.435	0.435	0.05
8	0.752	0.434	0.425	2.08
9	0.767	0.451	0.452	0.08
10	0.753	0.438	0.427	2.69
11	0.758	0.433	0.435	0.44
12	0.770	0.453	0.457	0.70
13	0.774	0.472	0.464	1.53
14	0.776	0.467	0.467	0.00
15	0.775	0.467	0.465	0.42
16	0.769	0.466	0.455	2.51
17	0.769	0.466	0.455	2.51

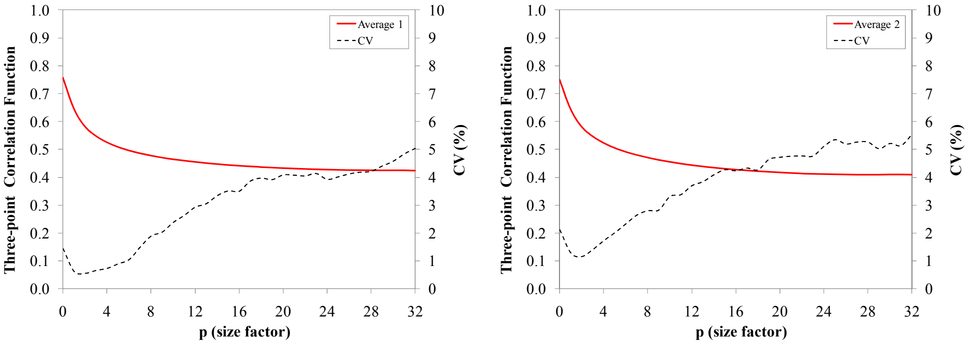

Figure 5.35. 3-point correlation function for mixtures 1 and 2 and CV

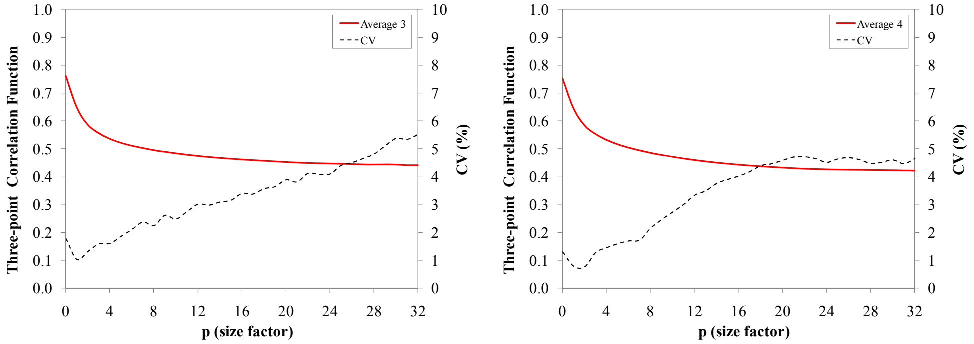

Figure 5.36. 3-point correlation function for mixtures 3 and 4 and CV

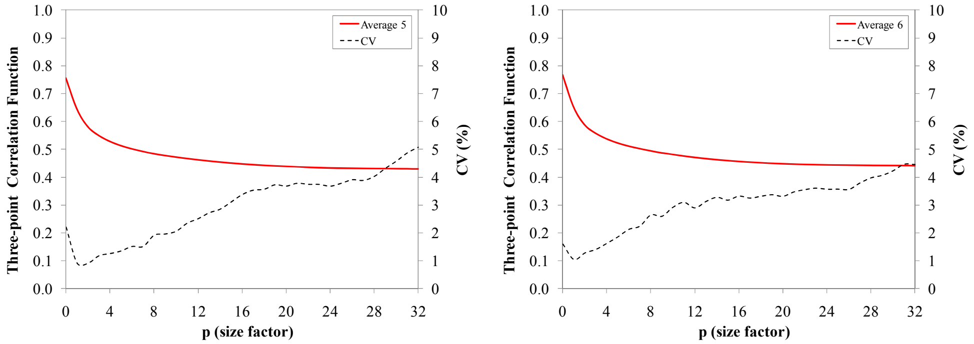

Figure 5.37. 3-point correlation function for mixtures 5 and 6 and CV

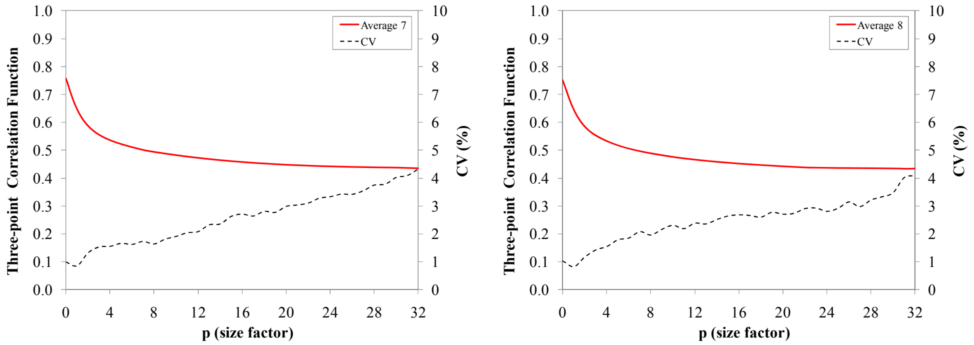

Figure 5.38. 3-point correlation function for mixtures 7 and 8 and CV

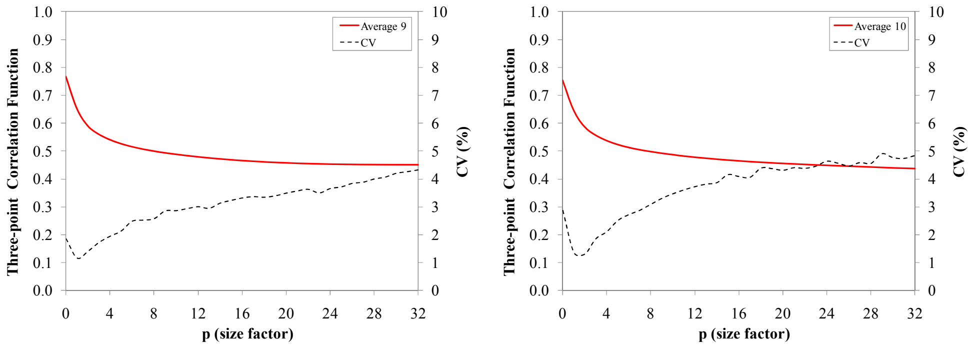

Figure 5.39. 3-point correlation function for mixtures 9 and 10 and CV

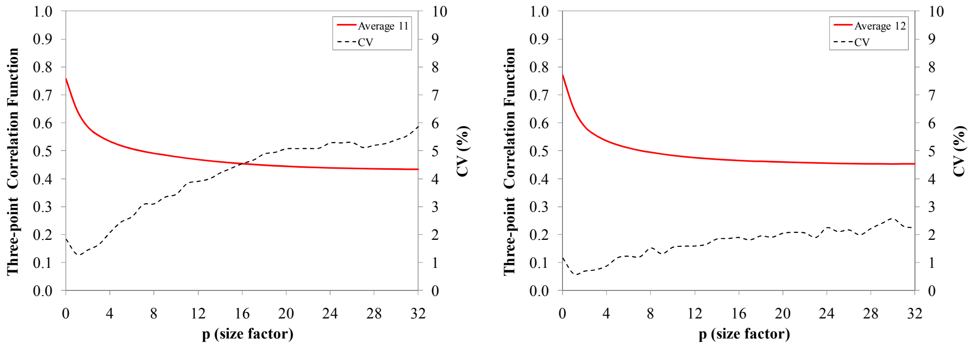

Figure 5.40. 3-point correlation function for mixtures 11 and 12 and CV

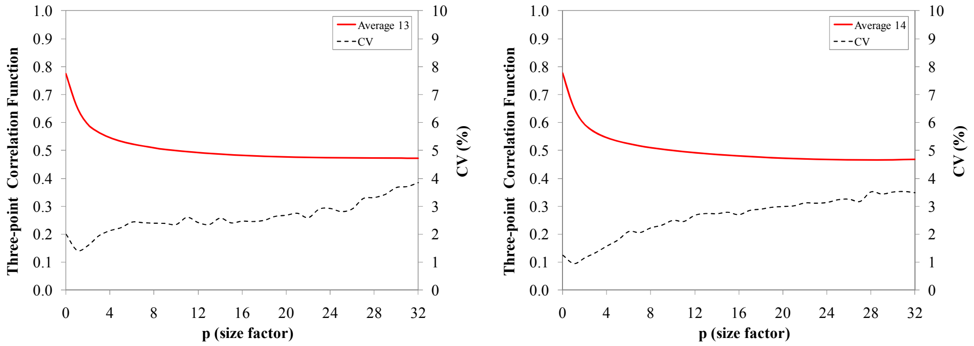

Figure 5.41. 3-point correlation function for mixtures 13 and 14 and CV

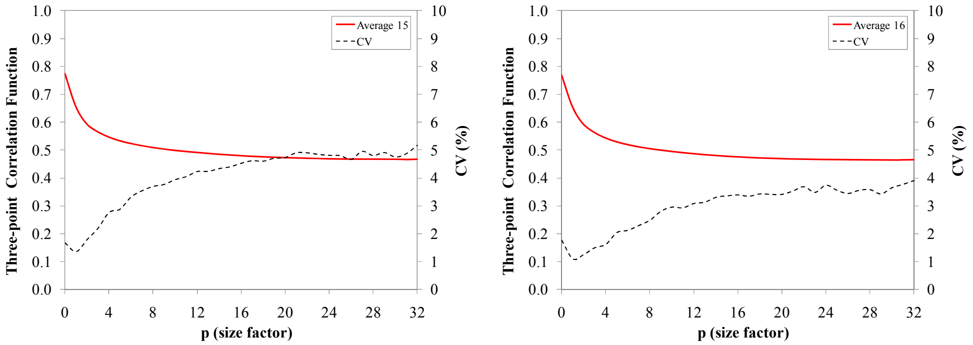

Figure 5.42. 3-point correlation function for mixtures 15 and 16 and CV

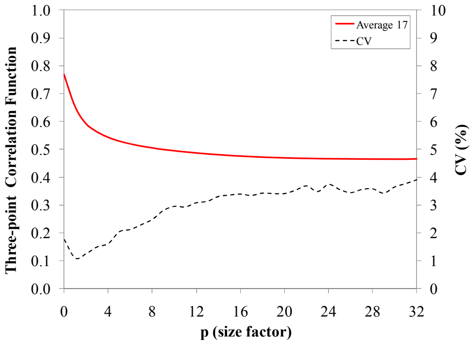

Figure 5.43. 3-point correlation function for mixture 17 and CV

The average 3-point correlation functions computed for asphalt mixtures materials (Figures 5.35 - 5.43) has a similar pattern for all the seventeen asphalt mixtures considered in this thesis. No large fluctuations on S_3 are observed as the size of the triangle p increases. S_3 begins at $\phi_{aggregate}$ and smoothly drops to $\phi_{aggregate}^3$. The maximum coefficient of variation measured for S_3 is 5.86%.

Chapter 6. Modeling

This Chapter deals with the inverse problem in asphalt mixture. The prediction of the asphalt binder bulk properties, and specifically of the asphalt binder creep stiffness form the asphalt mixture creep stiffness experimental data obtained from BBR testing, is investigated. For this purpose two of the models mentioned in Chapter 2 are selected based on literature review and previous research: Hirsch model (*Hirsch, 1962*; *Christensen et al.*, *2003*) and Huet model (*Huet, 1963*) and its application to asphalt mixture at low temperature (*Cannone Falchetto et al., 2011*). In order to validate the models the back calculated asphalt binder creep stiffness is used as input in a two-dimensional finite element simulation to calculate the original creep stiffness of the asphalt mixtures from which the binder stiffness was obtained.

6.1. Inverse Problem in Low Temperature Asphalt Mixture Characterization

Solving inverse problems is not trivial and may require some sophisticated procedures. *Zofka* (*2007*) found that Self-Consistent Model (SCM) (*Yin et al., 2006*) is not a good candidate for the inverse problem since it does not produce good prediction in the case of the forward model. Analogously, *Milton* (*1981*) and GSCS - Generalized Self-Consistent Scheme (*Christensen 1979, Christensen and Lo 1979*) – models present complicated expressions and require additional adjustment factors. This may results in bigger errors both in the case of forward and the potential inverse solutions.

In the next sections two models, Hirsch (*Christensen et al., 2003*) and Huet (*Huet, 1963*) and their applications to asphalt mixture characterization at low temperature are used to back calculate asphalt binder creep stiffness S_{binder} from the corresponding asphalt mixture creep stiffness S_{mix} obtained experimentally from BBR asphalt mixtures beams. The calculation will be performed on a limited number of the mixtures investigated in this thesis: the selected mixtures are 1, 2, 3, 4, 5, 6, 7, and 8 and the specimens considered are those cut from one single slice of the mixtures obtained from one single gyratory compacted cylinder. This is done to limit the number of simulations and thus the required computational time in the finite element simulations (section 6.2 of this Chapter). Moreover to reduce the number of variables involved in the problem, time temperature superposition principle was not considered and thus only the highest testing temperature data (-6°C) was investigated. This was found to be convenient since

BBR experimental data for the extracted binders of mixtures 2, 3, 5, 6, 7 and 8 were available at testing temperature of -6°C (Chapter 3). The graphical results of the back calculated and extracted asphalt binder creep stiffness are presented at the end of section 6.1.

6.1.1. Hirsch Model

In this dissertation the method proposed by *Zofka et al.* (*2005*) is used to investigate the inverse problem with the Hirsch model. First, based on the volumetric properties of the mixtures (Table 3.1), plots of binder creep stiffness versus predicted mixture stiffness using modified equation [2.38] are generated for binder stiffness values between 50 to 1000MPa as shown in Figures 6.1 to 6.4 for all the eight mixtures considered.

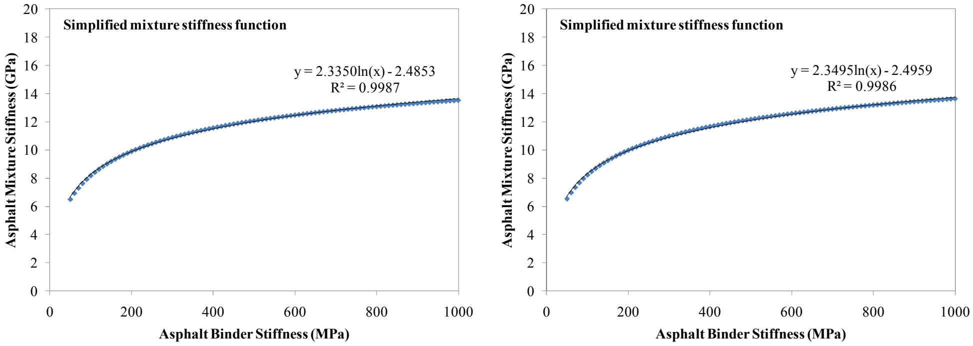

Figure 6.1. Simplified mixture stiffness function for mixtures 1 and 2, T=-6°C

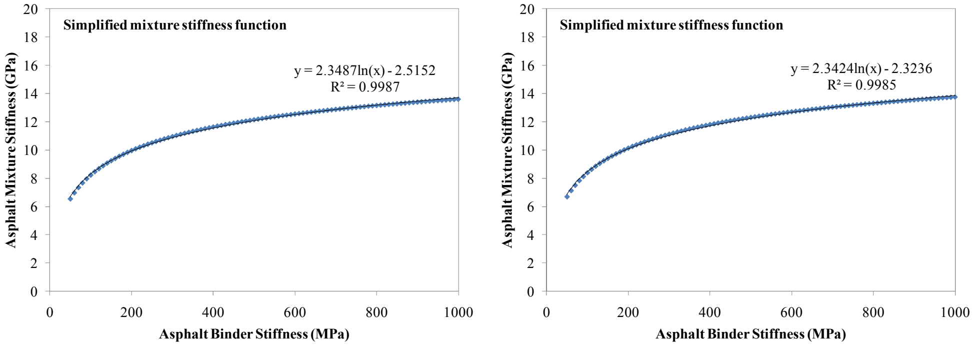

Figure 6.2. Simplified mixture stiffness function for mixtures 3 and 4, T=-6°C

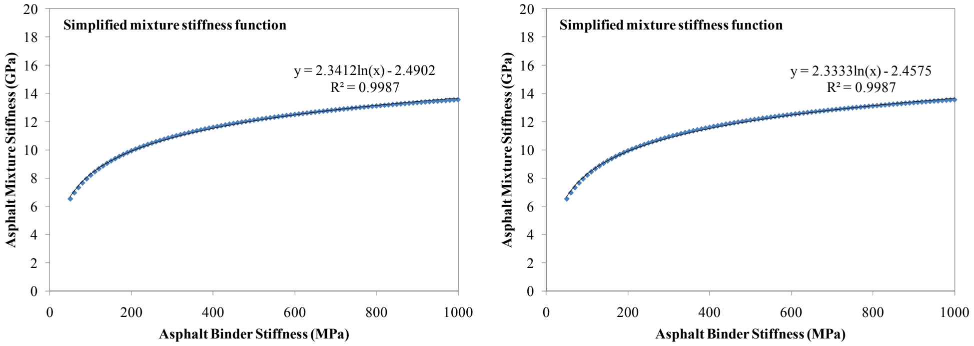

Figure 6.3. Simplified mixture stiffness function for mixtures 5 and 6, T=-6°C

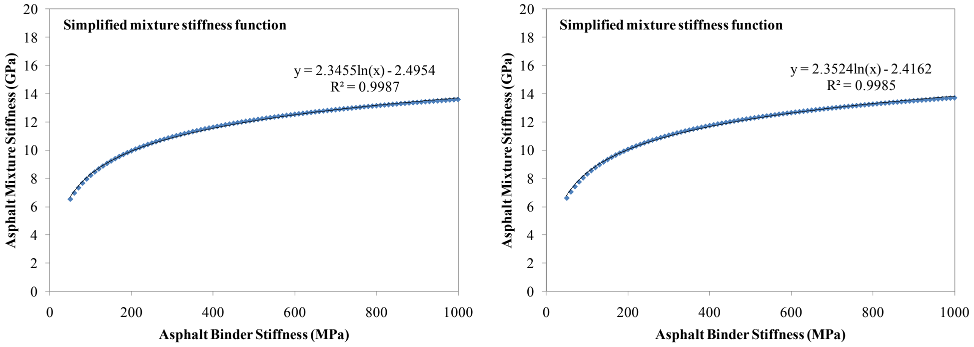

Figure 6.4. Simplified mixture stiffness function for mixtures 7 and 8, T=-6°C

Based on the alternative formulation of the Hirsch model (*Zofka et al., 2005*) the value of the aggregate modulus for all the eight mixtures investigated in this phase was assumed E_{agg}=3625942psi (25GPa) instead of E_{agg}=4200000psi (29GPa of [2.38]). The aggregate modulus was imposed to be equal for all the mixtures since it was assumed that the aggregate in the recycled materials (RAP in particular) was similar to limestone that has, as already mentioned in Chapter 3, a modulus close to that of the Dolostone, used as virgin aggregate in the mixtures. Then, a very simple function is fitted to the mix log stiffness versus binder log stiffness data, as shown in Figures 6.1 to 6.4:

$$E_{mix} = a \cdot \ln(E_{binder}) + b \qquad [6.1]$$

where *a* and *b* are regression parameters.

Finally, the binder stiffness is simply calculated using equation [6.1] over the entire range of loading time.

6.1.2. Huet Model and ENTPE Transformation

Among the analogical models reviewed in Chapter 2 the only model with continuous spectrum that presents an expression in the time domain for the creep compliance is the Huet model (*Huet, 1963*) [2.52]. This model does not have the additional dashpot in series and the spring in parallel that are present in the 2S2P1D model (*Olard et al., 2003; Olard, 2003; Di Benedetto et al., 2004*) since the BBR experimental data are obtained at low temperatures or high frequencies. At low temperature and/or high frequency Huet model and 2S2P1D model give the same results while at higher temperatures and/or lower frequencies, the analysis would need to use 2S2P1D model. Based on Huet model, an expression that relates asphalt mixture creep stiffness and asphalt mixture creep compliance to asphalt binder creep stiffness and asphalt binder creep compliance, respectively was found by *Cannone Falchetto* (*2010*) and *Cannone Falchetto et al*., (*2011*) [2.62]. This expression represents a specific case of the ENTPE transformation [2.60] (*Di Benedetto et al., 2004*) in the time domain for low temperatures and high frequencies. In the same work this expression was also used to backcalculate the creep stiffness for the asphalt binder from the creep stiffness of the corresponding asphalt mixtures (inverse problem) [6.2] and [6.3]:

$$D_{mix}(t) = D_{binder}(t10^{-\alpha})\frac{E_{\infty\_binder}}{E_{\infty\_mix}} \qquad [6.2]$$

$$S_{mix}(t) = S_{binder}(t10^{-\alpha})\frac{E_{\infty\_mix}}{E_{\infty\_binder}} \qquad [6.3a]$$

$$S_{binder}(t) = S_{mix}(t10^{\alpha})\frac{E_{\infty\_binder}}{E_{\infty\_mix}} \qquad [6.2b]$$

where:

$S_{mix}(t)$	creep stiffness of mixture,
$S_{binder}(t)$	creep stiffness of binder,
$D_{mix}(t)$	creep compliance of mixture,
$D_{binder}(t)$	creep compliance of binder,
E_{∞_mix}	glassy modulus of mixture,
E_{∞_binder}	glassy modulus of binder,
t	time,
α	regression parameter which may depend on mix design, expressed as:

$$\tau_{mix} = 10^{\alpha}\tau_{binder} \qquad [6.4]$$

where:

τ_{binder}	characteristic time of binder,
τ_{mix}	characteristic time of mixture.

Expressions [6.2], [6.3] and the Huet model (*Huet*, *1963*) are used in this dissertation for the backcalculation of the asphalt binder creep stiffness from the corresponding asphalt mixture creep stiffness for all the eight mixtures investigated. In order to do that the following Huet model equations for asphalt binder and asphalt mixture creep compliance were considered (*Cannone Falchetto, 2010* and *Cannone Falchetto et al*., *2011*) [6.5] and [6.6]:

$$D_{binder}(t) = \frac{1}{E_{\infty\_binder}}\left(1 + \delta\frac{(t/\tau_{binder})^{k}}{\Gamma(k+1)} + \frac{(t/\tau_{binder})^{h}}{\Gamma(h+1)}\right) \qquad [6.5]$$

$$D_{mix}(t) = \frac{1}{E_{\infty\_mix}}\left(1 + \delta\frac{(t/\tau_{mix})^{k}}{\Gamma(k+1)} + \frac{(t/\tau_{mix})^{h}}{\Gamma(h+1)}\right) \qquad [6.6]$$

where

$D_{binder}(t)$, $D_{mix}(t)$	creep compliance of binder and mixture,
E_{∞_binder}, E_{∞_mix}	glassy modulus of binder and mixture,
τ_{binder}, τ_{mix}	characteristic time of binder and mixture.
h, k	exponents such that $0<k<h<1$,
δ	dimensionless constant,
t	time,
Γ	gamma function,
τ_{binder}	characteristic time of binder,
τ_{mix}	characteristic time of mixture.

Since the experimental asphalt mixture creep stiffness data were available, expression [6.3a] was manipulated using equations [6.4], [6.5] and [6.6], obtaining the following formula:

$$S_{mix}(t,h,k,\delta,\tau_{mix}) = S_{binder}(t,h,k,\delta,10^{\alpha}\tau_{binder})\frac{E_{\infty\_mix}}{E_{\infty\_binder}} \qquad [6.7]$$

The five constants (δ, k, h, E_{∞}, and τ) required by the [6.7] and thus by the embedded Huet model are determined through the minimization of the sum of the distances between the experimental asphalt mixture creep stiffness and that of expression [6.7] (Huet-ENTPE) at n time points [6.8].

$$\min\left(\sum_{i=1}^{n}\left[S^{\exp}(t)-S^{Huet-ENTPE}(t)\right]^{2}\right) \qquad [6.8]$$

where:

$S^{exp}(t)$ experimental creep stiffness,

$S^{Huet\text{-}ENTPE}(t)$ model creep stiffness.

Since from previous studies (*Olard et al., 2003; Olard, 2003; Di Benedetto et al., 2004, Cannone Falchetto, 2010* and *Cannone Falchetto et al*., *2011*) it was found that the Huet model parameters are the same for binder and corresponding mixture, the only unknown that strictly characterizes the difference between asphalt binder and asphalt mixture is represented by the α parameter that relates the characteristic time of binder to the characteristic time of mixture. The value of α was obtained during the minimization process (equation [6.8]) starting form initial values of δ, k, h, E_∞, τ and α found in literature (*Huet, 1963; Olard et al., 2003; Olard, 2003; Di Benedetto et al., 2004, Cannone Falchetto, 2010* and *Cannone Falchetto et al*., *2011*). Figures 6.5 to 6.8 present the asphalt mixture creep compliance for the experimental data and Huet model prediction for the eight mixtures considered and tested at -6°C. The plots present the creep compliance curves since it is easier to appreciate the goodness of the fitting compared the creep stiffness representation.

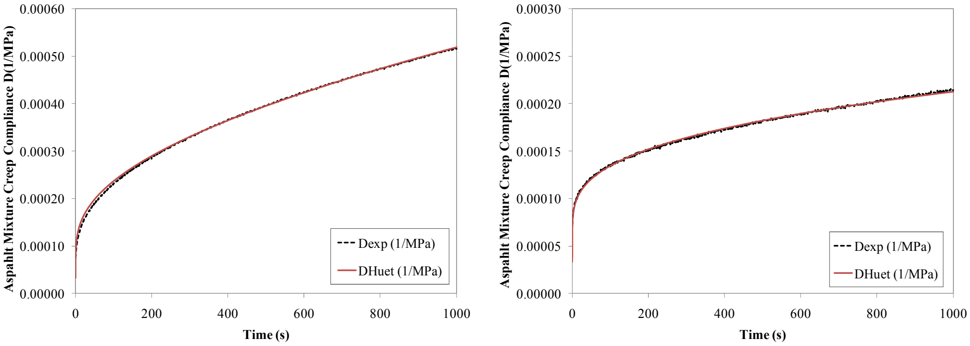

Figure 6.5. Huet model for mixture 1 and 2, T=-6ºC

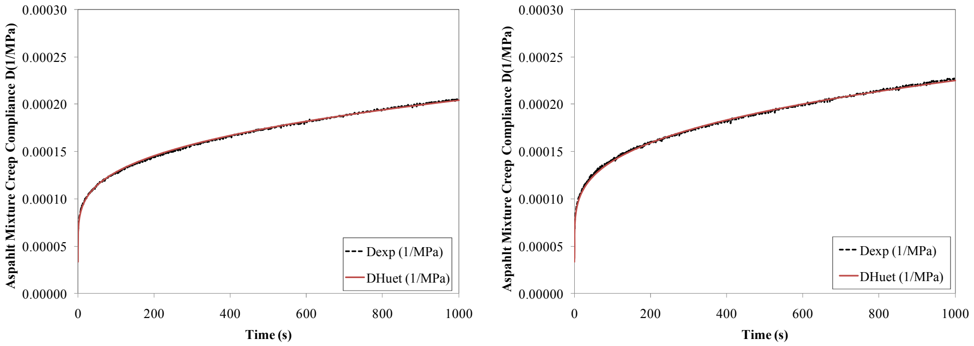

Figure 6.6. Huet model for mixture 3 and 4, T=-6°C

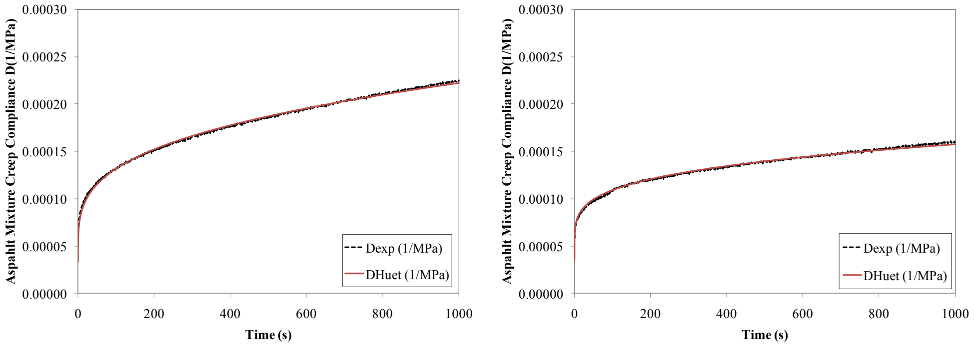

Figure 6.7. Huet model for mixture 5 and 6, T=-6°C

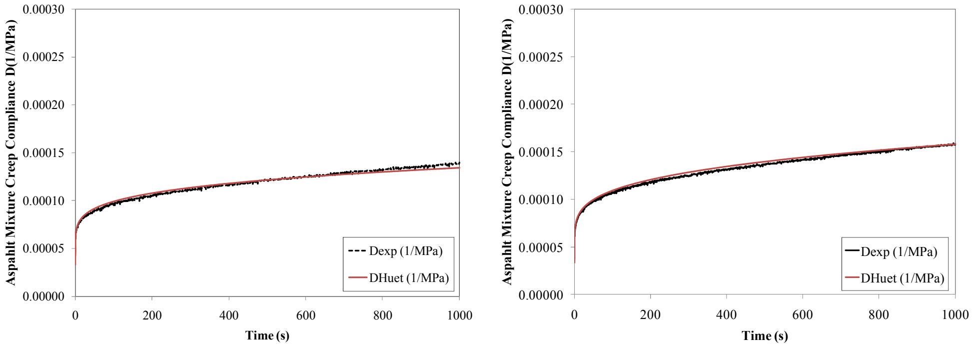

Figure 6.8. Huet model for mixture 7 and 8, T=-6°C

Table 6.1 presents the Huet model parameters for the eight asphalt mixtures evaluated and corresponding backcalculated asphalt binders while Table 6.2 shows the α parameters.

Table 6.1. Huet model parameters for mixtures and corresponding backcalculated binders

Material		δ	k	h	E_∞(MPa)	Log(τ)
Binder	1	4.00	0.20	0.70	3000.00	-1.00
	2	2.07	0.12	0.44	3000.00	-0.73
	3	3.77	0.20	0.59	3000.00	0.11
	4	3.66	0.19	0.54	3000.00	-0.50
	5	5.73	0.25	0.80	3000.00	0.60
	6	2.98	0.16	0.45	3000.00	0.50
	7	3.06	0.15	0.45	3000.00	-0.16
	8	2.53	0.15	0.46	3000.00	-0.22
Mixtures	1	4.00	0.20	0.70	30000.00	1.84
	2	2.07	0.12	0.44	30000.00	2.18
	3	3.77	0.20	0.59	30000.00	3.03
	4	3.66	0.19	0.54	30000.00	2.81
	5	5.73	0.25	0.80	30000.00	3.37
	6	2.98	0.16	0.45	30000.00	3.28
	7	3.06	0.15	0.45	30000.00	3.78
	8	2.53	0.15	0.46	30000.00	3.05

Table 6.2. α parameter for mixtures and corresponding backcalculated binders

Mixture/binder	1	2	3	4	5	6	7	8
α	2.84	2.91	2.92	3.31	2.76	2.78	3.94	3.27

As expected the characteristic time seems to be peculiar of the specific mixture-binder considered.

6.1.3. Binder Backcalculation Results Comparison

This section presents a graphical and qualitative comparison between the creep stiffness of asphalt binders predicted from the Hirsch model, the Huet-ENTPE formulation and the experimentally determined creep stiffness obtained from the extracted asphalt binder using BBR testing. As already mentioned in Chapter 3 the extraction and the BBR test on the extracted asphalt binder were performed at the Minnesota Department of Transportation and no control on the testing was possible. Moreover BBR data on the recovered binders are available just up to 240s of testing while the asphalt mixtures were tested up to 1000s in the BBR. For this reason, in the following plots, the creep stiffness curves of the extracted binder are shorter than those predicted by the models. It must also be mentioned that no extracted asphalt binder data are available for mixtures 1 and 4. Figures 6.9 to 6.12 presents the creep stiffness for the back calculated and extracted binders in log scale.

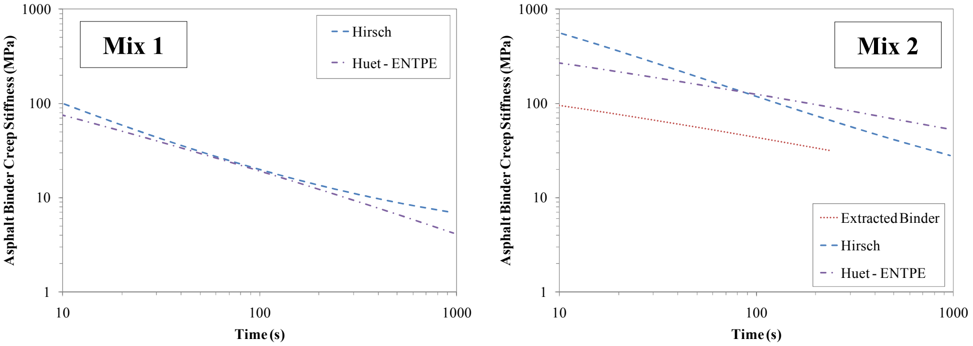

Figure 6.9. Creep stiffness of backclaculated and extracted asphalt binder for mixture 1 and 2, T=-6ºC

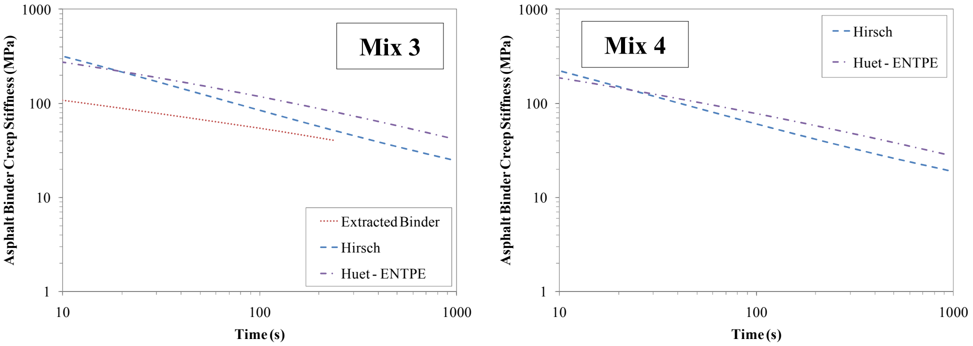

Figure 6.10. Creep stiffness of backclaculated and extracted asphalt binder for mixture 3 and 4, T=-6ºC

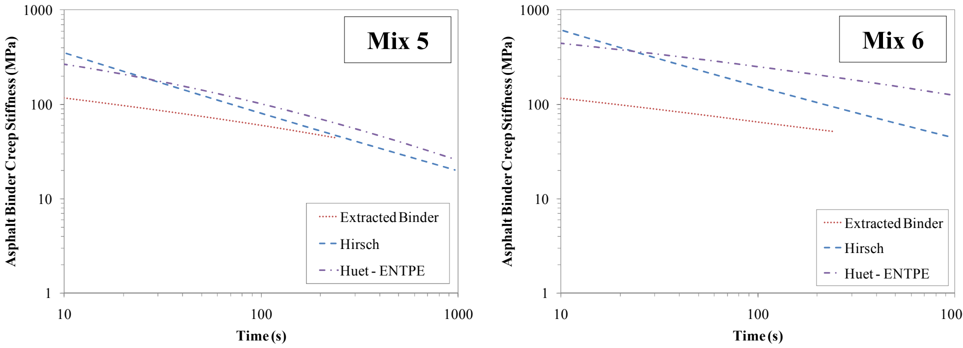

Figure 6.11. Creep stiffness of backclaculated and extracted asphalt binder for mixture 5 and 6, T=-6ºC

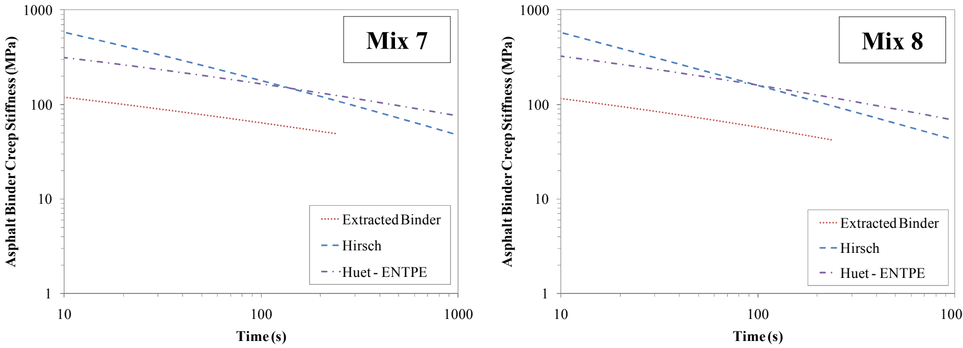

Figure 6.12. Creep stiffness of backclaculated and extracted asphalt binder for mixture 7 and 8, T=-6ºC

A visual comparison between the predictions of the Hirsch model and Huet-ENTPE formulation shows that the former model seems to gives and higher estimation of the asphalt binder creep stiffness for shorter time and smaller values for longer time. Another particular aspect of the Hirsch model is evident from Figure 6.9 mixture 1, where the asphalt binder creep stiffness curve bends upward suggesting that for smaller stiffness values the model is affected by the aggregate effect.

On the other hand creep stiffness curves obtained from the ENTPE transformation (coupled with Huet model) look smoother and when a comparison is possible they seem to be parallel to the extracted binder creep stiffness curves. Overall both Hirsch model and Huet-ENTPE formulation predict higher creep stiffness values compared to those measured on the extracted binder. An explanation on this point results complicated since an opposite trend, where the extracted binder is stiffer than the backcalculated predictions, would have been expected. This is because, during chemical extraction, a total blending of virgin and oxidized binder, contained in RAP, TOSS or MWSS, should take place providing a rejuvenator effect. Moreover some authors such as *Bonaquist* (*2007*) suggested that there may be a partial or little melting of the aged shingle binder when mixed with virgin material in the asphalt mixture production plant.

To further investigate the behavior of the binder results, Huet model (*Huet, 1963*) was also fitted to the experimental determined creep stiffness obtained from the extracted asphalt binders. Figures 6.13 to 6.15 present asphalt binder creep compliance curves for the experimental data and Huet model predictions for the extracted asphalt binders (# 2, 3, 5, 6, 7 and 8) tested at -6°C, while Table 6.3 presents the corresponding Huet model parameters:

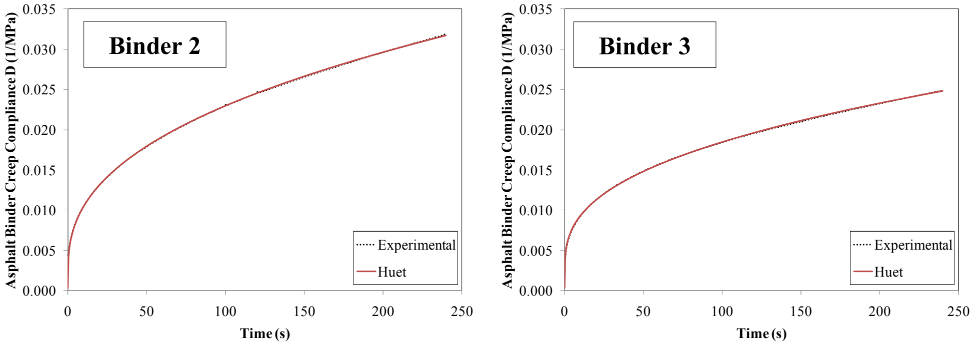

Figure 6.13. Huet model for extracted asphalt binder 2 and 3, T=-6°C

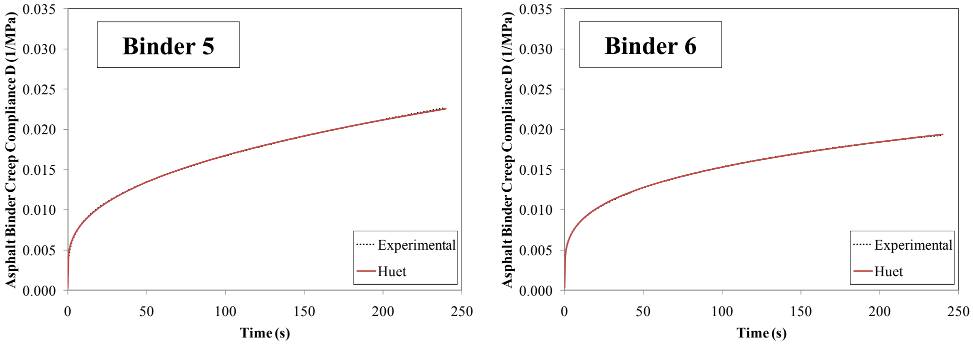

Figure 6.14. Huet model for extracted asphalt binder 5 and 6, T=-6°C

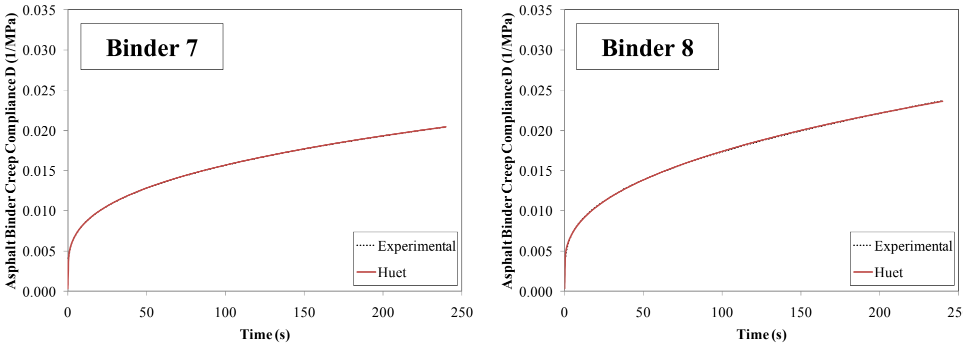

Figure 6.15. Huet model for extracted asphalt binder 7 and 8, T=-6°C

Table 6.3. Huet model parameters for extracted asphalt binders

Material		δ	k	h	E_∞(MPa)	Log(τ)
Binder	2	3.84	0.12	0.42	3000.00	-2.00
	3	7.70	0.18	0.48	3000.00	-0.87
	5	7.19	0.11	0.46	3000.00	-1.18
	6	3.60	0.15	0.34	3000.00	-2.17
	7	4.88	0.11	0.38	3000.00	-1.79
	8	7.14	0.05	0.43	3000.00	-1.63

Table 6.4 shows the difference in percentage between the Huet model parameters obtained from back calculation of the asphalt binder creep stiffness (Table 6.1) and those obtained from the extracted binder data fitting (Table 6.3).

Table 6.4. Huet model parameters comparison: mixture predicted vs. extracted

Binder	Difference %			
#	δ	k	h	Log(τ)
2	-85.51	0.00	4.55	-173.97
3	-104.24	10.00	18.64	-890.91
5	-25.48	56.00	42.50	-296.67
6	-20.81	6.25	24.44	-534.00
7	-59.48	26.67	15.56	-1018.75
8	-182.21	66.67	6.52	-640.91

From Table 6.4 it is evident that there are significant differences between *δ, k, h* and log*τ* evaluated from backcalculation and extracted binder fitting, respectively. However is noticeable the negative change in the *δ* and log*τ* with the highest difference for the characteristic time. Varying one by one the single parameters it was found that the main contribution to the translation of the asphalt binder predicted curve is related to the value of the characteristic time. However this is not the only contribution. The two parameters *δ* and *k*, that indentify the behavior of one of the parabolic elements of the Huet model, provide a sort of translation combined with a rotation (steepening or flattening) affecting the global shape of the predicted curve. Finally *h* seems to influence the shape of the creep stiffness curve as well, affecting mainly curvature. It must be mentioned that these considerations were obtained visually and further investigation, through a sensitivity study is required to provide a deeper understanding of each single parameter.

6.2. Finite Element Investigation of the Inverse Problem Models

Two-dimensional plane stress finite element models of asphalt mixture BBR beams were used to validate the models used in the former sections.

6.2.1. Detail of Finite Element Simulations

Three point bending creep test simulations were performed on asphalt mixture beams considered as a two phase material, aggregates plus mastic (e.g. asphalt binder + aggregates smaller than 250 μm), using *ABAQUS* (*2009*). Both phases are assumed to be linear elastic materials and the properties used for the simulations are presented in Table 6.3.

Table 6.5. Material properties for finite element simulations

Property	Value
$E_{aggregate}$ (GPa)	25
E_{mastic} (GPa)	Know from backcalculation
$\nu_{aggregate}$	0.3
ν_{mastic}	0.3

As in the case of back calculation models a single value of the aggregates modulus was assumed (25GPa) considering that the aggregates were mainly made of Dolostone (similar to Limestone). The values of the relaxation modulus of mastic were obtained form the back calculated and extracted modulus of the asphalt binder, and using the elastic-viscoelastic correspondence principle (*Findley, 1989*) combined with the Euler-Bernoulli elementary beam theory. The assumptions of the Euler-Bernoulli beam theory are: material is linear and isotropic, plane sections remain plane after load is applied, all material points are on plane stress state and strains and deflections are small (*Gere and Timoshenko, 1990*). It must be noted that the mastic phase used in the finite element simulations is actually a mixture made with fine material with a maximum grain size up to 250 μm. This is because the minimum dimension of a single triangular finite element used in the meshing of the BBR beam geometry is not smaller than 250 μm. Based on the stiffening ratios suggested by *Buttlar et al.* (*1999*), on the micromechanical modeling work proposed by *Masad and Somadevan* (*2002*) and on the minimum dimension of a single finite element assumed, a stiffening factor of 10 is used for the estimation of the stiffness of the mastic starting from the stiffness of the binder.

The microstructure of the finite element models was extracted from the binary images of the asphalt mixtures BBR beams used in Chapter 5. A simple *MATLAB* (*2008*) code was written to map the pixel matrix of the binary image into a CPS6M elements mesh (i.e. 6-node modified quadratic plane stress triangle element) with either aggregate or mastic properties. Those types of elements were chosen to allow more flexibility in the reconstruction of an irregular microstructure typical of a two-phase heterogeneous random material as asphalt mixture. Figure 6.16 shows an example of the FEM reconstruction of an asphalt mixture BBR beam.

Figure 6.16. Processed image of asphalt mixture beam used as input structure into ABAQUS (red represents mastic and black aggregates)

The number of elements included in the mesh was obtained from different trials and based on literature. *Velasquez* (*2009*) used three different meshes to evaluate the representative volume element of asphalt mixtures through uniaxial tension finite element simulations. He found that using a mesh of 819000 elements is extremely expensive in terms of computational time and that good balance between computational time and minimum size of aggregate simulated in the FE models was obtained when a mesh of 900 × 227=204300 elements is used. *Zofka* (*2007*) run more than 1500 finite element simulations on BBR asphalt mixtures beams both in 2D and 3D configuration. In the two dimensional simulation a square mesh with CPS8R elements (plane stress quadratic reduced integration element), was used with the side length corresponding to 0.508mm for a total of 2200 elements. In this dissertation the number of element was limited to 23130. This was considered a good compromise in terms of microstructure reconstruction accuracy and computational time.

6.2.2. Finite Element Simulations Results

The asphalt binder creep stiffness obtained from the backcalculation performed with Hirsch model, Huet-ENTPE formulation and the experimental determined creep stiffness of the extracted binder at -6°C was used as input in the finite element simulations. To further reduce the computational time the simulations were run for selected point on the creep stiffness curve and specifically for creep stiffness at 8, 15, 30, 60 120, 240 480, 960s. Each simulation was performed for each side of the two small sides (~115 × 6.25 mm) of the specific asphalt mixture BBR beam specimen and the results averaged. The results of the FEM simulations are graphically compared to those obtained experimentally form on the asphalt mixtures beams (Figures 6.17 to 6.20).

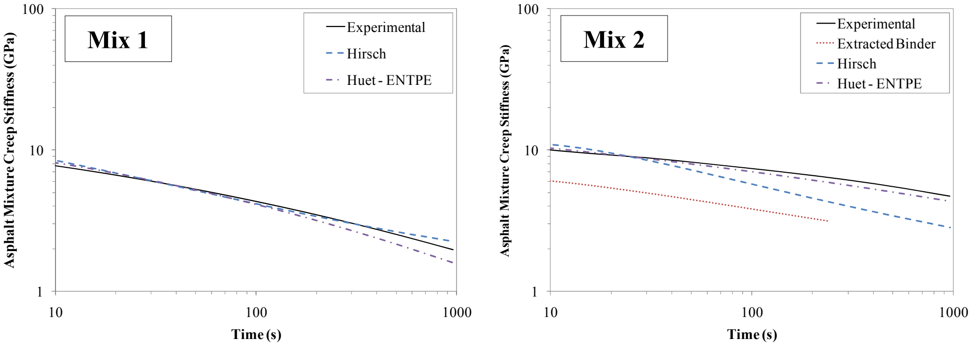

Figure 6.17. Finite element simulation comparison for mixture 1 and 2, T=-6ºC

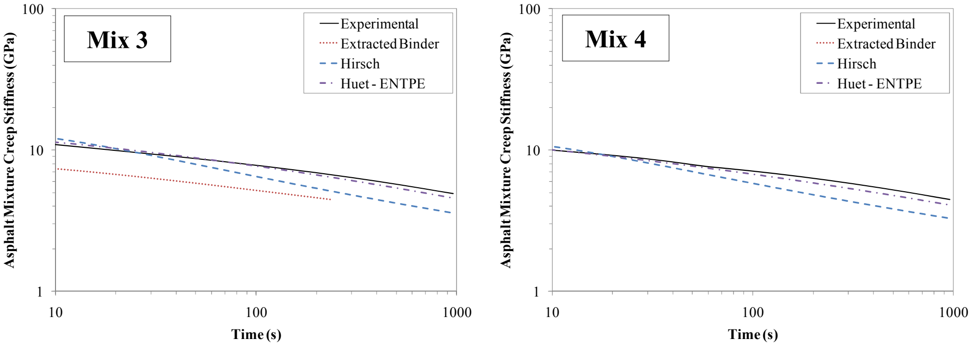

Figure 6.18. Finite element simulation comparison for mixture 3 and 4, T=-6ºC

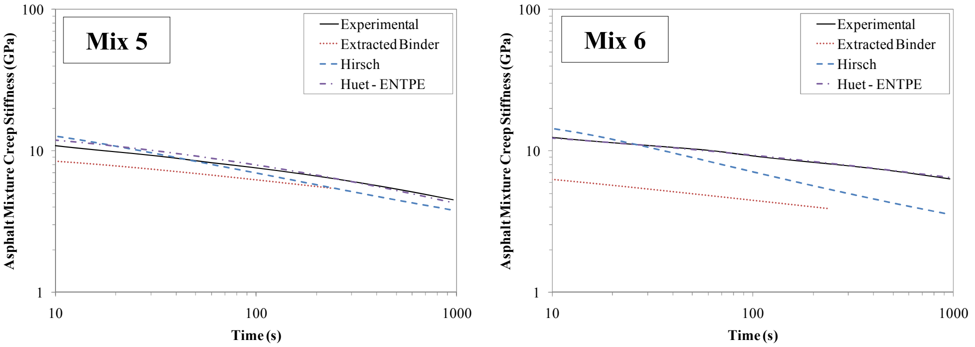

Figure 6.19. Finite element simulation comparison for mixture 5 and 6, T=-6ºC

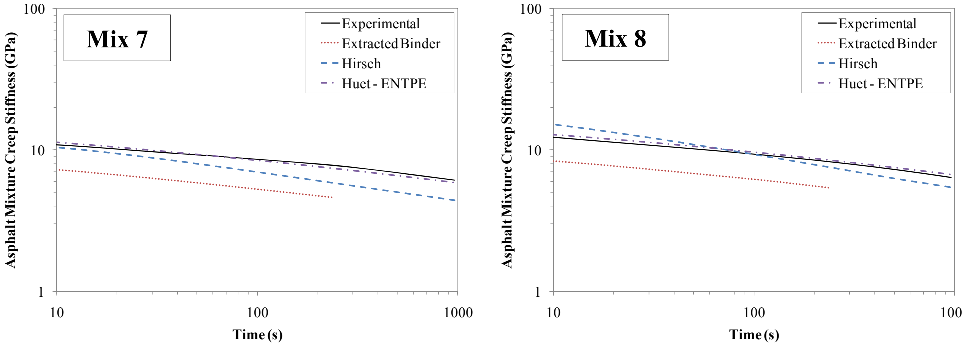

Figure 6.20. Finite element simulation comparison for mixture 7 and 8, T=-6ºC

From the plots it is evident that the finite element simulations that use the back calculated asphalt binder stiffness obtained from the Huet model, coupled with the ENTPE transformation, [6.7] as input, are more accurate than those performed using the Hirsch model predictions and for sure much closer to the asphalt mixture creep stiffness experimental data than what are the simulations that use the creep stiffness of the extracted asphalt binder. However, as in the case of the back calculation of the asphalt binder creep stiffness, it seems that the simulations based on Huet-ENTPE approach and extracted binder data present parallel curves in log scale.

Overall, based on the finite element simulations, the Huet-ENTPE formulation seems to provide the best asphalt binder creep stiffness prediction. Anyway the strong assumption made at the beginning of this Chapter of assuming a single identical value for the aggregate modulus, may be not realistic. Further information is required on the characteristics of RAP and shingles (TOSS and MWSS) included in the different mixtures to elaborate more precise finite element simulation since it may be that such an assumption is masking some effects of the aggregates and the good results obtained may be biased by this.

As in the case of asphalt binder creep stiffness, the simulation results obtained from the extracted asphalt binder data and those obtained from backcalculation are significantly different with higher values for the modeling input. This was expected since the asphalt binder creep stiffness of the extracted binder was much smaller than that predicted from both Huet-ENTPE expression [6.7] and Hirsch model. However, this cannot be related to the finite element simulations itself, even though a more sophisticated 3D geometry reconstruction of the asphalt mixtures beam through X-Ray CT tomography may provide more accurate results. On the other hand, the price to pay for such an accuracy improvement would be an increased computational time of simulations.

It turns out that also the FE simulations seem to put a spot light on the actual interaction between the aged binder (contained in RAP, TOSS and MWSS) and the virgin binder when mixed together both in the case of mixture preparation (laboratory or plant) and chemical extraction. As mention in the previous section it may be that the very stiff asphalt binder present in the recycled material cannot melt and/or partially blend with the virgin one after heating and mixing. However other explanations can be given for significant difference between the results.

In the case of the mixtures containing only RAP, it was hypnotized that the higher stiffness showed from the backcalculated binder prediction, compared to that of the extracted binder, may be due to an erroneous mixture preparation, where a smaller amount of virgin binder was used, resulting in dryer asphalt mixtures. This can lead to much stiffer asphalt mixtures. On the other hand, when extraction is performed, the asphalt binder blend obtained from virgin and oxidized asphalt binders, presents much different characteristics with smaller creep stiffness.

When analyzing the results for the four asphalt binders - asphalt mixtures containing both RAP and RAS (mixtures # 5, 6, 7 and 8) particular attention should be carried since one of the basic components of shingles is paper backing. This material has fibrous characteristics and thus it significantly contribute to the stiffness of the asphalt mixtures. However when binder extraction is performed fiber are washed away during the extraction process and thus their contribution to the asphalt binder creep stiffness is then removed. This may be an explanation to the significantly higher results obtained from asphalt binder creep stiffness backcalculation compared to the extracted asphalt binder creep stiffness. Analogous conclusions were drawn by *Cascione et al*. (*2010*) when investigating the dynamic modulus of asphalt mixtures containing both RAP and RAS and the PG grade of the corresponding extracted asphalt binder. It must be also mentioned that the detection of fibers is not possible during the scanning process and thus they cannot be represented in the finite element simulations.

As for backcalculation models and for Hirsch model in particular, it is known that micromechanical models present some limitations since their formulations relate asphalt binders and asphalt mixtures properties in a fundamental way. On the other hand, Huet -ENTPE expression [6.7] can be categorized as phenomenological model. The advantage of this type of model is that they are directly fitted to the experimental data. However, little is known about the physical meaning of the parameters they are built on. For this reason a more in dept study should be carried on to investigate how δ, k, h, E_∞, and τ affect the predicted properties.

Chapter 7. Conclusion and Closing Remarks

7.1. Summary

In this dissertation, the use of different type of recycled asphalt materials in asphalt pavement with applications to low temperatures was investigated based on statistical analysis and modeling of an extensive set of experiments.

The experimental part consisted of three-point bending creep tests performed in the Bending Beam Rheometer (BBR) on thin asphalt mixtures beams with dimensions 6.25 × 12.5 × 101.6 mm. Seventeen asphalt mixtures were tested at two low pavement service temperature levels: high temperature level (PG low limit + 22˚C), intermediate temperature level (PG low limit + 10˚C).

Statistical analyses were performed to compare the results of the different mixtures based on the experimental data obtained. The influence of Reclaimed Asphalt Pavement (RAP), Tear-off Scrap Shingles (TOSS) and Manufacturer Waste Scrap Shingles (MWSS) on the asphalt mixtures creep stiffness, *m*-value, thermal stress and critical temperature were investigated using ANOVA.

In the theoretical part, the different asphalt mixtures specimens (two-dimensional projections of the beams) were analyzed based on digital image analysis, micromechanical and analogical models, and finite element modeling. The volumetric fractions and particle size distributions of the different mixtures were estimated from their binary images after digital processing. Detailed information on the internal structure of the asphalt mixtures material was investigated by calculating the 2- and 3-point correlation functions of the BBR specimens.

For a limited number of mixtures, micromechanical Hirch model and analogical Huet model coupled with ENTPE trasnformation were used to backcalculate the asphalt binder bulk properties (asphalt binder creep stiffness) of the binder present in the mixtures (inverse problem) and compared to the asphalt binder creep stiffness experimental data provided by the Minnesota Department of Transportation. Finally the results from two-dimensional finite element simulations of three point bending test, based on the reconstructed microstructure of the asphalt mixture beams, were used to validate the models used in the backcalculation of the mixture asphalt binder mechanical properties.

7.2. Conclusion

Several conclusions can be drawn from the different Chapters and sections of this thesis. For asphalt mixture creep stiffness and *m*-value it can be concluded that:

- Significant increase in asphalt mixture creep stiffness is experienced for a 25% RAP content when RAP is the only recycled material included in the mixtures. On the other hand a significant decrease of the *m*-value and thus of the relaxation properties of the mix are shown for all RAP percentage investigated.
- For a fixed RAP content of 15% mixtures containing up to 3% of Tear-off Scrap Shingles (TOSS) presents a decrease in creep stiffness. On the other hand when 5% Manufacturer Waste Scarp Shingles (MWSS) are added to the mix creep stiffness increases significantly. Neither TOSS nor MWSS statistically affect the *m*-value.
- Tear-off Scrap Shingles and Manufacturer Waste Scrap Shingles do not affect the creep stiffness of mixtures designed with 25% of RAP. However an increase in TOSS is negatively correlated to the *m*-value resulting in mixture with poorer relaxation properties.
- When using softer binder there is a decrease in creep stiffness for asphalt mixtures containing 5% of Tear-off Scrap Shingles, while there is no binder type effect when Manufacturer Waste Scrap Shingles are present. An increase in *m*-values is however experienced for softer binder meaning that using a PG 52-34 is beneficial to the relaxation characteristics of the mixtures.

The main findings for thermal stress and critical temperature can be summarized as follow

- When only RAP is present in the mixtures both cooling rate and RAP content are statistically significant. They are positively correlated with thermal stress and critical temperature meaning that, for an increase in RAP content and cooling rate, there is an increase in thermal stress and critical temperature resulting in a more brittle and temperature susceptible mixture.
- For mixture containing 15% of RAP cooling rate has a positive correlation with thermal stress and critical temperature. However the contribution of Recycled Asphalt Shingles to thermal stress is highly significant only for TOSS at 3% resulting in an increase of the stress in the pavement. A significant critical temperature increase is experienced only for a TOSS content of 3%.
- When 25% of RAP is present in the mixtures there is a significant increase in thermal stress when TOSS or MWSS are present up to a 3%. Critical temperature is affected

by all the factors levels showing an increase as the recycled material content increases. Cooling rate is positively correlated both with thermal stress and critical temperature.

- A softer binder type shows to be statistically significant and negatively correlated with thermal stress. As a result softer binder helps reducing the thermal stress in pavement. However depending on the type of recycled material included in the mixtures (TOSS or MWSSS) it may not be helpful in decreasing the critical temperature of the specific mixture.

From the digital image analysis it was found that:

- The volumetric fraction and the average distribution of aggregates for the different asphalt mixtures are very similar suggesting that the mixtures were designed for the same amount of aggregate in volume even though they include various type of recycled asphalt material.
- Based on the average values of the particle size distribution obtained from two-dimensional images, the mixtures show very similar gradation curves. This impression is also confirmed by a visual comparison of the mixtures with similar characteristics in terms of RAP, Tear-off Scrap Shingles (TOSS) and Manufacturer Waste Scrap Shingles (MWSS) content.
- The 2- and 3-point correlation functions calculated for asphalt mixtures behave similarly to what would be expected from a theoretical solution using the penetrable spheres model. No large variations are observed between the 2- and 3-point correlation functions. The results contained in S_2 and S_3 suggest that there is no unexpected pattern in the asphalt mixtures microstructure and thus that the recycled materials added to the mixtures do not deviate the distribution of the mixtures constituents, and in particulars of the aggregates, from that of a typical random heterogeneous material.

From the modeling section it can be concluded that:

- The Hirsch model and the Huet model, coupled with the ENTPE transformation, predict higher asphalt binder creep stiffness than those obtained from the Bending Beam Rheometer testing on the extracted asphalt binder.
- In general the asphalt binder creep stiffness obtained using Huet-ENTPE formulation are parallel to the creep stiffness of the extracted asphalt binder up to 240s in log scale.
- The two dimensional finite element simulations performed using as input the asphalt binder creep stiffness obtained from Hirsch model, Huet-ENTPE approach and from

the extracted binder suggest that, under the assumed hypothesis on the aggregates properties, the ENTPE transformation, with the embedded Huet model, provides a good estimation of the asphalt binder creep stiffness of the mixtures investigated. On the other hand Hirsch model doesn't seem to give good asphalt binder creep stiffness predictions.

- The two dimensional finite element simulations seem also to indicate that the creep stiffness of the extracted asphalt binder is not representative of the real properties of the binder when in the mix. This is something expected since extraction results in a complete blending of the different binder present in the mixtures and coming from different sources (virgin, RAP, TOSS and MWSS).
- The fibrous materials contained in RAS may contribute to the global stiffness of the recycled asphalt mixtures, however they may be just one of the reason for the difference between the backcalculated and extracted asphalt binder creep stiffness.

7.3. Recommendations and Future Work

Based on the findings from this dissertation, the following recommendations for future work are made:

- Include all the recycled materials type investigated (RAP, TOSS and MWSS) in the mix design so that the interaction between Tear-off Scrap Shingles and Manufacturer Waste Scrap Shingles may be evaluated in terms of asphalt mixture creep stiffness, *m*-value, thermal stress and critical temperature.
- Improve the algorithm for the calculation of the grain size distribution to solve the difficulty of having several particles in contact.
- Investigate the orientation of the particles in the mixtures since this may give more insight on the influence of Reclaimed Asphalt Pavement (RAP), Tear-off Scrap Shingles (TOSS) and Manufacturer Waste Scrap Shingles (MWSS) on the asphalt mixtures microstructure.
- Evaluate the complete 3-point correlation function.
- Conduct a sensitivity study on Huet model parameter to investigate how they are related to the predicted properties.

- Evaluate the Huet model and ENTPE transformation on a larger number of mixtures containing different amount of RAP since this may help in finding an expression for the α parameter.
- Run two-dimensional finite element models with finer mesh so to reduce the effect of coarser particle size in the mastic phase.

References

AASHTO T 313-02, Determining the flexural creep stiffness of asphalt binder using the Bending Beam Rheometer (BBR), American Association of State Highway and Transportation Officials, 2006.

AASHTO T 314-02, Standard Method of Test for Determining the Fracture Properties of Asphalt Binder in Direct Tension (DT), American Association of State Highway and Transportation Officials, 2002.

AASHTO T 322-03, Determining the creep compliance and strength of hot-mix asphalt (HMA) using the Indirect Tensile test device, American Association of State Highway and Transportation Officials, 2006.

ABAQUS, help documentation, ver. 6.9-1, 2009.

Abbas A. R., Papagiannakis A. T., Masad E. A., Linear and nonlinear viscoelastic analysis of the microstructure of asphalt concretes, Journal of Materials in Civil Engineering, vol. 16(2), pp. 133-139, 2004.

Ahn J., Kang S. and Kwon Y., A flexible inverse Laplace transform algorithm and its application, Computing, vol. 71(2), 2003.

Alfrey T., Non-homogenous stresses in visco-elastic media, Quarterly of Applied Mathematics, vol. 2, pp. 113-119, 1944.

Amin A. F. M. S., Alam M. S., Okui Y., An improved hyperelasticity relation in modeling viscoelasticity response of natural and high damping rubbers in compression: experiments, parameter identification and numerical verification, Mechanics of Materials, vol. 34, pp. 75-95, 2002.

Anderson, D.A., and Kennedy, T., Development of SHRP binder specification, Journal of Association of Asphalt Paving Technologists, vol. 62, pp. 481-507, 1993.

Anderson D. A., Christensen D. W., Bahia H., Physical properties of asphalt cement and the development of performance related specifications, Journal of the Association of Asphalt Paving Technologist, vol. 60, pp. 437-475, 1991.

Arutyunyan N. K., Zevin, A.A., Design Structures Considering Creep, Taylor & Francis, Rotterdam, Netherlands, 1988.

ASTM D 225-07 American Society for Testing and Materials, ASTM D 225-07, Standard specification for asphalt shingles (organic felt) surfaced with mineral granules, Annual Book of ASTM Standards, Volume 4.04, 2007.

ASTM D 225-07 American Society for Testing and Materials, ASTM D 3462/3462-10a, Standard specification for asphalt shingles made from glass felt and surfaced with mineral granules, Annual Book of ASTM Standards, Volume 4.04, 2010.

Bahia H., Anderson D. A., Christensen D., The Bending Beam Rheometer: a simple device for measuring low-temperature rheology of asphalt binders, Journal of the Association of Asphalt Paving Technologists, vol. 61, pp. 117-153, 1992.

Basu A., An evaluation of the time-temperature equivalence factor and of the physical hardening effects on low temperature asphalt binder specifications, MS thesis, University of Minnesota, Minneapolis, 2002.

Bell F. G., Engineering Properties of Soils and Rocks, Blackwell Sicence, 2000.

Beran, M., Statistical Continuum Theories, Interscience, New York, 1968.

Berryman, J. G., Measurement of spatial correlation functions using image processing techniques, Journal of Applied Physics, vol. 57, pp. 2374-2384, 1985.

Better Roads, Recycling Alternatives Studied and Tried, vol. 67, no. 3, 1997.

Bocciarelli M., Bolzon G., Maier G., Parameter identification in anisotropic elastoplasticity by indentation and imprint mapping, Mechanics of Materials, vol. 37, pp. 855-868, 2005.

Bodin D., Pijaudier-Cabot G., De La Roche C., Piau J., Chabot C., Continuum Damage Approach to Asphalt Concrete Fatigue, Modeling, Journal of Engineering Mechanics, ASCE, June 2004.

Bonaquist R., A new tool to design and characterize higher RAP HMA, Presentation, Presented at 2007 Greater Iowa Asphalt Conference, Des Moines, IA, 2007.

Bonaquist R., Can I Run More RAP?, Hot Mix Asphalt Technology, pp. 11-13, September/October 2007.

Bouldin M. G., Dongre R. N., Sharrock M. S., Rowe G. M. and Anderson D. A., Predicting Thermal Cracking of Pavements from Binder Properties – Theoretical Basis and Field Validation, Journal of the Association of Asphalt Paving Technologists, vol. 69, pp 455-496, 2000.

Brown E. R., Evaluation of properties of recycled asphalt concrete hot mix, Final Report CL-84-2. U.S. Army Engineer Waterways Experiment Station, Vicksburg, Mississippi, 1984.

Buttlar W.G., Roque R., Development and evaluation of the Strategic Highway Research Program measurement and analysis system for Indirect Tensile Testing at low temperatures, Transportation Research Record, vol. 1454, pp. 163-171, 1994.

Buttlar W. G., Roque R., Evaluation of empirical and theoretical models to determine asphalt mixture stiffnesses at low temperatures, Journal of the Association of Asphalt Paving Technologists, vol. 65, pp. 99-141, 1996.

Buttlar W. G., Bozkurt D., Al-Khateeb G. G., Waldhoff A. S., Understanding asphalt mastic behavior through micromechanics, Transportation Research Record, vol. 1681, pp.157-166, 1999.

Buttlar W. G., Dave E. V., A micromechanics-based approach for determining presence and amount of recycled asphalt pavement material in asphalt concrete, Journal of the Association of Asphalt Paving Technologists, vol. 74, pp. 829-883, 2005.

Button J. W., Williams D. and Scherocman J. A., Roofing shingles and toner in asphalt pavements, Research Report 1344, Research Study no. 0-1344, Texas Transportation Institute, The Texas A&M University System, 1996.

Cannone Falchetto A., Micromechanics and analogical models for forward and inverse problems in asphalt materials low temperature characterization, MS thesis, University of Minnesota, Minneapolis, August 2010.

Cannone Falchetto A., Marasteanu M. O. and Di Benedetto H. Analogical based approach to forward and inverse problems for asphalt materials characterization at low temperatures, Journal the Association of Asphalt Paving Technologists, vol 80, 2011 (in press).

Cascione A.A., Willimas R. C. Gillen S. L., and Haugen D. S. Utilization of post consumer recycled asphalt shingles and fractioned recycled asphalt pavement in hot mix asphalt, Proceeding of the 2010 Mid-Continent Transportation Research Forum, 2010.

Chabot A., Chupin O., Deloffre L., Duhamel D., Viscoroute 2.0: a tool for the simulation of moving load effects on asphalt pavement, Road Material and Pavement Design, Special Issue on Recent Advances in Numerical Simulation of Pavements, 2010.

Chen J.S., Shiah M.S. and Chen H.J., Quantification of coarse aggregate shape and its effect on engineering properties of hot-mix asphalt mixtures, Journal of Testing and Evaluation, vol. 29, pp. 513–519, 2001.

Chen J.S. and Liao M.C., Evaluation of internal resistance in hot-mix asphalt concrete, Construction and Building Materials, 16, pp. 313-319, 2002.

Chen J.S., Wong S.Y. and Lin K.Y., Quantification of movements of flat and elongated particles in hot-mix asphalt subject to wheel load test, Journal of Materials and Structures, vol. 38(3), pp. 395-402, 2005.

Christensen R. M., Mechanics of composite materials, Dover Publications, INC., Mineola, New York, 1979.

Christensen R. M., Theory of viscoelasticity, an introduction, Academic Press, 1982.

Christensen D. W., Analysis of creep data from indirect tension tests on asphalt concrete, Journal of the Association of Asphalt Paving Technologists, vol. 67, pp. 458-477, 1998.

Christensen D., Pellinen T., Bonaquist R. F. Hirsch model for estimating the modulus of asphalt concrete, Journal of the Association of Asphalt Paving Technologists, vol. 72, pp. 97-121, 2003.

Cook R. D. and Weisberg S., Applied regression including computing and graphics, Wiley-Interscience, August 6, 1999.

Corson, P., Correlation functions for predicting properties of heterogeneous materials. I. Experimental measurement of spatial correlation functions in multiphase solids, Journal of Applied Physics, vol. 45, no 7, pp. 3159-3170, 1974.

Daniel J. S., Kim Y. R. and Lee H. J., Effects of aging on viscoelastic properties of asphalt-aggregate mixtures, Transportation Research Record, vol. 1630, pp. 21-27, 1998.

De La Roche C., Module de rigidité et comportement en fatigue des enrobés bitumineux. Expérimentations et nouvelles perspectives d'analyse. Thèse de Doctorat : Ecole Centrale Paris, 189 p., Décembre 1996 [In French].

Di Benedetto H., Partl M. N., Francken L., De La Roche, Stiffness testing for bituminous mixtures, Materials and Structure, vol. 34, pp. 66-70, 2001.

Di Benedetto H., Olard F., Sauzéat C., Delaporte B., Linear viscoelastic behaviour of bituminous materials : from binders to mixes, Road Material and Pavement Design, vol. 5 – Special Issue, pp.163-202, 2004.

Di Benedetto H., Delaporte B., Sauzeat C., Three-dimensional linear behavior of bituminous materials: experiments and modeling, International Journal of Geomechanics, vol. 7(2), pp. 149-157, 2007.

Di Benedetto H., Neifar M., Sauzéat C., Olard F. Three-dimensional thermo-viscoplastic behavior of bituminous materials. The DBN law, Road Material and Pavement Design, vol. 8, pp.285-315, 2007.

Delaporte B., Di Benedetto H., Chaverot P., Gauthier G., Linear viscoelastic properties of bituminous materials : from binders to mastics, Journal of the Association of Asphalt Paving Technologists, vol. 76, pp. 455-494, 2007.

Eriksen K., and Wegan V., Optical methods for the evaluation of asphalt concrete and polymer-modified bituminous binders, Note 244, Danish Road Institute, 1993.

Ferry J. D., Viscoelastic properties of polymers, 3rd ed.,Wiley and Sons, New York, 1980.

Findley W. N., Lai J. S., Onaran K., Creep and relaxation of nonlinear viscoelastic materials, Dover Publications, INC., New York, 1989.

Gere J. M. and Timoshenko S. P., Mechanics of materials, pws-kent publishing company, Boston, 3rd edition, 1990.

Gonzales R., Woods R., Eddins S., Digital Image Processing using MATLAB, Pearson Prentice Hall, 2004.

Graham G. A. C., The correspondence principle of linear viscoelastiity theory for mixed boundary value problems involving time-dependent boundary regions, Quarterly of Applied Mathematics, vol 26(2), pp. 167-174, 1968.

Hanson D. I., Foo K. Y. and Lynn T. A., Evaluation of roofing shingles in HMA, Final Report, NCAT—National Center for Asphalt Technology, Auburn University, 1997.

Hashin Z., Shtrikman S., A variational approach to the theory of the elastic behavior of multiphase materials, Journal of the Mechanics and Physics of Solids, vol. 11, pp. 127-140, 1963.

Hill, R., A self consistent mechanics of composite materials, Journal of the Mechanics and Physics of Solids, vol. 13, pp. 213-222, 1965.

Hirsch T. J., Modulus of elasticity of concrete affected by elastic moduli of cement paste matrix and aggregate, Journal of the American Concrete Institute vol. 59(3), pp. 427-452, 1962.

Hopkins I. L., Hamming R. W., On creep and relaxation, Journal of Applied Physics, vol. 28, pp. 906-909, 1957.

Huang Y., Mogilevskaya S. G., Crouch S. L., Semi-analytical solution for a viscoelastic plane containing multiple circular holes, Journal of Mechanics of Materials and Structures, vol. 1(3), pp. 471-501, 2006.

Huet, C., Etude par une méthode d'impédance du comportement viscoélastique des matériaux hydrocarbonés. Thèse de doctorat d'ingénieur, Faculté des Sciences de l'Université de Paris, 69 p. [In French], October 1963.

Jackson N. M. and Vinson T. S., Analysis of thermal fatigue distress of asphalt concrete pavements, Transportation Research Record, vol. 1545, pp. 43-49, 1996.

Janisch D. and Turgeon C. Minnesota's experience with scrap shingles in bituminous pavements, Report No. MN/PR – 96/34, Minnesota Department of Transportation, 1996.

Jiao, Y., Stillinger, F.H. and Torquato, S., Modeling heterogeneous materials via two-point correlation functions: Basic principles, Physical Review, E76, 031110, 2007.

Johnson E., Johnson G., Dai S., Linell D., McGraw J. and Watson M., Incorporation of recycled asphalt shingles in hot-mixed asphalt pavement mixtures, Final Report MN/RC 2010-08, Minnesota Department of Transportation, 2010.

Jordaan I. J. and Khalifa M. A., Creep analysis of reinforced and prestressed concrete structures under non-uniform temperature distributions, using elastic solutions, International Journal for Numerical Methods in Engineering, vol. 11, pp. 883-895, 1977.

Jung D. and Vinson T. S., Low temperature cracking resistance of asphalt concrete mixtures, Journal of the Association of Asphalt Paving Technologists, vol. 62, pp. 54–92, 1993.

Karlsson R. and Isacsson U., Bitumen rejuvenator diffusion as influenced by ageing, Road Materials and Pavement Design. vol. 3/2, pp. 167-182, 2002.

Karlsson R. and Isacsson U., Bitumen structural stability characterization using turbidimetric titration, Energy & Fuels, vol. 17, pp. 1407-1415, 2003.

Karlsson R. and Isacsson U., Application of FTIR-ATR to characterization of bitumen rejuvenator diffusion, Journal of Materials in Civil Engineering, ASCE, vol. 15/2, pp. 157-165, 2003.

Karlsson R. and Isacsson U., Laboratory studies of diffusion in bitumen using markers, Journal of Material Science, vol. 33/13, pp. 2835-2844, 2003.

Kandhal P. S., Rao S. S., Watson D. E. and Yound B., Performance of recycled hot mix asphalt mixtures. Research Report 95-1, National Center for Asphalt Technology, Auburn, Ala., 1995.

Kandhal P. S. and Foo K. Y., Designing recycled hot mix asphalt mixture using superpave technology, Paper prepared for publication in ASTM STP, vol. 1322, 1997.

Kim Y. R., Lee Y. C. and Lee H. J., Correspondence principle for characterization of asphalt concrete, Journal of Materials in Civil Engineering, vol. 7(1), pp. 59-68, 1995.

Kim Y. R., Little D. N., Linear viscoelastic analysis of asphalt mastics, Journal of Materials in Civil Engineering, vol. 16(2), pp. 122-132, 2004.

Kim S., Kreider K. L., Parameter identification for nonlinear elastic and viscoelastic plates, Applied Numerical Mathematics, vol. 56(12), pp. 1538-1554, 2006.

Kose S., Guler M., Bahia H.U. and Masad, E., Distribution of Strains within Hot-mix Asphalt Binders: Applying Imaging and Finite Element Techniques, Transportation Research Record, vol. 1728, pp. 21-27, 2000.

Leaderman H., Elastic and creep properties of filamentous materials and other high polymers, Textile Foundation, 1943.

Lee E. H., Stress analysis in visco-elastic bodies, Quarterly of Applied Mathematics, vol 13(2), pp. 183-190, 1955.

Lee S. S. and Kim Y. J., Time-domain boundary element analysis of cracked linear viscoelastic solids, Engineering Fracture Mechanics, vol. 51(4), 585–590, 1995.

Lee K. W., Supharath N., Shukla A., Franco C. A. and Manning F. J., Rheological and mechanical properties of blended asphalts containing recycled asphalt pavement binders, Journal of the Association of Asphalt Paving Technologists, vol-68, pp 89-118, 1999.

Little D. H., Holmgreen Jr. R. J, and Epps J. A., Effect of recycling agents on the structural performance of recycled asphalt concrete materials, Journal of the Association of Asphalt Paving Technologists, vol. 50, pp. 32–63, 1981.

Li X., Marasteanu M. O., Williams R. C. and Clyne T. R., Effect of reclaimed asphalt pavement (proportion and type) and binder grade on asphalt mixtures, Transportation Research Record, vol. 2051, pp. 90-97, 2008.

Li Y., Metcalf J. B., Two-step approach to prediction of asphalt concrete modulus from two-phase micromechanical models, Journal of Materials in Civil Engineering, vol. 17(4), pp. 407-415, 2005.

Lundstrom R. and Isacsson U., An investigation of the applicability of Schapery´s work potential model for characterization of asphalt fatigue behavior, Journal of the Association of Asphalt Paving Technologists, vol. 73, pp. 657-696, 2004.

Lytton R. L., Uzan J., Rogue R., Hiltunen D., Stoffel, S. M., Development and validation of performance prediction models and specifications for asphalt binder and paving mixes", SHRP-A-357, Strategic Highway Research Program , National Research Council, Washington, DC, 1993.

MacANOVA version 5.05, release 1, Oehlert W. G. and Bingham C., University of Minnesota, http://www.stat.umn.edu/macanova/ , 2006.

Maillard S., Fissuration et autoreparation des liants bitumineux – apport de l'essai de rupture locale repetee sur bitumen -. Thèse de doctorat d'ingénieur, L'Ecole Central de Nantes et l'Université de Nantes, Juin 2005. [In French].

Marasteanu M. O., Anderson D. A., Time-temperature dependency of asphalt binders-an improved model, Journal of the Association of Asphalt Paving Technologists, vol. 65, pp. 408-435, 1996.

Marasteanu M. O., Anderson D. A., Comparison of moduli for asphalt binders obtained from different test devices, Journal of the Association of Asphalt Paving Technologists, vol. 69, pp. 574-606, 2000.

Marasteanu M., Velasquez R., Cannone Falchetto A., and Zofka A., Development of a simple test to determine the low temperature creep compliance of asphalt mixture, IDEA Program Final Report NCHRP 133, 2009, Transportation Research Board of the National Accademies.

Marks V. J. and G. Petermeier, Let Me Shingle Your Roadway, Iowa Department of Transportation, Ames, 1997.

Martínez-Martínez J., Benavente D., García Del Cura M. A. and Cañaveras J. C., Application of ultrasonics to brecciated dolostones for assessing their mechanical properties, IAEG2006, Engineering Geology for Tomorrow's Cities, The 10th IAEG International Congress, Nottingham, United Kingdom, 6-10 September 2006.

Masad E., Muhunthan B., Shashidhar N., and Harman T., Aggregate orientation and segregation in asphalt concrete, Geotechnical Special Publication, vol 85, pp. 69-80, 1998.

Masad E., Muhunthan B., Shashidhar N. and Harman, T., Internal structure characterization of asphalt concrete using image analysis, Journal of Computing in Civil Engineering., ASCE, 13(2), pp. 88-95, 1999.

Masad E., Somadevan N., Microstructural Finite-Element analysis of influence of localized strain distribution on asphalt mix properties, Journal of Engineering Mechanics, vol. 128(10), pp. 1105-1114, 2002.

Masad, E. and Button J., Implications of experimental measurements and analyses of the internal structure of hot-mix asphalt, Transportation Research Record 1891, pp. 212-220, 2004.

Masad E., Dessouky S., Little D., Development of an elastoviscoplastic microstructural-based continuum model to predict permanent deformation in hot mix asphalt, International Journal of Geomechanics, vol. 7(2), pp. 119-130, 2007.

MATLAB, help documentation, R2008a, 2008.

McDaniel R. S. and Anderson R. M., NCHRP Report 452: Recommended Use of reclaimed asphalt pavement in the superpave mix design method: technician's manual. TRB, National Research Council, Washington, D.C., 2002.

McGraw J., Zofka A., Krivit D., Schroer J., Olson, R. and Marasteanu, M. Recycled asphalt shingles in hot mix asphalt, Journal of the Association of Asphalt Paving Technologists, vol. 76, pp. 235-274, 2007.

McNichol D., Paving the way: asphalt in America, National Asphalt Pavement Association, 2005.

Mead D. W., Numerical interconversion of linear viscoelastic material functions, Journal of Rheology, vol. 38(6), pp. 1769-1795, 1994.

Meyers F., Tessier G. R., Haas R. and Kennedy T. W., Study of hot mix recycling of asphalt pavements, Report TP 2964 E, Roads and Transportation Association of Canada, Ottawa, Ontario, 1983.

Milton G. W., Bounds on the electromagnetic, elastic, and other properties of two-component composites, Physical Review Letters, vol. 46(8), pp. 542-545, 1981.

Minnesota Department of Transportation, Combined 2350/2360 plant mixed asphalt pavement, standard specifications for construction, Minnesota Department of Transportation, 2008.

Monismith, C. L., Secor, K. E., Viscoelastic behavior of asphalt concrete pavements, Journal of the Association of Asphalt Paving Technologists, vol. 34, pp. 248-285, 1962.

Moon K. H., Comparison of thermal stress calculated form asphalt binder and asphalt mixture creep compliance, MS thesis, University of Minnesota, Minneapolis, 2010.

Moore D. S., McCabe G. P. and Craig C., Introduction to the Practice of Statistics, W. H. Freeman; 6th edition, December 25, 2007.

NAPA, National Asphalt Pavement Association, Virtual Superpave laboratory, CD-ROM, 2005.

National Cooperative Highway Research Program, Recommended Use of Reclaimed Asphalt Pavement in the Superpave Mix Design Method: Guidelines, Research Results Digest 253, 2001

National Cooperative Highway Research Program, Recommended Use of Reclaimed Asphalt Pavement in the Superpave Mix Design Method: Technician's Manual, Transportation Research Board, Report 452, 2001.

NCAT, National Center for Asphalt Technology, Hot mix asphalt materials, mixture design and construction, 2009.

Neifar M., Comportement thermomécanique des enrobés bitumineux : expérimentation et modélisation. Thèse de Doctorat ENTPE-INSA Lyon, pp. 289, 1997 [In French].

Neifar M. Di Benedetto H., Thermo-viscoplastic law for bituminous mixes, Road Material and Pavement Design, vol. 2, Issue 1, 2001.

Newcomb D., Stroup-Gardiner M., Weikle B. and Drescher A., Influence of roofing shingles on asphalt concrete mixture properties, Report no. MN/RC-93/09, Minnesota Department of Transportation, St. Paul, MN, 1993.

Oehlert G. W., A first course in desing and analysis of experiments, W. H. Freeman; 1st edition, January 19, 2000.

Offrell P. and Magnusson R., In situ photographic survey of crack propagation in flexible pavements, International Journal of Pavement Engineering, vol. 5 (2), pp. 91-102, 2004.

Ohkami T., Swoboda G., Parameter identification of viscoelastic materials, Computers and Geotechnics, vol. 24, pp. 279-295, 1999.

Olard F., Di Benedetto H., Dony A., Vaniscote J.C., Properties of bituminous mixtures at low temperatures and relations with binder characteristics, 6th international RILEM Symposium on Performance Testing and Evaluation of Bituminous Materials, Zurich, April 2003.

Olard F., Comportement thermomécanique des enrobes bitumineux a basses températures – relation entre les propriétés du liant et de l'enrobe, Thèse de Doctorat : Ecole Nationale des Travaux Publics de l'Etat, 226 p., Octobre 2003 [In French].

Olard F., Di Benedetto H., General "2S2P1D" model and relation between the linear viscoelastic behaviors of bituminous binders and mixes. Road Material and Pavement Design, vol. 4/2 – Special Issue, pp.185-224, 2003.

Olard F., Di Benedetto H., The "DBN" Model: A Thermo-Visco-Elasto-Plastic Approach for Pavement Behavior Modeling, Journal of the Association of Asphalt Paving Technologists, vol. 74, 2005.

Papagiannakis A. T., Abbas A., Masad E., Micromechanical analysis of viscoelastic properties of asphalt concretes, Transportation Research Record, vol. 1789, pp. 113-120, 2002.

Park S. W., Kim Y. R., Interconversion Between relaxation modulus and creep compliance for viscoelastic solids, Journal of materials in Civil Engineering, vol. 11(1), pp. 76-82, 1999.

Paulino G. H. and Jin Z. H., Correspondence principle in viscoelastic functionally graded materials, Journal of Applied Mechanics, vol. 68, pp. 129-132, 2001.

Pellinen T. K., Witczak M. W., Stress dependent master curve construction for dynamic (complex) modulus, Journal of the Association of Asphalt Paving Technologists, vol. 71, pp. 281-309, 2002.

Roque R., Buttlar W. G., The development of a measurement and analysis system to accurately determine asphalt concrete properties using the Indirect Tensile mode, Journal of the Association of Asphalt Paving Technologists, vol. 61, pp. 304-328, 1992.

Roque R., Birgisson B., Zhang Z., Sangpetngam B., Grant T, Implementation of SHRP Indirect Tension tester to migrate cracking in asphlat pavements and overlays. University of Florida, Final Report submitted to Florida Department of Transportation, May 2002.

Sayegh G., Variation des modules de quelques bitumes purs et enrobés bitumineux. Thèse de doctorat d'ingénieur, Faculté des Sciences de l'Université de Paris, 74p., June 1965 [In French].

Schafer A., Teyssen T., Size, shape and orientation of grains in sand stones- image analysis applied to rock thin-sections, Sedimentary Geology, vol. 52, pp. 251-271, 1987.

Secor K. E., Monismith C. L., Analysis and interrelation of stress-strain-time data for asphalt concrete, Transactions of the Society of Rheology, vol. 8, pp. 19-32, 1964.

Schapery R. A., A method of viscoelastic stress analysis using elastic solutions, Journal of The Franklin Institute, vol. 279(4), pp. 268-289, 1965.

Shenoy A., Single-event cracking temperature of asphalt pavements directly from the Bending Beam Rheometer data, Journal of Transportation Engineering, vol. 128, issue 5, pp. 465-471, 2002.

SPSS v.17.1., www.spss.com, 2008.

Torquato, S., and Stell, G., Microstructure of two-phase random media. III. The n-point matrix probability functions for fully penetrable spheres, Journal of Chemical Physics, vol. 79, pp. 1505, 1983.

Torquato S., Random heterogeneous media: microstructure and improved bounds on effective properties, Applied Mechanics Review, vol. 44(2), pp. 37-76 1991.

Torquato S., Effective stiffness tensor of composite media: II. Applications to isotropic dispersions, Journal of the Mechanics and Physics of Solids, vol. 46(8), pp. 1411-1440, 1998.

Torquato, S., Morphology and effective properties of disordered heterogeneous media, International Journal of Solids and Structures vol. 35, pp. 2385-2406, 1998.

Torquato, S., Modelling of physical properties of composite materials, International Journal of Solids and Structures, vol. 37, pp. 411-422, 2000.

Torquato S., Random heterogeneous materials, Springer-Verlag, New York, 2002.

Tsien H. S., Generalization of Alfrey's theorem for visco-elastic media, Quarterly of Applied Mathematics, vol. 8(1), pp. 104-106, 1950.

Turgeon C., waste tire and shingle scrap bituminous paving test sections on the munger recreational trail gateway segment, Report No. MN/RD-91/06; 9PR6002, Minnesota Pollution Control Agency, Minnesota Department of Natural Resources and Minnesota Department of Transportation, St. Paul, MN, 1991.

Underwood E., Quantitative stereology, Addison-Wesley, Reading, MA, 1970.

University of Wisconsin, AASHTO draft standard: Determining aggregate structure in asphalt mixes by means of planar imaging, (2010).

Velasquez R.A., On the representative volume element of asphalt concrete with application to low temperature, PhD thesis, University of Minnesota, Minneapolis, July 2009.

Velasquez R. A., Cannone Falchetto A., Marasteanu M.O., From mixtures to binder. Can the inverse problem be solved?, Road Material and Pavement Design, vol. 11 – Special Issue, pp.225-250, 2010.

Wang L. B., Wang X., Mohammad L., Wang Y., Application of mixture theory in the evaluation of mechanical properties of asphalt concrete, Journal of Materials in Civil Engineering, vol. 16(2), pp. 167-174, 2004.

Wang J., Birgisson B., Roque R., Effects of viscoelastic stress redistribution on the cracking performance of asphalt pavements, Journal of the Association of Asphalt Paving Technologists, vol. 75, pp. 637-675, 2006.

Watson D. E., Johnson A. and Sharma H. R., Georgia's experience with recycled roofing shingles in asphaltic concrete, Transportation Research Record, vol. 1526, pp. 129-133, 1998.

Weissberg, H., Effective diffusion coefficient in porous media, Journal of Applied Physics, vol. 34, pp.2636 - 2638, 1963.

Williams M. L., Landel R. F., Ferry J. D., The temperature dependence of relaxation mechanism in amorphous polymers and other glass-forming liquids, Journal of the American Chemical Society, vol. 77(14), pp. 3701-3707, 1955.

Wistuba M, Lackner R., Blab R., Spiegl M., Low-temperature performance prediction of asphalt mixtures used for LLP—new approach based on fundamental test methods and numerical modeling, International Journal of Pavement Engineering, Vol. 7, No. 2, 121–132, June 2006.

Yin H. M., Buttlar W. G., Paulino G. H., Di Benedetto H., Micromechanics-based model for asphalt mastics considering viscoelastic effects, presented at 10th International Conference on Asphalt Pavements, August 12-17 2006, Quebec City, Canada, 2006.

Yue Z., Bekking W. and Morin, I., Application of digital image processing to quantitative study of asphalt concrete microstructure, Transportation Research Record 1492, pp. 53-60, 1995.

Yue Z. Q. ,Chen S., Tham L. G., Finite element modeling of geomaterials using digital image processing, Computers and Geotechnics, Vol. 30, pp 375-397, 2003.

Zelelew H.M. and Papagiannakis A.T. and Masad E., Application of digital image processing techniques for aspahtl concrete mixture images, The 12th International Conference of International Association for Computer Methods and Advances in Geomechanics (IACMAG), 1-6 October, 2008, Goa, India

Zelelew H.M., Simulation of the permanent deformation of asphalt concrete mixtures using discrete element method (DEM), PhD thesis, Washington State University, Pullman, May 2008.

Zevin A.A., Approximation of functions of Volterra operators in Boundary Value Problems for aging materials," Ivestiya Vuzov AN SSSR MTT (Proceedings of Universities of the Academy of Science of USSR, Mechanics of Solid Bodies), no. 3, pp. 127-134, 1979 (in Russian).

Zhang W., Drescher A., Newcomb D. E., Viscoelastic analysis of diametral compression of asphalt concrete, Journal of Engineering Mechanics, vol. 123(6), pp. 596-603, 1997.

Zofka A., Marasteanu M., Li X., Clyne T., McGraw J., Simple method to obtain asphalt binders low temperature properties from asphalt mixtures properties, Journal of the Association of Asphalt Paving Technologists, vol. 74, pp.255-282, 2005.

Zofka A., Marasteanu M., Turos M., Investigation of asphalt mixture creep behavior using thin beam specimens, Presented at Multiscale and Functionally Graded Materials Conference, Honolulu, Hawaii, USA, 2006.

Zofka A., Investigation of asphalt concrete creep behavior using 3-point bending test, PhD thesis, University of Minnesota, Minneapolis, July 2007.

Zubeck H. K. and Vinson T. S., Prediction of low-temperature cracking of asphalt concrete mixtures with thermal stress restrained specimen test results, Journal of the Transportation Research Board, vol. 1545, pp. 50-58, 1996.

Zubeck H. K., Zeng H.-Y., Vinson T. S. and Janoo V. C., Field validation of thermal stress restrained specimen test: six case histories, Journal of the Transportation Research Board, vol. 1545, pp. 67-74, 1996.

Appendix A. (Chapter 3)

A.1. Beam Dimensions

Table A.1. Asphalt mixtures BBR beams geometric properties

Mixture	Binder	Recycled Material			Replicate	Dimension	
ID	PG	RAP (%)	TOSS (%)	MW (%)	#	Width (mm)	Thickness (mm)
1-1	58-28	0	0	0	3	12.46	6.38
					5	12.45	6.79
					6	12.45	6.60
					7	12.47	6.40
					8	12.51	6.37
					10	12.57	6.42
1-2	58-28	0	0	0	3	12.55	6.14
					4	12.69	6.30
					5	12.70	6.01
					6	12.71	6.58
					8	12.89	6.60
					9	12.96	6.21
2-1	58-28	15	0	0	3	12.55	6.63
					4	12.45	6.58
					5	12.46	6.30
					6	12.40	6.39
					7	12.31	6.28
					8	12.27	6.47
2-2	58-28	15	0	0	3	12.49	5.89
					4	12.48	6.91
					5	12.37	6.93
					6	12.52	6.52
					7	12.41	6.89
					8	12.44	6.76
3-1	58-28	25	0	0	3	12.44	6.48
					4	12.42	6.32
					5	12.39	6.68
					6	12.33	6.58
					7	12.29	6.57
					8	12.22	6.45
3-2	58-28	25	0	0	3	12.36	6.39
					4	12.35	6.49
					5	12.48	6.10
					6	12.51	6.57
					7	12.50	6.56
					8	12.47	6.32
4-1	58-28	30	0	0	3	12.37	6.88
					4	12.37	6.84
					5	12.38	6.98
					6	12.34	6.69
					7	12.34	6.48
					8	12.34	6.67
4-2	58-28	30	0	0	3	12.44	6.38
					4	12.56	6.24
					5	12.60	6.30
					6	12.66	6.53
					7	12.65	6.57
					8	12.70	6.58
5-1	58-28	15	0	5	3	12.23	6.16
					4	12.25	6.52
					5	12.40	6.56
					6	12.45	6.49
					7	12.52	6.51
					8	12.57	6.27
5-2	58-28	15	0	5	3	12.47	6.48
					4	12.47	6.07
					5	12.49	6.34
					6	12.55	6.33
					7	12.59	6.36
					8	12.65	6.23

Mixture ID	Binder PG	Recycled Material			Replicate #	Dimension	
		RAP (%)	TOSS (%)	MW (%)		Width (mm)	Thickness (mm)
6-1	58-28	15	5	0	3	12.58	6.64
					4	12.63	6.56
					5	12.59	6.56
					6	12.54	6.47
					7	12.58	6.61
					8	12.47	6.52
6-2	58-28	15	5	0	3	12.33	6.44
					4	12.42	6.56
					5	12.47	6.50
					6	12.51	6.44
					7	12.57	6.53
					8	12.65	6.45
7-1	58-28	25	5	0	3	12.61	6.46
					4	12.55	6.37
					5	12.44	6.62
					6	12.37	6.51
					7	12.36	6.46
					8	12.27	6.57
7-2	58-28	25	5	0	3	12.39	6.56
					4	12.44	6.61
					5	12.51	6.58
					6	12.55	6.47
					7	12.51	6.40
					8	12.57	6.27
8-1	58-28	25	0	5	3	12.65	6.43
					4	12.57	6.32
					5	12.50	6.34
					6	12.45	6.54
					7	12.44	6.47
					8	12.41	6.92
8-2	58-28	25	0	5	3	12.45	6.66
					4	12.38	6.51
					5	12.37	6.63
					6	12.33	6.60
					7	12.27	6.44
					8	12.15	6.45
9-1	52-34	25	5	0	3	12.56	6.73
					4	12.53	6.75
					5	12.47	6.82
					6	12.49	6.70
					7	12.35	6.56
					8	12.40	6.68
9-2	52-34	25	5	0	3	12.63	6.73
					4	12.59	6.60
					5	12.61	6.56
					6	12.58	6.56
					7	12.61	6.55
					8	12.57	6.61
10-1	52-34	25	0	5	3	12.30	6.66
					4	12.27	6.50
					5	12.28	6.56
					6	12.30	6.55
					7	12.31	6.47
					8	12.29	6.49
10-2	52-34	25	0	5	3	12.3/9	6.50
					4	12.38	6.66
					5	12.33	6.48
					6	12.38	6.61
					7	12.31	6.35
					8	12.34	6.48

Mixture ID	Binder PG	Recycled Material			Replicate #	Dimension	
		RAP (%)	TOSS (%)	MW (%)		Width (mm)	Thickness (mm)
11-1	58-28	25	3	0	3	12.46	6.63
					4	12.42	6.56
					5	12.71	6.55
					6	12.61	6.63
					7	12.53	6.50
					8	12.44	6.55
11-2	58-28	25	3	0	3	12.50	6.67
					4	12.45	6.54
					5	12.47	6.58
					6	12.63	6.62
					7	12.48	6.60
					8	12.47	6.58
12-1	58-28	25	0	3	3	12.45	6.60
					4	12.60	6.48
					6	12.50	6.70
					7	12.51	6.71
					9	12.51	6.60
					10	12.56	6.19
12-2	58-28	25	0	3	3	12.56	6.65
					4	12.52	6.49
					5	12.53	6.75
					6	12.54	6.64
					7	12.47	6.46
					8	12.48	6.59
13-1	58-28	15	3	0	3	12.57	6.41
					4	12.59	6.54
					5	12.64	6.45
					6	12.65	6.44
					7	12.80	6.56
					8	12.78	6.50
13-2	58-28	15	3	0	3	12.45	6.50
					4	12.41	6.26
					5	12.37	6.61
					6	12.29	6.07
					7	12.31	6.56
					10	12.22	6.48
14-1	58-28	15	0	3	3	12.70	6.55
					4	12.72	6.66
					5	12.77	6.60
					6	12.87	6.50
					7	12.90	6.48
					8	13.01	6.58
14-2	58-28	15	0	3	3	12.54	6.49
					4	12.60	6.70
					5	12.63	6.58
					6	12.67	6.46
					7	12.70	6.52
					8	12.74	6.64
15-1	58-28	10	5	0	3	12.83	6.50
					5	12.67	6.54
					6	12.67	6.58
					7	12.65	6.68
					8	12.61	6.03
					10	12.59	6.50
15-2	58-28	10	5	0	3	12.86	6.36
					4	12.84	6.67
					5	12.74	6.57
					6	12.66	6.38
					7	12.66	6.46
					8	12.57	6.43

Mixture ID	Binder PG	Recycled Material			Replicate #	Dimension	
		RAP (%)	TOSS (%)	MW (%)		Width (mm)	Thickness (mm)
16-1	58-28	15*	5	0	3	12.26	6.58
					4	12.31	6.59
					5	12.36	6.58
					6	12.47	6.65
					7	12.54	6.50
					8	12.62	6.58
16-2	58-28	15*	5	0	3	12.32	6.69
					4	12.43	6.61
					5	12.50	6.64
					6	12.52	6.55
					7	12.48	6.53
					8	12.59	6.42
17-1	58-28	0	5	0	3	12.37	6.56
					4	12.44	6.50
					5	12.49	6.34
					6	12.54	6.57
					7	12.56	6.64
					8	12.62	6.50
17-2	58-28	0	5	0	3	12.52	6.47
					5	12.59	6.48
					6	12.49	6.59
					7	12.44	6.46
					8	12.43	6.53
					10	12.44	6.62

*Different RAP source

Appendix B. (Chapter 4)

B.1. Aspahlt Mixtures Creep Stiffness and *m*-value

Table B.1. Asphalt mixtures BBR creep stiffness and *m*-value

Mixture ID	Binder PG	Recycled Material			Replicate #	Temperature (ºC)	S(60) (MPa)	m(60) -
		RAP (%)	TOSS (%)	MW (%)				
1-1	58-28	0	0	0	3	-6	7863.5	0.183
					5	-6	6400.6	0.266
					6	-18	11941.5	0.151
					7	-6	4148.4	0.296
					8	-18	14232.8	0.154
					10	-18	10818.3	0.131
1-2	58-28	0	0	0	3	-6	9153.3	0.220
					4	-18	14057.8	0.159
					5	-6	4123.9	0.296
					6	-18	12471.8	0.161
					8	-18	13791.3	0.165
					9	-6	8119.0	0.206
2-1	58-28	15	0	0	3	-6	11477.9	0.151
					4	-18	11510.6	0.106
					5	-6	5211.6	0.135
					6	-18	14068.9	0.095
					7	-6	7307.5	0.169
					8	-18	15364.1	0.127
2-2	58-28	15	0	0	3	-6	5472.2	0.194
					4	-18	16809.3	0.138
					5	-6	6850.4	0.187
					6	-18	17436.9	0.138
					7	-6	8300.2	0.200
					8	-18	15995.9	0.136
3-1	58-28	25	0	0	3	-6	7929.5	0.185
					4	-18	11639.8	0.107
					5	-6	8586.5	0.167
					6	-18	17048.3	0.126
					7	-6	8963.1	0.140
					8	-18	17571.2	0.126
3-2	58-28	25	0	0	3	-6	8991.7	0.150
					4	-18	18607.3	0.122
					5	-6	8522.4	0.158
					6	-18	14325.7	0.120
					7	-6	8761.9	0.153
					8	-18	22118.7	0.111
4-1	58-28	30	0	0	3	-6	8654.5	0.157
					4	-18	13909.9	0.111
					5	-6	7384.8	0.167
					6	-18	15356.3	0.134
					7	-6	6784.6	0.174
					8	-18	14115.4	0.139
4-2	58-28	30	0	0	3	-6	7729.1	0.169
					4	-18	10544.2	0.116
					5	-6	7381.2	0.162
					6	-18	13662.9	0.105
					7	-6	7210.3	0.176
					8	-18	11903.4	0.100
5-1	58-28	15	0	5	3	-6	7690.8	0.195
					4	-18	14520.8	0.128
					5	-6	7652.0	0.180
					6	-18	14908.6	0.133
					7	-6	9358.2	0.167
					8	-18	18198.7	0.113
5-2	58-28	15	0	5	3	-6	6676.0	0.156
					4	-18	15276.7	0.129
					5	-6	7158.6	0.179
					6	-18	18714.0	0.134
					7	-6	7380.5	0.164
					8	-18	18080.8	0.136

Mixture ID	Binder PG	Recycled Material			Replicate #	Temperature (ºC)	S(60) (MPa)	m(60) -
		RAP (%)	TOSS (%)	MW (%)				
6-1	58-28	15	5	0	3	-6	10308.5	0.116
					4	-18	12000.7	0.120
					5	-6	9940.6	0.157
					6	-18	17942.9	0.124
					7	-6	10085.8	0.151
					8	-18	15243.2	0.133
6-2	58-28	15	5	0	3	-6	8567.3	0.173
					4	-18	11171.1	0.105
					5	-6	10471.9	0.161
					6	-18	15941.2	0.128
					7	-6	8295.2	0.165
					8	-18	17358.8	0.113
7-1	58-28	25	5	0	3	-6	11376.6	0.117
					4	-18	18087.8	0.071
					5	-6	5461.8	0.104
					6	-18	19695.0	0.124
					7	-6	10346.3	0.118
					8	-18	15869.3	0.106
7-2	58-28	25	5	0	3	-6	8371.8	0.161
					4	-18	11381.5	0.094
					5	-6	7874.8	0.145
					6	-18	17311.6	0.123
					7	-6	8423.8	0.119
					8	-18	12903.1	0.103
8-1	58-28	25	0	5	3	-6	9909.9	0.126
					4	-18	19759.6	0.150
					5	-6	8819.7	0.127
					6	-18	13369.8	0.092
					7	-6	11121.9	0.139
					8	-18	12774.9	0.084
8-2	58-28	25	0	5	3	-6	8000.7	0.150
					4	-18	14819.4	0.118
					5	-6	8773.4	0.159
					6	-18	25252.8	0.135
					7	-6	10949.3	0.115
					8	-18	15239.4	0.128
9-1	52-34	25	5	0	3	-6	6288.1	0.161
					4	-18	14225.4	0.096
					5	-6	8842.2	0.205
					6	-18	16296.6	0.144
					7	-6	5393.0	0.188
					8	-18	13333.5	0.143
9-2	52-34	25	5	0	3	-6	7848.3	0.161
					4	-18	10129.0	0.085
					5	-6	7087.5	0.176
					6	-18	14792.0	0.152
					7	-6	5641.6	0.190
					8	-18	16064.7	0.160
10-1	52-34	25	0	5	3	-6	10633.7	0.159
					4	-18	14315.5	0.163
					5	-6	7106.9	0.211
					6	-18	14626.5	0.160
					7	-6	8176.4	0.195
					8	-18	11419.8	0.124
10-2	52-34	25	0	5	3	-6	5490.0	0.195
					4	-18	15427.1	0.159
					5	-6	6361.5	0.202
					6	-18	13646.9	0.129
					7	-6	7825.8	0.195
					8	-18	17461.3	0.136

Mixture	Binder	Recycled Material			Replicate	Temperature	S(60)	m(60)
ID	PG	RAP (%)	TOSS (%)	MW (%)	#	(ºC)	(MPa)	-
11-1	58-28	25	3	0	3	-6	9962.4	0.148
					4	-18	9326.0	0.053
					5	-6	4788.1	0.155
					6	-18	19725.2	0.120
					7	-6	12795.4	0.114
					8	-18	17063.2	0.122
11-2	58-28	25	3	0	3	-6	14202.6	0.155
					4	-18	15144.5	0.085
					5	-6	9253.9	0.094
					6	-18	15565.4	0.103
					7	-6	9217.3	0.143
					8	-18	17482.3	0.099
12-1	58-28	25	0	3	3	-6	7417.7	0.143
					4	-18	15444.6	0.131
					6	-18	9945.5	0.082
					7	-6	13269.5	0.094
					9	-6	9181.5	0.141
					10	-18	13101.3	0.112
12-2	58-28	25	0	3	3	-6	8977.1	0.124
					4	-18	17327.6	0.135
					5	-6	11810.0	0.170
					6	-18	16192.6	0.134
					7	-6	9175.1	0.134
					8	-18	15502.3	0.143
13-1	58-28	15	3	0	3	-6	7075.5	0.151
					4	-18	12717.7	0.086
					5	-6	8236.3	0.142
					6	-18	12197.7	0.117
					7	-6	7526.2	0.146
					8	-18	14926.0	0.135
13-2	58-28	15	3	0	3	-6	6612.4	0.155
					4	-18	11734.3	0.111
					5	-6	7221.6	0.176
					6	-18	11032.9	0.115
					7	-6	7825.8	0.146
					10	-18	12472.2	0.136
14-1	58-28	15	0	3	3	-6	7764.6	0.177
					4	-18	15286.6	0.127
					5	-6	7068.8	0.163
					6	-18	14318.7	0.133
					7	-6	6325.0	0.170
					8	-18	13736.6	0.125
14-2	58-28	15	0	3	3	-6	5663.8	0.167
					4	-18	12945.5	0.087
					5	-6	7172.8	0.176
					6	-18	11701.0	0.121
					7	-6	5410.4	0.181
					8	-18	13589.3	0.137
15-1	58-28	10	5	0	3	-6	7347.3	0.173
					5	-6	6080.9	0.160
					6	-18	12432.4	0.123
					7	-6	6921.4	0.179
					8	-18	13994.5	0.127
					10	-18	11555.2	0.122
15-2	58-28	10	5	0	3	-6	5211.8	0.159
					4	-18	14093.6	0.143
					5	-6	6848.5	0.164
					6	-18	12980.7	0.134
					7	-6	6538.3	0.152
					8	-18	20063.9	0.134

Mixture ID	Binder PG	Recycled Material			Replicate #	Temperature (ºC)	S(60) (MPa)	m(60) -
		RAP (%)	TOSS (%)	MW (%)				
16-1	58-28	15*	5	0	3	-6	8314.7	0.170
					4	-18	12946.4	0.131
					5	-6	5507.4	0.172
					6	-18	25134.3	0.135
					7	-6	10511.3	0.160
					8	-18	12429.1	0.100
16-2	58-28	15*	5	0	3	-6	8774.3	0.146
					4	-18	19429.6	0.138
					5	-6	7573.6	0.168
					6	-18	18840.9	0.135
					7	-6	9330.6	0.166
					8	-18	19456.3	0.136
17-1	58-28	0	5	0	3	-6	6039.6	0.158
					4	-18	13007.9	0.125
					5	-6	5939.2	0.180
					6	-18	11387.5	0.120
					7	-6	7797.9	0.174
					8	-18	10117.3	0.114
17-2	58-28	0	5	0	3	-6	7429.8	0.179
					5	-6	5206.2	0.193
					6	-18	15588.4	0.160
					7	-6	5849.3	0.180
					8	-18	13537.1	0.102
					10	-18	22233.0	0.117

*Different RAP source

B.2. Thermal Stress Computation Procedure

The following section present a general procedure of thermal stress calculation used in this dissertation. The computational process involves two main steps: first relaxation modulus *E*(*t*) master curves are generated and then Gaussian quadrature approximation method is applied to calculate the thermal stress.

From Bending Beam Rheometer (BBR) test on asphalt mixtures the creep stiffness is calculated as:

$$S(t) = \frac{\sigma}{\varepsilon(t)} = \frac{P \cdot l^3}{4 \cdot b \cdot h^3 \cdot \delta(t)} \qquad [B.1]$$

where

S(t)	flexural creep stiffness, function of time,
σ	maximum bending stress in the beam, MPa,
ε(t)	bending strain (mm/mm), unction of time,
P	constant load = 980±50mN ,
l	length of specimen (101.6mm),
b	width of specimen (12.5mm),
h	height of specimen (6.25mm),
δ(t)	deflection at the midspan of the beam at time t, and
t	time.

The creep compliance *D*(*t*) is obtained as the inverse of the creep stiffness:

$$D(t) = \frac{1}{S(t)} \qquad [B.2]$$

The relaxation modulus *E*(*t*) and creep compliance *D*(*t*) are related through the Volterra integral:

$$t = \int_0^t E(t')D(t-t')dt' \qquad [B.3]$$

Using Laplace transform [B.3] can be rewritten as:

$$\overline{E}(s) \cdot \overline{D}(s) = \frac{1}{s^2} \qquad [B.4]$$

However the use of Laplace domain to manipulate the relaxation modulus $E(t)$ and creep compliance $D(t)$ is often not convenient when the inverse Laplace transform is applied. An alternative numerical approach was implemented by *Hopkins and Hamming* (*1957*) to calculate $E(t)$ as function of $D(t)$ and vice versa. *Basu* (*2002*) and *Moon* (*2010*) used this procedure to convert the experimental determined BBR creep compliance to relaxation modulus. This interconversion procedure involves different steps:

1. Time interval t_n is selected

   $$t_0 = 0, t_1 = 1, t_2 = 2, \cdots t_{1000} = 1000 \qquad [B.5]$$

2. The creep compliance $D(t_n)$ is obtained from the experimentally determined creep stiffness $S(t_n)$ according to:

   $$D(t_n) = \frac{1}{S(t_n)} \qquad [B.6]$$

3. The function $f(t)$ is defined as:

   $$f(t) = \int_0^t D(t)dt \qquad [B.7]$$

4. The value of the $f(t)$ is calculated using the trapezoidal rule:

   $$f(t_{n+1}) = f(t_n) + \frac{1}{2} \cdot (D(t_{n+1}) + D(t_n)) \cdot (t_{n+1} - t_n) \qquad [B.8]$$

5. Combining equations [B.3] and [B.8] the following discretized expression is obtained:

   $$t_{n+1} = \int_0^{t_n+1} E(t') \cdot D(t_{n+1} - t')dt' = \sum_{i=0}^{n} \int_{t_i}^{t_i+1} E(t') \cdot D(t_{n+1} - t')dt' \qquad [B.9]$$

6. Each integral of equation [B.9] is expressed as function of $f(t)$ as:

   $$\int_{t_i}^{t_i+1} E(t') \cdot D(t_{n+1} - t')dt' = -E(t_{i+1/2}) \cdot [f(t_{n+1} - t_{i+1}) - f(t_{n+1} - t_i)] \qquad [B.10]$$

   where:

   $$t_{i+\frac{1}{2}} = \frac{1}{2} \cdot (t_{i+1} + t_i) \qquad [B.11]$$

7. Finally [B.9] can be restated as:

   $$t_{n+1} = -\sum_{i=0}^{n-1} E(t_{i+1/2}) \cdot [f(t_{n+1} - t_{i+1}) - f(t_{n+1} - t_i)] + E(t_{n+1/2}) \cdot f(t_{n+1} - t_n) \qquad [B.12]$$

8. and solving for $E(t_{n+1/2})$ the previous expression becomes:

$$\begin{aligned} E(t_{n+1/2}) &= \frac{t_{n+1} - \sum_{i=0}^{n-1} E(t_{i+1/2}) \cdot [f(t_{n+1} - t_i) - f(t_{n+1} - t_{i+1})]}{f(t_{n+1} - t_n)} \\ E(t_{n+1/2}) &= \frac{t_{n+1} - \sum_{i=0}^{n-1} E(t_{i+1/2}) \cdot [f(t_{i+1}) - f(t_i)]}{f(t_{n+1}) - f(t_n)} \end{aligned} \qquad [B.13]$$

with the following set of initial conditions:

$f(t_0) = 0$

$E(t_0) = 0$

$E(t_1) = \frac{t_1}{f(t_1)}$

After the interconversion procedure the relaxation modulus *E*(*t*) master curves are constructed using the CAM model (*Marasteanu and Anderson, 1996*):

$$E(t) = E_g \cdot \left[1 + \left(\frac{t}{t_c} \right)^{v} \right]^{-w/v} \qquad [B.14]$$

where:

$E(t)$	relaxation modulus,
E_g	glassy modulus (generally 3GPa for binder and 30GPa for mixtures),
v, w	model parameters,
t_c	cross over time,
t	time.

In this thesis two different temperature levels were used during testing: PG low temperature + 22°C and PG low temperature + 10°C and thus a single shift factor was determined from the relaxation modulus *E*(*t*) master curves. However hereafter a more general case in which all three temperature level are assumed is considered and outlined. An example of a master curve obtained from three testing temperatures and with the application of CAM models is presented in Figure B.1 (*Moon, 2010*). This master curve requires two shift factors.

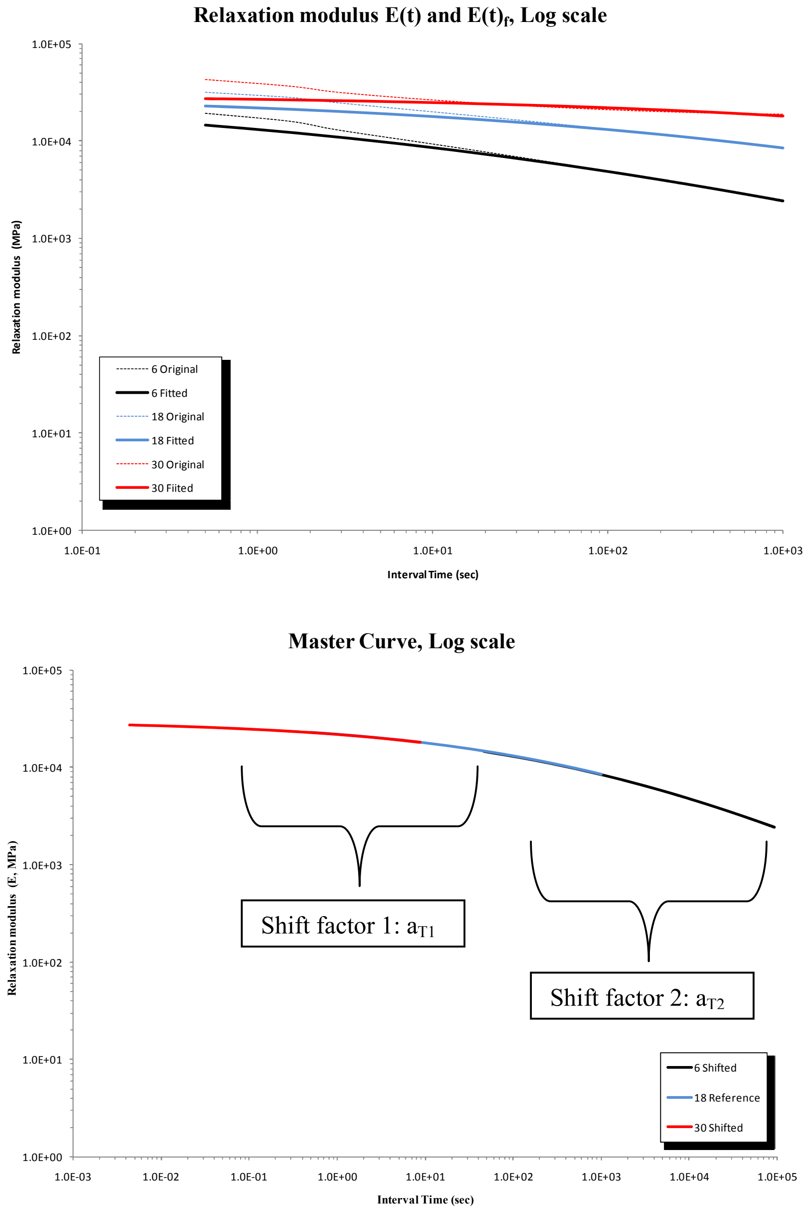
Relaxation modulus E(t) and $E(t)_f$, Log scale

Master Curve, Log scale

Figure B.1 Relaxation modulus master curve – (*Moon, 2010*)

The shift factors are calculated according to:

$$a_{T1} = 10^{C_1 + C_2 \cdot T} \quad [B.15]$$

$$a_{T2} = 10^{K_1 + K_2 \cdot T} \quad [B.16]$$

where:

C_1, C_2, K_1, K_2	fitting parameters,
T	reference temperature, °C.

Generally the intermediate temperature level corresponding for BBR asphalt mixture testing to PG low temperature + 10˚C is assumed as reference temperature and its relaxation modulus curve is set as reference curve which the other curve are shifted to. As a consequence shift factor a_{T1} relates the relaxation modulus master curve at reference temperature to the relaxation modulus master curve at lower temperature while shift factor a_{T2} relates the relaxation modulus master curve at reference temperature to the relaxation modulus master curve at higher temperature. After a log transformation of the two shift factors:

$$\log a_{T1} = C_1 + C_2 \cdot T \quad [B.17]$$

$$\log a_{T2} = K_1 + K_2 \cdot T \quad [B.18]$$

Introducing [B.17] and [B.18] into [B.14], the CAM model expression can be rewritten as:

$$\log E(t) = \log E_g - \frac{w}{v} \cdot \left[1 + \left(10^{\log t + \log a_{T1} - \log t_c} \right)^{v} \right] \quad [B.19]$$

$$\log E(t) = \log E_g - \frac{w}{v} \cdot \left[1 + \left(10^{\log t + \log a_{T2} - \log t_c} \right)^{v} \right] \quad [B.20]$$

The five constants (v, w, t_c, a_{T1} and a_{T2}) required by the CAM model are then determined fitting at the same time expressions [B.19] and [B.20] to the experimentally determined data running a minimization with a least squares error limit of 0.03-10.

Considering the case for the single shift factor a_{T1} (the case for a_{T2} would be analogous), the following expression for temperature can be assumed:

$$T = T_i - C_0 \cdot t \quad [B.21]$$

where:

C_0	constant temperature drop rate,
T_i	initial temperature, (22°C in this dissertation).

Substituting [B.21] into equation [B.15] the shift factor a_{T1} can be expressed as:

$$a_{T1} = 10^{C_1 + C_2 T} = 10^{C_1 + C_2 \cdot (T_i - C_0 t)} = 10^{(C_1 + C_2 T_i) - C_2 C_0 t} = 10^{C_3 + C_4 t} \quad [B.22]$$

And after a simple manipulation:

$$a_{T1} = 10^{C_3 + C_4} = 10^{C_3} \times 10^{C_4 t} = A_0 \cdot 10^{C_4 t} \qquad \text{[B.23]}$$

Assuming time temperature superposition principle it can be written that:

$$E(T, t) = E(T_0, \xi) \qquad \text{[B.24]}$$

and

$$\xi = \frac{t}{a_T(T)} \qquad \text{[B.25]}$$

where:

T_0 reference temperature, and

ξ reduced time.

Formula [B.25] can be re-expressed in integral form:

$$\xi = \frac{t}{a_T[T]} = \int_0^t \frac{dt'}{a_T[T(t')]} \qquad \text{[B.26]}$$

where:

t' arbitrary time prior to time *t*.

Introducing [B.23] into [B.26] the reduced time can be rewritten as:

$$\xi = \int_0^t \frac{dt'}{a_T[T(t')]} = \int_0^t \frac{dt'}{A_0 \cdot 10^{C_4 \cdot t'}} = \frac{1}{A_0} \int_0^t 10^{-C_4 \cdot t'} dt' = \frac{1}{A_0} \cdot \left[-\frac{10^{-C_4 t'}}{C_4 \cdot \ln 10} \right]_0^t$$
$$\xi = \frac{1}{A_0} \cdot \left[\frac{1}{C_4 \cdot \ln 10} \cdot \left(1 - 10^{-C_4 t}\right) \right] = \frac{1}{A_0 \cdot C_4 \cdot \ln 10} \cdot \left[1 - 10^{-C_4 t}\right] = A_1 \cdot \left[1 - 10^{-C_4 t}\right] \qquad \text{[B.27]}$$

where:

$$A_1 = \frac{1}{A_0 \cdot C_4 \cdot \ln 10} = \frac{1}{10^{C_1 + C_2 \cdot T_i} \cdot C_2 \cdot C_0 \cdot \ln 10} \qquad \text{[B.28]}$$

The stress is calculated according to:

$$\sigma(t) = \int_{-\infty}^{t} E(\xi - \xi') \frac{\partial \varepsilon(\xi')}{\partial \xi'} d\xi' \qquad \text{[B.29]}$$

where:

$$t = \frac{\Delta T}{C_0} \qquad \text{[B.30]}$$

Expressing the monodimensional strain as:

$$\varepsilon = -\alpha \cdot \Delta T \qquad \text{[B.31]}$$

and substituting in [B.29] the stress can be expressed according to:

$$\sigma(\xi) = \int_{-\infty}^{t} E(\xi-\xi')\frac{\partial\varepsilon(\xi')}{\partial\xi'}d\xi' = -\alpha\cdot\int_{0}^{t} E(\xi-\xi')\frac{\partial(\Delta T)}{\partial\xi'}d\xi' \qquad \text{[B.32]}$$

where:

ξ' arbitrary reduced time prior to ξ.

Since

$$\Delta T = C_0 \cdot t \qquad \text{[B.33]}$$

and its partial derivative with respect to ξ is:

$$\frac{\partial(\Delta T)}{\partial\xi} = C_0 \qquad \text{[B.34]}$$

it is possible to rewrite equation [B.32] as:

$$\sigma(\xi) = -\alpha\cdot\int_{0}^{t} E(\xi-\xi')\frac{\partial(\Delta T)}{\partial\xi'}d\xi' = -\alpha\cdot C_0\cdot\int_{0}^{t} E(\xi-\xi')d\xi' \qquad \text{[B.35]}$$

It is finally possible to introduce the CAM model into equation [B.35]:

$$\sigma(\xi) = -\alpha\cdot C_0\cdot\int_{0}^{t} E(\xi-\xi')d\xi' = -\alpha\cdot C_0\cdot\int_{0}^{t} E_g\cdot\left[1+\left(\frac{\xi-\xi'}{t_c}\right)^{v}\right]^{-\frac{w}{v}}d\xi' \qquad \text{[B.36]}$$

Analytical integration is unpractical for equation [B.36]. For this reason Gaussian quadrature with 24 Gauss points approximation is used:

$$\begin{aligned}\sigma(\xi) &= -\alpha\cdot C_0\cdot\int_{0}^{t} E(\xi-\xi')d\xi' = -\alpha\cdot C_0\cdot\int_{-1}^{1}\frac{t}{2}\cdot E(\xi-\xi')d\xi' \\ \sigma(\xi) &= -\alpha\cdot C_0\cdot\frac{t}{2}\cdot\sum_{i=1}^{24} w_i\cdot E(\xi-\xi_i')\end{aligned} \qquad \text{[B.37]}$$

where:

$$\xi = \frac{1}{10^{C_1+C_2\cdot T_i}\cdot C_2\cdot C_0\cdot\ln 10}\cdot\left[1-10^{-C_4\cdot t}\right] \qquad \text{[B.38]}$$

$$\xi' = \frac{1}{10^{C_1+C_2\cdot T_i}\cdot C_2\cdot C_0\cdot\ln 10}\cdot\left[1-10^{-C_4\cdot t'}\right] \qquad \text{[B.39]}$$

$$t' = \frac{t}{2}\cdot x_i + \frac{t}{2} \qquad \text{[B.40]}$$

x_i Gauss points (1 to 24)

B.3. Thermal Stress Curves and Critical Temperature plots

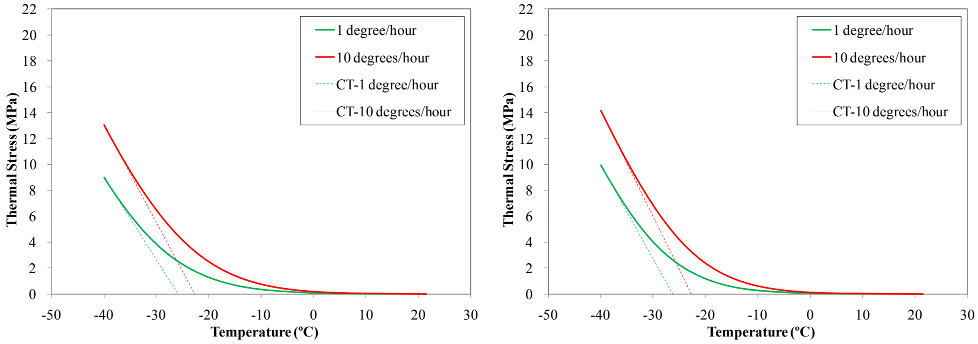

Figure B.2. Thermal stress and critical temperature curve for mixture 1 – slice 1 and 2

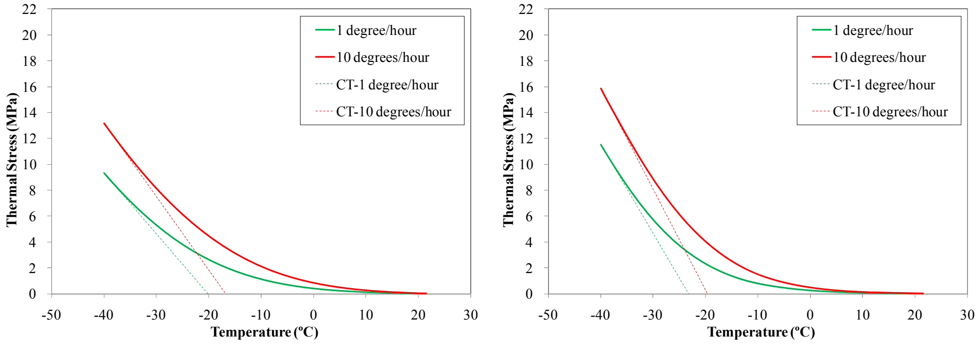

Figure B.3. Thermal stress and critical temperature curve for mixture 2 – slice 1 and 2

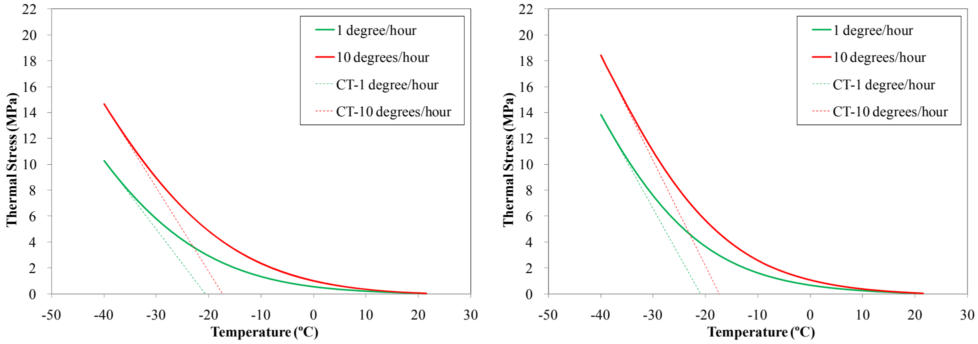

Figure B.4. Thermal stress and critical temperature curve for mixture 3 – slice 1 and 2

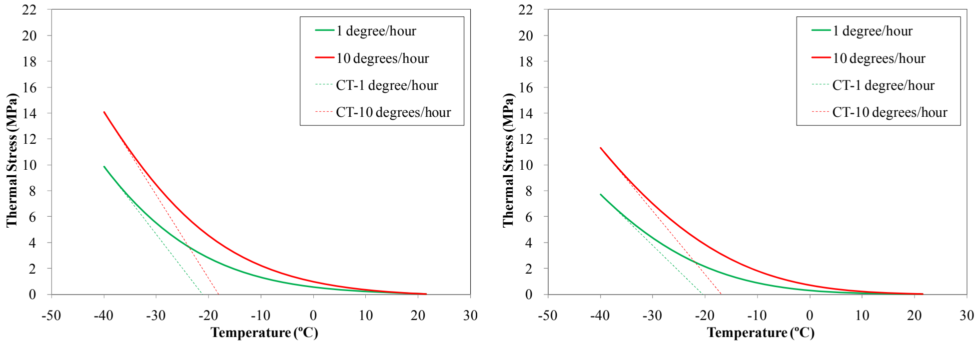

Figure B.5. Thermal stress and critical temperature curve for mixture 4 – slice 1 and 2

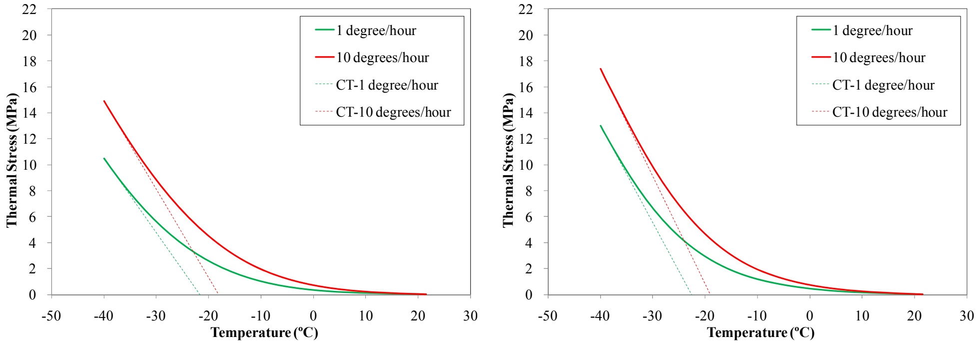

Figure B.6. Thermal stress and critical temperature curve for mixture 5 – slice 1 and 2

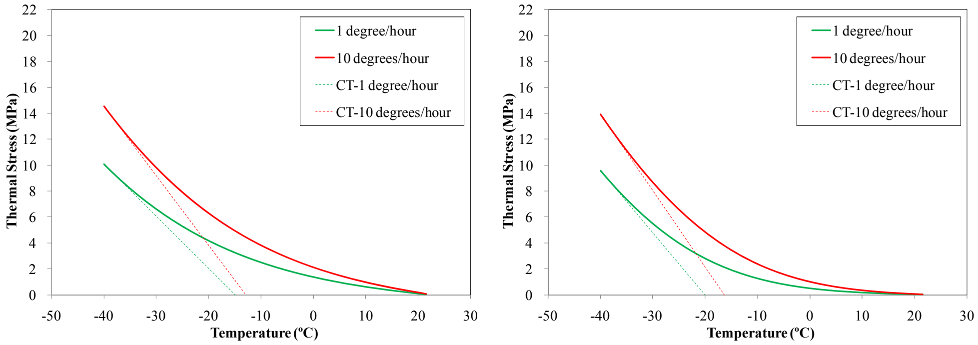

Figure B.7. Thermal stress and critical temperature curve for mixture 6 – slice 1 and 2

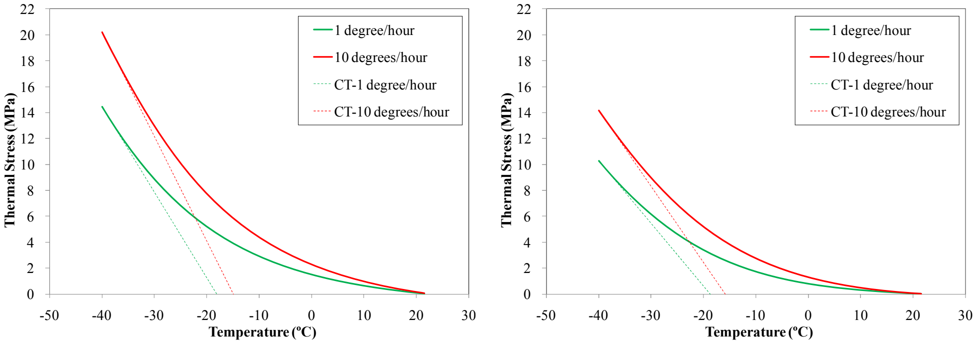

Figure B.8. Thermal stress and critical temperature curve for mixture 7 – slice 1 and 2

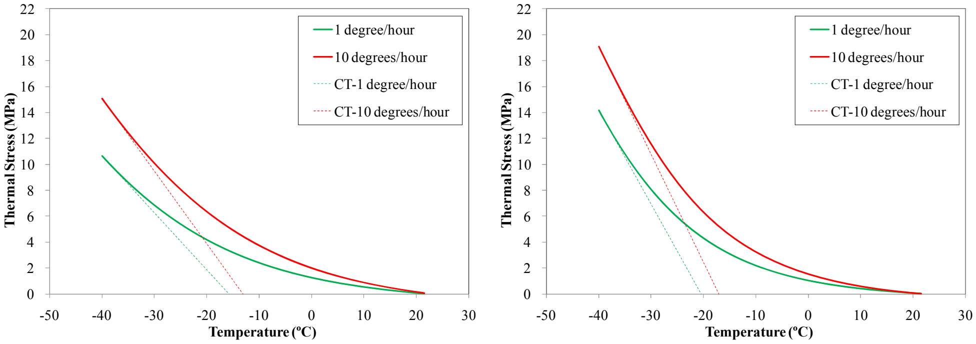

Figure B.9. Thermal stress and critical temperature curve for mixture 8 – slice 1 and 2

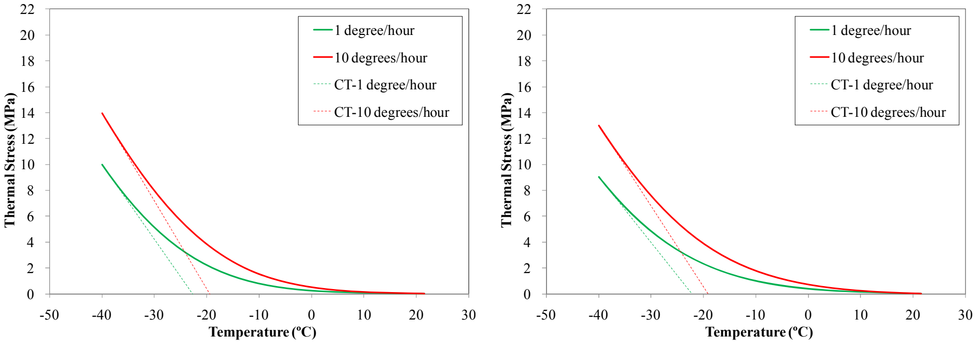

Figure B.10. Thermal stress and critical temperature curve for mixture 9 – slice 1 and 2

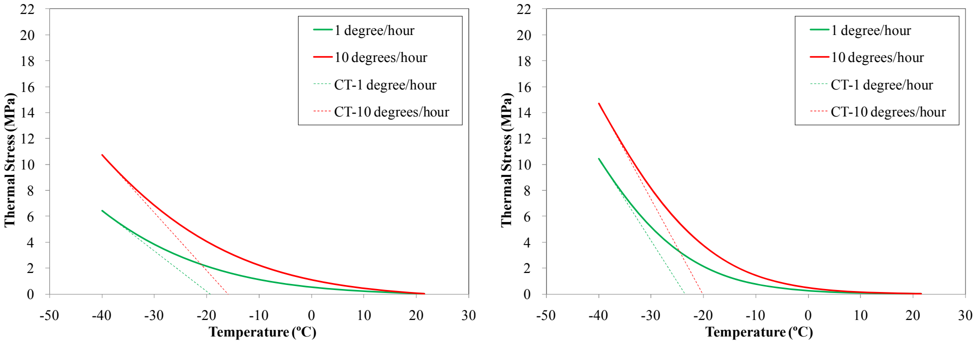

Figure B.11. Thermal stress and critical temperature curve for mixture 10 – slice 1 and 2

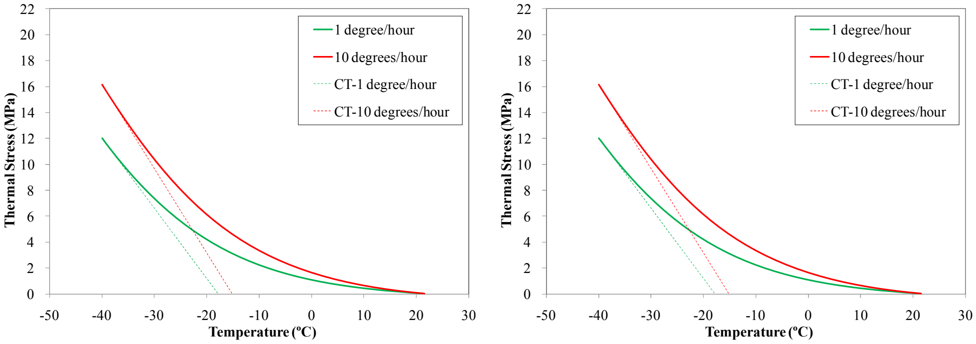

Figure B.12. Thermal stress and critical temperature curve for mixture 11 – slice 1 and 2

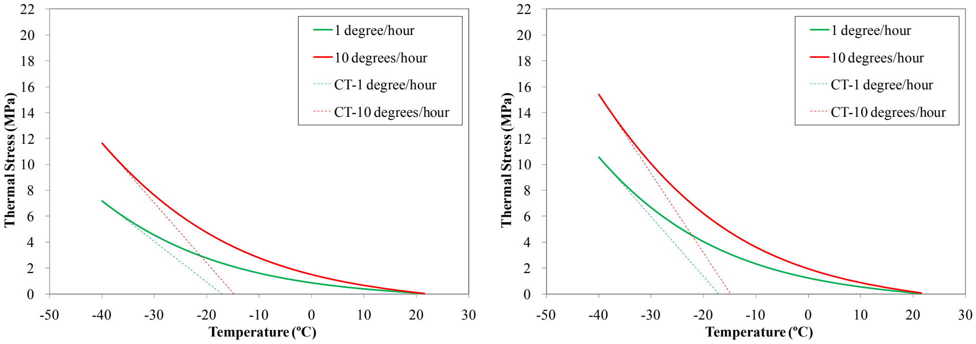

Figure B.13. Thermal stress and critical temperature curve for mixture 12 – slice 1 and 2

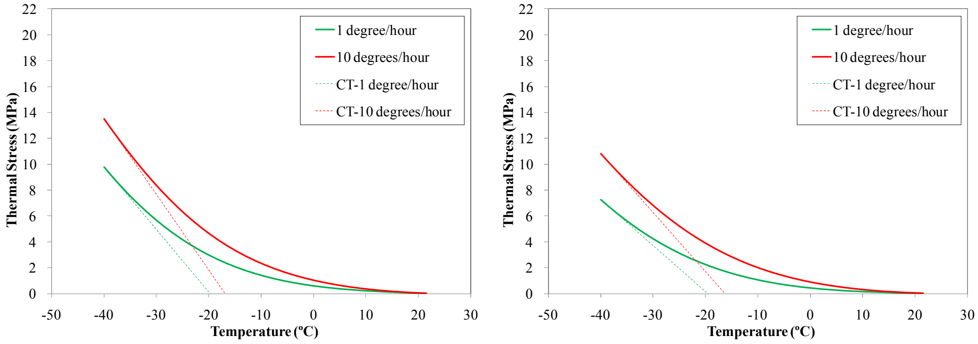

Figure B.14. Thermal stress and critical temperature curve for mixture 13 – slice 1 and 2

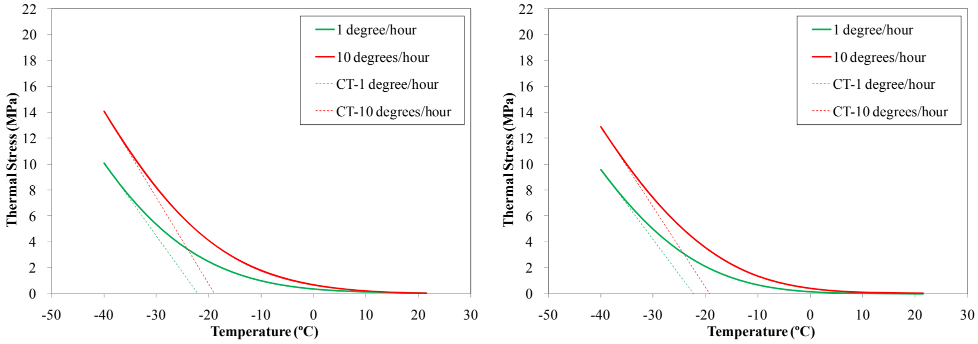

Figure B.15. Thermal stress and critical temperature curve for mixture 14 – slice 1 and 2

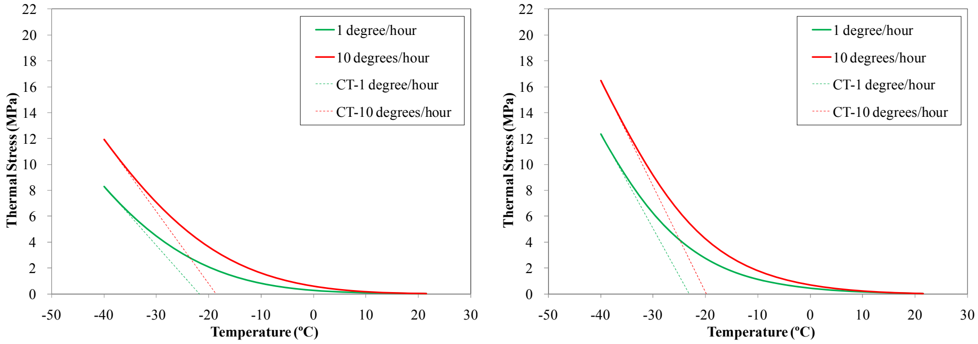

Figure B.16. Thermal stress and critical temperature curve for mixture 15 – slice 1 and 2

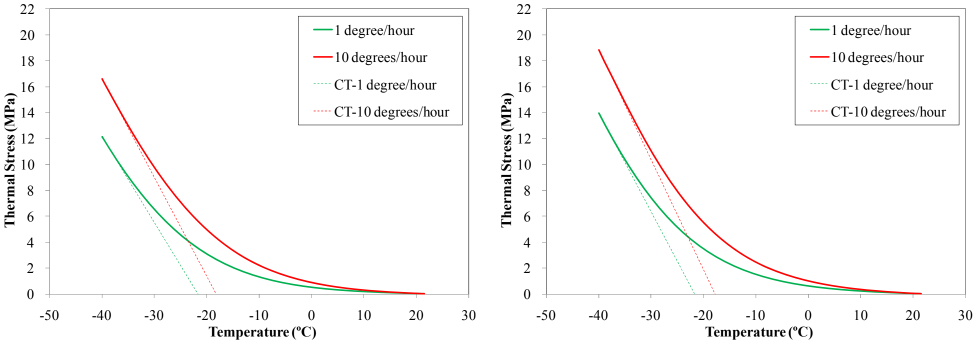

Figure B.17. Thermal stress and critical temperature curve for mixture 16 – slice 1 and 2

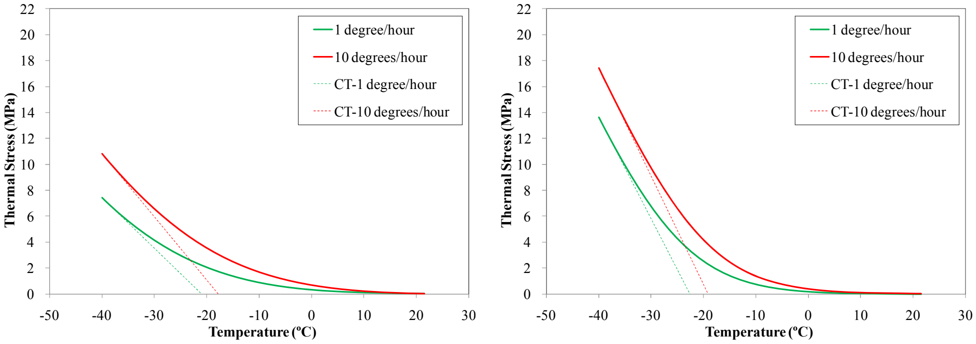

Figure B.18. Thermal stress and critical temperature curve for mixture 17 – slice 1 and 2

Appendix C. (Chapter 5)

C.1. Grain Size Distribution

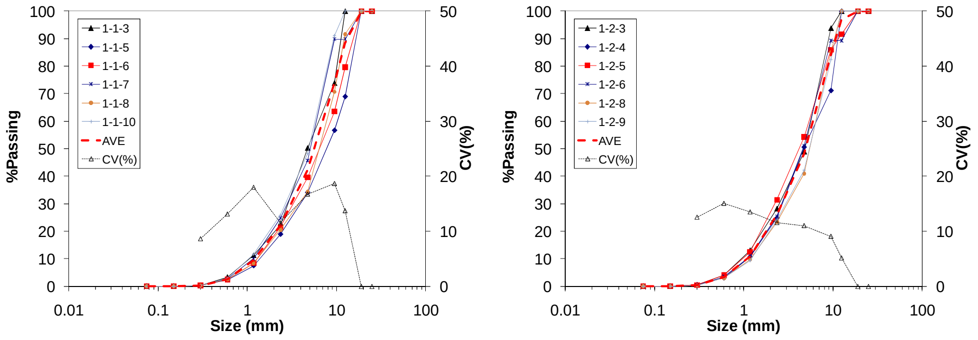

Figure C.1. Grain size distribution for mixture 1 – slice 1 and 2

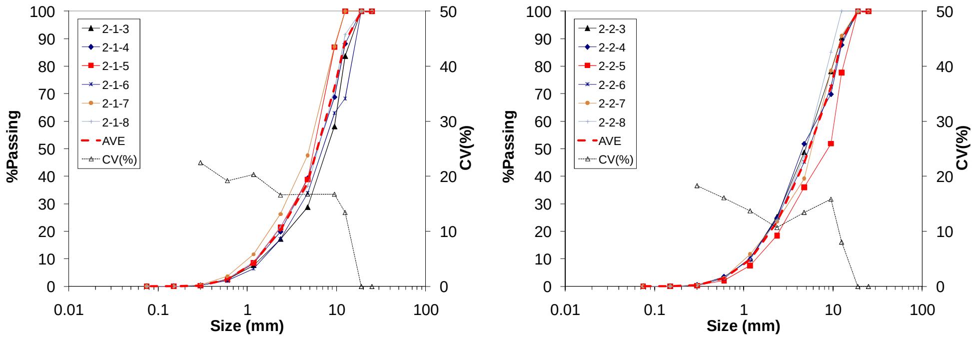

Figure C.2. Grain size distribution for mixture 2 – slice 1 and 2

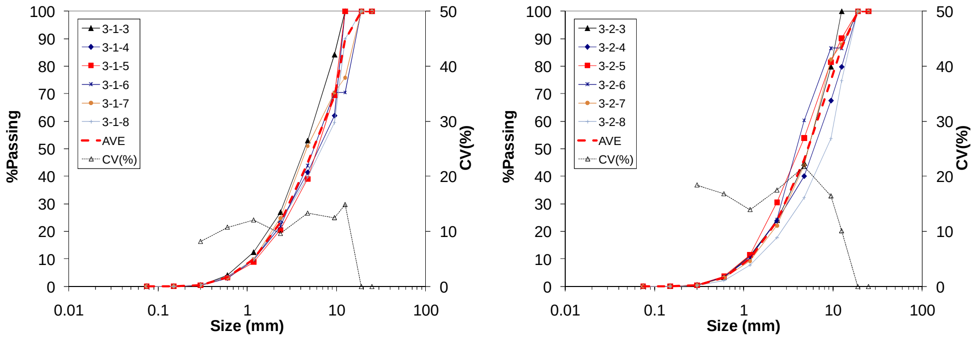

Figure C.3. Grain size distribution for mixture 3 – slice 1 and 2

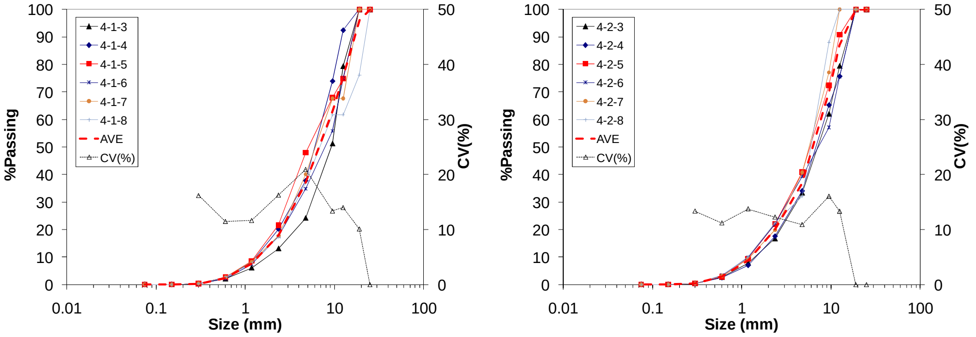

Figure C.4. Grain size distribution for mixture 4 – slice 1 and 2

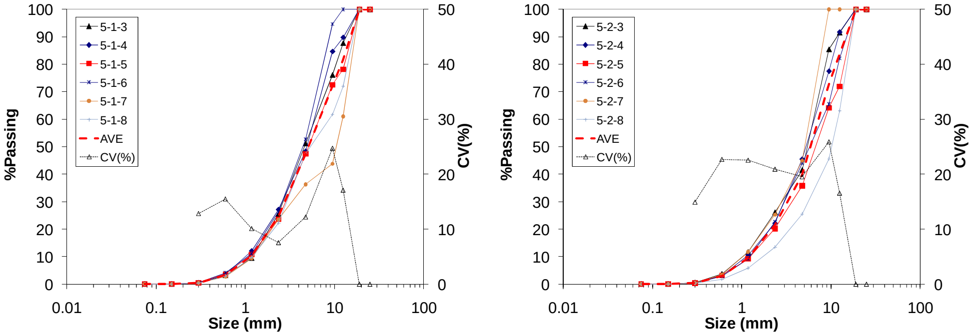

Figure C.5. Grain size distribution for mixture 5 – slice 1 and 2

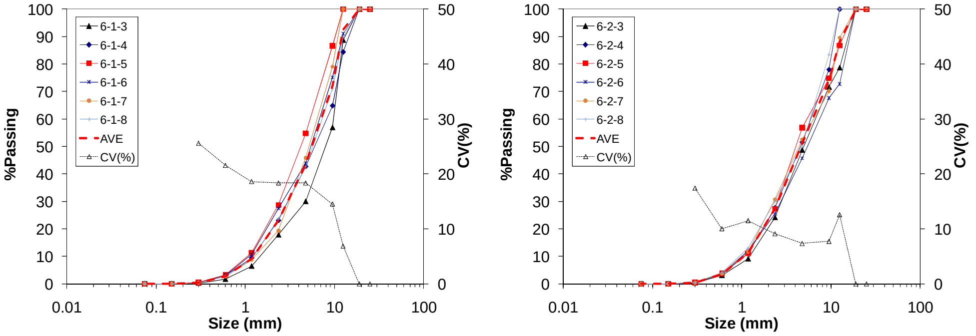

Figure C.6. Grain size distribution for mixture 6 – slice 1 and 2

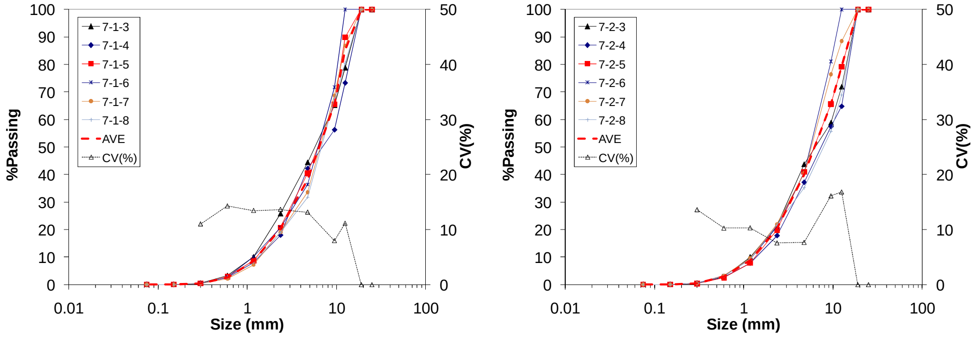

Figure C.7. Grain size distribution for mixture 7 – slice 1 and 2

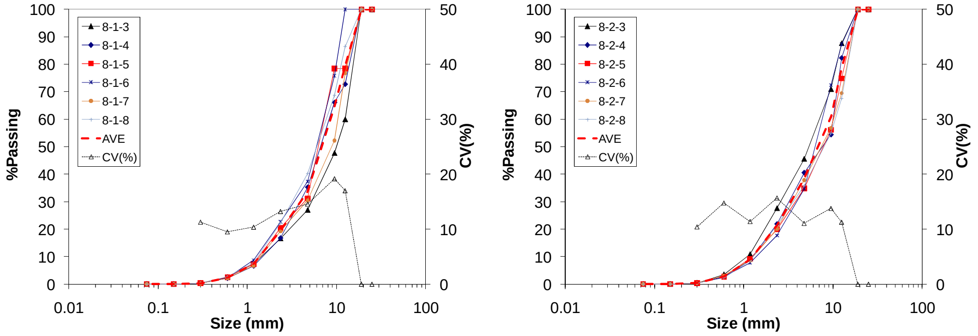

Figure C.8. Grain size distribution for mixture 8 – slice 1 and 2

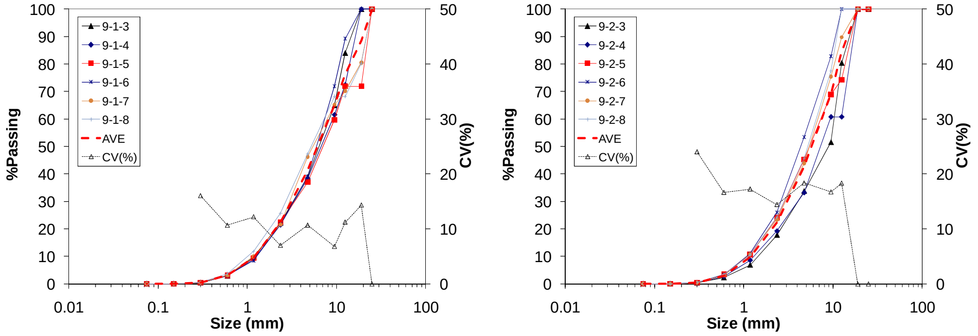

Figure C.9. Grain size distribution for mixture 9 – slice 1 and 2

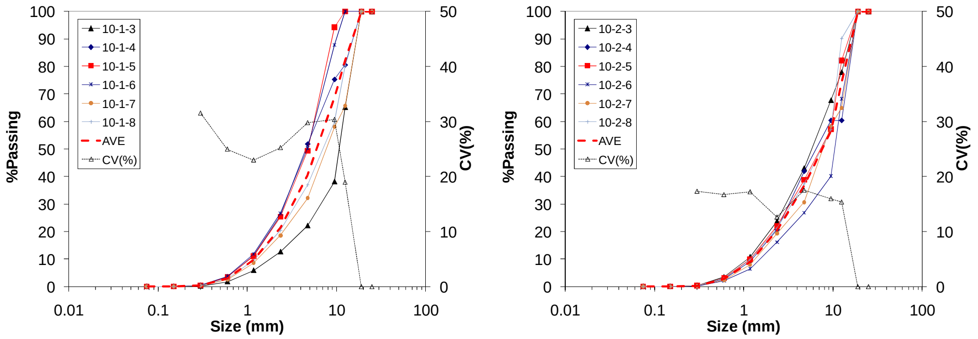

Figure C.10. Grain size distribution for mixture 10 – slice 1 and 2

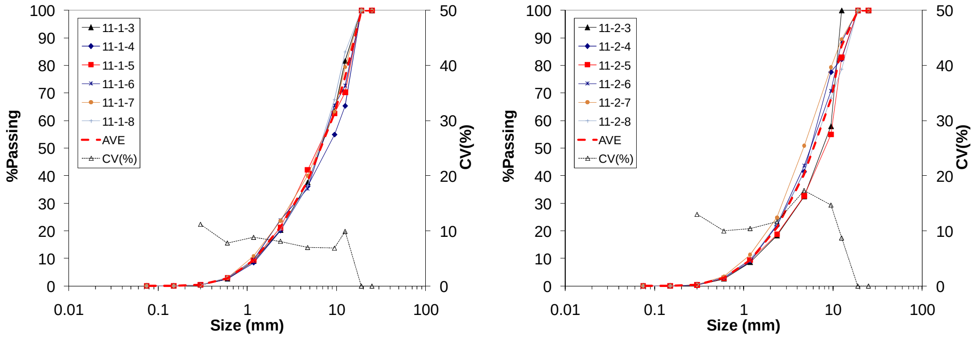

Figure C.11. Grain size distribution for mixture 11 – slice 1 and 2

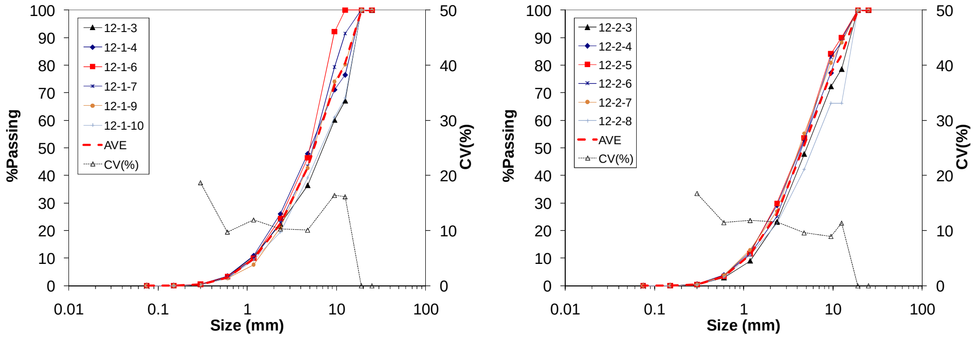

Figure C.12. Grain size distribution for mixture 12 – slice 1 and 2

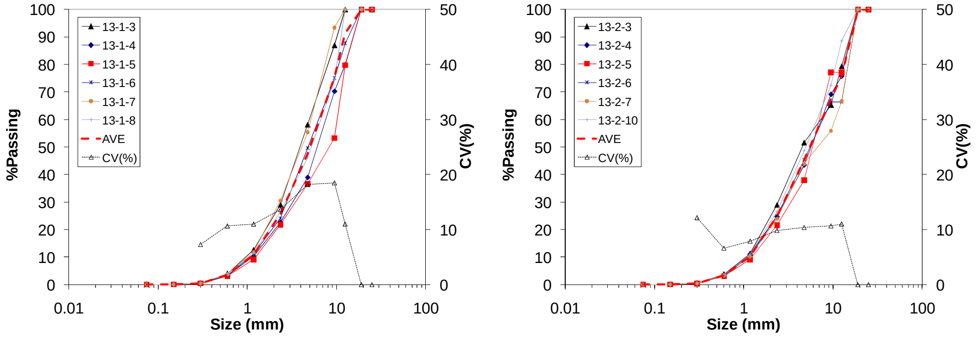

Figure C.13. Grain size distribution for mixture 13 – slice 1 and 2

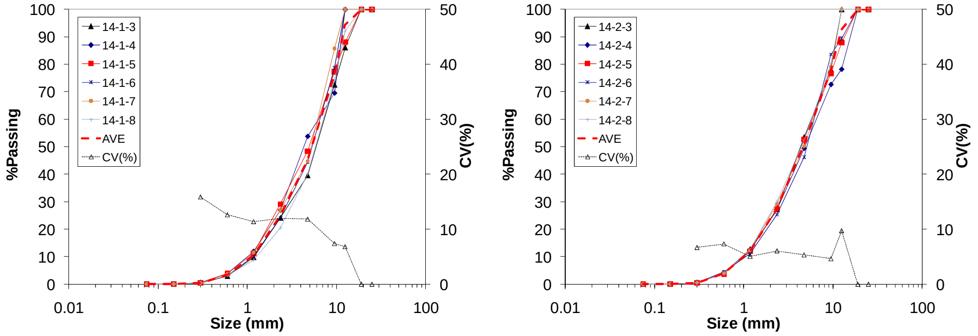

Figure C.14. Grain size distribution for mixture 14 – slice 1 and 2

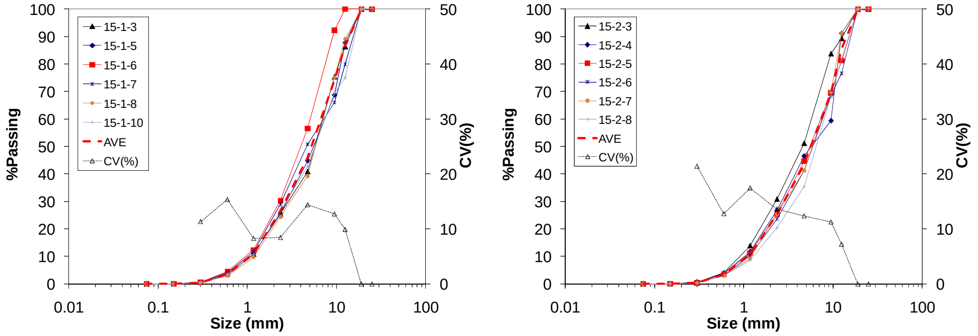

Figure C.15. Grain size distribution for mixture 15 – slice 1 and 2

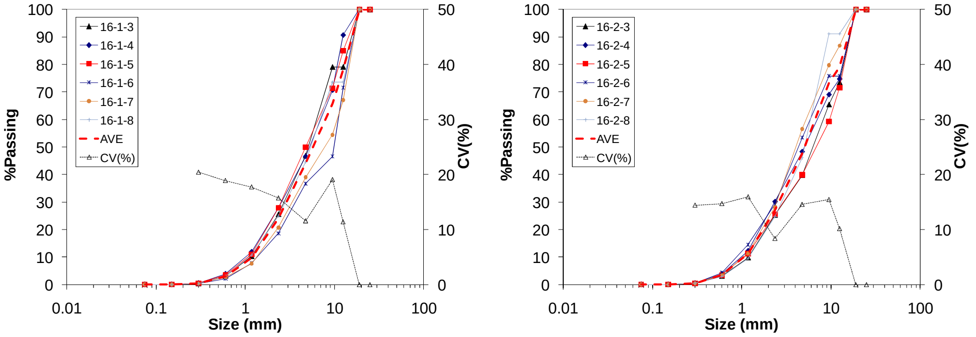

Figure C.16. Grain size distribution for mixture 16 – slice 1 and 2

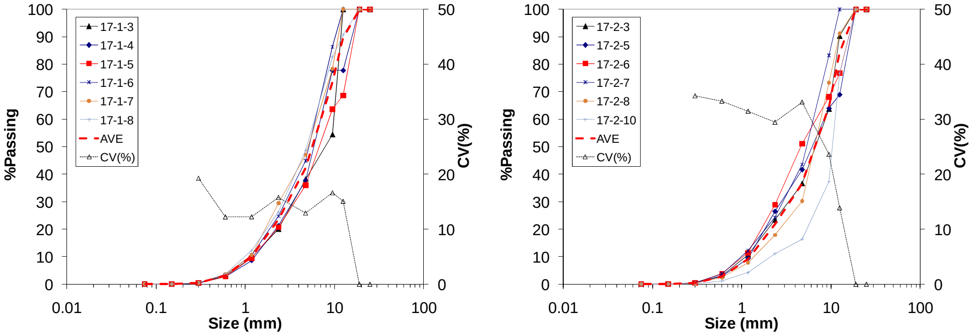

Figure C.17. Grain size distribution for mixture 17 – slice 1 and 2

C.2. 2-point Correlation Functions

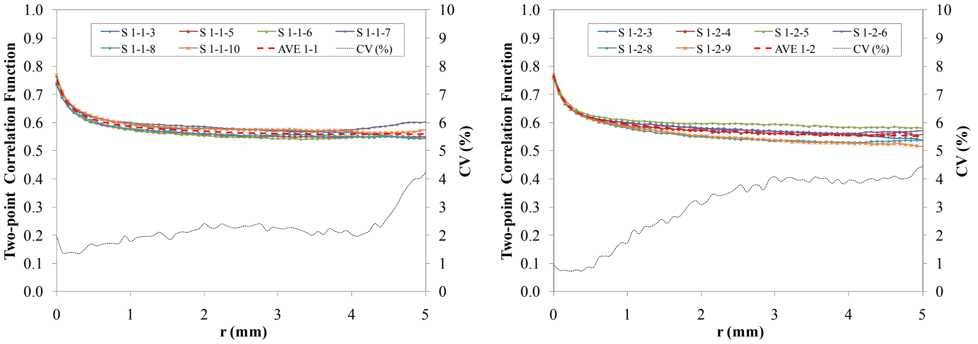

Figure C.18. 2-point correlation functions for mixture 1 – slice 1 and 2

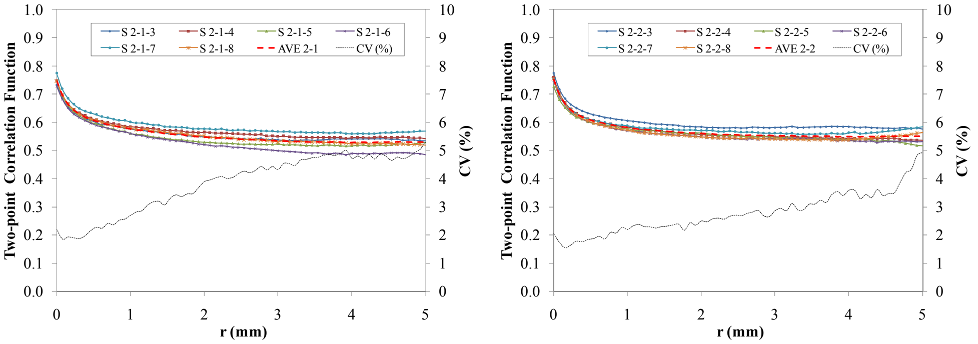

Figure C.19. 2-point correlation functions for mixture 2 – slice 1 and 2

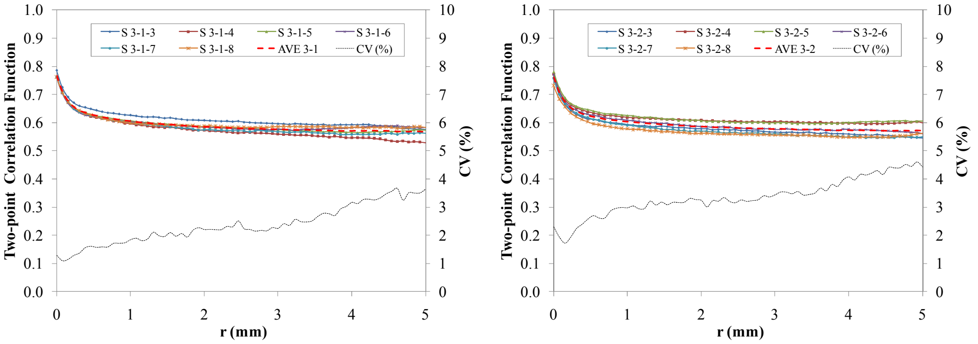

Figure C.20. 2-point correlation functions for mixture 3 – slice 1 and 2

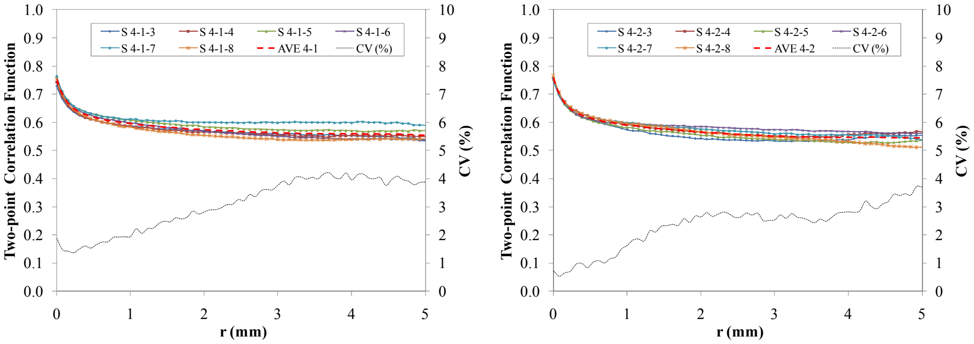

Figure C.21. 2-point correlation functions for mixture 4 – slice 1 and 2

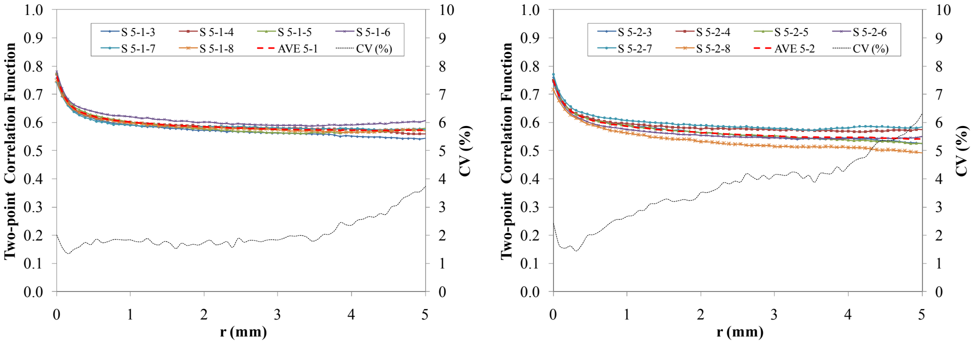

Figure C.22. 2-point correlation functions for mixture 5 – slice 1 and 2

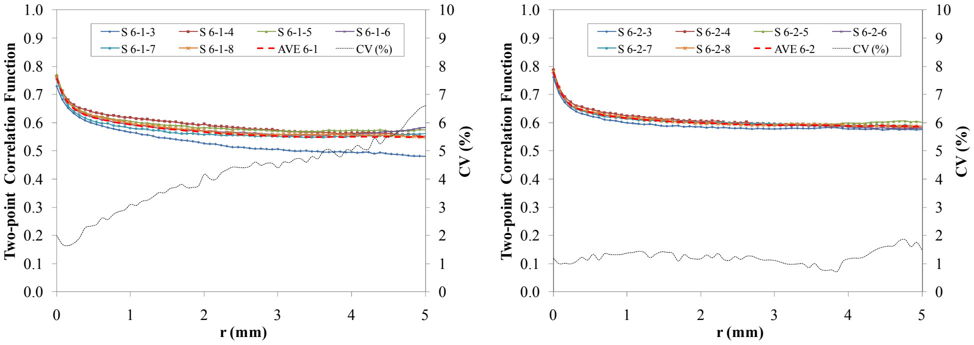

Figure C.23. 2-point correlation functions for mixture 6 – slice 1 and 2

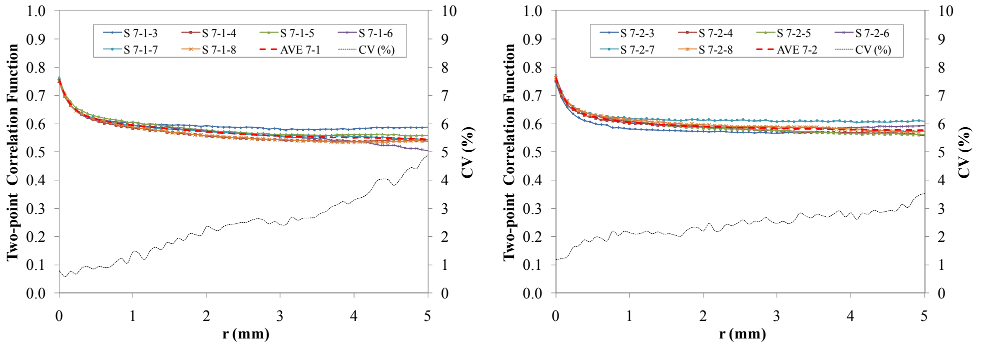

Figure C.24. 2-point correlation functions for mixture 7 – slice 1 and 2

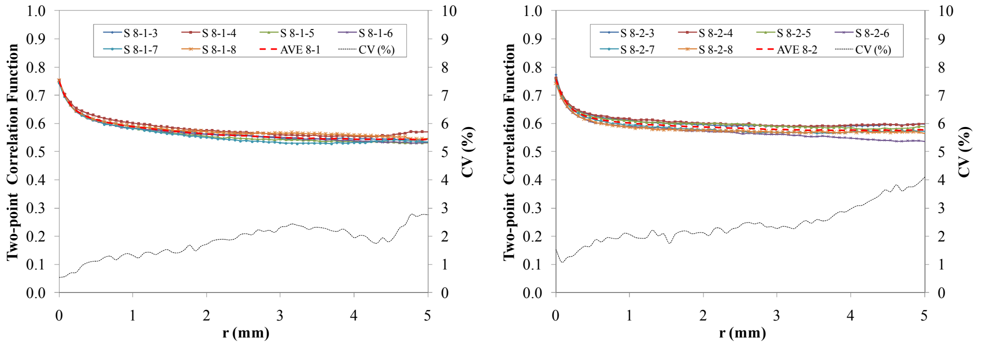

Figure C.25. 2-point correlation functions for mixture 8 – slice 1 and 2

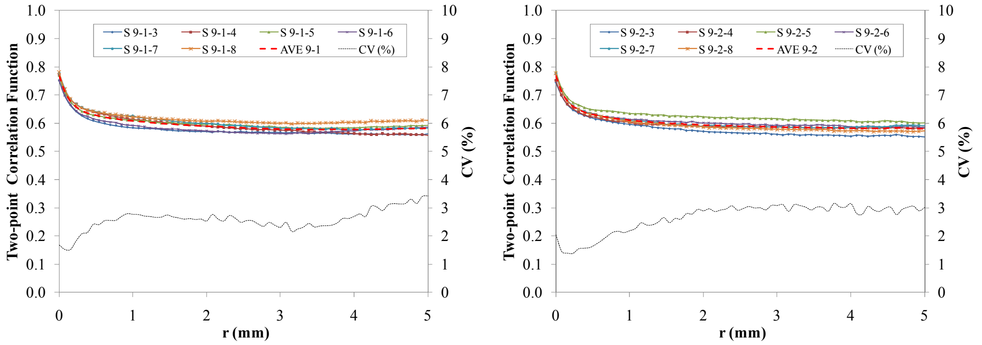

Figure C.26. 2-point correlation functions for mixture 9 – slice 1 and 2

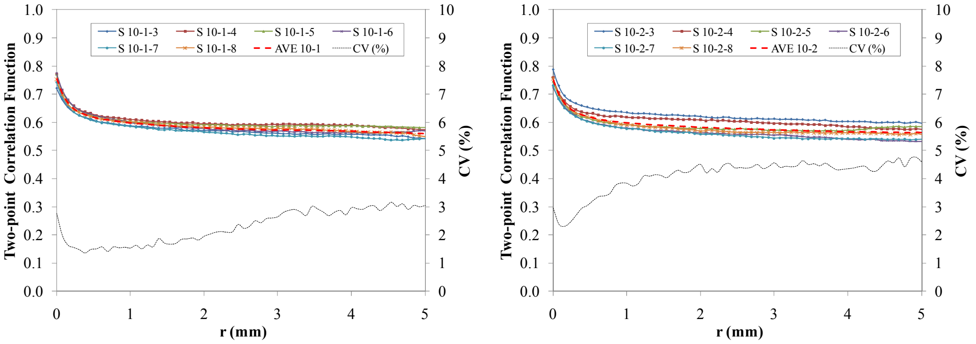

Figure C.27. 2-point correlation functions for mixture 10 – slice 1 and 2

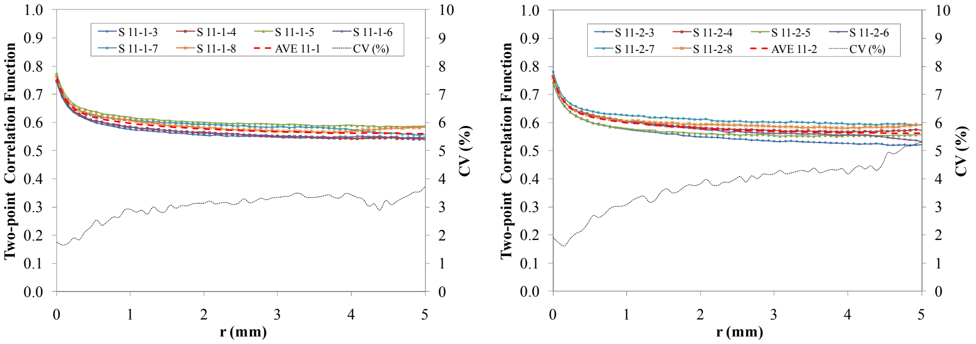

Figure C.28. 2-point correlation functions for mixture 11 – slice 1 and 2

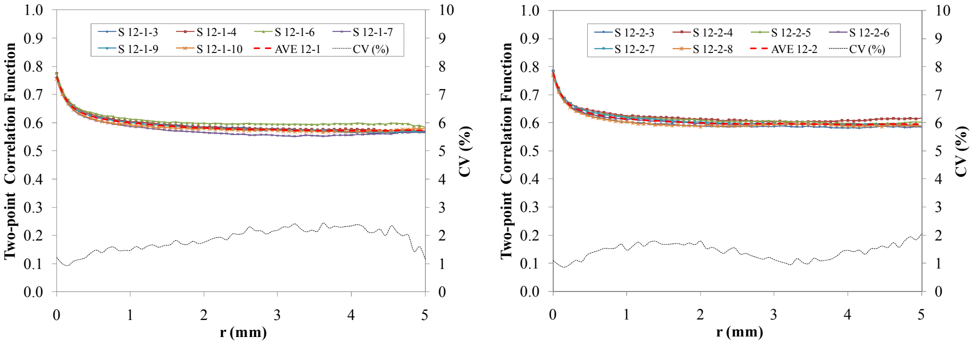

Figure C.29. 2-point correlation functions for mixture 12 – slice 1 and 2

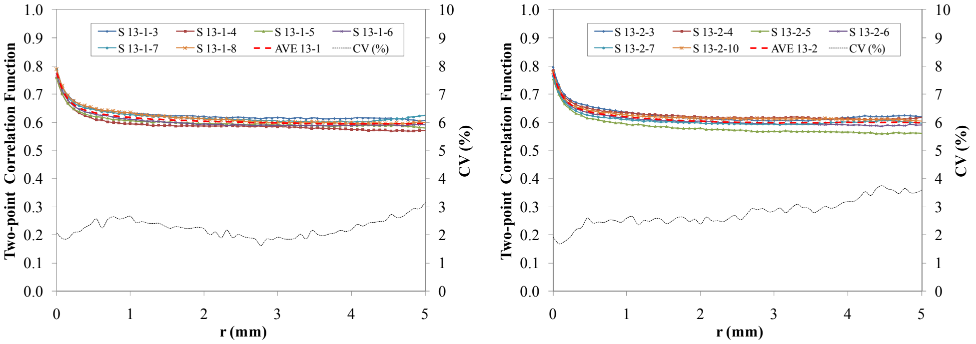

Figure C.30. 2-point correlation functions for mixture 13 – slice 1 and 2

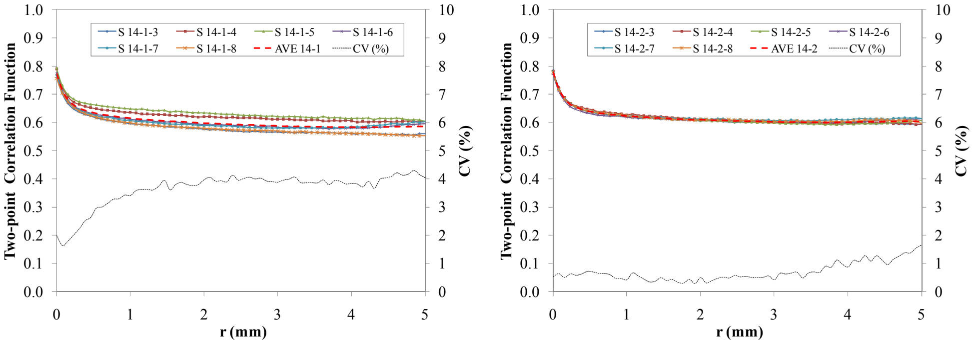

Figure C.31. 2-point correlation functions for mixture 14 – slice 1 and 2

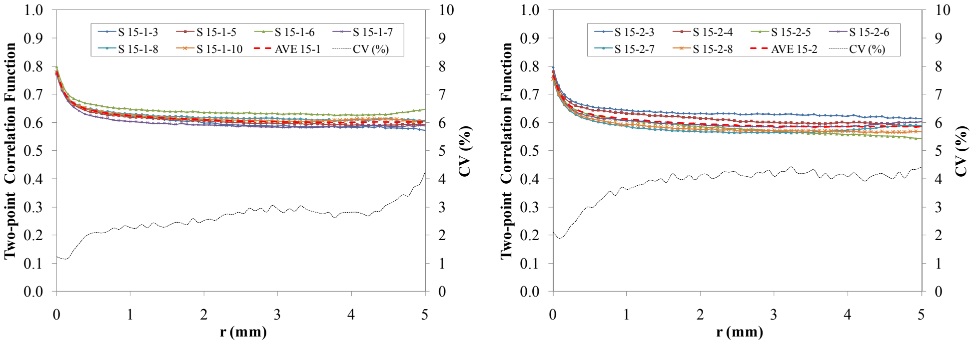

Figure C.32. 2-point correlation functions for mixture 15 – slice 1 and 2

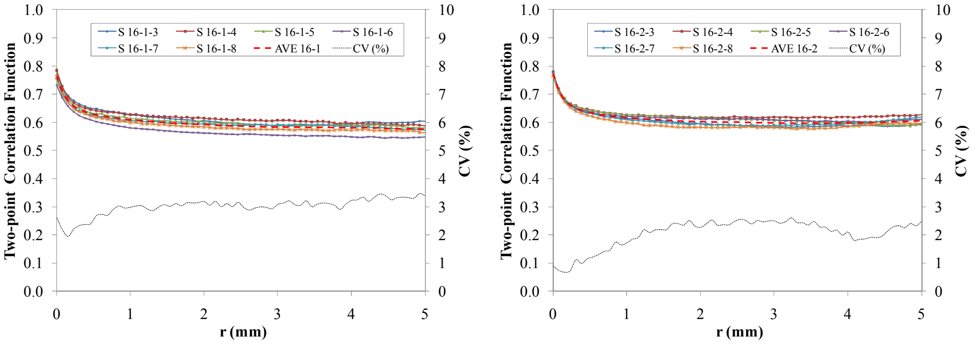

Figure C.33. 2-point correlation functions for mixture 16 – slice 1 and 2

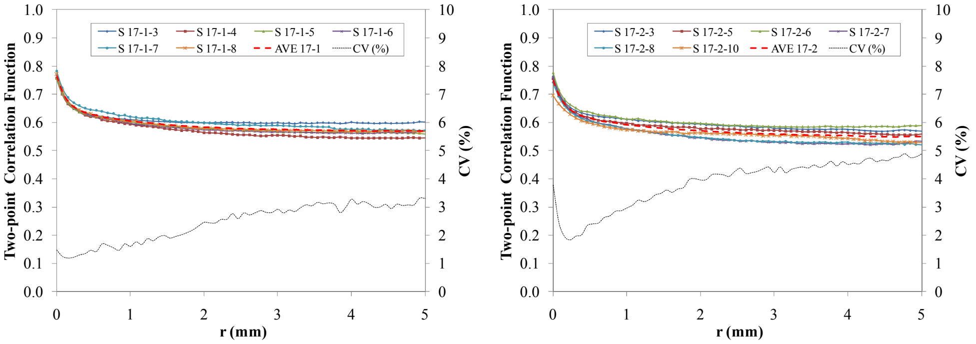

Figure C.34. 2-point correlation functions for mixture 17 – slice 1 and 2

C.3. 3-point Correlation Functions

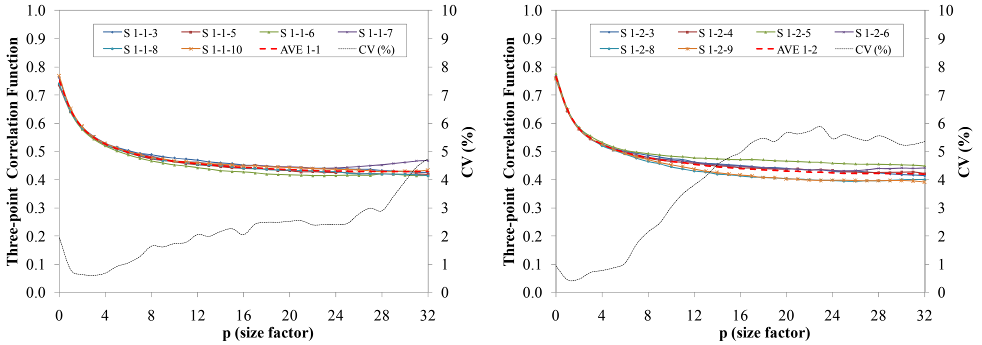

Figure C.35. 3-point correlation functions for mixture 1 – slice 1 and 2

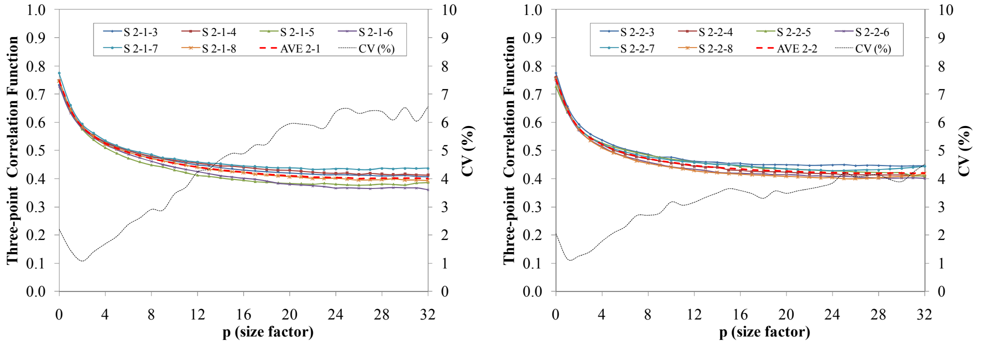

Figure C.36. 3-point correlation functions for mixture 2 – slice 1 and 2

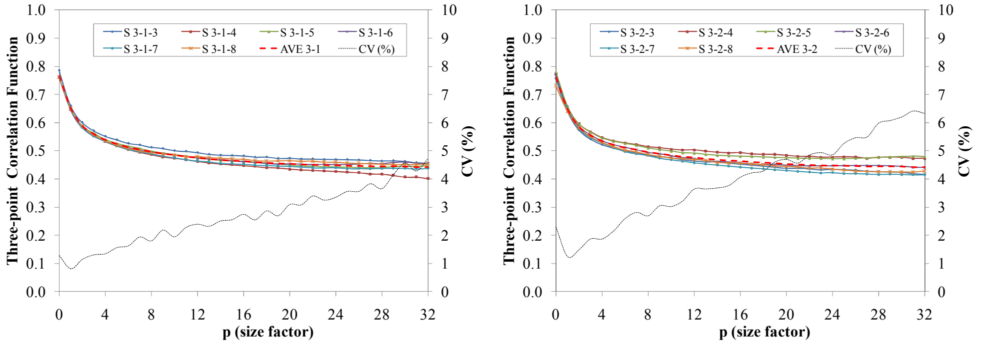

Figure C.37. 3-point correlation functions for mixture 3 – slice 1 and 2

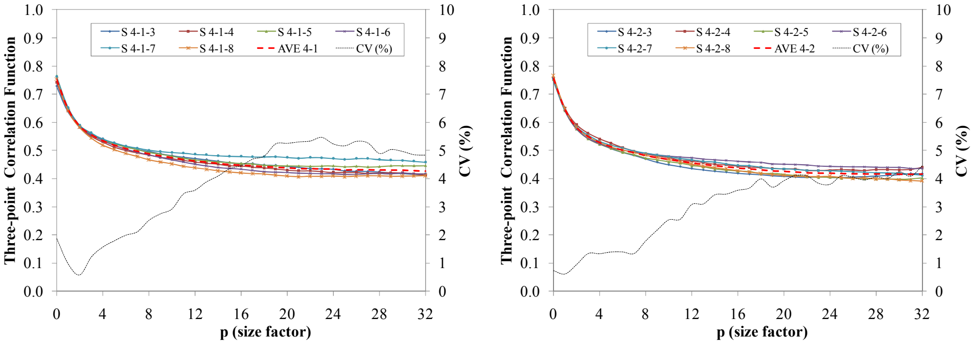

Figure C.38. 3-point correlation functions for mixture 4 – slice 1 and 2

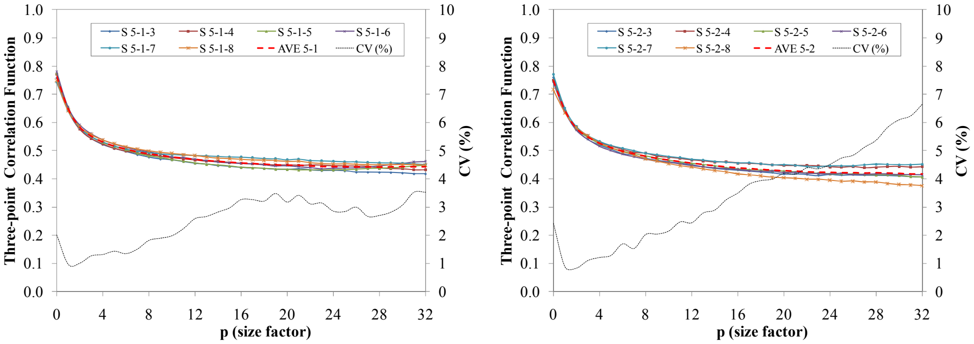

Figure C.39. 3-point correlation functions for mixture 5 – slice 1 and 2

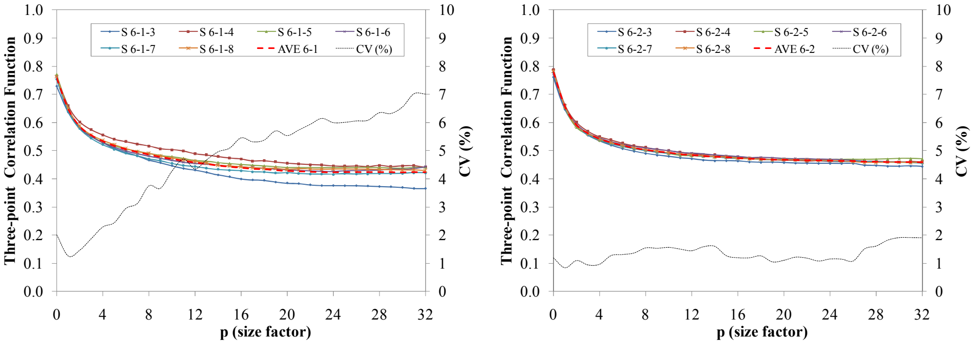

Figure C.40. 3-point correlation functions for mixture 6 – slice 1 and 2

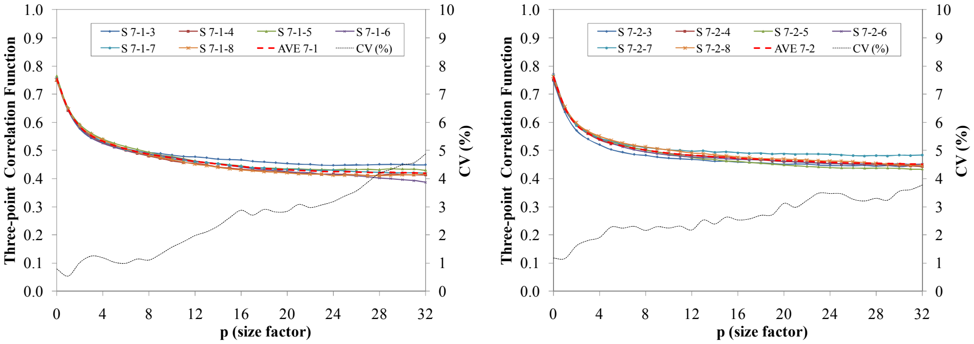

Figure C.41. 3-point correlation functions for mixture 7 – slice 1 and 2

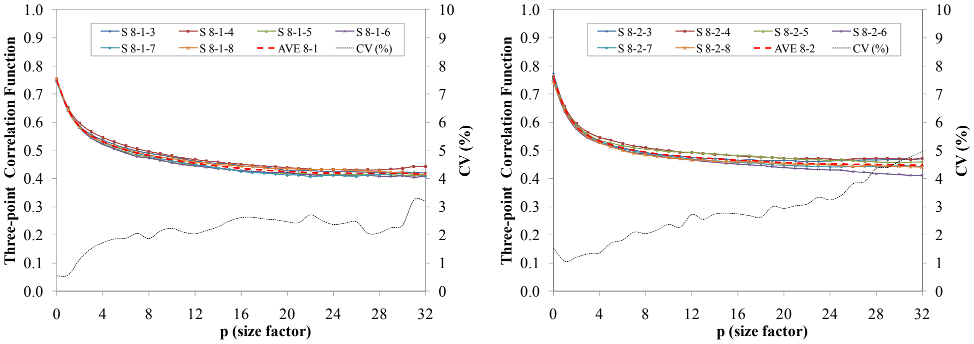

Figure C.42. 3-point correlation functions for mixture 8 – slice 1 and 2

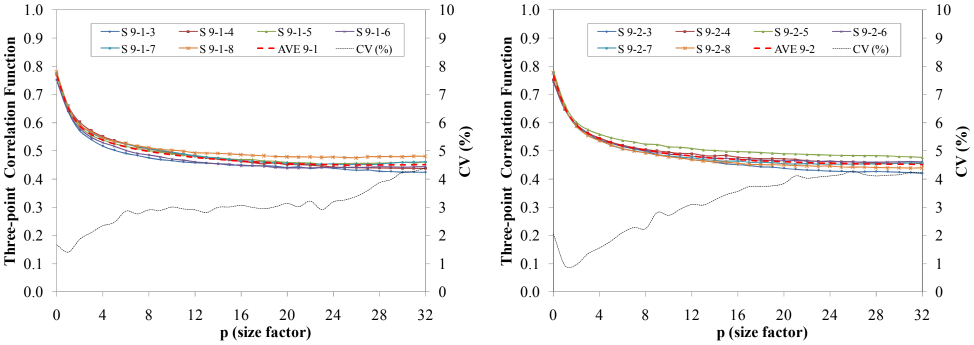

Figure C.43. 3-point correlation functions for mixture 9 – slice 1 and 2

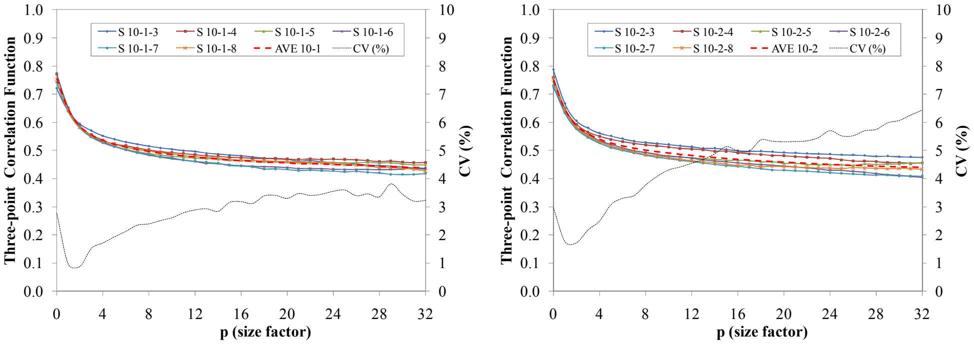

Figure C.44. 3-point correlation functions for mixture 10 – slice 1 and 2

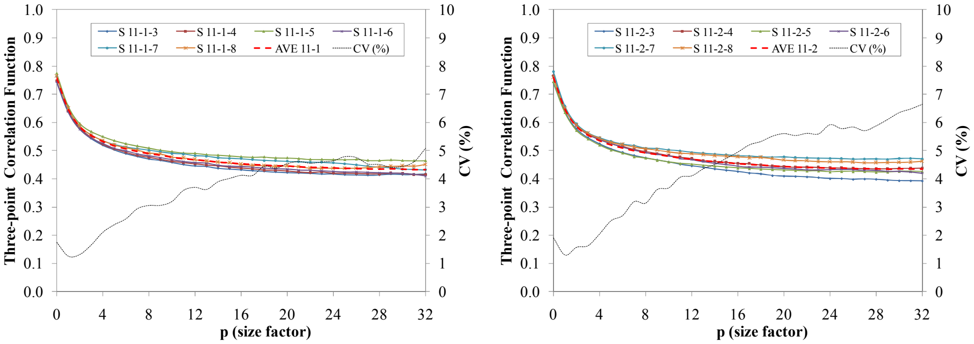

Figure C.45. 3-point correlation functions for mixture 11 – slice 1 and 2

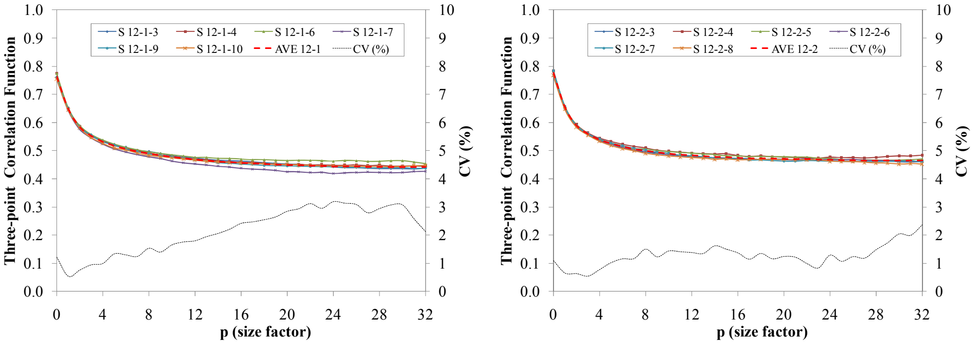

Figure C.46. 3-point correlation functions for mixture 12 – slice 1 and 2

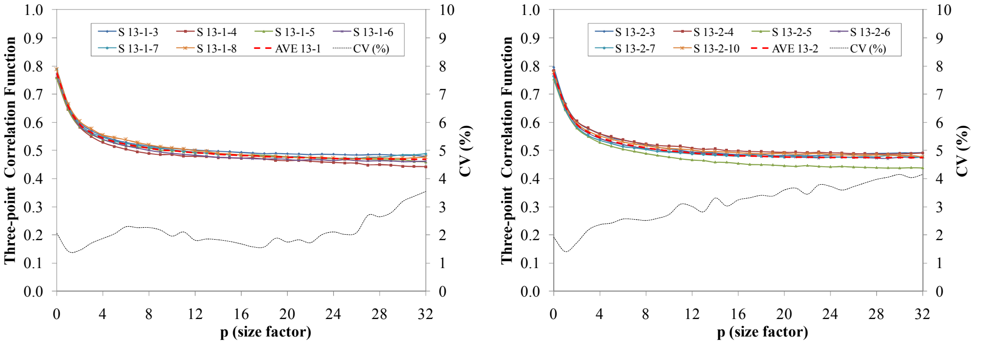

Figure C.47. 3-point correlation functions for mixture 13 – slice 1 and 2

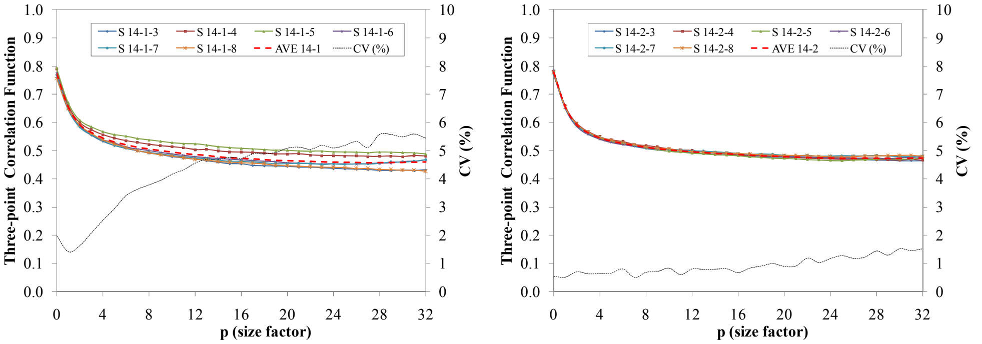

Figure C.48. 3-point correlation functions for mixture 14 – slice 1 and 2

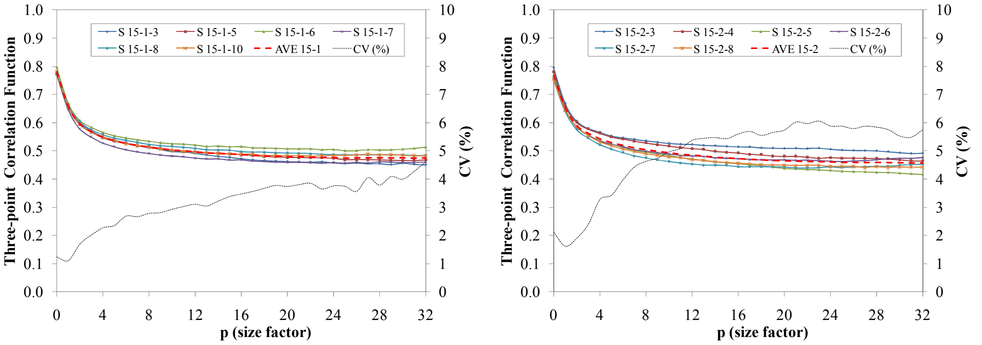

Figure C.49. 3-point correlation functions for mixture 15 – slice 1 and 2

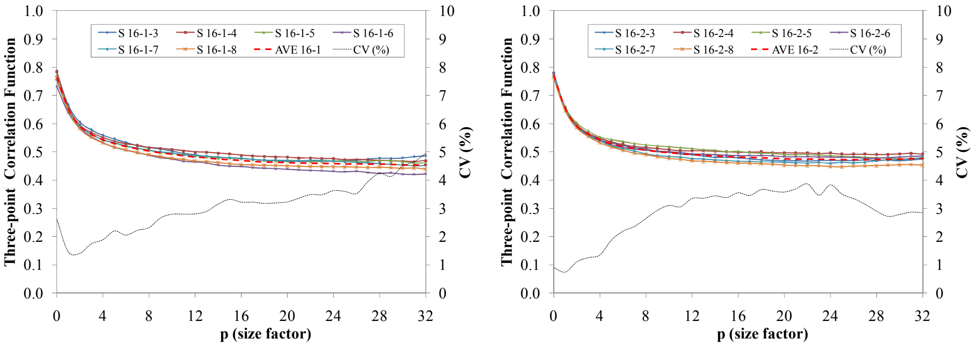

Figure C.50. 3-point correlation functions for mixture 16 – slice 1 and 2

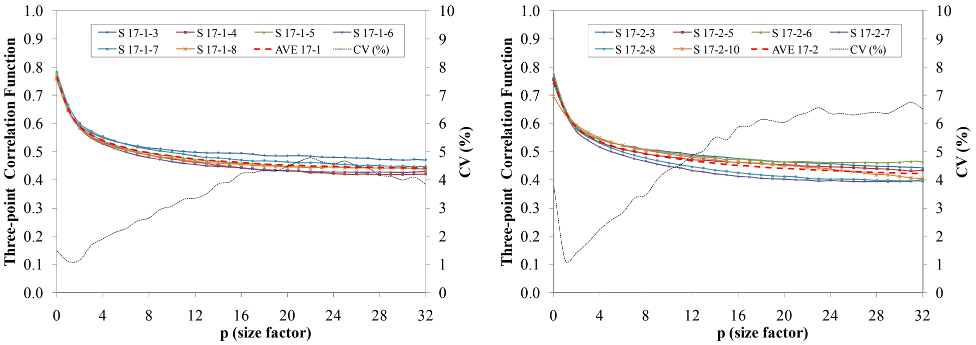

Figure C.51. 3-point correlation functions for mixture 17 – slice 1 and 2